THE POTENTIAL FOR GROUNDWATER CONTAMINATION ARISING FROM A LEAD/ZINC MINE TAILINGS IMPOUNDMENT

Thomas Maarten Vergunst

B.Sc. (Hons)

Submitted in fulfilment of the academic requirements for the degree of

Master of Science

in

Soil Science

School of Environmental Sciences

University of KwaZulu-Natal

Pietermaritzburg

December 2006

DECLARATION

I hereby certify that the research reported in this thesis is the result of my own investigation, except as acknowledged herein, and that it has not been submitted for a higher degree at any other university or institution.

Signed: ..... Date: 11 April 2007

Thomas M. Vergunst

Signed: ..... Date: 11/04/2007

Mr H.C Bester
(supervisor)

ABSTRACT

The mining industry produces vast quantities of overburden and mill tailings. In many instances the disposal of these wastes on the Earth's surface have caused local, and occasionally even regional, water resources to become contaminated. Contamination typically arises from the oxidation of metal sulfide minerals contained within these wastes. Upon oxidation these minerals release sulfate, their associated metal cations and acidity into solution. This study investigated the potential for groundwater contamination arising from a Pb/Zn tailings impoundment in the North West Province of South Africa (Pering Mine).

The tailings is composed predominantly of dolomite, which imparts to the material an alkaline pH and a high acid buffering capacity. Acid-base accounting (ABA) established that the capacity of the tailings to buffer acidity surpasses any acid producing potential that could arise from pyrite (FeS_2), galena (PbS) and sphalerite (ZnS) oxidation. These minerals account for about 3 to 6% of the tailings by mass. Total elemental analysis (XRF) showed that the material has high total concentrations of Fe (19083 mg kg^{-1}), Zn (5481 mg kg^{-1}), Pb (398 mg kg^{-1}), S (15400 mg kg^{-1}), Al (9152 mg kg^{-1}) and Mn (29102 mg kg^{-1}). Only a very small fraction of this, however, was soluble under saturated conditions. An estimation of potentially available concentrations, using the DTPA extraction method, indicated that high concentrations of Zn (1056 mg kg^{-1}), and moderate concentrations of Pb (27.3 mg kg^{-1}) and Cu (6.01 mg kg^{-1}) could potentially be available to cause contamination.

A number of leaching experiments were undertaken to accurately quantify the release of elements from the tailings material. These experiments were aimed at determining the potential for groundwater contamination and also provided a means whereby the long-term release of contaminants could be modelled using the convection-dispersion equation for solute transport. Four leaching treatments were investigated. Two consisted of using distilled water under intermittent and continuous flow, while a third used intermittent flow of deoxygenated distilled water to assess leaching under conditions of reduced oxygen. The mobilisation of potential contaminants under a worst case scenario was assessed by means of leaching with an acetic acid solution at pH 2.88 (after the US Environmental Protection Agency's toxicity characteristic leaching procedure).

The acid buffering potential of the tailings was considerable. Even after 8 months of weekly leaching with 1 pore volume of acetic acid solution the pH of the effluent was maintained above pH 5.90. The protracted acidity caused very high concentrations of Pb, Zn, Mn, Ca, Mg, Hg and S to be released into solution. Leaching the tailings with distilled water also caused the effluent to have noticeable traces of contamination, most importantly from S, Mg, Mn and Zn. In many instances concentrations significantly exceeded guideline values for South African drinking water. Modelling solute transport with the convection-dispersion equation predicted that SO_4^{2-} and Mn contamination could persist for a very long period of time (±700 years under continuous saturated leaching), while Mg and Zn concentrations would most likely exceed recommended limits for a much shorter period of time (±300 years under the same conditions). In light of the various column leaching experiments it was concluded that seepage from the Pering tailings impoundment could cause groundwater contamination.

A drill-rig and coring system were used to collect both tailings and pore-water samples from eight boreholes spread out across the tailings impoundment. These investigations showed that most of the impoundment was aerobic (E_h ranged from +323 to +454 mV) and alkaline (pH 8.0 to 9.5). This chemical environment favours sulfide oxidation and as a consequence high concentrations of S have been released into the pore-water of the impoundment (S concentrations ranged from 211 to 1221 mg l^{-1}). The acidity released as a by-product of sulfide oxidation was being buffered by dolomite dissolution, which in turn was releasing high concentrations of Mg (175 to 917 mg l^{-1}) and Ca (62.6 to 247 mg l^{-1}) into solution. Metal concentrations in the pore-water were low as a result of the strong metal sorbing capacity of the tailings and possible secondary precipitation. The only metal which significantly exceeded recommended limits throughout the impoundment was Hg (concentrations were between 100 and 6000 times the recommended limit of 0.001 mg l^{-1}). Under the current geochemical conditions it is expected that Hg, S and Mg will likely pose the greatest threat to groundwater.

The main concerns associated with mine tailings are that of mine drainage and dust blow off. In order to eradicate the latter problem, the tailings impoundment at Pering Mine was covered with a layer of rocks. Modelling the water balance of the impoundment using the computer model *HYDRUS-2D* showed that the rock cladding has potentially increased the volume of drainage water seeping from the impoundment. In light of the leaching

experiments and field work, which proved that water passing through the tailings became enriched with various potentially toxic elements, it is expected that the problem of groundwater contamination around Pering Mine has been further exacerbated by the rock cladding. It was therefore concluded that there would be a strong likelihood of groundwater contamination in the vicinity of the mine.

ACKNOWLEDGMENTS

There are many people I would like to thank, each of them has in some way helped me to realise this project.

First and foremost I would like to thank my supervisor Christopher Bester for all his input and supervision over the course of the project. Without him this project would not have materialised let alone come together in the way it has. Your assistance in all aspects has been much appreciated.

I would also like to extend thanks to Louis Titshall. He has provided endless support and help throughout my project, from the long days of sampling at Pering right through to arbitrary requests for information and references right at the end. He always has, somehow, had time to offer assistance. Professor Jeff Hughes has also provided much guidance on the academic and written aspects of this thesis. For this I am also very grateful.

Much of my laboratory work would not have been possible without the assistance of Essack Abib and Tad Dorasamy. Thank you both for your help and time. Dorothea Smith also needs special mention for her calm guidance and work in the laboratory, both of which have contributed towards the completion of this thesis.

Special thanks must go to Professor Simon Lorentz of the Hydrology Department for his detailed explanations and patient help with setting up and modelling some of the column experiments. His time and expertise were greatly appreciated.

I would also like to acknowledge Ritva Muhlbauer of BHP Billiton SA Ltd. for making this project possible and for ensuring financial support. In the same capacity I would also like to thank Sashnee Raja.

On a final note I would like to acknowledge my friends Ian Kiephill and Evan Brauteseth for helping to keep me sane, not only through good rides but also through good friendship. To Jess. Thanks for everything; your English lessons, patient support and love have all meant so much to me over the last two years.

November 2006, Pietermaritzburg

TABLE OF CONTENTS

CHAPTER 2

CHAPTER 3

LIST OF FIGURES

LIST OF TABLES

LIST OF APPENDICES

INTRODUCTION

Since the mid 1800's mining in South Africa has increased consistently, to become one of the most significant contributors to the national economy. The mining industry has helped to fuel both economic and social development for many decades. In 2002 the industry contributed R 80.6 billion (8.1%) to the country's GDP (Chamber of Mines, 2006). Associated with the mining industry however, is its inevitable impact upon the environment (Dudka and Adriano, 1997; Wilson, 1998). These impacts vary widely and, in line with legislation and public concern, are receiving increased attention both locally and abroad (Salmons, 1995; Wilson, 1998; Aucamp and van Schalkwyk, 2003; Naicker *et al.*, 2003; Xenidis *et al.*, 2003).

The mining of base and precious metals produces vast quantities of waste rock and mill tailings. Due to processing and economic limitations these wastes often contain traces of a variety of heavy metals. These metals are typically bound up in sulfide minerals, which are unstable in the oxidising environment of our atmosphere. As oxygen and water penetrate into discarded tailings, the sulfide minerals undergo oxidation. This releases sulfate, acidity and metal cations into the surrounding pore-water (McGregor *et al.*, 1998; Moncur *et al.*, 2005). As infiltrating water percolates through the waste the metal-rich pore-water may leach into local rivers or groundwater systems and cause considerable contamination (Salmons, 1995; Wilson, 1998; España *et al.*, 2005; Blodau, 2006).

Due to the environmental concerns which surround mining operations and the disposal of their wastes, an environmental assessment of a recently decommissioned Pb/Zn mine in the North West Province of South Africa was undertaken. This project forms part of a larger investigation which focused on various aspects of contamination in and around the mine. It will be the exclusive focus of this thesis to investigate the mineralogy, geochemistry and leaching potential of the tailings impoundment.

The mine is located on Pering Farm about 70 km southwest of Vryburg. Prior to discovery of the ore body, the farm was used for the grazing of livestock and game. Mining operations began in 1986 and continued through to January 2003. During this time approximately 19.12 Mt of ore, with an average grade of 2.60% Zn and 0.59% Pb, was

mined from two neighbouring pits (personal communication Ms S. Raja). The sphalerite (ZnS) and galena (PbS) deposits were concentrated in almost horizontal carbonates of the Lower Proterozoic Reivilo Formation (Transvaal Supergroup). In addition to sphalerite and galena, minor traces of pyrite (FeS_2) and chalcopyrite ($CuFeS_2$) were also reported to have been present in the ore (du Toit, 1998). The metal sulfides were separated from the milled ore by froth flotation. The sulfide concentrate was then transported by road and rail for final smelting and processing offsite.

The development of froth flotation in the early 1900s revolutionised extraction efficiencies, but has also resulted in greater reactivity of tailings due to the ore being finely milled for this process (Moncur *et al.*, 2005). The method consists of placing finely milled ore in water and adding a frothing or foaming agent which selectively coats the sulfide mineral particles, making them hydrophobic. Air is then bubbled through the system, causing the coated particles to rise to the surface of the solution, from where they are scooped off and sent for final processing (Cowey, 1998). The uncoated minerals sink to the bottom of the reaction tank as tailings. The remaining frothing solution and tailings are then siphoned away and deposited in slurry form into a dam/impoundment close to the mill. Over the years at Pering Mine the discarded tailings were built up layer by layer, eventually reaching a height of 30 m and covering an area of approximately 522 000 m^2.

Water percolation through the large volume of tailings could potentially cause a range of contaminants to be leached into the local groundwater. It was the objective of this project to quantify the nature and severity of this risk. This was achieved by both laboratory and field based investigations. The tailings material was characterised on the basis of its mineralogy, total elemental composition and basic chemical properties. The potential for contamination was assessed by means of a number of batch extractions and leaching column experiments. This was augmented by a detailed field investigation, in which eight boreholes were drilled through the impoundment. Both solid and pore-water samples were collected from these boreholes, which enabled the risk of groundwater contamination to be assessed and understood in context of the geochemical conditions within the impoundment. Since closure of the mine all infrastructure has been removed, and the shape and surface coverage of the impoundment has been modified in an attempt to reduce erosion and dust blow off. These modifications were made in September 2004 and consisted of constructing retainer walls around the upper perimeter of the impoundment, which has given the upper

surface of the tailings a dam like shape (the retainer walls are about 2 to 3 m high and approximately 10 to 15 m wide). The entire impoundment was also covered with a layer of rocks, ranging from about 30 to 50 cm thick. It is thought that these modifications have altered the movement of water across the upper boundary of the impoundment, and will therefore most likely affect the volume of mine drainage entering the groundwater. In order to understand the full effect of these modifications on the water balance of the impoundment, water movement through the profile was modelled using the computer model *HYDRUS-2D* (Šimůnek *et al.*, 1999).

The first chapter of this thesis provides a theoretical background to the environmental implications associated with mine tailings and the factors which control the release of contaminants from these wastes. The second chapter deals with characterisation aspects, while the third moves on to investigate the leachability of the Pering tailings by means of leaching column type experiments. The fourth chapter provides an overview of the geochemical conditions within the impoundment based on detailed borehole sampling. The final chapter of this thesis was dedicated to modelling the water balance of the tailings impoundment using *HYDRUS-2D*.

CHAPTER 1

OXIDATION, SPECIATION AND MOBILITY OF SULFIDE MINERALS AND THEIR BY-PRODUCTS IN MINE TAILINGS

1.1 Introduction

A large proportion of the World's economic metals are obtained from metal sulfide ores (Ross, 1994; Dudka and Adriano, 1997). The mining of these ores from the Earth's crust and their subsequent processing produces large amounts of solid wastes in the form of overburden and mill tailings. Ore reserves often contain a variety of different metal sulfide minerals. Due to economic and processing limitations not all of these minerals are removed from the ore (Dudka and Adriano, 1997) and as a result tailings typically contain traces of heavy metals. Some of the more commonly occurring metal sulfides include pyrite (FeS_2), pyrrhotite ($Fe_{x-1}S$), galena (PbS), sphalerite (ZnS), cinnabar (HgS) and chalcopyrite ($CuFeS_2$). Tailings are most commonly disposed of onsite and, after years of deposition, tailing impoundments may build up to cover many thousands of square metres. Extended exposure of these tailings to the weathering processes at the Earth's surface causes the sulfide minerals to undergo oxidation, releasing sulfate, their associated metals and hydrogen ions into the pore-water of the tailings. Over time this enriched pore-water may percolate into groundwater systems or surface streams (Lin, 1997; Bain *et al.*, 2000; Sharma and Al-Busaidi, 2001; Moncur *et al.*, 2005) and cause severe contamination (Salmons, 1995; Rösner and van Schalkwyk, 2000; Naicker *et al.*, 2003; Heyden and New, 2004; España *et al.*, 2005).

The oxidation of a typical metal sulfide ($Me^{2+}S^{2-}$) by oxygen, with the subsequent release of H^+ ions, metal cations (Me^{2+}) and sulfate (SO_4^{2-}), can be broadly demonstrated by the following equation:

$$Me^{2+}S^{2-} + O_2 + 2H_2O \rightarrow Me^{2+} + SO_4^{2-} + 4H^+ \qquad (1.1)$$

The rate of metal sulfide oxidation is controlled by the rate at which oxygen can penetrate into the surface of the tailings impoundment (Elberling *et al.*, 1994; Wunderly *et al.*, 1996). This diffusion of oxygen into the pore space of the tailings and then into the water films surrounding the sulfide minerals is the first step to sulfide oxidation (Figure 1.1). If no oxidised coating or surface precipitates cover the sulfide minerals, oxidation will begin

without much delay. However if surface coatings are present, oxidation will only occur at the rate at which 0_2 can penetrate these layers (Wunderly *et al.*, 1996). Over extended periods of time these processes lead to the formation of stratified oxidation layers within the tailings as shown in Figure 1.1.

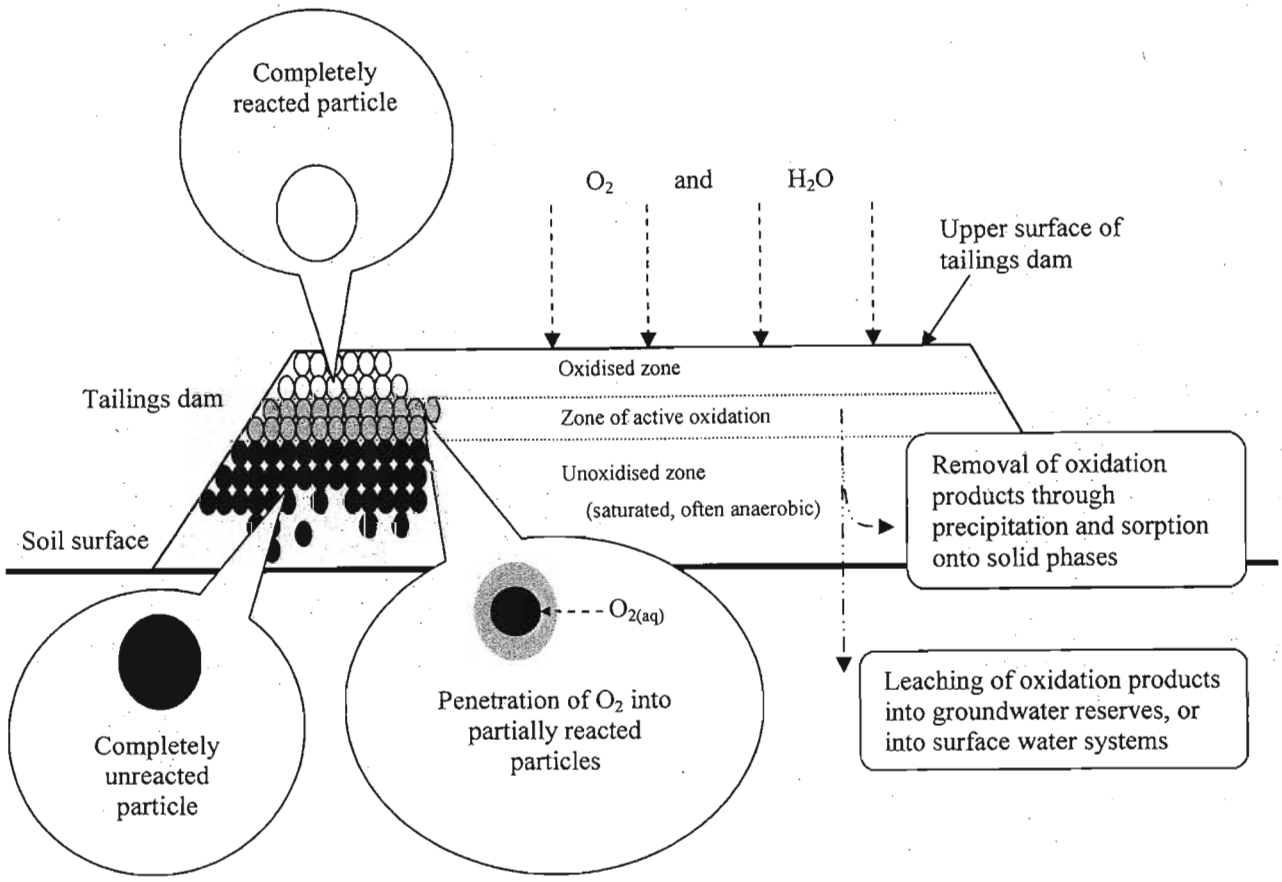

Figure 1.1 Typical conditions and processes occurring in abandoned tailings impoundments after extended exposure to atmospheric weathering (modified from Wunderly *et al.*, 1996).

The extent of sulfide oxidation tends to decrease with depth (Blowes *et al.*, 1998; McGregor *et al.*, 1998; Moncur *et al.*, 2005). After a number of years a clearly defined oxidised zone often becomes visible. This layer is characterised by low levels of sulfur and heavy metals. Underlying this layer is the region of active oxidation in which acid, sulfate and metal rich leachate are created by means of Equation 1.1. As this leachate passes down through the profile, it comes into contact with the unweathered, typically anaerobic zone of the tailings dam. The mineralogy and chemical conditions of this zone tend to be very

different to those of the oxidising layers above. As a result a vast number of chemical transformations can occur here, including acid buffering, precipitation, adsorption and reduction reactions. Thus, if the mineralogy and chemistry of the tailings favour these processes, the release of acidity and heavy metals from the impoundment may be significantly retarded (Lin, 1997; Al *et al.*, 2000; Ljungberg and Öhlander, 2001; Moncur *et al.*, 2005).

Due to the reported environmental consequences associated with acid mine drainage, it is essential to understand the mechanisms of sulfide oxidation, and the subsequent chemical interactions of the oxidation products in the lower zones of the tailings impoundment (Salmons, 1995; Dudka and Adriano, 1997; Blodau, 2006). The kind of interactions that take place will determine how mobile the contaminants will be in the environment. These reactions are dependent upon the prevailing chemical conditions within the impoundment, the mineralogical composition of the tailings and the chemical composition of the leaching pore-water. This chapter will first examine the processes and mechanisms of sulfide oxidation, and then move on to describe the factors that control the behaviour of the sulfide oxidation products in the lower parts of a typical tailings impoundment.

1.2 Sulfide oxidation in mine tailings

Residual sulfide minerals have been reported to account for as much as 60%, by mass, of unweathered tailings (Moncur *et al.*, 2005). However ranges of approximately 5 to 10% are more commonly reported (e.g. Blowes *et al.*, 1998; McGregor *et al.*, 1998; Bain *et al.*, 2000). An understanding of how these sulfide minerals undergo oxidation provides the first step towards explaining the potential for environmental contamination.

1.2.1 Controlling factors

Sulfur has a number of oxidation states, ranging from -2 to +6, and consequently a wide variety of sulfur species are possible, which may occur in solid, aqueous or gaseous forms. Possible sulfur species include sulfides (S^{2-}; HS^-; H_2S), sulfites (SO_3^{2-}, HSO_3^-, HSO_3), thiosulfates ($S_2O_3^{2-}$, $HS_2O_3^-$), sulfates (SO_4^{2-}, HSO_4^-, H_2SO_4) and elemental sulfur (S^0). Transformations between these species can occur when electrons and hydrogen ions are gained or lost. Minerals and aqueous species which contain sulfur in its lower oxidation

states tend to be stable under reducing conditions, whereas in oxidising environments the higher oxidation states of sulfur predominate. This is clearly demonstrated in Equation 1.1 where the anaerobically formed metal sulfide (sulfur as S^{2-}) was shown to release sulfate (S^{6+}) and H^+ ions on oxidation. Thus the stability of any given species in an aqueous environment is described by the combined effect of redox potential (E_h) and pH.

E_h – pH diagrams have been widely used to depict the interaction of various solid, aqueous and gaseous species in geochemical environments. The details of these diagrams have been covered in depth by, among others, Garrels and Christ (1965), Lindsay (1979), Brookins (1988) and Bartlett and James (1993). For this reason, a detailed description of their theoretical background will not be given here. Instead, just a brief description of the sulfur, oxygen and hydrogen system, and its importance in terms of predicting sulfur speciation will be included. The primary variables, E_h and pH, are not the only controlling factors in these systems. Boundaries between species are also controlled by differences in concentrations, temperature and partial pressure of gasses. An E_h – pH diagram for important naturally occurring sulfur species is shown in Figure 1.2. The activity of all species is assumed to be equal at 10^{-3} *M* under conditions of standard temperature and pressure. Increasing the concentration or altering the activities between different species will shift the equilibrium lines only marginally. This is demonstrated in the diagrams presented by Garrels and Christ (1965) who described systems containing much higher sulfur activities (10^{-1} *M*). The equilibrium lines illustrated by those authors do not differ significantly from those of Brookins (1988) shown in Figure 1.2.

The predominance of sulfate is clearly evident throughout most of the pH and E_h ranges, with the sulfide forms only being stable under highly reducing conditions (Figure 1.2). Thus, by way of example, it would follow that a tailings system with a pH of 7 and having an E_h of 200 mV would favour the formation of SO_4^{2-}. Any sulfur in the system contained in lower oxidation states, such as metal sulfides, would have a thermodynamic tendency to be transformed to sulfate. Likewise, the reverse may happen if the lower part of a tailings impoundment is sufficiently reduced (E_h < -200 mV at pH 7). Under these conditions sulfate leaching down from the oxidising zone may be reduced to sulfides (HS^-, H_2S) and undergo precipitation with heavy metals, thereby reforming metal sulfides (Adriano, 1986; Fergusson, 1990; McBride, 1994).

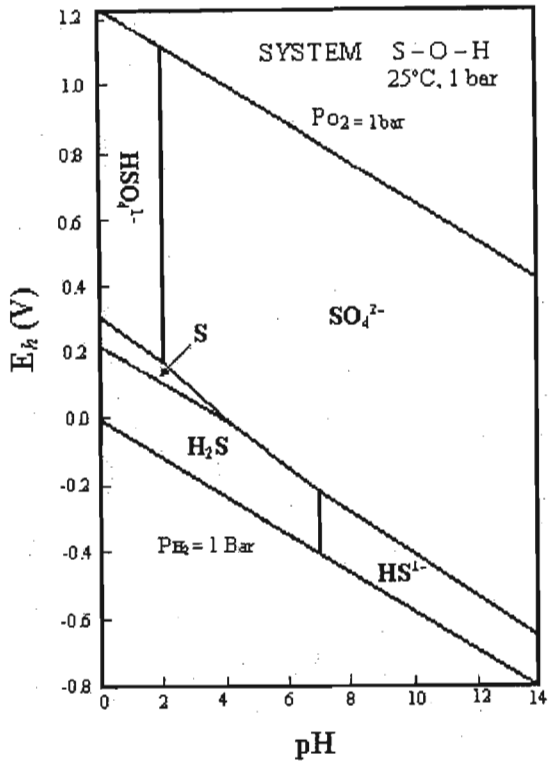

Figure 1.2 Relationship between sulfur species at different pH and E_h values (Brookins, 1988).

Most metal sulfides are unstable in oxidising aqueous solutions, in air they are reported to be unstable only at the very outer surface (Vaughan *et al.*, 1997). Thus water containing dissolved oxygen, or other oxidants, is essential for full mineral oxidation. When sulfides are brought to the Earth's surface, as is the case with mining operations, they become exposed to moisture and a number of naturally occurring oxidants. These oxidants accept electrons from the reduced sulfur atom in the metal sulfide mineral. With each successive loss of an electron, an intermediate sulfur species is formed. This stepwise transition between species makes the entire process of sulfide oxidation very difficult to quantify (Rimstidt and Vaughan, 2003).

Oxygen is primarily responsible for the oxidation of metal sulfides. However, ferric iron (Fe^{3+}) is also widely reported to be an important oxidant, often speeding up the rates of oxidation under acid conditions (pH < 4). At higher pH Fe^{3+} tends to precipitate out as iron oxide or hydroxide (Janzen *et al.*, 2000; Gleisner and Herbert, 2002; Belzile *et al.*, 2004; Weisner *et al.*, 2004). The oxidative pathways of O_2 and Fe^{3+} are summarised for the more commonly occurring metal sulfides in Table 1.1.

Table 1.1 Oxidation reactions for several metal sulfides commonly found in mine tailings (Malmström *et al.*, 2006).

Mineral	*Summarised reaction yielding final oxidation products*
Pyrite (oxygen path)	$FeS_{2(s)} + H_2O + 3½O_{2(aq)} \rightarrow Fe^{2+} + 2SO_4^{2-} + 2H^+$
Pyrite (iron path)	$FeS_{2(s)} + 14Fe^{3+} + 8H_2O \rightarrow 15Fe^{3+} + 2SO_4^{2-} + 16H^+$
Pyrrhotite (oxygen path)	$Fe_{1-x}S_{(s)} + (2 - ½x)O_{2(aq)} + xH_2O \rightarrow (1 - x)Fe^{2+} + SO_4^{2-} + 2xH^+$
Pyrrhotite (iron path)	$Fe_{1-x}S_{(s)} + (8 - 2x)Fe^{3+} + 2H_2O \rightarrow (9 - 3x)Fe^{2+} + SO_4^{2-} + 8H^+$
Sphalerite (oxygen path)	$ZnS_{(s)} + 2O_{2(aq)} \rightarrow Zn^{2+} + SO_4^{2-}$
Sphalerite (iron path)	$ZnS_{(s)} + 8Fe^{3+} + 4H_2O \rightarrow Zn^{2+} + SO_4^{2-} + 8Fe^{2+} + 8H^+$
Chalcopyrite (oxygen path)	$CuFeS_{2(s)} + 4O_{2(aq)} \rightarrow Cu^{2+} + Fe^{2+} + 2SO_4^{2-}$
Chalcopyrite (iron path)	$CuFeS_{2(s)} + 16Fe^{3+} + 8H_2O \rightarrow Cu^{2+} + 17Fe^{2+} + 2SO_4^{2-} + 16H^+$
Galena (oxygen path)	$PbS_{(s)} + 2O_{2(aq)} \rightarrow Pb^{2+} + SO_4^{2-}$
Galena (iron path)	$PbS_{(s)} + 8Fe^{3+} 4H_2O \rightarrow Pb^{2+} + SO_4^{2-} + 8Fe^{2+} + 8H^+$

Considerable research has been completed on the mechanisms of metal sulfide oxidation in order to improve commercial extraction processes, and to understand the dynamics controlling acid mine drainage. Most attention has been given to the more commonly occurring sulfide ores, such as pyrite (Chernyshova, 2003; Rimstidt and Vaughan, 2003; Belzile *et al.*, 2004), galena (Chernyshova, 2003; Gerson and O'Dea, 2003; da Silva, 2004), chalcopyrite (Yin *et al.*, 1995; Hiroyoshi *et al.*, 2001; Sandström *et al.*, 2005) and sphalerite (Weisner *et al.*, 2004; Shi *et al.*, 2006). The factors governing oxidation are similar for most metal sulfides. In a detailed study on the reaction mechanisms of pyrite oxidation, Rimstidt and Vaughan (2003) proposed that these principles could be extrapolated to "most, if not all, sulfide minerals." For this reason, pyrite will be used by way of example to demonstrate the overall process of metal sulfide oxidation.

1.2.2 Pyrite oxidation

Pyrite is one of the most commonly occurring mineral sulfides (Vaughan *et al.*, 1997; Rimstidt and Vaughan, 2003). In many instances its extraction and processing is uneconomical, which has resulted in many reports of acid mine drainage arising almost exclusively from pyrite oxidation (Blowes *et al.*, 1998; McGregor *et al.*, 1998; Bain *et al.*, 2000; Blodau, 2006).

In its purest form pyrite occurs as FeS_2. There are however, many derivatives of pyrite formed through associations with other trace elements and varying ratios of Fe to S. These variations give rise to sulfides with differing chemistry and electrical properties (Abraitis *et*

al., 2004). The oxidation of pyrite is an electrochemical process and thus these variations can affect the rate of oxidation. The oxidation of pyrite, and most other metal sulfides, consists of three steps (Figure 1.3). These steps include:

1. the cathodic reaction;
2. electron transport; and
3. the anodic reaction.

These reactions occur virtually simultaneously, but for the sake of clarity, they will be discussed separately.

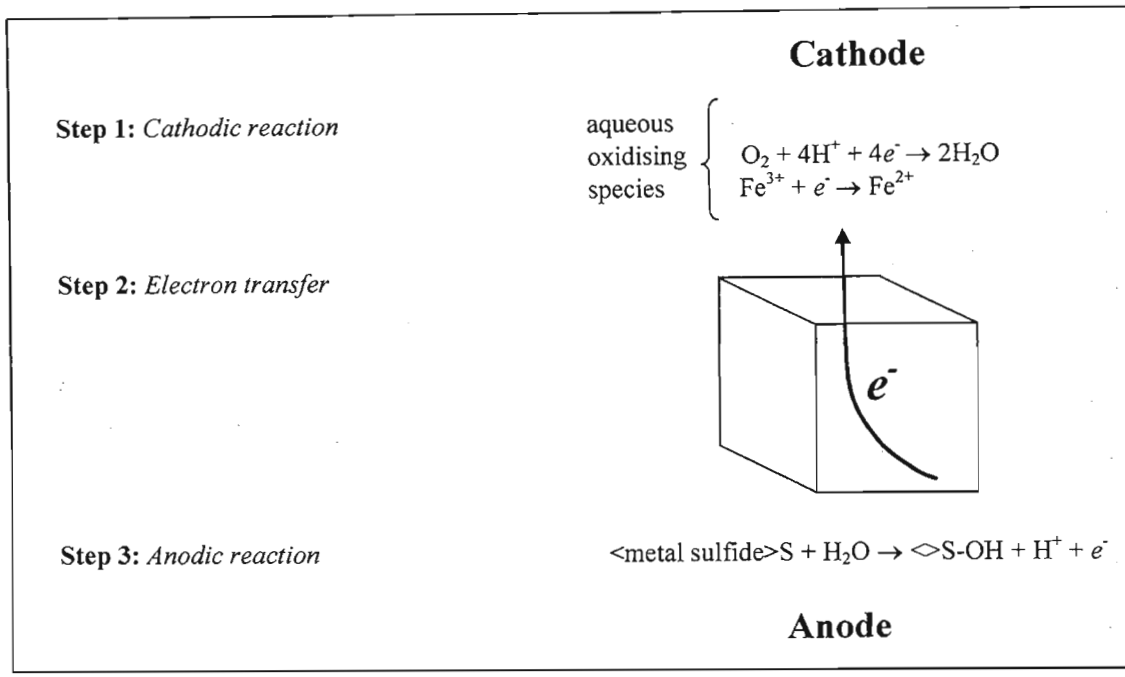

Figure 1.3 The three steps involved in pyrite oxidation (Rimstidt and Vaughan, 2003).

Step 1: *Cathodic reaction*

The cathodic reaction involves the reduction of an aqueous species by the donation of electrons (e^-) from the pyrite surface. The overall reactions defining the reduction of pyrite by O_2 and Fe^{3+} are given by Equations 1.2 and 1.3, respectively (Rimstidt and Vaughan, 2003).

$$FeS_2 + 3½O_2 + H_2O \rightarrow Fe^{2+} + 2SO_4^{2-} \quad (1.2)$$

$$FeS_2 + 14Fe^{3+} + 8H_2O \rightarrow 15Fe^{2+} + 16H^+ + 2SO_4^{2-} \quad (1.3)$$

Reactions 1.2 and 1.3 show that sulfur is oxidised while iron remains in its +2 oxidation state. Research suggests however, that electrons are first transferred from the metal sites in

the sulfide mineral to the aqueous oxidant, as opposed to the direct transfer of electrons from the S atom itself (Rosso *et al.*, 1999). The subsequent transfer of electrons to the cathodic site (Step 2, Figure 1.3) replaces electrons lost by Fe. It is the initial transfer of electrons from the sulfide to the aqueous oxidant, at the cathodic site, that controls the rate of pyrite oxidation (Brown and Jurinak, 1989). According to Rimstidt and Vaughan (2003) this also holds true for galena, sphalerite, chalcopyrite, arsenopyrite and, most likely, other sulfide minerals as well.

Step 2: *Electron transfer*

This consists of the transfer of electrons from the sulfur atom at the anodic site to iron at the cathodic site. As the Fe^{2+} ions at the pyrite surface lose electrons to the aqueous oxidant they become oxidised to Fe^{3+}, this is almost immediately reversed by the donation of an electron from the anodic site. This in turn allows the Fe^{2+} to donate another electron, thereby allowing the process of electron loss to continue. The transfer of electrons through pyrite is made possible by the fact that most sulfide minerals are semiconductors (Vaughan *et al.*, 1997; Abraitis *et al.*, 2004). Conductivity varies widely due to vast variations in the chemical composition of iron sulfides, where inclusions of many heavy metals are common (Abraitis *et al.*, 2004). However, these variations in conductivity seem to have little effect on controlling the rate of oxidation. According to Rimstidt and Vaughan (2003) variations in reactive surface area tend to override any differences in conductivity.

Step 3: *Anodic reaction*

In order for sulfide ions to be fully oxidised to SO_4^{2+}, a total of $7e^-$ from disulfide sulfur (e.g. FeS_2) and $8e^-$ from sulfide sulfur (e.g. FeS, PbS, ZnS) need to be removed. During this process many intermediate sulfur species may form, most of which tend to remain in some way associated with the mineral surface. Rimstidt and Vaughan (2003) outlined this oxidative process in some detail, but report that the intermediate species that result from weathering pyrite are not commonly found in acid mine drainage which tends to be dominated by SO_4^{2-} ions. The dominance of SO_4^{2-} in mine drainage is widely reported and thus the equations outlined in Table 1.1 show the general response of metal sulfides to oxidation in tailings (Jaynes *et al.*, 1984; McGregor *et al.*, 1998; Moncur *et al.*, 2005; Salmon and Malmström, 2006).

1.3 Acid buffering in mine tailings

The latent acidity released by sulfide oxidation in the aerated zones of the tailings impoundment may be buffered by the dissolution of surrounding minerals such as carbonates, oxyhydroxides and aluminosilicates. Soluble minerals such as calcite and dolomite tend to buffer the tailings pore-water close to neutrality. As the production of acidity continues, these minerals may be completely removed, a drop in pH will then ensue as the drainage water becomes buffered by less soluble minerals. This gives rise to the widely reported stratified layering of pore-water pH in many tailings impoundments (Lin, 1997; Al *et al.*, 2000; Johnson *et al.*, 2000; Ljungberg and Öhlander, 2001; Moncur *et al.*, 2005).

Jurjovec *et al.* (2002) gave the example of a sequentially buffered tailings dam, in which the pH of the pore-water was first controlled by the dissolution of calcite ($CaCO_3$), followed by siderite ($FeCO_3$), gibbsite ($Al(OH)_3$), iron hydroxide ($Fe(OH)_3$) and finally aluminosilicate minerals (Figure 1.4). In a carbonaceous tailings system this sequence has been reported to follow the stepwise dissolution of calcite, dolomite, ankerite, and finally siderite (Al *et al.*, 2000). The buffering capacity of tailings often retards the advancement of the acid plume as it moves down through the impoundment and into the underlying soil and rock structures (Johnson *et al.*, 2000; Ljungberg and Öhlander, 2001; Jurjovec *et al.*, 2002). In some instances this buffering may be sufficient to prevent the release of acidic drainage waters altogether (Ferguson and Erickson, 1988). Table 1.2 lists a number of minerals the dissolution of which has been reported to buffer acidity within mine tailings.

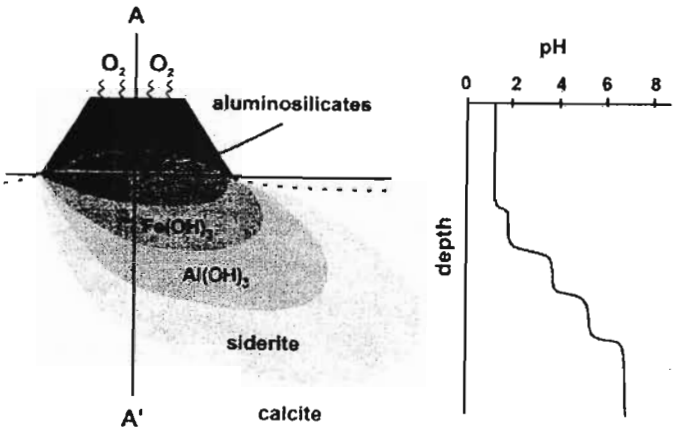

Figure 1.4 An example of pH buffering below a tailings impoundment (Jurjovec *et al.*, 2002).

Table 1.2 Typical buffering reactions reported to occur in mine tailings.

Mineral	*Dissolution reaction*		*Reference*
Calcite	$CaCO_3 + H^+ \rightarrow Ca^{2+} + HCO_3^-$	(at pH > 6.45)	a; b; d
	$CaCO_3 + 2H^+ \rightarrow Ca^{2+} + CO_{2(g)} + H_2O$	(at pH < 6.50)	
Dolomite	$CaMg(CO_3)_2 + H^+ \rightarrow Ca^{2+} + Mg^{2+} + HCO_3^-$		a; b
Siderite	$FeCO_3 + 2H^+ \rightarrow Fe^{2+} + H_2CO_3$		a; b; c; e
Rhodochrosite	$MnCO_3 + 2H^+ \rightarrow Mn^{2+} + H_2CO_3$		b
Gibsite	$Al(OH)_3 + 3H^+ \rightarrow Al^{3+} + 3H_2O$		c; d; f
Iron hydroxide	$Fe(OH)_3 + 3H^+ \rightarrow Fe^{3+} + 3H_2O$		d
Aluminosilicate minerals	Biotite → Vermiculite → Kaolinite		f

Decreasing solubility ↓

a: Blowes *et al.* (1998) b: Al *et al.* (2000); c: Johnson *et al.* (2000); d: Ljungberg and Öhlander (2001); e: Jurjovec *et al.* (2002); f: Moncur *et al.* (2005)

The presence of carbonate minerals (e.g. calcite [$CaCO_3$], dolomite [$CaMg(CO_3)_2$], ankerite [$Ca(Fe,Mg)(CO_3)_2$] and siderite [$FeCO_3$]) are of major environmental importance when found in association with economic sulfide deposits, due to their ability to neutralise acid leachate in tailings material. Despite extensive research on the acid producing effects of sulfide oxidation, there has been little investigation into the beneficial processes of acid neutralisation by carbonate minerals within mine tailings themselves (Blowes *et al.*, 1998; Strömberg and Banwart, 1999; Al *et al.*, 2000; Jurjovec *et al.*, 2002). However, the studies that have been done have shown carbonate minerals to be highly effective in treating acid mine drainage (Gazea *et al.*, 1996; Cravotta and Trahan, 1999; Potgieter-Vermaak *et al.*, 2006) and reducing concentrations of dissolved metals through precipitation, co-precipitation and adsorption processes (Bruno *et al.*, 1998; Al *et al.*, 2000).

The surfaces of carbonate minerals are known to be highly reactive and thus much research has been aimed at describing the interaction of trace elements with these surfaces under varying conditions of pH, moisture, temperature, electrolyte type and ionic strength. These trace element interactions have been described by surface complexation of metals with carbonate minerals (Zachara *et al.*, 1989; Brady *et al.*, 1999; Gómez del Río *et al.*, 2004; Lee *et al.*, 2006), co-precipitation of trace elements with dissolved carbonates (Rouff *et al.*, 2005) and sorption onto, and eventually into, the carbonate surfaces (Louise and Stipp, 1998; Schosseler *et al.*, 1999; Martin-Garin *et al.*, 2003). As a result of this adsorption and precipitation, the presence of carbonates have been reported to not only retard the advancement of the acid front, but also the movement of metals through soils and tailings (Al *et al.*, 2000; Johnson *et al.*, 2000; Elzahabi and Yong, 2001; de Matos *et al.*, 2001; Dorronsoro *et al.*, 2002; Jurjovec *et al.*, 2002).

1.4 Factors controlling the mobility of sulfate and heavy metals

The processes involved in the generation of acidity, through pyrite oxidation, and the subsequent immobilisation of metal cations through sorption, precipitation and reduction are summarised in Figure 1.5. This final section will briefly discuss precipitation and the environmental chemistry of heavy metals, which will help to explain the potential for metal immobilisation within an impoundment or within the surrounding soils.

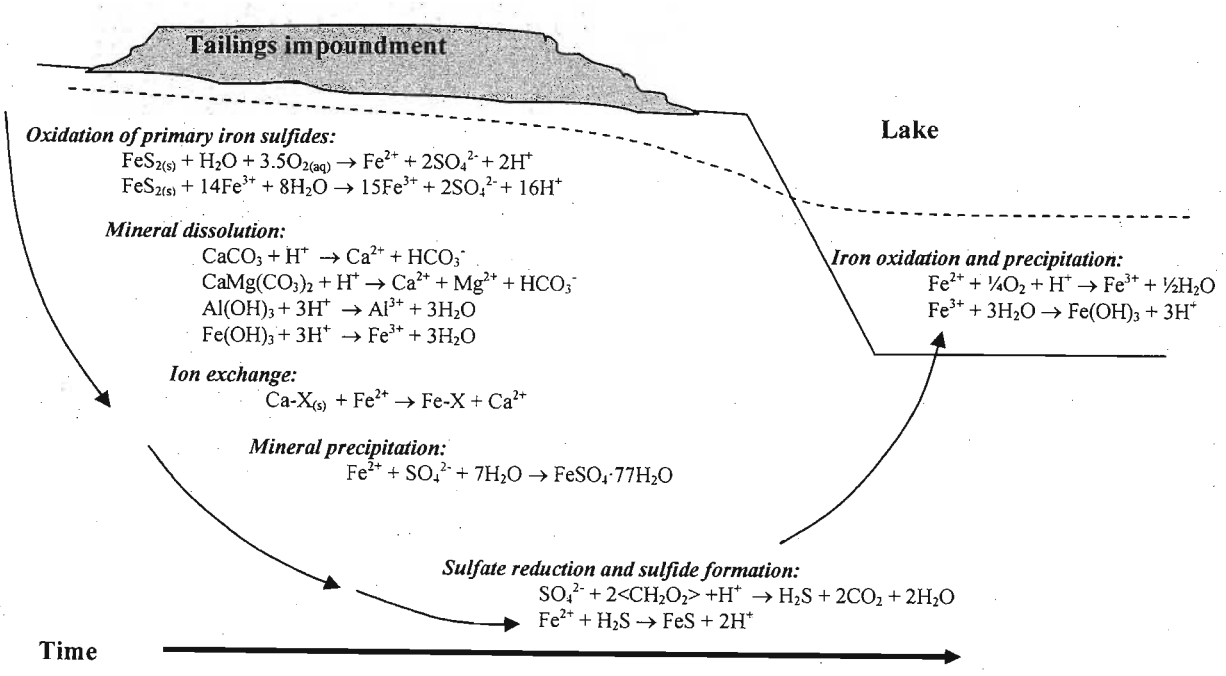

Figure 1.5 Diagrammatic representation of the processes involved in acidity, and metal generation and consumption in mine dumps and lakes (after Blodau, 2006).

1.4.1 Mineral precipitation

The precipitation of solid phases from the pore-water of abandoned mine tailings helps to retard the downward movement of SO_4^{2-} and metal cations (Lin, 1997; Johnson *et al.*, 2000; McGregor and Blowes, 2002; Gieré *et al.*, 2003). Precipitation of a particular solid phase occurs when the concentration of its constituent ions in solution are in excess of its solubility product (K_{sp}). The K_{sp} values can vary considerably within the same mineral type, depending on the level of substitution by other elements and its degree of crystallisation (high defect versus low defect).

The likelihood of a solid phase precipitating out of a solution can be predicted by comparing the ratio of the ion activity product (IAP) to the K_{sp} of the crystalline solid. The log of this ratio is known as the saturation index (SI), thus:

$$SI = \log IAP - \log K_{sp} \quad (1.4)$$

If the SI for a given solid is greater than 0 the system is said to be supersaturated and precipitation will occur. When equal to 0 the system is in equilibrium (i.e. the rate of dissolution equals the rate of precipitation). At values less than 0 the solution is regarded as being undersaturated and no precipitation will occur. A large number of precipitates can potentially form in tailings due to the diverse chemistry of these systems. Table 1.3 lists a number of minerals which have been reported to precipitate in tailings.

Table 1.3 Some examples of precipitation reactions reported to occur in mine tailings.

Mineral	*Reaction*	*Reference*
Goethite	$Fe^{3+} + 2H_2O \rightarrow FeOOH + 3H^+$	b; d; e; f
Iron hydroxide	$Fe^{3+} + 3H_2O \rightarrow Fe(OH)_3 + 3H^+$	a; b
Jarosite	$K^+ + 3Fe^{3+} + 2SO_4^{2-} + OH^- \rightarrow KFe_3(SO_4)_2(OH)_6$	b; d; e; f
Gypsum	$Ca^{2+} + SO_4^{2-} + 2H_2O \rightarrow CaSO_4 \cdot 2H_2O$	b; c; e; f
Siderite	$Fe^{2+} + HCO_3^- \rightarrow FeCO_3 + H^+$	b
Rhodochrosite	$Mn^{2+} + HCO_3^- \rightarrow MnCO_3 + H^+$	c
Anglesite	$Pb^{2+} + SO_4^{2-} \rightarrow PbSO_4$	c
Melanterite	$Fe^{2+} + SO_4^{2-} + 7H_2O \rightarrow FeSO_4 \cdot 7H_2O$	f

a: Lin (1997); b: McGregor *et al.* (1998); c: Al *et al.* (2000); d: Johnson *et al.* (2000); e: McGregor and Blowes (2002); f: Moncur *et al.* (2005)

As the pore-water becomes supersaturated with respect to certain solid phases, surface precipitates may begin to coat the surrounding minerals. This reduces their ability to adsorb trace metals and buffer pH changes (Booth *et al.*, 1997; Al *et al.*, 2000; Martin-Garin *et al.*, 2003; Cave and Talens-Alesson, 2005). Booth *et al.* (1997) demonstrated this by exposing polished calcite surfaces to a 0.1 *M* H_2SO_4 solution in a flow-through reactor. It was found that the rate of calcite dissolution decreased significantly, within 17 minutes, due to the formation of a protective gypsum ($CaSO_4 \cdot 2H_2O$) layer. Thus protective precipitate coverings might result in an acid front moving through tailings faster than would otherwise be expected.

A number of authors (e.g. Lin, 1997; Johnson *et al.*, 2000; McGregor and Blowes, 2002; Moncur *et al.*, 2005) have also reported on the formation of hardpans within abandoned tailings impoundments. These are horizontal layers of precipitated minerals which act to cement the tailings material, often limiting the penetration of oxygen and water to lower

layers. Hardpans commonly occur just below the zone of active oxidation, where dissolved concentrations of inorganic ions are highest. Thus, depending on the nature and extent of the precipitate, these hardpans may help to slow down the advancing oxidation front.

1.4.2 Factors controlling the mobility of heavy metals

Many authors have identified mining activities as being sources of significant contamination to plants, animals and humans (Palmer and Kucera, 1980; Gulson *et al.*, 1994; Manz and Castro, 1997; Milton *et al.*, 2002). It is therefore important to understand the factors which control metal mobility in these environments. Voegelin *et al.* (2003) state that the "environmental impact of heavy metal contaminants strongly depends on the metal's speciation, mobility, and bioavailability in soil." The bioavailability or toxicity of a metal contaminant is dependent on the pathway and rate of exposure, the chemical nature of the contaminant and the physiology of the organism under threat (Baksi, 1982; WHO, 2001). A contaminant only becomes bioavailable if it is mobile in the environment. McBride (1994) states that the mobility of heavy metals in soils are controlled by:

1. the chemical form and nature of the metal (the element's speciation);
2. the chemical and mineralogical properties of the soil; and
3. the prevailing hydrology.

These three factors apply equally to tailings which are also physically and chemically active. In order to understand and make predictions about heavy metal mobility in various settings, it is necessary to have a grasp of how these three aspects operate in the environment.

1.4.2.1 The chemical form and nature of the heavy metals

The availability of trace metals in soils and tailings is dependent in part on the valency of the heavy metal in association with its ionic radius. Figure 1.6 classifies a number of elements into four commonly recognised groups, based on variations in their ionic potential (ratio of valency to ionic radius). Elements from each group tend to behave in a characteristic way within soils and therefore their mobility also tends to differ. For example the availability of Fe^{2+} and Mn^{2+} (Group 2, Figure 1.6) will most likely be controlled by reversible sorption onto negatively charged colloidal material, whereas their

oxidised forms Fe^{3+} and Mn^{3+} (Group 3), are most likely to be immobilised through precipitation.

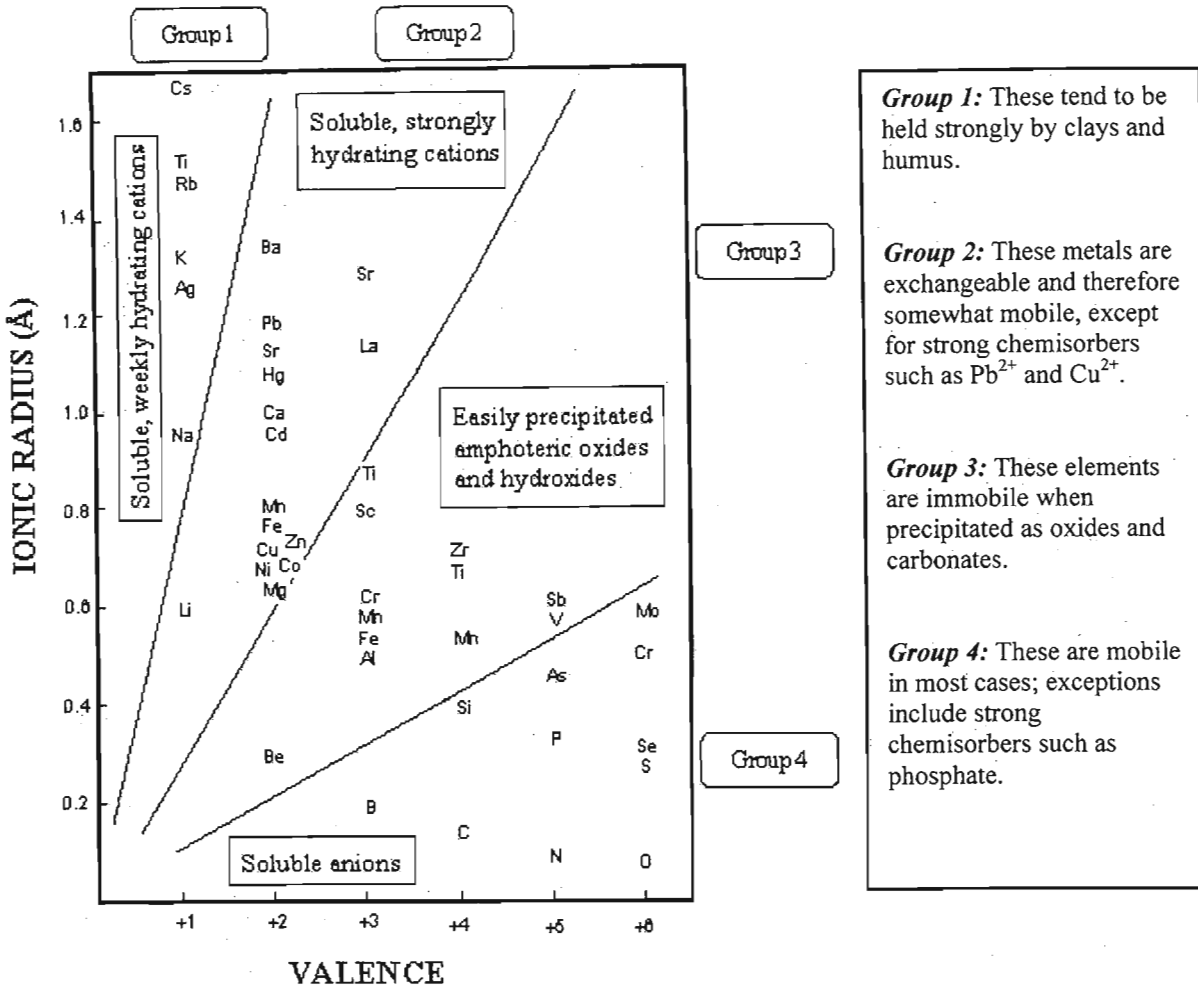

Figure 1.6 Classification of elements into four groups, based on valency and ionic radius, which give an indication of their general mobility in soils (McBride, 1994).

1.4.2.2 The mineralogical properties of the tailings

The mineralogical composition of a tailings impoundment plays a significant role in determining the overall mobility of heavy metals within it. The mineralogy of tailings can vary greatly from mine to mine, depending on the type of rock in which the metal sulfides were precipitated. Tailings typically consist of varying amounts of metal sulfides, metal oxides, carbonates and silicate minerals (see for example Blowes *et al.*, 1998; Al *et al.*, 2000; Moncur *et al.*, 2005; Salmon and Malmström, 2006). The different mineral phases which may play a role in controlling aqueous concentrations of metal cations are shown in

Figure 1.7. Soluble ion pairs (e.g. MoO_4^{2-}, BO_3^{3-}) or free ions (e.g. Pb^{2+}, Zn^{2+}) in the pore-water may be reversibly or irreversibly bound to aluminosilicate clays (Bradl, 2004; Bellir *et al.*, 2005; Potgieter *et al.*, 2006), metal oxides (Al-Abadleh and Grassian, 2003; Koschinsky *et al.*, 2003; Al-Abadleh *et al.*, 2005) and/or carbonate minerals (Bruno *et al.*, 1998; Brady, 1999; Al *et al.*, 2000; Lee *et al.*, 2006). If present in sufficient quantities these minerals may considerably reduce the mobility of trace metals in tailings. The degree of sorption, however, is also dependent on the chemical conditions within the tailings. If conditions are unfavourable metals may be released into solution from these minerals by desorption, oxidation and/or dissolution (Figure 1.7).

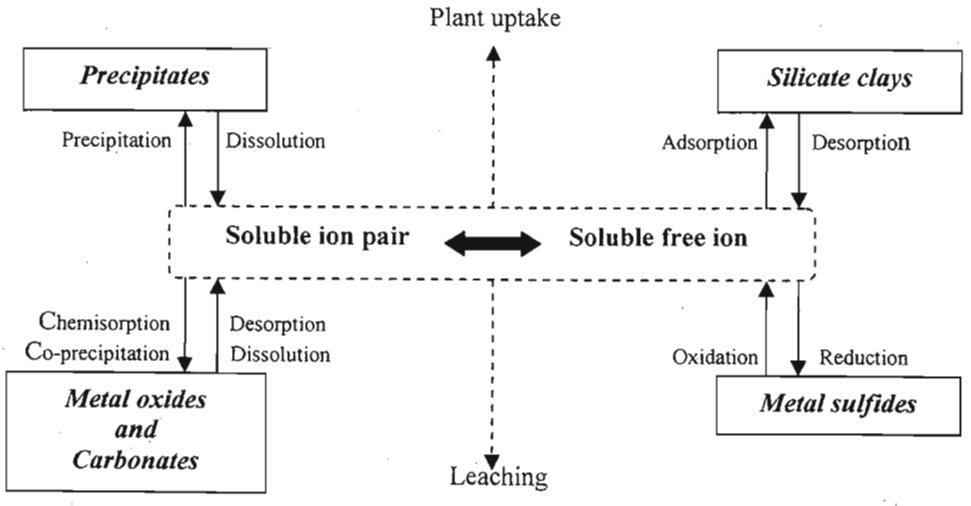

Figure 1.7 Dynamic interactive processes governing the availability of heavy metals and other ions for leaching and plant uptake from mine tailings (modified from McBride, 1994).

The two most important chemical parameters controlling metal ion availability, as demonstrated by the equilibrium between the solid and aqueous phases in Figure 1.7, are pH and E_h. These two variables are often referred to as the "master variables" in soil and play a significant role in controlling metal availability (McBride, 1994; Bradl, 2004).

1.4.2.3 The effect of pH on metal mobility

As previously discussed (Section 1.3), there are often dramatic variations in pH within abandoned sulfidic tailings. The availability of metals for leaching tends to vary in accordance with these changes in pH. There are two mechanisms by which pH affects the availability of trace metals:

1. By altering the surface charge of the colloidal material, and thus the adsorptive capacity of the tailings.
2. By controlling the dissolution and precipitation of metal containing minerals at low and high pH, respectively.

Under acidic conditions, such as those created by acid mine drainage, heavy metal mobility is greatly enhanced (Bain *et al.*, 2000; Shu *et al.*, 2001; Moncur *et al.*, 2005). As pH increases to above pH 5 or 6, cationic sorption begins to increase rapidly. This is due to the increasing negative charge associated with the surfaces of soil organic matter, metal oxides and clays (McBride, 1989; Alloway, 1990; Frimmel and Hube, 1996; Bradl, 2004; Al-Abadleh *et al.*, 2005). Higher pH (> 6) also tends to favour the co-precipitation of trace elements with hydroxides, carbonates and phosphates (Lindsay, 1979; Badawy *et al.*, 2002; Dorronsoro *et al.*, 2002; Rouff *et al.*, 2005; Saxena and D'Souza, 2006), which further contributes to the immobilisation of heavy metals under alkaline conditions. It is therefore generally accepted that the mobility of heavy metals in soils and tailings decreases with increasing pH (Gupta, 1992; Lin, 1997; Blowes *et al.*, 1998; Elzahabi and Yong, 2001; Al *et al.*, 2000; Hall *et al.*, 2001; Bradl, 2004).

Under acid conditions metal cations may be displaced from exchange sites by high concentrations of H^+ ions and other competing cations. Acidity also causes the solublisation of many minerals, which will cause physically bound elements to be released into solution (see Table 1.2).

1.4.2.4 Oxidation and reduction reactions

The substantial influence of redox potential on the speciation and mobility of different elements in soils has been widely described in the literature (Garrels and Christ, 1965; Brookins, 1988; Bartlett and James, 1993; McBride, 1994; Bartlett, 1999). Figure 1.8 shows the most common redox transformations that are likely to occur in soils at varying conditions of pH and E_h (McBride, 1994). The inclined lines represent the E_h at which the redox half-reactions of NO_3^-, Mn, Fe, N_2, SO_4^{2-}, and CO_2 are at equilibrium for a given pH. For a soil system undergoing reduction the oxidised elements on the left are reduced to the compounds on their right. The reverse is true for a system undergoing oxidation. Thus, for example, if a section of a tailing impoundment was highly reduced to an E_h below the

SO_4^{2-}/H_2S equilibrium line it would be expected that the metal sulfides would be stable. However, if a strong oxidant penetrated into the tailings, such as atmospheric oxygen, the redox potential of the tailings would rise. This would create an oxidising environment for the metal sulfides and the metals would consequently be released into solution.

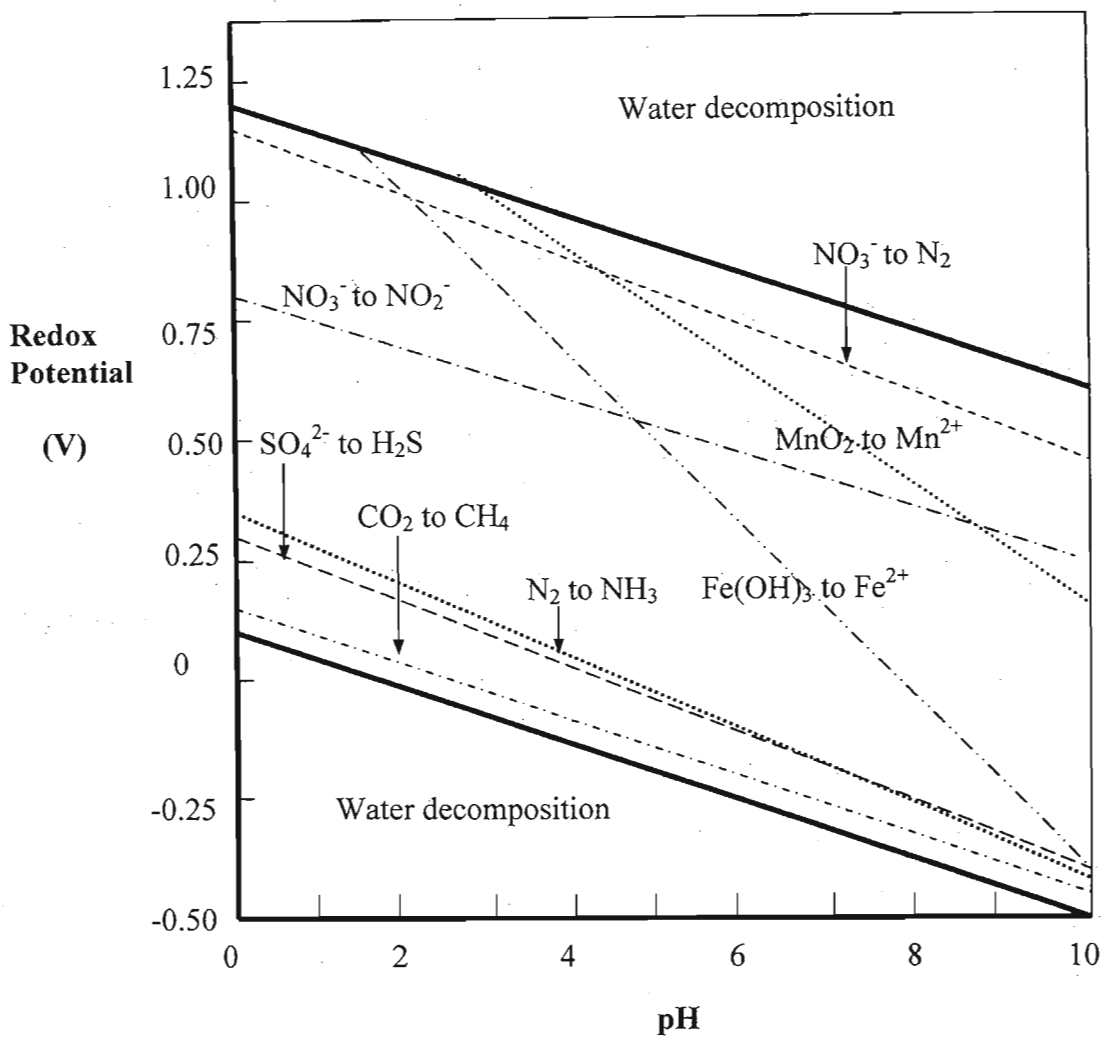

Figure 1.8 The relationship between redox potential (E_h) and pH for important half-cell reactions in water. The bold solid lines indicate the E_h at which water is oxidised to O_2 (upper line) or reduced to H_2 (lower line) (McBride, 1994).

Applying a surface cover of organic materials, clays, fly ash, or water films to old mine tailings is a technique which has been widely used to reduce oxygen diffusion into the tailings and thereby stabilise the sulfide minerals (Vigneault *et al.*, 2001; Romano *et al.*, 2003; Hallberg *et al.*, 2005). These treatments are only effective if they are able to reduce the tailings and elevate the pH sufficiently to inhibit the action of *Thiobacilli*, an acidiophilic bacteria species, which is most commonly responsible for sulfide oxidation.

As shown by Figure 1.8 there are a number of redox transformations which occur before sulfate becomes reduced. Thus, if large parts of the tailings impoundment are already above the SO_4^{2-}/H_2S line and if significant amounts of MnO_2, $Fe(OH)_3$, or FeOOH are present, a drop in the redox potential may be buffered by the reduction of these compounds, which would result in Mn^{2+} and Fe^{2+} being released into solution. It is therefore essential to examine the redox buffering capacity of oxidising tailings prior to using a remediation technology that aims to stabilise sulfide oxidation through reduction.

1.4.2.5 Prevailing hydrological parameters

The availability of an element for leaching in a tailings dam does not necessarily mean that it will migrate over any significant distance. However, with the movement of water through the profile, considerable migration may occur. In high rainfall regions, downward leaching will predominate while in arid environments the net movement of water may be upwards, due to high levels of surface evaporation. It is thus the mass-flow of water in a profile which determines the overall rate at which free ions can move. Therefore, in order to make predictions about the mobility of any given element in a tailings dam, it is necessary to describe both its availability within the tailings and the prevailing hydrological conditions.

1.5 Direction of study: a project outline

This chapter was aimed at providing a theoretical background to the factors which control the oxidation of metal sulfides and the subsequent leaching of contaminants from mine tailings. In order to quantify some of these factors and to better understand the potential for groundwater contamination at the Pering Mine, a number of laboratory experiments along with a detailed field investigation were undertaken. The approach used was similar to that of Xenidis *et al.* (2003) who provided a recent risk assessment of carbonate-rich mine tailings in Greece. An outline of the basic methods which were used in the current study and their sequence is presented in Figure 1.9. A chemical and mineralogical analysis is essential for any risk assessment and forms the foundation of assessing whether a waste possesses potential to cause contamination. The mineralogy also plays a significant role in determining buffering, sorption and precipitation reactions. If a waste is shown to have contaminating elements, such as heavy metals, it is then necessary to quantify what

fraction of the total elemental pool is potentially available to cause environmental contamination. This is typically done by means of batch and leaching column experiments, both of which were used in this study.

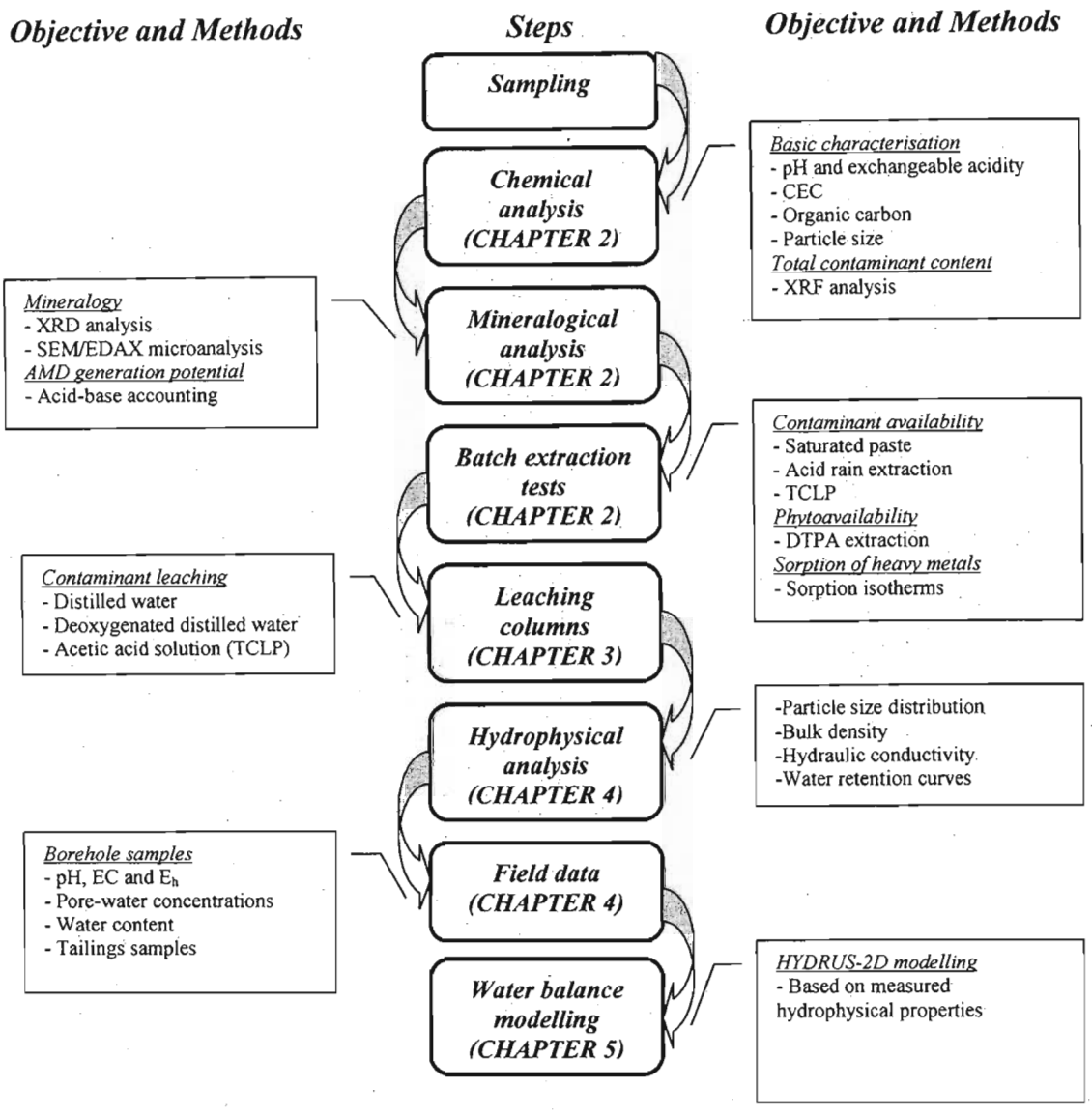

Figure 1.9 Sequential methodology used in this study for the environmental characterisation of Pering Mine's tailings impoundment. The relevant chapters in which each aspect is dealt with are also shown.

It was shown in this chapter how the stability of sulfide minerals depends on the prevailing chemical conditions within an impoundment. It was therefore necessary to determine the geochemical conditions within the Pering tailings impoundment. This forms the focus of Chapter 4, which also describes the hydrophysical properties of the tailings (Figure 1.9). The final chapter concludes by modelling the water balance of the tailings with the newly constructed retainer walls and rock cladding.

CHAPTER 2

CHEMICAL AND MINERALOGICAL CHARACTERISATION OF THE PERING MINE TAILINGS MATERIAL

2.1 Introduction

There is endless variation in the mineralogical and elemental composition of mine tailings across the world. This variation is the result of mining activities which extract a wide array of economic minerals from various ore bodies, which are embedded in different geological formations. The leaching of hazardous contaminants from abandoned tailings impoundments is very much dependent on this mineralogy. Tailings can contain anywhere from 0.5 to 60% sulfide minerals by mass (Bain *et al.*, 2000; Moncur *et al.*, 2005; Blodau, 2006). These metal sulfides undergo oxidation when brought into contact with the Earth's atmosphere and weathering cycles and consequently release heavy metals, sulfate and acidity into the pore-water of the tailings. The rate at which these potentially hazardous by-products will move through the tailings is in turn dependent on the degree to which the remaining minerals in the tailings are able to buffer acidity, and immobilise the heavy metals and sulfate through sorption and precipitation (McGregor *et al.*, 1998). Therefore the first requirement for any environmental assessment of mine tailings would be a detailed characterisation of the material's mineralogical and chemical properties (Xenidis *et al.*, 2003).

This chapter aims to characterise the Pering tailings and provide some initial predictions on the potential risk posed by the material. Interpretations will be based on the material's mineralogy, chemistry and a number of batch extractions which have been designed to estimate the potential for contaminant leaching.

2.2 Site description

Pering Mine is located approximately 18 km northeast of Reivilo in the North West Province of South Africa (Figure 2.1). During the 17 years of operation the ore was excavated from the two opencast pits (Figure 2.1). The overburden from the two pits was deposited onto the northern and southern rock piles. The recovered ore was taken to the milling plant, where it was finely milled before the lead and zinc sulfides, galena and

sphalerite, were separated off by froth flotation. After separation the tailings were siphoned off and deposited into the tailings dam, which now has a volume of approximately 12.5 million m^3 and a footprint area of about 522 000 m^2. These tailings overlie a Mispah soil (Soil Classification Working Group, 1991), which is underlain by fractured dolomite.

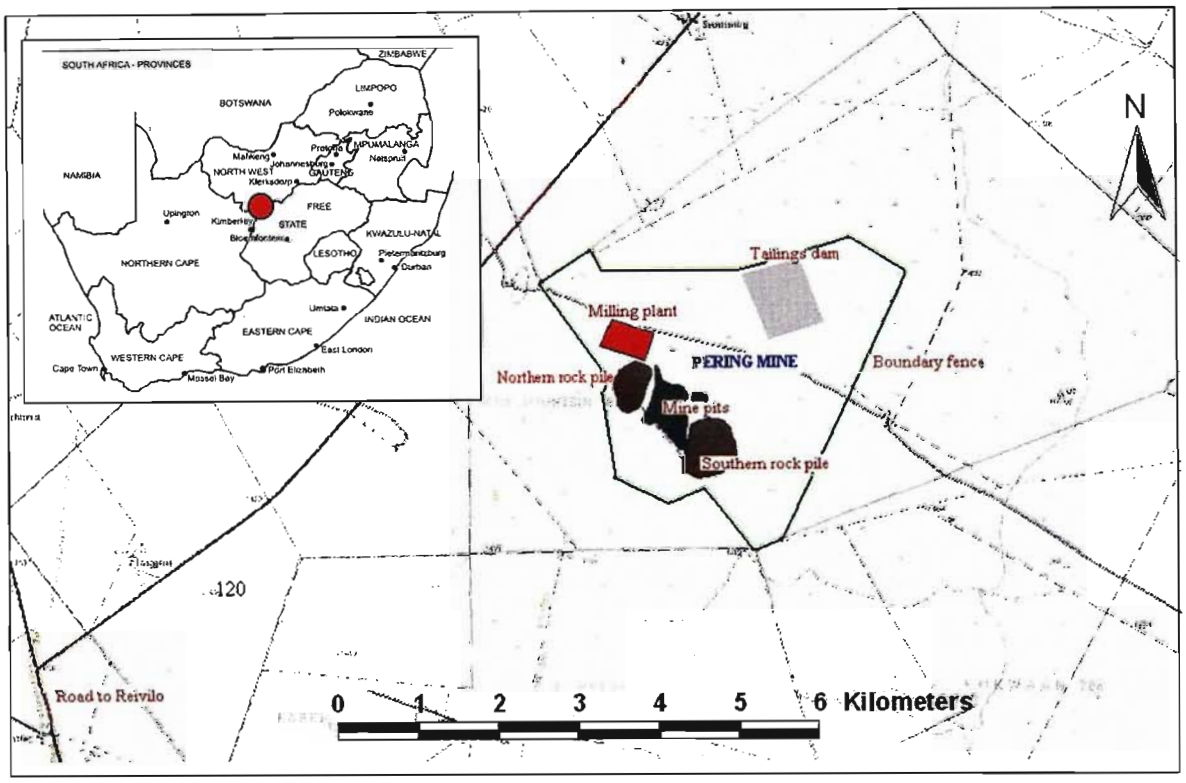

Figure 2.1 The general location of Pering Mine is shown by the red dot on the inset map (27°26′ South; 24°16′ East). The main image gives the layout of the mine, showing the location of the tailings dam (grey) and mine pits (black) as well as the milling plant (red) and the waste rock piles (brown).

Pering Mine is situated at an altitude of approximately 1400 m above mean sea level. The local topography is flat and sparsely vegetated. Low and Rebelo (1996) classified the vegetation of this area as Kalahari Plateau Bushveld (savanna biome), which is a dense bushveld composed of shrubs, trees and patches of mixed grassland. Prior to this, Acocks (1988) described this region as Kalahari Thornveld, sub-type Vryburg Shrub Bushveld (vegetation type 16b). The climate in the Reivilo region is classified as being arid, with a highly variable summer rainfall pattern. The mean annual precipitation is 413 mm, which tends to fall predominantly between February and April in the form of scattered thundershowers. Temperatures range from an average of 25 °C in January to 11 °C in June. However, temperatures often rise above 40 °C in summer and fall below 0 °C on winter nights. The mean annual potential evaporation (A-pan) for the region is reported to be

2100 mm (Land Type Survey Staff, 1986), which means that there is a significant water deficit.

2.3 Sample collection

Subsequent to mine closure in January 2003, two bulk samples were collected from the surface of the tailings impoundment. The first sample was collected during February 2004 and the second in August of the same year. During the initial visit tailings material was gathered from the side of the impoundment (TS sample), while during the second visit in August, material was collected from the top of the impoundment (TT sample). Prior to analysis the bulk samples were air-dried and well mixed.

2.4 Laboratory procedures

The TT sample was chosen for characterising the Pering tailings material as it was less weathered than the TS material which had been deposited a number of years earlier on the drier outer flanks of the impoundment.

2.4.1 General classification of the Pering tailings

The pH and electrical conductivity (EC) of the TT sample was measured in distilled water using a Radiometer PHM210 pH meter and a Radiometer CDM83 electrical conductivity meter. A solid to solution ratio of 1:2.5 was used (10 g of tailings to 25 m*l* of solution). The tailings and distilled water were stirred occasionally while being allowed to stand for approximately 45 minutes before measurements were taken. The pH was also measured in a 1 *M* KCl solution, at the same solid to solution ratio.

Extractable cations and cation exchange capacity (CEC) were measured by saturation with ammonium (NH_4^+) and subsequent exchange with potassium (K^+) at pH 7 (Soil Classification Working Group, 1991). The nitrate (NO_3^{2-}) and ammonium (NH_4^+) concentrations within the tailings were determined by extraction with 2 *M* KCl (Maynard and Kalra, 1993), with the concentrations of the extracted solutions being analysed colorimetrically using a TRAACS 2000 continuous flow auto analyser. Extraction with AMBIC (ammonium bicarbonate) solution was used to approximate plant available

phosphorus, the concentration of which was determined colorimetrically (The Non-Affiliated Soil Analysis Work Committee, 1990) on a Varian Cary 1E UV-Visible spectrophotometer (UV-Vis). Exchangeable acidity and exchangeable aluminium were measured by the method of Sims (1996), with the aluminium concentrations being measured by atomic absorption spectrophotometry (AAS, Varian SpectraAA-200). The acid neutralising capacity of the material, as a percentage of $CaCO_3$, was measured by back titration according to the method given by Jackson (1958). Organic carbon was determined titrimetrically after potassium dichromate oxidation (Walkley, 1947). All procedures were done in triplicate.

The particle size distribution of the TT sample was determined by an adapted version of the Gee and Bauder (1986) pipette method (see Appendix 5).

2.4.2 Mineralogy and total elemental composition

The mineralogy of the TT material was determined by X-ray diffraction (XRD). Analyses were done on randomly oriented powder samples using a Phillips PW1050 diffractometer, with monochromated Co Kα radiation from 3° to 75° 2θ with a scanning step of 0.02° at 1° per minute counting interval. The diffraction data were captured by a Sietronics 122D automated micro-processor attached to the X-ray diffractometer. Samples were then qualitatively analysed to determine major mineralogical components. The total elemental composition of the TS and TT samples was determined by X-ray fluorescence spectrometry (XRF, School of Geological Sciences, University of KwaZulu-Natal, Durban).

2.4.3 Metal extractability

An estimate of the concentrations of metals available for leaching or plant uptake was assessed by a number of methods. Plant available concentrations of Cd, Cr, Cu, Fe, Pb, Mn, Ni and Zn were determined by DTPA extraction (Liang and Karamanos, 1993). The DTPA solution was prepared by dissolving 149.20 g of TEA, 19.67 g of DTPA and 14.70 g of $CaCl_2 \cdot H_2O$ in approximately 200 m*l* of distilled water. This solution was then diluted to 9 *l* and the pH adjusted to 7.30 ±0.05 with 1:1 HCl before final dilution to 10 *l*. The extraction consisted of adding a 25 m*l* aliquot of DTPA solution to 5 g of tailings in a

plastic centrifuge tube and shaking on a horizontal shaker for 2 hours at 150 strokes min^{-1}. Samples were then centrifuged at 2500 rpm for 5 minutes and filtered through Whatman No. 42 filter paper. The supernatant liquid was analysed for the above metals by AAS (Varian SpectraAA-200).

The concentration of elements which may potentially be leached from the tailings material was also assessed by the toxicity characterisation leaching procedure (TCLP) and an acid rain extraction (DWAF, 2005). The TCLP solution was made up by adding 5.7 m*l* of glacial acetic acid to 1 *l* of distilled water to give a final pH of 2.88 ±0.05. The acid rain solution was made up by bubbling CO_2 gas through distilled water to create a saturated carbonic acid solution. The pH of the solution was then decreased to pH 3.80 by the addition of HNO_3. For both the TCLP and acid rain extractions 400 m*l* of the respective solutions were added to 20 g of tailings and shaken at 30 rpm for 20 hours in an incubation oven set at 23 °C (analyses were all done in triplicate). The solutions were then filtered through Whatman No. 42 filter paper and analysed for Ca, Cd, Co, Cr, Cu, Fe, K, Mg, Mn, Na, Ni, Pb and Zn by AAS (Varian SpectraAA-200).

The water soluble fraction of the tailings was determined by a saturated paste extract (Soil Salinity Laboratory Staff, 1954). The extracted solution was analysed for Al, Ba, Ca, Cd, Co, Cr, Cu, Fe, Hg, K, Mg, Mn, Na, Ni, P, Pb, S, Se, Sr, V and Zn by inductively coupled spectrophotometry (ICP, Varian Liberty X150). Nitrogen in the solution was determined by the ammonia probe method.

2.4.4 Metal sorption isotherms

The metal sorbing capacity of the TT sample was determined by accurately weighing 1 g of tailings material into each of eleven centrifuge tubes. Zinc stock solutions were made up in distilled water, from zinc chloride ($ZnCl_2$), to have concentrations of 0, 2, 4, 8, 16, 32, 64, 125, 250, 500 and 1000 mg l^{-1}. Twenty-five millilitres of a given stock solution was added to each pre-weighed sample, and shaken for 24 hours on an end-over-end shaker. Following this, the samples were centrifuged at 3000 rpm for 5 minutes and the supernatant liquid filtered through Whatman No. 42 filter paper. Equilibrium Zn concentrations were then measured by AAS (Varian SpectraAA-200). This procedure was

done in triplicate. Sorption isotherms for the metals Pb, Cu and Ni were also undertaken, using $PbCl_2$, $CuCl_2.2H_2O$ and $NiCl_2.6H_2O$ salts, respectively.

2.5 Results and discussion

2.5.1 General classification of the Pering Mine tailings material

The ore at Pering Mine was excavated from a dolomite deposit (du Toit, 1998) and as a consequence the tailings are rich in carbonate minerals. This has resulted in the waste having a high acid buffering capacity and a slightly alkaline pH of 7.85 (Table 2.1). The relative neutralising capacity, in relation to pure calcite ($CaCO_3$), of the tailings was calculated to be 56.39%[1]. It is widely accepted that the presence of carbonate minerals in tailings plays a significant role in mitigating the effects of acid mine drainage and reducing heavy metal mobility (Blowes *et al.*, 1998; Al *et al.*, 2000; Banwart and Malmström, 2001; Shu *et al.*, 2001). The presence of dolomite in the Pering tailings is therefore highly beneficial and will most likely help to minimise contamination.

Table 2.1 Basic physico-chemical properties of the Pering tailings material.

pH	H_2O	7.85
	1 *M* KCl	8.83
Electrical conductivity (EC)	mS m^{-1}	366
Organic carbon	%	0.49
AMBIC P	mg kg^{-1}	2.03
NH_4^+	mg kg^{-1}	6.78
NO_3^{2-}	mg kg^{-1}	2.37
Total N	%	0.0006
Base cations $cmol_+ kg^{-1}$	Ca	4.00
	Mg	1.75
	Na	0.04
	K	0.02
Cation exchange capacity	$cmol_+ kg^{-1}$	2.26
Exchangeable acidity	$cmol_+ kg^{-1}$	0.01
Exchangeable aluminium	$cmol_+ kg^{-1}$	bd
Calcium carbonate equivalence	%	56.4
Particle size analysis mass %	clay	1.88
	silt	13.4
	very fine sand	21.9
	fine sand	57.4
	medium sand	5.35
	coarse sand	0.05

bd: below detection

[1] Given the large amount of dolomite this value appears low. It is speculated that this was due to the formation of secondary coatings which protected the dolomite from acid attack (see Booth *et al.*, 1997).

The cation exchange capacity (CEC) of the tailings was low at 2.26 $cmol_+ kg^{-1}$. This may be partly due to the coarseness of the material, which limits surface area for sorption. Particle size analysis of the TT sample found that it fitted the standard classification of a loamy sand, with the sand fraction further classified as a fine sand (Soil Classification Working Group, 1991). Based on the chemical properties alone, ignoring factors such as the arid climate, the ability of the tailings to support plant life appears limited. This is evident from the low CEC, high EC (366 mS m^{-1}) and the low levels of plant available nitrogen (6.78 mg kg^{-1} as NH_4^+ and 2.37 mg kg^{-1} as NO_3^{2-}) and phosphorus (2.03 mg kg^{-1}).

Total organic carbon in the tailings was measured at 0.49%, which is similar to that reported for other unvegetated Pb/Zn mine tailings (Shu *et al.*, 2002; Ye *et al.*, 2002). The presence of organic matter in these instances is surprising, because unlike soils where natural processes add organic matter, tailings are derived from inorganic origins. Thus the presence of organic carbon would have to have occurred by some other means. The most likely explanation for this, in the case of Pering Mine, is the use of organic dispersants in the froth flotation process (Cowey, 1998). This would also explain the observation of an oily blackish- brown layer found floating on the tailings/water solution while measuring the pH of borehole samples (see Chapter 4). In certain instances, the presence of organic fractions has been reported to increase the mobility of heavy metals (McBride, 1989; McBride 1994; Almås *et al.*, 1999; Shuman, 1999). Thus, enhanced metal mobility could result, if the assumption that organics have been added to the tailings is correct. The effects of this potential risk would require further investigation.

2.5.2 Mineralogy and total elemental composition

X-ray diffraction (XRD) analysis of ground tailings taken from the side (TS sample) and the top of the tailings impoundment (TT sample) showed that the material consisted predominantly of dolomite ($CaMg(CO_3)_2$), with traces of quartz (SiO_2), potassium feldspar ($(K,Al)_2SiO_4$), pyrite (FeS_2) and sphalerite (ZnS). The total elemental composition of these two samples was determined by XRF analysis. The more recently deposited TT material was found to have higher concentrations of all heavy metals, other than Fe, which would suggest that it has undergone less weathering (Table 2.2).

The presence of pyrite and sphalerite account for the high concentrations of Fe (19083 mg kg^{-1}), Zn (5481 mg kg^{-1}) and S (15400 mg kg^{-1}) measured in the TT material (Table 2.2). The presence of Cu (22.6 mg kg^{-1}) and Pb (398 mg kg^{-1}) may also be an indication that small amounts of chalcopyrite and galena are present in the tailings. This is very probable as these sulfide minerals are known to have been present in the ore (du Toit, 1998). Observations of the tailings with a scanning electron microscope (SEM), fitted with EDAX, identified all of the aforementioned sulfide minerals, except for chalcopyrite (Appendix 1). During these observations pyrite was the most frequently identified metal sulfide, followed by sphalerite and then galena. This sequence follows the total concentrations of Fe, Zn and Pb recorded in the material.

Table 2.2 XRF analyses (mg kg^{-1}) of the TT and TS bulk samples.

Sample	*Al*	*As*	*Ba*	*Ca*	*Ce*	*Cr*	*Cu*	*Na*
TT	9152	109	11.5	354712	0	3.6	22.6	3116
TS	7829	85	0.8	356571	3	2.8	6.2	1929
	Fe	*Ga*	*K*	*La*	*Mg*	*Mn*	*Nb*	*Nd*
TT	19083	5	8051	0	194528	29102	0	0
TS	28170	2	6308	0	196397	28328	0	0
	Ni	*P*	*Pb*	*Rb*	*S*	*Sc*	*Si*	*Sn*
TT	0.1	87.2	398	8.80	15400	0.5	28113	0
TS	4.4	87.2	311	8.00	18564	0.3	22743	0
	Sr	*Th*	*Ti*	*U*	*V*	*Y*	*Zn*	*Zr*
TT	15.0	6.5	689	0	11.8	2.2	5481	7.2
TS	17.2	3.9	325	0	5.5	0.8	2170	5.3

From the total recorded concentrations of Fe, Zn and Pb, assuming that these elements were contained exclusively within sulfide minerals, it is possible to calculate the approximate sulfide content of the tailings. Based on the measured mass of each element in the tailings (Table 2.2) and the molar mass of the individual sulfide minerals, the TT material was calculated to have a total sulfide content of 49.62 g per kilogram of tailings. Of this 79.94% was present as FeS_2, 19.61% as ZnS and 0.45% as PbS. In the TS material the total sulfide content was calculated to be 64.11 g per kilogram of tailings, of which FeS_2 comprised 93.57%, ZnS 6.15% and PbS 0.28%.

It is also possible to estimate the sulfide load of the tailings from the total S content of the material, assuming that all S is either contained in the sulfide form or at least originated

from the oxidation of sulfide minerals. The TT sample contained 15400 mg of S kg^{-1} of tailings and the TS sample 18564 mg kg^{-1} (Table 2.2). Assuming that all S was contained as FeS_2 the TT and TS samples would have an equivalent pyrite content of 28.8 g kg^{-1} and 34.7 g kg^{-1}, respectively. If galena and sphalerite had to be included in this composition the sulfide content would be marginally higher, due to the higher molar mass of Pb and Zn. Calculating the sulfide content of the tailings from the total S gives a value less than that reported in the calculations, in which the total Fe, Zn and Pb concentrations were used. Discrepancies between the different values are most likely the result of preferential leaching of S, which would have resulted in an underestimation of the sulfide content in the second set of calculations. The two methods combined provide the safest approximation of the total sulfide content within the tailings. A range of 2.88 to 6.41% (by mass) can therefore be expected, which is well within the range reported in the literature (e.g. Blowes *et al.*, 1998; McGregor *et al.*, 1998; Bain *et al.*, 2000).

Total concentrations of Pb and Zn in the tailings of abandoned Pb/Zn mines vary hugely. For Zn, concentrations have been reported to range between 1583 and 36500 mg kg^{-1}, and for Pb between 1042 and 34300 mg kg^{-1} (Sidle *et al.*, 1991; Lan *et al.*, 1998; Ye *et al.*, 2000; Shu *et al.*, 2001; Shu *et al.*, 2002; Ye *et al.*, 2002; Romero *et al.*, 2005). In relation to the values reported by these authors the total Zn concentration (5481 mg kg^{-1}) in the Pering tailings is moderate to high, while that of Pb (398 mg kg^{-1}) is low. In addition to Fe, Pb, Zn and Cu, the TT tailings contained a number of other metals. These include As (109 mg kg^{-1}), Cr (3.6 mg kg^{-1}), Mn (29102 mg kg^{-1}), Sr (6.5 mg kg^{-1}), Ti (689 mg kg^{-1}), V (11.8 mg kg^{-1}) and Zr (7.2 mg kg^{-1}). Some of these elements are potentially toxic (DWAF, 1996a; WHO, 2004) and can therefore cause groundwater contamination if released in sufficient quantities from the tailings.

2.5.3 Element availability

There is generally a very poor relationship reported between total element concentrations in soils and wastes, and concentrations which are considered mobile or bioavailable (Gupta *et al.*, 1996; Milton *et al.*, 2002). For this reason, a number of standardised extraction procedures have been developed, which aim to approximate the release or availability of heavy metals from wastes. The least aggressive of these extractions is a measure of the element concentrations released by dissolution under saturated conditions. This method

would theoretically represent element availability under neutral environmental conditions as could be expected after rainfall. The soluble fraction of a wide range of elements in the tailings, as determined by the saturated paste method (Soil Salinity Laboratory Staff, 1954), is given in Table 2.3. The soluble concentrations of most heavy metals were very low and, as would be expected, significantly less than total concentrations (Table 2.2). In terms of South African drinking water guidelines (SABS 241, 1999; DWAF, 1996a) and leaching limits for hazardous waste (DWAF, 2005) concentrations of Ca (520 mg l^{-1}), Mg (341 mg l^{-1}), S (915 mg l^{-1}) and Mn (0.92 mg l^{-1}) released from the tailings were all well over recommended limits (Appendix 2). Thus, even under very neutral conditions the Pering tailings material could potentially cause groundwater contamination.

Table 2.3 Results from a saturated paste extraction of the Pering tailings (TT) material.

Element	*Saturated Paste*	
	mg l^{-1}	*mg* kg^{-1}
Al	0.01	0.04
Ba	0.06	0.26
Ca	520	2252
Cd	bd	bd
Co	bd	bd
Cr	0.01	0.04
Cu	0.04	0.17
Fe	0.01	0.04
Hg	bd	bd
K	27.1	117
Mg	341	1477
Mn	0.92	3.99
N	4.38	18.9
Na	26.6	115
Ni	0.60	2.60
P	0.04	0.17
Pb	bd	bd
S	915	3963
Se	0.02	0.09
Sr	0.38	1.65
V	bd	bd
Zn	1.73	7.49
pH	8.09	
EC	356 mS m^{-1}	
Water content	0.23 kg kg^{-1}	

bd: below detection

The above mentioned extraction is generally not considered severe enough to be used in environmental risk assessments where the release of contaminants under a 'worst case scenario' provides a safer estimate of potential contamination. It is difficult to foresee

exactly what would constitute a worst case scenario for Pering Mine over an indefinite period of time. The most probable future risks could include the slow onset of acid rain as air pollution increases and the development of acidity as a result of sulfide oxidation. As a hypothetical assessment two generalised methods were chosen to simulate these conditions, the internationally recognised toxicity characteristic leaching procedure and the acid rain extraction method. Both methods were developed by the United States Environmental Protection Agency and have subsequently been accepted by the South African Department of Water Affairs and Forestry to be the best generalised methods for assessing the toxicity leaching characteristics of waste materials (DWAF, 2005). Because these methods are aimed at simulating waste leaching it is required that their concentrations be given in mg l^{-1} (DWAF, 2005). However, in order to make comparisons between the methods used here, element concentrations have also been reported on a mass basis i.e. mg of element extracted per kilogram of tailings (Table 2.4).

The TCLP is more aggressive than the acid rain extraction as it was developed to simulate leaching under conditions of co-disposal in landfill sites where leaching with organic acids is assumed (DWAF, 2005). High concentrations of Zn (1873 mg kg^{-1}), Mn (1197 mg kg^{-1}) and Pb (249 mg kg^{-1}) were extracted by this method (Table 2.4; Appendix 3). Most mine wastes are mono-disposed and thus are not exposed to organic leachates, but more likely to conditions of acid rain (DWAF, 2005). The acid rain extraction method provided a more conservative estimate of metal release from the tailings. The concentrations of Zn, Mn and Pb extracted by this method were 537 mg kg^{-1}, 4.07 mg kg^{-1} and 23.7 mg kg^{-1}, respectively. Contrary to what would be expected, the concentrations of Ca (592 mg kg^{-1}) and Mg (136 mg kg^{-1}) were substantially lower than the saturated paste. This is attributed to the CO_2 saturated water which is thought to have stabilised the dolomite.

When classifying Pb/Zn mine tailings, many authors have reported on both the total and DTPA extractable concentrations of heavy metals (Sidle *et al.*, 1991; Lan *et al.*, 1998; Ye *et al.*, 2000; Shu *et al.*, 2001; Shu *et al.*, 2002; Ye *et al.*, 2002; Romero *et al.*, 2005). The latter are typically significantly lower and are thought to provide a good approximation of plant available concnetrations. In comparison to the aforementioned studies on Pb/Zn tailings, very high concentrations of DTPA extractable Zn (1056 mg kg^{-1}) and moderate concentrations of Pb (27.3 mg kg^{-1}) and Cu (6.01 mg kg^{-1}) were extracted from the TT sample. At these concentrations, in conjunction with the poor nutrient status, it is likely

that plant growth in the tailings will be severely restricted (Shu *et al.*, 2002; Ye *et al.*, 2002).

Table 2.4 TCLP, acid rain and DTPA extractions of the Pering tailings material.

Element	*TCLP* [1]		*Acid Rain* [2]		*DTPA* [3]
	mg l^{-1}	*mg kg^{-1}*	*mg l^{-1}*	*mg kg^{-1}*	*mg kg^{-1}*
Ca	538	10751	29.6	592	nd
Cd	bd	bd	0.13	2.51	bd
Co	0.01	0.24	0.01	0.26	nd
Cr	bd	bd	bd	bd	bd
Cu	1.00	20.1	0.01	0.11	6.01
Fe	5.45	108.9	0.04	0.79	2.66
K	0.41	8.26	0.09	1.73	nd
Mg	293	5858	6.81	136	nd
Mn	59.9	1197	1.18	23.7	4.07
Na	nd	nd	1.06	21.2	nd
Ni	0.06	1.22	0.03	0.51	0.06
Pb	12.5	249	0.19	3.82	27.3
Zn	93.6	1873	26.9	537	1056
pH	5.11		7.00		

bd: below detection
nd: not determined
1: TCLP-2 solution - 5.7 m*l* of acetic acid in 1 *l* of distilled water, pH 2.88 ±0.05 (DWAF, 2005)
2: saturated solution of carbonic acid, pH 3.8 (DWAF, 2005)
3: DTPA-TEA at pH 7.3 (Liang and Karamanos, 1993)

Due to the severe toxicity effects of many heavy metals, relatively low concentrations can cause a water body to become contaminated (DWAF, 1996a; 1996b; WHO, 2004). Thus, even a marginal mobilisation of the total reserve of heavy metals in the tailings may cause severe problems. The batch extractions reported here provide insight into what elements pose the greatest risk and help to quantify potentially available concentrations. According to the above batch extractions the general availability of heavy metals in the tailings follows the order Zn>> Mn > Pb > Cu > Fe > Ni. With respect to South African regulatory guidelines, concentrations of Mg, Mn, Pb and Zn reported in Table 2.4 were all above guideline limits (Appendix 2). Thus, it must be assumed that high concentrations of these elements may potentially be mobilised from the tailings impoundment and may therefore be available to cause groundwater contamination.

2.5.4 Sorption of lead, zinc, copper and nickel

Sorption isotherms provide a means whereby the metal sorbing capacity of soils or tailings can be assessed and mathematically described. Many models which aim to simulate solute

movement through porous media use sorption isotherms to describe the interaction of a solute with the solid phase (Toride *et al.*, 1999; Šimůnek *et al.*, 1999; Hutson, 2001). The sorption characteristics of Zn, Pb, Cu and Ni, can be seen in Figure 2.2 (Appendix 3). In this figure the amount of solute sorbed onto the tailings (S) is related to the equilibrium concentration (C) of the solute in solution. The sorption of Zn and Cu were best described by the Langmuir isotherm (Travis and Etnier, 1981). The sorption isotherm for Zn was defined by $C/S = 0.0001C + 0.0074$ ($R^2 = 0.811$) and Cu sorption followed the trend $C/S = 7\times10^{-5}C + 5\times10^{-5}$ ($R^2 = 0.853$). Lead and Ni followed the Freundlich type sorption pattern (Travis and Etnier, 1981), with their respective sorption curves being defined by $\log S = 0.711\log C + 3.363$ ($R^2 = 0.976$) and $\log S = 0.679\log C + 1.779$ ($R^2 = 0.889$).

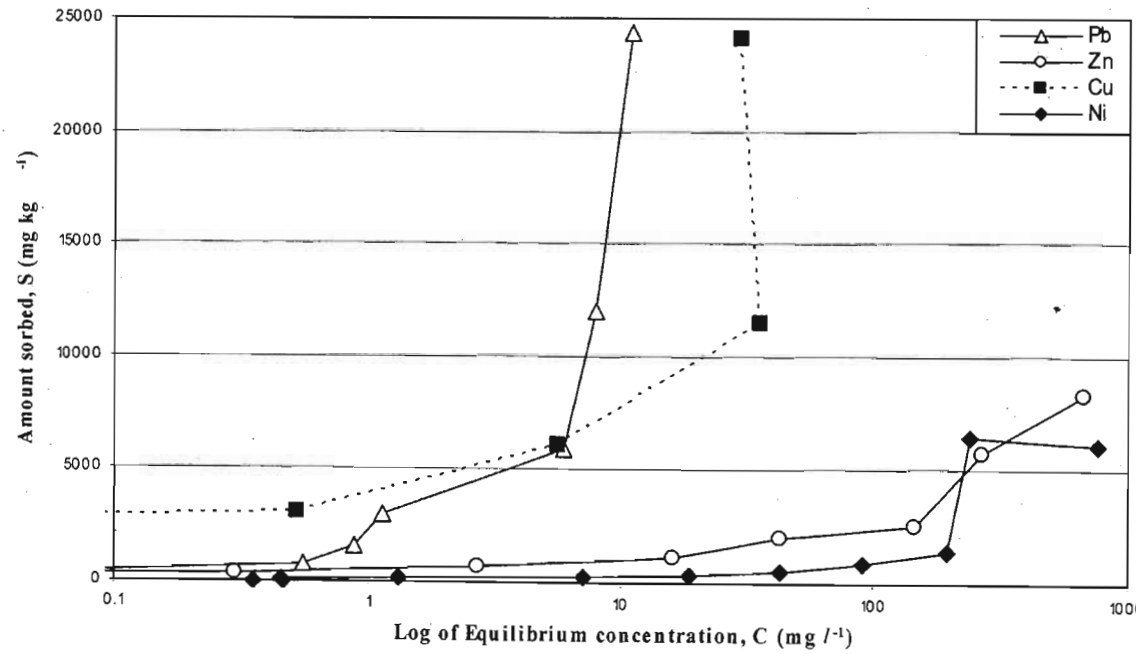

Figure 2.2 Sorption of Pb, Zn, Cu and Ni onto the Pering tailings (TT) material.

Despite the low CEC of the Pering tailings (2.26 $cmol_+ kg^{-1}$), its metal sorbing capacity was pronounced. Immobilisation was most likely the result of sorption onto the dolomite particles and possible precipitation, especially at higher concentrations (Louise and Stipp, 1998; Schosseler *et al.*, 1999; Al *et al.*, 2000; Martin-Garin *et al.*, 2003; Rouff *et al.*, 2005). Sorption of Pb and Cu was exceptionally high with no plateau being reached for these elements in the sorption experiments (Figure 2.2). This suggests that Pb and Cu movement through the tailings will be greatly retarded. Sorption of Zn and Ni increased slowly with increasing equilibrium concentration. A sudden increase in Zn and Ni sorption

was observed at about 150 mg l^{-1} and 200 mg l^{-1} respectively, most likely as the result of secondary oxy/hydroxide precipitation and not due to direct sorption. From this it appears that the mobility of these metals in the tailings will follow the decreasing order of Ni > Zn > Cu > Pb.

Based on the above sorption isotherms it is evident that the Pering tailings material has a marked ability to remove metal cations from solution. Thus, it can be expected that the release of metals from the impoundment will be greatly retarded, especially in the case of Pb and Cu.

2.5.5 Mineralogical prediction of acid mine drainage

Geochemical static tests, such as acid-base accounting (ABA) and the net acid generation (NAG) methods, are commonly used to predict the acid producing potential of mine wastes (Ferguson and Erickson, 1988; Shu *et al.*, 2001; Lei and Watkins, 2005). In many mines throughout the world, the acid producing potential of tailings exceeds its acid neutralising capacity. In such instances, where the buffering capacity is low, it may take only a few years before acid mine drainage begins to occur (Lei and Watkins, 2005), together with its consequent impacts (Aucamp and van Schalkwyk, 2003; Heyden and New, 2004; España *et al.*, 2005; Moncur *et al.*, 2005). As a result, a measure of the acid producing and neutralising potential of mine tailings provides a very important preliminary assessment for predicting the possible onset of acid mine drainage.

Different forms of pyrite react at different rates (Vaughan *et al.*, 1997; Rimstidt and Vaughan, 2003) and thus have varying acid producing potentials. The NAG method accounts for this variation in sulfide reactivity by measuring the net acid production directly from sulfide oxidation with H_2O_2. The ABA method, however, calculates the acid producing potential from the total measured sulfur in the tailings, which is assumed to react completely to form a stoichiometrically equivalent amount of acid. This method also assumes that all sulfur is contained as pyrite or some other sulfide mineral and not as sulfate or organic sulfur. The NAG method has been reported to provide more conservative, and possibly more realistic, estimates of the acid producing and neutralising capacities of tailings in comparison to the ABA method (Shu *et al.*, 2001). However, the

latter gives a better indication of the worst case scenario of acid production. Based on this, it was chosen for assessing the Pering tailings material.

It can be assumed that 2 moles of S per kilogram of tailings material will correspond to 1 mole of pyrite (as FeS_2), the oxidation of which will stoichiometrically release 2 moles of H^+ ions according to the equation:

$$FeS_{2(s)} + H_2O + 3.5O_{2(aq)} \rightarrow Fe^{2+} + 2SO_4^{2-} + 2H^+ \quad (2.1)$$

The degree of acid neutralisation is dependent on the acid neutralising capacity of the tailings. This neutralising capacity can be quantitatively determined in the laboratory by back titration (e.g. Jackson, 1958; Costigan *et al.*, 1981; Shu *et al.*, 2001) and is given as an equivalence to $CaCO_3$ i.e. the material's percentage effectiveness in neutralising acid in comparison to pure $CaCO_3$. The neutralisation of acidity by $CaCO_3$ at pH > 6 is given by:

$$CaCO_3 + 2H^+ \rightarrow Ca^{2+} + CO_{2(g)} + H_2O \quad (2.2)$$

From this it follows that 2 moles of H^+ ions will dissolve 1 mole of $CaCO_3$. Thus, overall, the acidity produced by the oxidation of 1 mole of sulfide sulfur will require 1 mole of pure $CaCO_3$ to be neutralised. If this neutralising potential is not available acid mine drainage will inevitably occur.

Total element analysis showed that the TT bulk sample had a total S content of 0.48 moles per kilogram of tailings. Assuming that all this sulfur is contained in the sulfide form and that it is completely reacted according to Equation 2.1, the release of 0.48 moles of H^+ ions per kilogram of tailings could be expected. This would require 0.24 mols of $CaCO_3$ to be neutralised according to Equation 2.2. The neutralising potential of the Pering tailings greatly exceeds this as the material has an effective neutralising capacity of 563.90 g of $CaCO_3$ per kilogram of tailings or 5.63 mols per kilogram (Table 2.1). From this it can be seen that the acid neutralising capacity of the tailings significantly exceeds the acid producing potential of the waste. Thus even after extended oxidation low pH waters will not be released from the Pering Mine tailings impoundment. Ferguson and Erickson (1988) describe this kind of situation as one in which the leachate will be characterised by both a high sulfate content and a high pH, a scenario which is quite different to the majority of mines where drainage waters are commonly acidic. Therefore, it can be expected that the negative effects of acidification will be mitigated at Pering but the remaining by-products

of sulfide oxidation (i.e. sulfate and metal cations) may still pose a risk to the local environment.

2.6 Conclusions

The Pering tailings material consists predominantly of dolomite and has an alkaline pH, a high buffering capacity and a low nutrient status. Within this dolomitic matrix, traces of pyrite, galena and sphalerite were identified. Based on the total recorded concentrations of S, Fe, Pb and Zn in the material it was calculated that metal sulfides account for approximately 2.88 to 6.41% of the tailings by mass. In addition to Fe, Pb and Zn a number of other heavy metals were also identified in the tailings. Element availability was assessed by means of the saturated paste, TCLP, acid rain and DTPA extraction methods. According to these extractions groundwater at the Pering Mine may be at risk from Mg, Mn, Pb, S and Zn contamination. In order to substantiate these findings further laboratory (Chapter 3) and field (Chapter 4) based investigations were undertaken.

CHAPTER 3

LEACHING STUDIES: ESTIMATING AND MODELLING THE LONG-TERM RELEASE OF CONTAMINANTS FROM THE PERING TAILINGS MATERIAL

3.1 Introduction

Discarded mine tailings may release contaminants into the surrounding environment for very long periods of time (Dudka and Adriano, 1997; Aucamp and van Schalkwyk, 2003; Moreno and Neretnieks, 2006). Some difficulty exists in quantifying which elements may be released and defining the duration over which concentrations are likely to exceed legal limits. In general three basic approaches have been used to define mobile, mobilisable or bioavailable pools of contaminants in soil, namely:

1. Single batch extractions using distilled water, salt solutions, acids, or other organic/inorganic extractants.
2. Sequential batch experiments in which metals associated with different solid phases are extracted by increasingly vigorous extractants.
3. Leaching column experiments

All three methods have been used to estimate contaminant release from tailings material (Lin, 1997; McGowen and Basta, 2001; Carlsson *et al.*, 2002; Cukrowska *et al.*, 2004; Mihaljevič *et al.*, 2004; Malmström *et al.*, 2006). In comparison to batch extractions, leaching column experiments provide a better representation of field conditions. At the same time they also provide the only means whereby the mechanisms governing solute transport can be simultaneously assessed and modelled. These two aspects integrate the two main objectives of this study and for this reason several leaching experiments were undertaken.

The release of potential contaminants from a number of leaching columns was determined under conditions of continuous saturated flow and under conditions of intermittent flow. Continuous flow, with constant water content, is required in order to describe the transport of solutes mathematically by the convection-dispersion equation (Toride *et al.*, 1999). Intermittent flow, with interceding weeks of stagnation is on the other hand, more realistic of field conditions. In these treatments the Pering tailings material was leached with an acetic acid solution, distilled water and deoxygenated distilled water. In order to quantify the impact that the tailings are expected to have on the local groundwater, it is necessary to

compare results with known guidelines which have been scientifically formulated to ensure environmental and human health. The water quality guidelines provided by the South African Bureau of Standards (SABS 241, 1999) and the Department of Water Affairs and Forestry (DWAF, 1996a; 1996b; 1996c; 2005) were chosen for this purpose (Appendix 2).

The tailings impoundment was deposited on a shallow Mispah soil (Soil Classification Working Group, 1991) which has a low CEC (10.46 $cmoles_+ kg^{-1}$). As a result it is expected to play an insignificant role in the long-term immobilisation of contaminants. There remains a possibility, however, that some degree of immobilisation may occur as the mine drainage enters the underlying fractured dolomite. This was not examined in the current study, but it is thought that sorption will be limited as a result of preferential water flow through fractures. Due to the lack of confirmatory groundwater data it was assumed that those elements mobilised from the tailings would be directly available to cause groundwater contamination. For these reasons the potential for contamination will be evaluated according to element availability in the actual tailings.

3.2 Theoretical background

3.2.1 Column breakthrough curves

If a solute of known concentration is applied to a soil its movement through the profile, or column, will be retarded by a number of factors. The physical makeup of soils causes the added solute to undergo dispersion and dilution as a result of tortuous flow paths and mixing with the surrounding pore-water. This results in a dispersive front moving down the profile. Thus, if the concentration of the solute were to be successively measured some distance below its point of application a gradual change in concentration would be observed, rising from zero up to some maximum as increasing volumes of solute are added to the surface of the profile (Figure 3.1, Curve b). This change in concentration gives an indication of how the solute is transported within the profile and is described by what is known as a breakthrough curve (BTC). If the solute was reactive its movement through the profile would be further retarded by sorption onto the soil particles, this in turn would alter the shape of the BTC (Figure 3.1, Curves b to e). The shape of the BTC is therefore determined by the chemical and physical characteristics of both the solute and the soil, and their combined interaction.

The shape of a BTC provides information on the mechanisms which maybe governing solute transport. Figure 3.1 gives examples of a number of BTCs determined in soils where different transport mechanisms are operating (Nielsen and Biggar, 1964). Under ideal situations of piston flow and zero diffusion complete breakthrough would be expected at exactly 1 pore volume (Figure 3.1, Curve a). Due to the porous nature of soils and solute diffusion this is seldom achieved. Curve b shows a typical BTC for a non-sorbing solute where, as a result of dispersion and diffusion, the breakthrough front is dispersed. In the case of reactive solutes breakthrough is retarded by sorption onto exchange sites (Curve c). Curves d and e represent alternative BTCs, which may arise as a result of rate limited sorption or water movement along preferential flow paths i.e. chemical and physical nonequilibrium transport mechanisms, respectively.

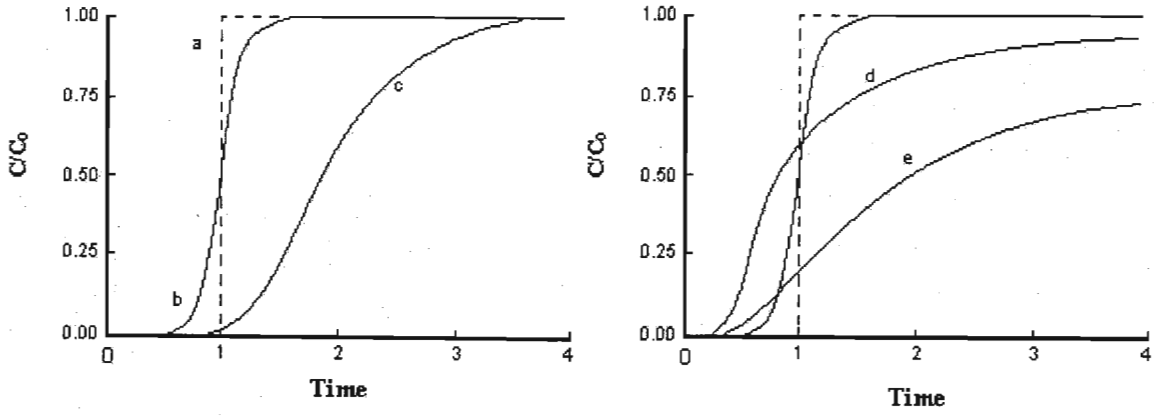

Figure 3.1 Some typical breakthrough curves (BTC) from leaching column miscible displacement experiments (Nielsen and Biggar, 1964).

In uncontaminated soils metal transport has typically been modelled by adding metal salt solutions via pulse or continuous flow to pre-packed columns and recording the corresponding BTC (e.g. Yong *et al.*, 2001; Voegelin *et al.*, 2003). According to McGowen and Basta (2001) less research has focussed on modelling the release of metals from contaminated soils. In such instances the contaminated soil is flushed with a leaching solution and the concentration of metals in the effluent measured. The BTCs determined in this way will form inverse shapes in comparison to those shown in Figure 3.1, starting at a maximum and decreasing as flushing continues. This type of BTC is typically achieved when leaching metal-rich mine tailings (Jurjovec *et al.*, 2002).

3.2.2 Defining solute movement

Mathematically, solute movement in porous media is described by the convection-dispersion equation (CDE, Toride *et al.*, 1999; Álvarez-Benedi *et al.*, 2005). In essence this equation describes the shape of the BTC for a particular solute. In its most simplistic form the CDE defines solute movement in porous media that is assumed to be homogeneous and in which all interphase mass transfer processes are assumed to be instantaneous (i.e. equilibrium assumption). Under these assumptions the equilibrium CDE for one-dimensional transport of a non-reactive solute is defined by (Álvarez-Benedi *et al.*, 2005):

$$\frac{\partial \theta c}{\partial t} = -\frac{\partial}{\partial z}\left(J_w C - \theta D \frac{\partial c}{\partial x}\right) + \theta \Gamma \tag{4.1}$$

where θ is the volumetric water content ($L^3\ L^{-3}$; L = length); c is the volume-averaged or resident solute concentration of the liquid phase ($M\ L^{-3}$; M = mass); t is time (T); x is the distance (L); J_w is the water flux ($L\ T^{-1}$); D is the dispersion coefficient ($L^2\ T^{-1}$); and Γ is the solute sink/source term ($M\ L^{-3}\ T^{-1}$). When the water content is constant (e.g. under saturated conditions), the above equation can be simplified to:

$$\frac{\partial c}{\partial t} = D\frac{\partial^2 c}{\partial x^2} - v\frac{\partial c}{\partial x} + \Gamma \tag{4.2}$$

where v is the average pore-water velocity ($L\ T^{-1}$) which is equal to J_w/θ. In the case of reactive solutes solid phase sorption needs to be taken into account. This leads to Equation 4.2 being modified to include a retardation factor, R, which describes sorption. The overall equation is written as:

$$R\frac{\partial c}{\partial t} = \theta D\frac{\partial^2 c}{\partial x^2} - v\frac{\partial c}{\partial x} + \Gamma \tag{4.3}$$

In the case of linear sorption R is equal to:

$$R = 1 + \frac{\rho_b K_d}{\theta} \tag{4.4}$$

where ρ_b is the bulk density of the soil ($M\ L^{-3}$) and K_d is an empirical distribution constant ($L^3\ M^{-1}$) defining the slope of the sorption isotherm.

3.2.3 Solute transport under conditions of nonequilibrium

The equilibrium CDE outlined above describes solute movement in homogeneous porous media under conditions of chemical and physical equilibrium. These assumptions are not always valid as soils seldom follow such 'ideals'. Situations of nonequilibrium often exist in both soils and tailings. In fine grained porous media it is not uncommon for zones of immobile water to accumulate. It is thus possible to separate the soil flow domain into mobile and immobile fractions. Solute exchange between these fractions affects the way in which solutes are transported through the soil and thus the mathematical formulation of the BTC (van Genuchten and Wierenga, 1977; Gerke and van Genuchten, 1993). As the presence of mobile/immobile phases is dependent on the physical structure of the porous medium, this type of situation is known as physical nonequilibrium.

Situations of chemical nonequilibrium are also common as soils are not homogeneous in their composition, but possess multiple sorption sites on various fractions, such as organic matter, clay particles and metal oxides. Sorption of a particular solute onto some, or all, of the available sorption sites is often a rate limited (i.e. kinetic) process. Thus models describing chemical nonequilibrium have been devised to take into account both sorption kinetics and sorption site heterogeneity (Cameron and Klute, 1977; van Genuchten and Wagenet, 1989).

Numerical models describing solute transport under conditions of chemical (Cameron and Klute, 1977; van Genuchten and Wagenet, 1989) and physical (van Genuchten and Wierenga, 1977; Gerke and van Genuchten, 1993) nonequilibrium have tended to split the equilibrium CDE into two parts. In the case of physical nonequilibrium the first part describes solute movement in the mobile phase, while the second part describes solute transfer between the immobile and mobile phases. Modelling chemical nonequilibrium assumes that sorption can be either an instantaneous or a rate limited process. The first half of the equation accounts for the fraction of exchange sites which undergo equilibrium sorption, while the second half describes the kinetic sorption of the solute on the remaining sites. As a result the CDEs defining chemical and physical nonequilibrium have become known as the two-site and two-region models, respectively.

Although the chemical and physical CDEs are based on different concepts Nekedi-Kizza *et al.* (1984) and van Genuchten and Wagenet (1989) devised a single equation, which has equivalent dimensionless parameters, to describe both types of nonequilibrium transport. Under conditions of steady state water flow, the two-site and two-region models are written as (Toride *et al.*, 1999; Álvarez-Benedi *et al.*, 2005):

$$\beta R\frac{\partial C_1}{\partial T}+(1-\beta)R\frac{\partial C_2}{\partial T}=\frac{1}{P}\frac{\partial^2 C_1}{\partial X^2}-v\frac{\partial C_1}{\partial X}-\mu_1 C_1+\gamma_1(X) \qquad \text{(Equilibrium phase)}$$

(4.5)

$$(1-\beta)R\frac{\partial C_2}{\partial T}=\omega(C_1-C_2)-\mu_2 C_2+\gamma_2(X) \qquad \text{(Nonquilibrium or immobile phase)}$$

In this equation C is the dimensionless solute concentration and the subscripts 1 and 2 denote concentrations in equilibrium (mobile liquid phase) and nonequilibrium (immobile phase) phases, respectively. T is dimensionless time ($T = vt/L$); X is dimensionless distance ($X = x/L$); P is the Peclet number ($P = vL/D$); R is the retardation factor (Equation 4.4); ω is a dimensionless mass transfer coefficient; β is a partitioning coefficient; μ is a dimensionless first-order decay constant (M L^{-3} T^{-1}) and γ is a dimensionless zero-order solute production constant (M L^{-3} T^{-1}). For the two-region model:

$$\beta=\frac{\theta_m+f\rho_b K_d}{\theta+\rho_b K_d} \qquad \omega=\frac{\alpha L}{\theta v} \qquad C_1=\frac{c_m}{c_0} \qquad C_2=\frac{c_{im}}{c_0}$$

ρ_b is the bulk density of the soil (M L^{-3}); K_d is an empirical distribution constant defining the slope of the linear sorption isotherm (L^3 M^{-1}); v is the pore water velocity (L T^{-1}); f is the dimensionless fraction of sorption sites in equilibrium with the mobile water; θ is the total volumetric water content (L^3 L^{-3}) and θ_m is the volumetric water content of the mobile water phase; α is a mass transfer coefficient between the two regions (T^{-}); c_m and c_{im} are the concentrations in the mobile and immobile phases respectively (M L^{-3}); c_0 and L represent a characteristic concentration and length, respectively. For the two-site model:

$$\beta=\frac{\theta+f\rho_b K_d}{\theta+\rho_b K_d} \qquad \omega=\frac{\alpha(1-\beta)RL}{v} \qquad C_1=\frac{c}{c_0} \qquad C_2=\frac{S_k}{(1-f)K_d c_0}$$

All parameters for the two-site model are the same as described above, except for f which designates the fraction of exchange sites that are always at equilibrium and α, which is a first-order kinetic rate coefficient (T^{-1}). S_k is the sorbed concentration of the solute on the kinetic sites (M M^{-1}).

Toride *et al.* (1999) developed the computer model *CXTFIT* which enables inverse fitting of the CDE to observed laboratory or field data obtained from miscible displacement experiments. In this way parameters in the CDE can be optimised and the BTC can be expressed in mathematical terms. By providing a mathematical definition of how a solute moves through a column it becomes possible to model its movement at larger scales.

3.3 Materials and methods

3.3.1 Leaching under continuous steady-state flow

Chloride (Cl^-) has been widely used as a non-reactive solute in many experimental designs and model simulations (Bain *et al.*, 2000; Malmström *et al.*, 2006). It is typically used to determine the dispersivity of a porous media, which is one of the most important parameters required to describe solute transport. For this reason a single leaching column was set up to exclusively measure the mobility of Cl^- in the tailings, while a second column was used to determine the rates at which potentially toxic contaminants were leached from the tailings by the addition of distilled water.

In order to accurately simulate water movement within the impoundment a fine grained bulk sample, collected from approximately 100 cm below the upper surface of the tailings dam, was used. When packed into a column the TT material had a much higher hydraulic conductivity than that which was found in the field (Appendix 6). The newer bulk sample (TN material), collected in July 2005, was found to better represent the bulk of the tailings and had similar hydrophysical properties.

The two columns used in this experiment were each packed as follows: 2 kg of the TN tailings was slowly brought to saturation by the slow addition of distilled water with vigorous stirring. A known mass of saturated tailings was then tightly compacted into a flat ended, clear Perspex leaching column (internal diameter 6 cm, length 23 cm) and sealed tightly with a Perspex lid. A thin plastic mesh and three layers of glass wool were placed at the point of water entry into the column to ensure even distribution of the leaching solution. The same was done at the top of the column in order to prevent upward dispersion of the tailings. Once sealed, the two packed columns were laid on their sides and allowed to equilibrate for 24 hours. Both columns were rotated every few hours to

maintain an even distribution of water. No duplicate columns were run in this experiment. In light of work carried out by Malmström *et al.* (2006) this was seen to be acceptable, as these authors successfully used similar sized columns (internal diameter 8 cm, length 21 cm) with no duplicates for their long term leaching experiments of mine tailings.

After the 24 hour equilibration period the columns were set upright. The bottom inlet valve was connected to an inlet tube which supplied the leaching solution from a constant head mariott bottle system that was set 160 cm above the base of the column (Lorentz *et al.*, 2001; see Appendix 7, Figure A7.1 for diagrammatic representation of the setup). The pressure head of the leaching solution at the base of the column caused the equilibrated pore-water to be displaced upwards. This displaced pore-water or effluent was collected in a sealed glass measuring cylinder. Once 10 to 20 m*l* of effluent had leached into the measuring cylinder the solution was collected and a clean measuring cylinder was immediately attached to the outlet tube to collect the second sample. In this way effluent samples were gathered continuously throughout the experiment. The volume of these samples and their time of collection were accurately recorded so that the pore-water velocity (v, in Equation 4.3) and hydraulic conductivity of the material could be determined. The pH (Radiometer PHM210 pH meter) and EC (CDM83 electrical conductivity meter) of alternate samples were measured. All samples were stored at 4 °C for later elemental analysis.

The first column was used for chloride leaching. This was done by passing a 980 mg l^{-1} Cl^- solution (made up from anhydrous $CaCl_2$) through the pre-packed column and measuring the concentration of Cl^- released in the effluent. After about 1.5 pore volumes, all the original pore-water in the column had been displaced and the Cl^- concentration in the effluent was very close to the concentration of the inflowing leaching solution. The original pore-water of the tailings had a Cl^- concentration of approximately 260 mg l^{-1}. Thus a complete BTC was not achieved initially (Appendix 7, Figure A7.3). In order to obtain a full BTC an additional pore volume of the Cl^- leaching solution was allowed to pass through the column. This ensured that the column was completely saturated with the Cl^- leaching solution. After this, the Cl^- solution in the mariott bottle was replaced with distilled water and the BTC was determined in reverse order. The Cl^- concentration in all effluent samples was determined by titration with 0.005 N $AgNO_3$, using a 5% potassium chromate solution as an indicator (Soil Salinity Laboratory Staff, 1954).

The second column was leached exclusively with distilled water in order to simulate rainfall. As mentioned above regular effluent samples were collected in a measuring cylinder throughout the experiment. Alternate samples were analysed for Al, Ba, Ca, Cd, Co, Cu, Cr, Fe, Hg, K, Mg, Mn, Na, Ni, P, Pb, S, Se, Sr and Zn by ICP-OES (Perkin Elmer Optima 5300DV). After six pore volumes of distilled water had passed through the column, elemental concentrations had decreased significantly. At this point the column was dismantled and the contents carefully collected and dried at 105 °C for 3 days. This enabled the water content, bulk density and porosity of the packed tailings to be determined.

3.3.2 Leaching with intermittent flow

As part of this investigation the tailings were leached with three different solutions: acetic acid (TCLP-2 solution), distilled water and deoxygenated distilled water. Some of these leaching columns were initiated prior to the collection of the TN bulk sample and therefore the TT sample was used throughout this set of experiments. The air-dried tailings were tightly compacted into Perspex columns (internal diameter 5.4 cm, length 15 cm) to a height of 10 cm. Packing was done to give bulk densities similar to that found in the field, i.e. 1.7 g cm^{-3} (Appendix 6). The tailings material was placed on top of perforated Perspex discs in order to allow the leachate to drain freely. A triple layer of glass wool was placed above and below the tailings in immediate contact with it, to prevent wash through and upward dispersion of the material. Once packed, the columns were sealed with rubber bungs, each of which contained a single glass tube to allow for water inflow and outflow (see Appendix 7, Figure A7.2 for diagrammatic representation of the column). The columns were then covered with aluminium foil to prevent growth of photosynthetic organisms. A constant temperature of 22 ±1 °C was maintained throughout the experimental procedures.

3.3.2.1 Treatment 1: Leaching with TCLP-2 solution

In order to assess element release under what would most certainly be a worst case scenario, three pre-packed columns were leached with the TCLP-2 solution on a weekly basis (DWAF, 2005). This solution was made up by adding 5.7 m*l* of glacial acetic acid to 1 *l* of distilled water to give a solution with a pH of 2.88 ±0.05. At day zero 1 pore volume

of the leaching solution was added to each of three columns and allowed to equilibrate for 1 week. After a week the equilibrated pore solution was displaced downwards by the addition of a second pore volume of TCLP solution. Leaching was continued in this way for a period of 44 weeks. The pH, EC and volume of the leachate samples were recorded each week. Solutions were acidified to below pH 2 with 2 *M* HNO_3 and stored at 4 °C for analysis of Al, Ba, Ca, Cd, Co, Cr, Cu, Fe, Hg, K, Mg, Mn, Na, Ni, P, Pb, S, Se, Sr, V and Zn using ICP (Varian Liberty X150).

3.3.2.2 Treatment 2: Leaching with distilled water

The readily mobile or water soluble fraction of the tailings was determined by leaching with distilled water (pH ±5.0 to 5.5). This was designed to simulate the infiltration of rainfall. The same leaching procedure was used as described above (Section 3.3.2.1); only the length of the experiment was reduced to 10 weeks. After this time period, all elements had reached steady outputs except for S and Zn. An additional week was run to confirm that equilibrium outputs of these two elements had been reached.

3.3.2.3 Treatment 3: Leaching under conditions of reduced oxygen

In order to examine the leachability of the tailings under conditions of reduced oxygen, the material was leached with deoxygenated distilled water. Oxygen was removed from the distilled water by vigorous boiling for 1 hour, followed by 1 hour exposure to nitrogen bubbling (Lu *et al.*, 1997; Sinha and Li, 2000). In order to maintain oxygen-free conditions within the tailings throughout the 10 week period, an airtight system was set up as shown in Figure 3.2. Prior to leaching, all oxygen was displaced out of the pore spaces of the tailings by passing a low pressure flow of nitrogen gas (N_2) through the columns for 4 hours. The leaching solution was then placed in the mariott bottle, over-gassed with N_2, and allowed to slowly drip into the columns. The outflow tubes of the columns were simultaneously opened and the leachate was allowed to pass through into sealed glass measuring cylinders, from which the oxygen had been removed by displacement with N_2 gas. After exactly 1 pore volume of leachate had passed through the tailings, the inflow and outflow tubes were resealed to prevent oxygen ingress into the column. As in the previous treatments the waste was leached on a weekly basis, with newly degassed distilled water.

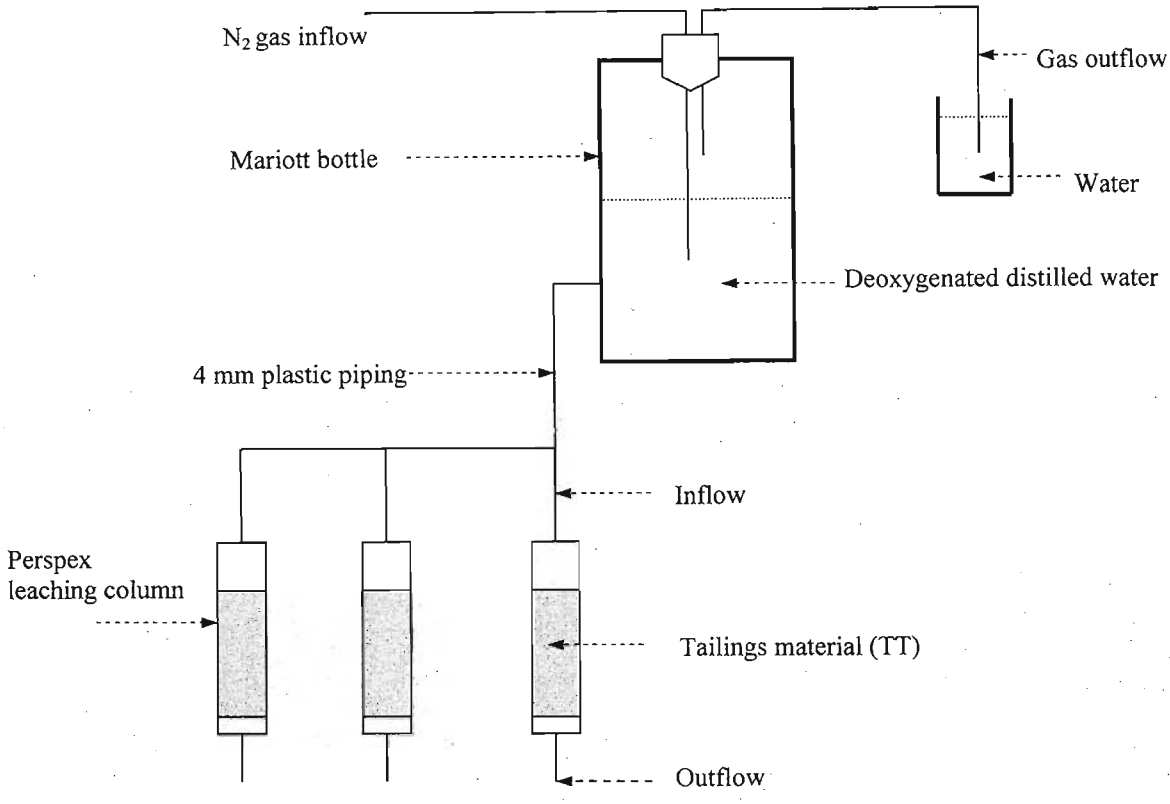

Figure 3.2 Leaching column setup used to leach the Pering tailings under oxygen free conditions.

The redox potential (Radiometer PHM210 redox meter with Ag/AgCl redox probe) of all the effluent samples collected from Treatments 1 and 2 were measured, under O_2 free conditions, immediately after leaching. This was followed by the measurement of EC and pH. All samples in these two experiments were also acidified with HNO_3 to below pH 2 by diluting 1:1 with 2 *M* HNO_3. The concentrations of Ca, Cu, Fe, Hg, K, Mg, Mn, Na, Pb, S and Zn in the effluent were determined by ICP (Varian Liberty X150).

3.3.3 Geochemical modelling

A number of models have been developed to predict the equilibria between aqueous, adsorbed and solid phases in environmental settings. The *MINTEQ-A2* (Allison *et al.*, 1991) model has been widely used for this purpose in many tailings systems (e.g. McGregor *et al.*, 1998; Al *et al.*, 2000; Bain *et al.*, 2000; Jurjovec *et al.*, 2002). This model was recently upgraded to include a Microsoft interface and is now known as *visual*

MINTEQ. This new version was used for geochemical modelling in this study. Measured elemental concentrations and pH of the column effluents were used as the starting values for all simulations. The *visual MINTEQ* program defaults to making no redox calculations, this default setting was accepted in all cases. This was seen to be acceptable as the leaching columns remained aerobic throughout the experimental procedures.

3.4 Results and discussion

3.4.1 Element release and solute transport under continuous flow

3.4.1.1 Element release

The two columns packed for this experiment had hydrophysical properties similar to that of five undisturbed cores collected from the surface of the tailings impoundment (Appendix 6). The bulk density of the packed tailings was slightly higher at 1.88 g cm^{-3} in comparison to the 1.71 g cm^{-3} measured for the surface tailings, and the saturated hydraulic conductivity slightly lower at 0.008 cm $hour^{-1}$ compared to 0.018 cm $hour^{-1}$ for Core 5. These values, however, may potentially be a better approximation of the internal tailings where bulk densities are often higher than at the surface and the hydraulic conductivities lower (Blowes *et al.*, 1998; McGregor *et al.*, 1998).

Mobility of calcium, magnesium and sulfate

Prior to leaching, the saturated tailings material was allowed to equilibrate for 24 hours. It was therefore expected that initial element concentrations displaced from the column would be at a maximum and after some time decline as the leaching water began to dilute the pore-water. This trend was followed by most elements (Figure 3.3). The first two effluent samples, however, had unexpectedly high concentrations of S at 2946 mg l^{-1} and 2883 mg l^{-1}, respectively. The initial sample also had a very high Mg concentration of 1515 mg l^{-1}. This initial peak may have been due to localised dissolution of epsomite ($MgSO_4$). As these initial concentrations were seen to be anomalous and would prevent accurate fitting of the CDE, they were ignored in the parameter optimisation process (see Section 3.4.1.2).

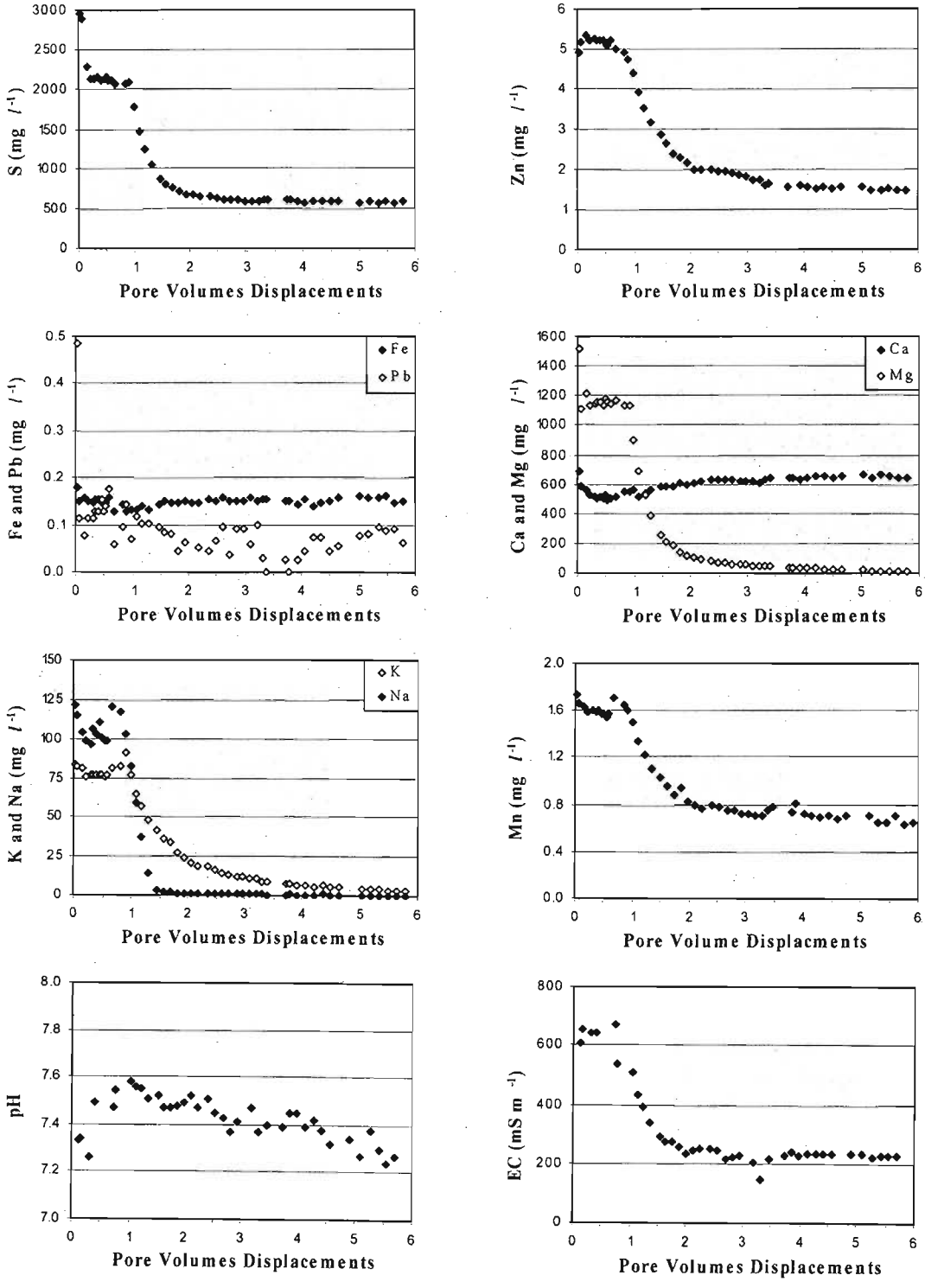

Figure 3.3 Concentrations of S, Zn, Fe, Pb, Ca, Mg, K, Na and Mn released from the Pering tailings under continuous saturated leaching. The pH and EC of the effluent solutions are also included (1 pore volume = 225 cm^3).

After the first two effluent samples S concentrations stabilised at just over 2000 mg l^{-1} (Figure 3.3). The release of S began to decline rapidly after approximately one pore volume and then stabilised at ±600 mg l^{-1} from about the third pore volume onwards. High concentrations of Mg were also released for the first pore volume, after which concentrations decreased rapidly. By the end of the leaching procedure, almost all of the easily soluble Mg had been flushed from the tailings. The release of Ca from the material appeared to be inversely related to pH (Figure 3.3). Initially the Ca concentration in the effluent decreased, after which it began to increase slowly to a maximum of 665 mg l^{-1}. The pH increased over the first pore volume and then decreased from a maximum of 7.58 to a minimum of 7.24. The EC reflects the removal of soluble species from the tailings. The rapid flushing of elements after about one pore volume can be seen by the sharp reduction in EC. The continual release of S, Ca and K after the second pore volume caused the EC of the effluent to remain at about 230 mS m^{-1} for the remainder of the experiment (Figure 3.3).

Geochemical modelling of the effluent indicated that it was undersaturated with respect to dolomite for the entire experiment (Appendix 7). This is an indication that the dissolution of dolomite was kinetically limited in this experiment (Al *et al.*, 2000; Jurjovec *et al.*, 2002). According to Jurjovec *et al.* (2002) dissolution can be kinetically limited if pore-water flow rates are high or if secondary precipitates begin to coat the mineral particles. It is likely that in this experiment the continuous flow of water prevented dolomite from achieving equilibrium with the pore-water. In addition, it was predicted that gypsum ($CaSO_4 \cdot 2H_2O$) could have been precipitating during the first pore volume. It is therefore possible that this mineral could have partially coated the dolomite particles and as a consequence limited its dissolution (Booth *et al.*, 1997; Al *et al.*, 2000; Jurjovec *et al.*, 2002).

Dolomite is the primary source of Mg and Ca in the tailings. The release of these two elements, however, followed markedly different trends (Figure 3.3). Geochemical modelling indicated that for the first pore volume the precipitation of gypsum was thermodynamically possible. After this point the column effluent was very close to equilibrium with respect to this mineral (Appendix 7, Figure A7.5). It is thus thought, that from this point on the release of Ca, and to a large extent S, was controlled by the continual

dissolution of $CaSO_4 \cdot 2H_2O$. Epsomite ($MgSO_4$) is more soluble than $CaSO_4 \cdot 2H_2O$ (Lindsay, 1979) and as a consequence it was predicted by *MINTEQ* to occur only as a dissolved aqueous species (Appendix 7). This would explain why the initial Mg concentration in the effluent was so much higher than that of Ca. The formation of the $MgSO_{4(aq)}$ complex is also likely to have contributed to the rapid flushing of Mg from the column.

Oppositely charged ions in solution tend to form complexes of various kinds (Sposito, 1989; Tan, 1998). Geochemical modelling showed that Mg^{2+} Na^{+}, K^{+}, Mn^{2+} and Zn^{2+} formed aqueous complexes with SO_4^{2-}, CO_3^{2-} and OH^{-} ions in the leaching water (Appendix 7, Table A7.5). These complexes are expected to have increased the mobility of these elements in the tailings, because they often have a neutral or net negative charge, which limits their sorption under high pH conditions.

Magnesium concentrations in the leachate remained above the SABS 241 (1999) guideline of 70 mg l^{-1} until about 2.5 pore volumes of leachate had passed through the column (Figure 3.3). The high concentration of Mg, in conjunction with the high sulfate concentration, may pose a significant threat to groundwater reserves if leached from the tailings impoundment. This is because $MgSO_{4(aq)}$ is a known laxative and bowel irritant (DWAF, 1996a; WHO, 1996). The effluent was measured for its total S concentration and not for the concentration of the sulfate ion, which is the expected species under the aerobic alkaline conditions (see Figure 1.2). Even with no conversion to account for SO_4^{2-}, the S concentrations reported in Figure 3.3 are all in excess of the SABS 241 (1999) guideline of 400 mg SO_4^{2-} per l^{-1}. Drinking water with SO_4^{2-} concentrations in excess of 600 mg l^{-1} will cause diarrhoea in most individuals, with there being little chance for long-term adaptation (DWAF, 1996a). The sustained release of S, shown in Figure 3.3, suggests that the Pering tailings material can potentially leach high concentrations of S for long periods of time.

Mobility of metals

Zinc and Mn are essential trace elements for humans and higher plants. However, at higher concentrations they are known to have a number of toxicological effects (DWAF, 1996a; 1996c; WHO, 1996). Zinc concentrations increased marginally over the first three samples, most likely due to continued dissolution after leaching was commenced. Concentrations

then stabilised at about 5.2 mg l^{-1} before beginning to decrease after approximately 0.75 pore volumes. The initial decrease was rapid, but slowed down after about 3 pore volumes. After this point the tailings continued to release Zn at a sustained rate. The release of Mn followed a similar trend (Figure 3.3), with concentrations in the effluent being consistently above the 0.1 mg l^{-1} recommended limit for drinking water (SABS 241, 1999; Appendix 2). Zinc concentrations, on the other hand, were only above drinking water guidelines for the first pore volume, thereafter they decreased to within acceptable limits (< 4 mg l^{-1}). From this it would appear that groundwater at Pering may also be at risk from Mn and Zn contamination.

Pyrite is the most abundant sulfide in the tailings. Despite this, very low levels of Fe were recorded in the leachate. The release of Fe from the tailings was consistent, ranging between 0.13 and 0.18 mg l^{-1} for the entire experiment. The release of Pb was much more random, with concentrations ranging between 0 and 0.49 mg l^{-1}. It is thus evident that the release of these metals from the tailings is very limited. This may be due to slow sulfide oxidation rates and/or the strong metal sorbing capacity of the tailings. Concentrations of Al, Ba, Cd, Co, Cu, Cr, Ni, P, Se and Sr in all leachate samples were also low (Appendix 7) and therefore groundwater is unlikely to be at risk from these elements.

3.4.1.2 Modelling solute transport

Parameter optimisation

The dispersivity of the Pering tailings material was determined from the chloride BTC. Figure 3.4A shows the measured concentration of chloride in the effluent, C, normalised to the initial concentration of 980 mg l^{-1}, C_0, as a function of time. The CDE was fitted to this BTC using the nonlinear least-squares parameter optimisation process in the *CXTFIT* computer program. From this the dispersivity of the tailings was calculated to be 0.0685 cm (Table 3.1). As a non-reactive solute Cl^- did not sorb onto the tailings, and thus its dispersion in the column was purely the result of physical mixing and diffusion. In order to account for sorption and possible nonequilibrium transport mechanisms in the BTCs of the more prominent contaminants, Mg, Mn, S and Zn, *CXTFIT* was set up to describe these curves according to the nonequilibrium CDE (Figure 3.4B and Table 3.1; see Appendix 8 for an example of the Mg input and out files).

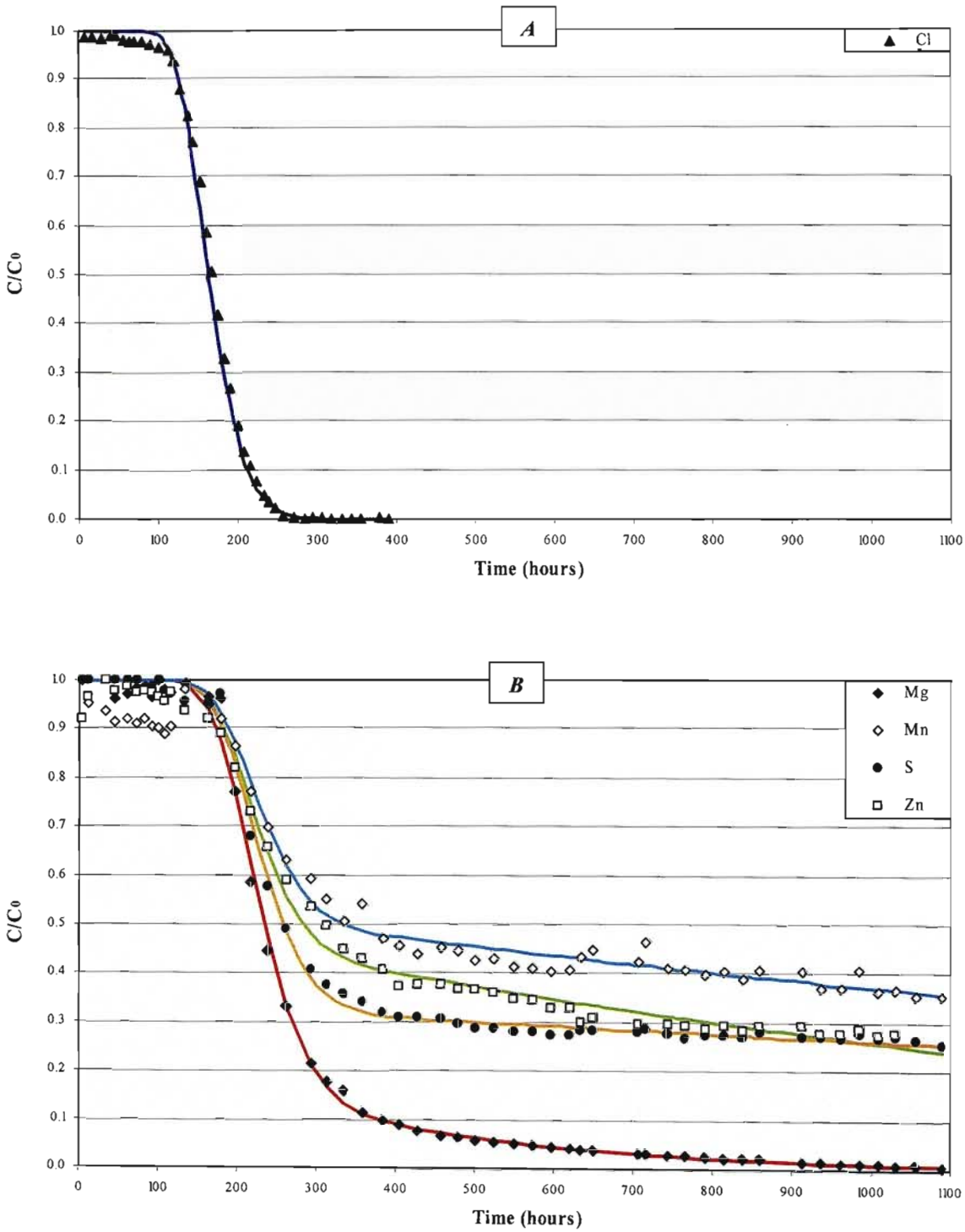

Figure 3.4 Relative concentrations of (A) chloride, and (B) magnesium, manganese, sulfur and zinc released from the tailings under continuous saturated leaching (symbols), with corresponding *CXTFIT* optimised CDEs (solid lines). (C_0 = initial or starting concentration at time zero and C = the measured concentration in the effluent at time T).

Table 3.1 Best fitting parameters defining the chloride, magnesium, manganese, sulfur and zinc BTCs shown in Figure 3.4.

Cl⁻ BTC	***Equilibrium CDE***	***Means of verification***
Pore-water velocity (v, cm hour^{-1})	0.1381	From experiment
Dispersivity (D, cm)	0.0685	*CXTFIT* optimisation
Retardation factor (R)	1.0000	For non-reactive solutes $R = 1$
Square for regression of observed vs. predicted	0.9969	p = 0.05
Mg^{2+} BTC	***Nonequilibrium CDE***	
Pore-water velocity (v, cm hour^{-1})	0.1302	From experiment
Dispersivity (D, cm)	0.0685	Optimised from Cl BTC
Retardation factor (R)	1.5510	*CXTFIT* optimisation
Beta (β)	0.8392	*CXTFIT* optimisation
omega (ω, hour^{-1})	0.1650	*CXTFIT* optimisation
Square for regression of observed vs. predicted	0.9977	p = 0.05
Mn^{2+} BTC	***Nonequilibrium CDE***	
Pore-water velocity (v, cm hour^{-1})	0.1302	From experiment
Dispersivity (D, cm)	0.0685	Optimised from Cl BTC
Retardation factor (R)	8.1330	*CXTFIT* optimisation
Beta (β)	0.1651	*CXTFIT* optimisation
omega (ω, hour^{-1})	0.7127	*CXTFIT* optimisation
Square for regression of observed vs. predicted	0.9653	p = 0.05
S BTC	***Nonequilibrium CDE***	
Pore-water velocity (v, cm hour^{-1})	0.1302	From experiment
Dispersivity (D, cm)	0.0685	Optimised from Cl BTC
Retardation factor (R)	7.9430	*CXTFIT* optimisation
Beta (β)	0.1668	*CXTFIT* optimisation
omega (ω, hour^{-1})	0.3910	*CXTFIT* optimisation
Square for regression of observed vs. predicted	0.9973	p = 0.05
Zn^{2+} BTC	***Nonequilibrium CDE***	
Pore-water velocity (v, cm hour^{-1})	0.1302	From experiment
Dispersivity (D, cm)	0.0685	Optimised from Cl BTC
Retardation factor (R)	4.7750	*CXTFIT* optimisation
Beta (β)	0.2746	*CXTFIT* optimisation
omega (ω, hour^{-1})	0.6041	*CXTFIT* optimisation
Square for regression of observed vs. predicted	0.9911	p = 0.05

The Cl^- BTC provides a comparison against which the movement of reactive solutes can be compared. All Cl^- contained in the pore-water of the column at the start of the leaching procedure, was displaced by the time 1.5 pore volumes of distilled water had leached through the column (Appendix 7, Figure A7.4). Manganese, Zn and S were released from the tailings much more slowly. Even after 1089 hours (45.75 days) of continuous leaching these elements were still present in the leaching solution (Figure 3.4B). The shape of these curves can be attributed to chemical rather than physical nonequilibrium, because if the tailings had both mobile and immobile water phases, this would have been evident from the Cl^- BTC. Tailings systems are chemically complex and thus the delay, or retardation, of the Mg, Mn, S and Zn curves may not exclusively be the result of sorption and desorption reactions, but could also be due to secondary precipitation, dissolution and continued

sulfide oxidation. These processes can add further complications to the CDE as they tend to increase or decrease the concentration of the solute in the pore-water, and thereby make it necessary to quantify and then add source or sink terms to the equation (γ and μ in Equation 4.5).

Despite the added complications of precipitation, dissolution and possible sulfide oxidation, the Mg, Mn, S and Zn BTCs in Figure 3.4B were all well described by the nonequilibrium CDE, with no added source or sink terms. The parameters defining these curves are reported in Table 3.1 (details on their meaning are given in Sections 3.2.2 and 3.2.3). From these parameters it is evident that the release of Mn from the tailings was the most strongly retarded (R = 8.1330), followed by S (R = 7.9430), Zn (R = 4.7750) and then Mg (R = 1.5510). The release of S was most likely retarded as a result of precipitation as gypsum, rather than by sorption of anionic sulfur species. The cations are expected to have been retarded by sorption onto the tailings.

Modelling the long-term release of magnesium, manganese, sulfur and zinc

In the previous section *CXTFIT* was used to fit the CDE to a number of experimentally determined BTCs by inverse optimisation. This program can also be used for direct modelling if the parameters defining solute transport are known. The parameters defining the release of Cl, Mg, Mn, S and Zn from the Pering tailings material (Table 3.1) were therefore inputted back into *CXTFIT*, to model the release of these elements from the base of the impoundment. In order to account for slower flow rates in the impoundment, the pore-water velocity (v) was assumed to be equal to the mean annual precipitation (i.e. 100% infiltration was assumed). As in the column study it was assumed that the pore-water of the impoundment was flushed by a continuous flow of water (413 mm year^{-1}). The initial concentrations in the pore-water were assumed to be the same as those found in the column effluent at the start of the leaching experiment (i.e. Mg = 1100 mg l^{-1}; Mn = 1.74 mg l^{-1}; Zn = 5.30 mg l^{-1}; and S, as SO_4^{2-} = 6400 mg l^{-1}; see Figure 3.3).

The predicted rate at which the individual elements were leached from the impoundment is shown in Figure 3.5. Predicted concentrations in the effluent, C, are given relative to the initial starting concentrations, C_0, which were assumed to be uniform across the 30 m depth of the impoundment at the start of the simulation (see Appendix 8 for direct outputs).

It was predicted that all Cl^- would be flushed from the impoundment in just less than 90 years (Figure 3.5A). As would be expected the reactive solutes were released over a much longer period of time (Figure 3.5B). The release of Mn and S were the most retarded (Figure 3.4B and Table 3.1) and as a consequence it was predicted that traces of these two elements would still be found in seepage waters after 700 years. After Cl, the movement of Mg through the column was the least retarded (Table 3.1), and thus it was predicted to be leached completely from the impoundment after about 350 years. Zinc concentrations leached from the profile remained equal to initial concentrations for about 280 years, before declining and disappearing altogether after about 450 years (Figure 3.5B).

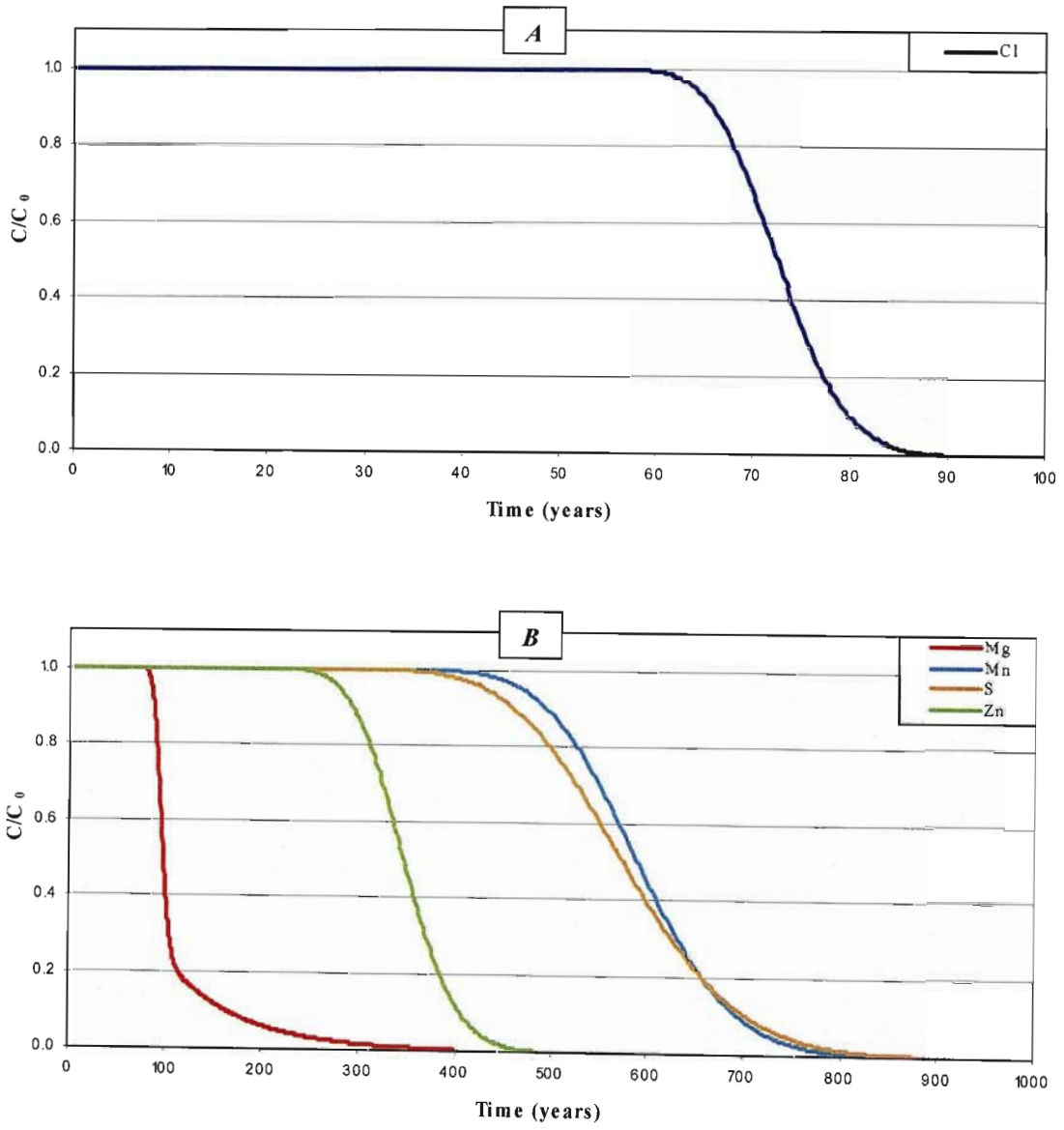

Figure 3.5 Predicted long-term release of (A) chloride, and (B) magnesium, manganese, sulfur and zinc from the Pering tailings impoundment.

In order to determine the long-term risk to groundwater, it is necessary to relate actual concentrations which may be released from the tailings impoundment to drinking water standards. Relative concentrations are given in Figure 3.5, these were obtained from the direct simulations, which used the above defined initial concentrations (see Appendix 8, Figures A8.1 and A8.2). According to these simulations, Mn and S concentrations only started declining after about 400 years and continued to do so until they were completely removed from the impoundment after about 800 years. During this time concentrations were above the SABS 241 (1999) drinking water guidelines for approximately 720 years. Magnesium and Zn concentrations exceeded recommended guidelines for 200 and 300 years, respectively. It is thus evident that S and Mn will most likely pose a long-term threat to groundwater, whereas the expected lifespan for Mg and Zn contamination will be somewhat shorter.

Modelling the movement of solutes in the Pering tailings with the CDE has highlighted some important trends. However, it must be noted that the above trends are based on a number of assumptions, which may not hold true in the field. One of the most limiting assumptions is that of continuous saturated flow, as this is seldom achieved in the field for any significant length of time. Much of the Pering tailings impoundment was found to be saturated (see Chapter 4), thus saturated flow is realistic, but not on a continual basis. The parameters are also based on an idealised BTC determined under conditions of continuous saturated flow. Intermittent cycles of wetting and drying in the field could cause variations in mineral weathering and sulfide oxidation (Kovács *et al.*, 2006). Such variations may create effects which could not be simulated, and therefore accounted for, in a continuous flow laboratory column. These are the two main limitations which may cause the predicted rates in Figure 3.5 to deviate from reality. More realistic predictions could be achieved if variations in pore-water velocity were taken into account. This would require more complex modelling, beyond the scope of *CXTFIT*, in which solute movement is modelled in conjunction with an accurate water balance of the tailings.

3.4.2 Element release under intermittent flow

3.4.2.1 Treatment 1: Leaching with TCLP-2 solution

Long-term leaching with TCLP-2 solution was used to estimate element mobilisation in a worst case scenario.

pH buffering

The tailings material has a significant ability to buffer acidity. Throughout the 44 weeks of leaching the pH of the effluent did not fall below pH 5.93 (Appendix 7). This is highly favourable as heavy metal mobility is greatly enhanced under acidic conditions (Bain *et al.*, 2000; Shu *et al.*, 2001; Moncur *et al.*, 2005; Malmström *et al.*, 2006). Two distinct buffering phases were observed in Reps 1 and 2 (Figure 3.6), the first at around pH 6.80 to 7.00, which dropped off after about 19 pore volumes. The second phase stabilised at about pH 6.00 and was maintained for the remainder of the experiment. Geochemical analysis with *MINTEQ* was unable to identify any secondary minerals which may have been responsible for buffering the pore-water during these two phases. It is therefore expected, that buffering throughout the experiment was the result of kinetically limited dolomite dissolution (all effluent samples were predicted to be undersaturated with respect to this mineral). The two buffering phases could then be attributed to the initial rapid dissolution of fine dolomite particles, followed by the slower dissolution of larger grains. Greater buffering in Rep 3 is thus likely to have been due to the presence of finer granules in this column.

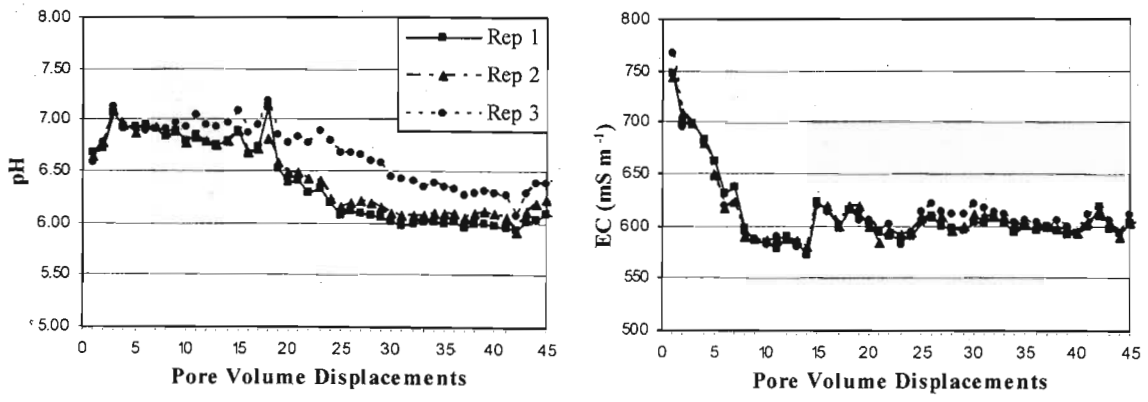

Figure 3.6 pH and EC of the effluent which was leached from three columns receiving 1 pore volume of TCLP-2 solution on a weekly basis (1 pore volume = 93.7 cm^3).

Calcium concentrations increased over the first 3 pore volumes up to about 1700 mg l^{-1}, before declining rapidly over the next 9 pore volumes to around 900 mg l^{-1}. After this point Ca dissolution continued at more or less the same level, with a few random peaks as a result of incongruent dissolution (Figure 3.7). According to *MINTEQ* calculations, the release of Ca was controlled by the dissolution of gypsum for the first five pore volumes. This is supported by the fact that high concentrations of S were mobilised over this period. After this point, the release of Ca is expected to have been controlled by dolomite dissolution. Magnesium concentrations released into solution over the first 9 pore volumes were consistent, ranging from about 450 to 550 mg l^{-1}. During this phase it is expected that all soluble Mg was flushed from the column. Following this the release of Mg was random and attributed to incongruent dolomite dissolution (Figure 3.7).

Mobilisation of metals

Leaching the Pering tailings with the TCLP-2 solution mobilised very high concentrations of Zn and Mn (Figure 3.7). Zinc concentrations tended to decrease over time from a maximum of 1228 mg l^{-1} to a minimum of 25.7 mg l^{-1} at the end of leaching (Appendix 7). In contrast the amount of Mn released into solution increased over time, with the concentration starting at about 40 mg l^{-1} and reaching a maximum of 177 mg l^{-1} (Rep 1, Figure 3.7). The release of Fe and Cu into solution was very limited, with concentrations remaining below 0.12 and 0.40 mg l^{-1}, respectively. Likewise only very low concentrations of Ba, Cd, Co, Cr, Ni, Se and V were mobilised (Appendix 7).

Lead concentrations decreased consistently, from approximately 7 mg l^{-1} to about 1 mg l^{-1}, for the first 14 pore volumes (Figure 3.7). After this point concentrations began to increase, but with no consistent trend between the three columns. In the initial phase the more mobile Pb was flushed out of the column, while in the latter phase increases were most likely the consequence of more severe mineral dissolution which coincided with the drop in pH. For example, Rep 3 experienced a less severe drop in pH than the other two columns (Figure 3.6) and therefore lower concentrations of Pb, Zn, Mn, Mg and Ca were mobilised from this column after about the 15th pore volume. In most instances, element release from the columns followed very similar trends for about the first 15 pore volumes. After this point, and approximately coinciding with the drop in pH, element release increased and became more random as desorption and mineral dissolution increased.

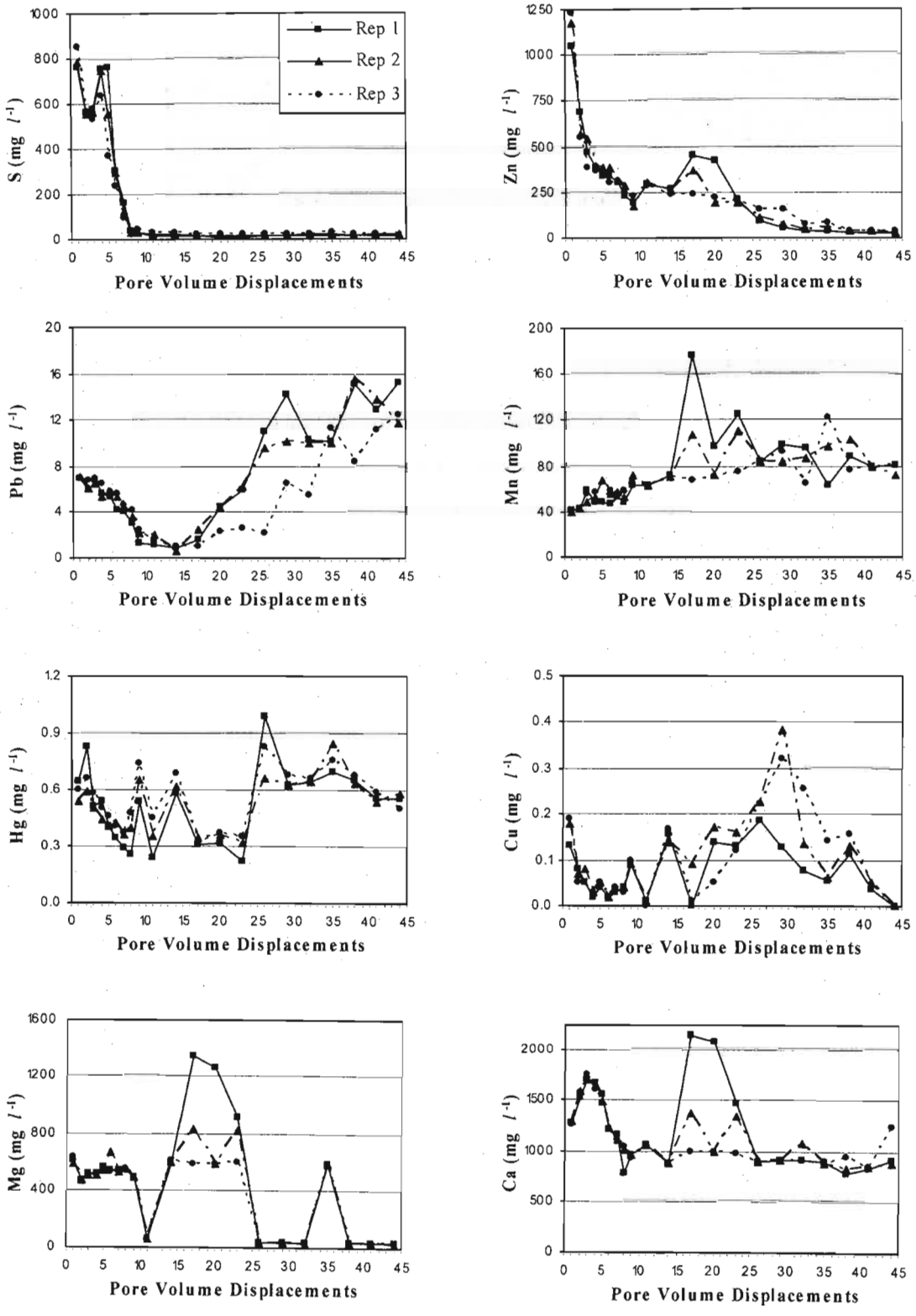

Figure 3.7 Concentrations of S, Zn, Pb, Mn, Hg, Cu, Mg and Ca mobilised from the Pering tailings as a result of weekly leaching with 1 pore volume of TCLP-2 solution (1 pore volume = 93.7 cm^3).

Jurjovec *et al.* (2002) and Malmström *et al.* (2006) both found that Zn was mobile in tailings, even at neutral pH, while Pb only became mobile at lower pH (≤ 4) and Cu remained associated with solid phases even at very low pH (≤ 1.3). In the case of soils Voegelin *et al.* (2003) found that acid inputs mobilised Zn long before the neutralising capacity of the soil was depleted, while Pb and Cu were only mobilised once the leachate itself became acidic. These findings are consistent with the current study of the Pering tailings, which have shown that Zn is much more mobile in comparison to either Cu or Pb. Given the high buffering capacity of the tailings material and the fact that acid conditions are unlikely to develop (see Section 2.5.5) it is expected that the release of Cu and Pb will always be inhibited. As a result of its greater mobility Zn, out of the three elements, will most certainly pose the greatest threat to groundwater.

Evidence of Hg contamination was also found in the column effluent. Mercury is often geochemically associated with sulfide minerals such as pyrite and sphalerite, where it typically occurs as cinnabar (HgS, Alloway, 1990). Its presence at Pering can therefore be expected, although it was not detected in the XRD analysis (Section 2.5.2) or in the SEM/EDAX observations (Appendix 1). After the second pore volume, Hg concentrations declined until about the seventh pore volume, after which point concentrations increased inconsistently in all three columns. Mercury in its various forms is known to be highly toxic (DWAF, 1996a; WHO, 1996) and thus guideline limits considered safe for drinking water are very low (Appendix 2). The range of Hg concentrations in the effluent, 0.22 to 0.99 mg l^{-1}, exceeded these limits considerably.

3.4.2.2 Treatment 2 and 3: Leaching with distilled water

Leaching with distilled water was aimed at simulating the oxidative potential of rainfall. In general, however, this is only applicable for the upper 200 cm or so of the impoundment, below this most tailings are reported to be devoid of free oxygen (Blowes *et al.*, 1998; McGregor *et al.*, 1998; Moncur *et al.*, 2005). It was thus also necessary to examine element mobility under conditions of reduced oxygen. Leaching under oxygen free conditions caused slight decreases in the E_h of the effluent (Figure 3.8). In both treatments however, the E_h was within aerobic limits (E_h > 350 mV, McBride, 1994). Throughout the experiment the pH remained close to neutrality. The initial EC was relatively low at about 280 mS m^{-1} and over time it declined consistently as soluble components were flushed out.

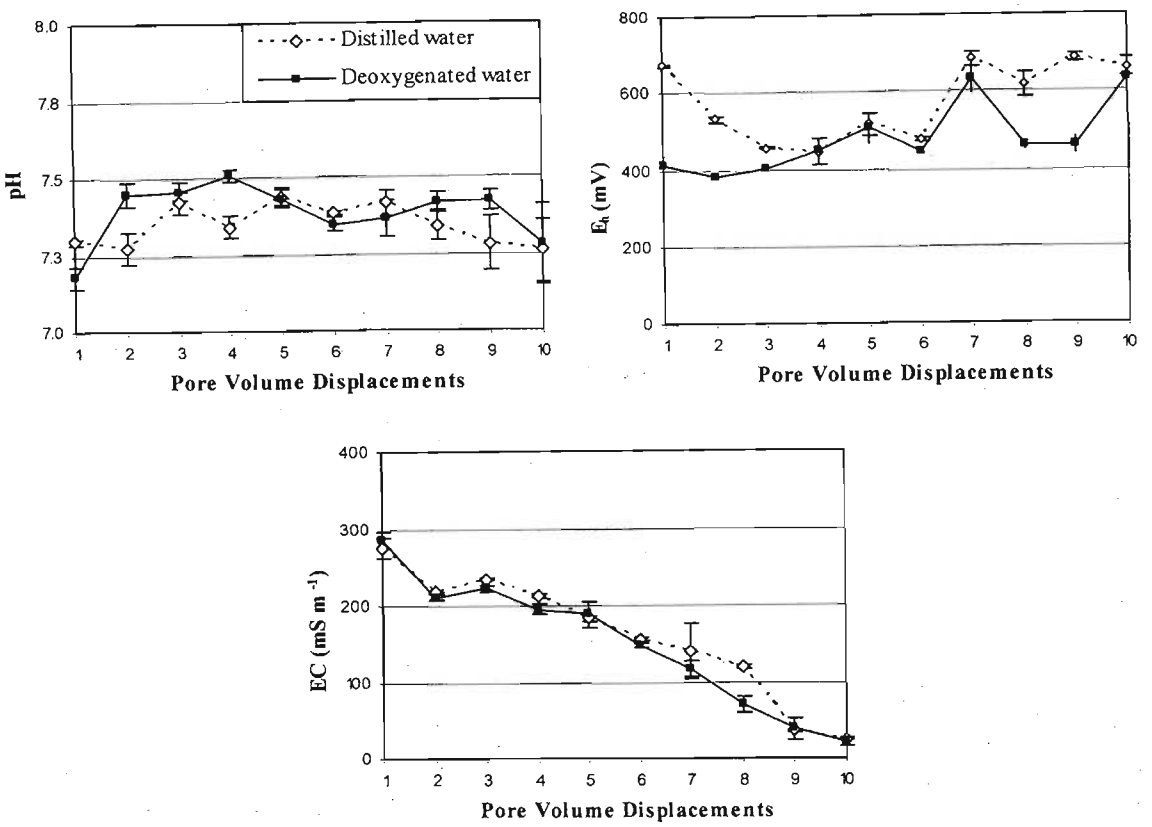

Figure 3.8 pH, EC and E_h of the effluent after leaching the Pering tailings with distilled water and deoxygenated distilled water (bar lines represent ±SD, n = 3; 1 pore volume = 91.3 cm^3).

Mobilisation of calcium, magnesium and sulfur

Initial flushing of the TT material with 1 pore volume of solution caused 714 mg l^{-1} and 766 mg l^{-1} of S to be released from the distilled water and the deoxygenated distilled water columns, respectively (Figure 3.9; Appendix 7). Further leaching caused the S concentrations to decline slowly over 10 weeks. These concentrations are considerably lower than those mobilised from the finer TN material in the continuous leaching column experiment. This is most likely the result of the experimental setup. In these experiments 1 pore volume of fresh solution was flushed through the column on a weekly basis and the elemental composition of the displaced pore solution was then measured. The Cl^- BTC showed that the tailings can cause up to a 50% dilution of the wetting front (i.e. after leaching the Cl^- saturated column with 1 pore volume of distilled water only 50% of the Cl^- had been displaced; Appendix 7). Thus, flushing the column with an entire pore volume in this experiment would have caused approximately a 50% dilution in comparison to the

initial concentrations released from the continuous flow experiment. In addition, Mihaljevič *et al.* (2004) and Salmon and Malmström (2006) showed that in both batch and column experiments, fine grained tailings were more reactive than their coarse grained counterparts. This could be a further explanation for the reduced S concentrations. However, this is expected to have had a limited effect because of the week long equilibration time which would have counteracted the limitations of the kinetic reactions in the previous experiment.

Magnesium was washed from the columns very rapidly (Figure 3.9), which would suggest that only a small amount of soluble Mg was present in the TT material. Calcium reached a maximum concentration of 585 mg l^{-1} in the second pore volume and then began to decline slowly over the remaining 10 weeks. Calcium concentrations were above the recommended target range for drinking water given by the Department of Water Affairs and Forestry (DWAF, 1996a) for the first 9 pore volumes. Magnesium exceeded these guidelines for only 2 pore volumes.

Mobilisation of metals

Despite the dilution factor, or possible influences of particle size, concentrations of Fe, Mn, Pb and Zn mobilised from the TT material under intermittent flow were greater than those mobilised from the TN sample under continuous flow. In general these elements were released at similar rates in both the distilled water and the deoxygenated distilled water treatments, only Zn showed marked variation. The deoxygenated water caused lower concentrations of Zn to be mobilised (Figure 3.9). This may be due to the lack of free oxygen which helped to stabilise the sphalerite minerals.

Manganese and Fe concentrations released from the deoxygenated columns tended to be slightly elevated in comparison to the aerated columns. This often occurs under conditions of reduced oxygen where Mn/Fe oxides are reduced and in the process dissolve to release Mn^{2+} and Fe^{2+} into solution. Metals which may have previously been bound to the oxide minerals will then also be mobilised (McBride, 1994; Bartlett, 1999). In both columns Mn and Hg concentrations were well above guideline limits for the entire leaching period (Appendix 2).

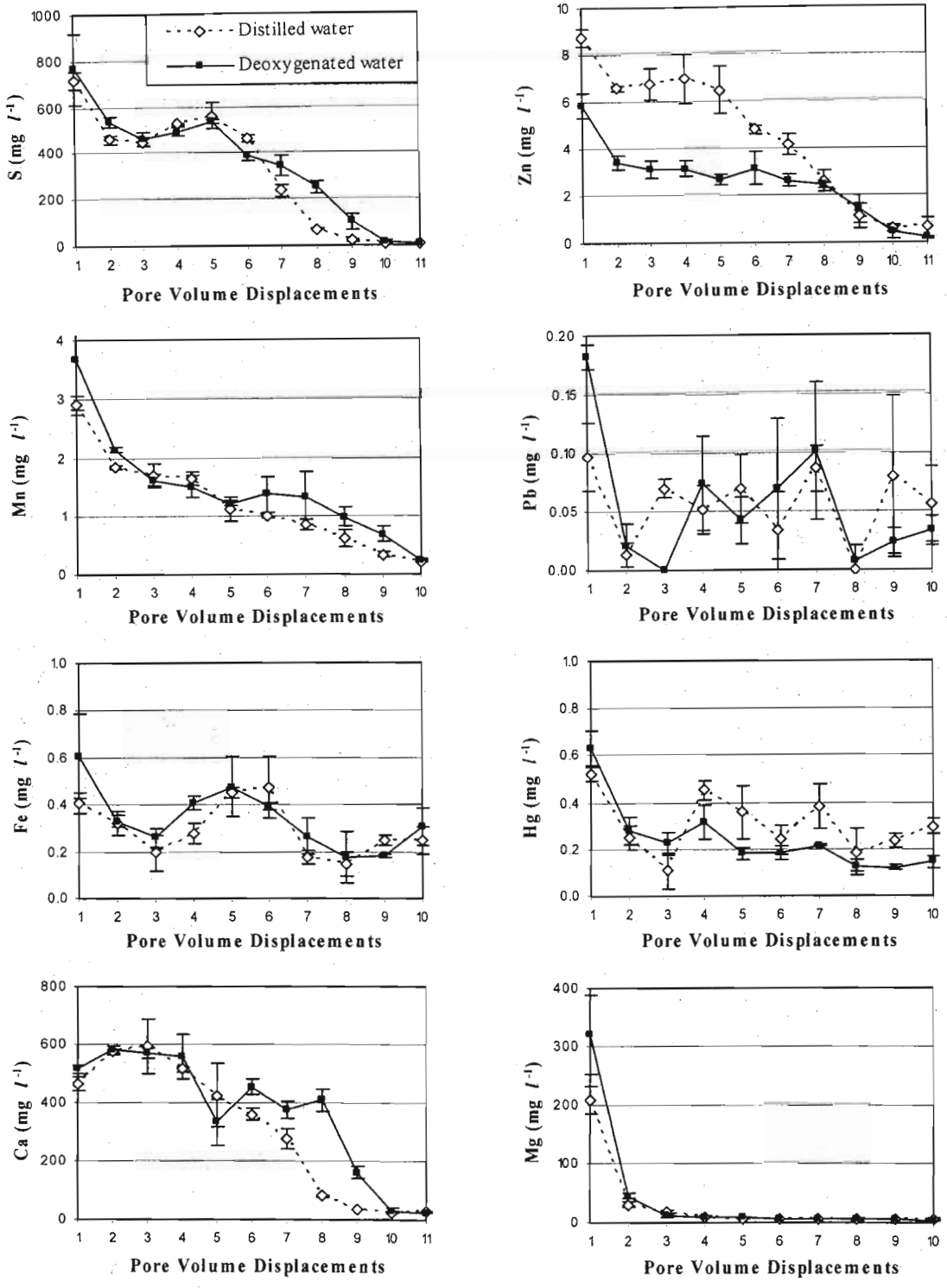

Figure 3.9 Concentrations of S, Zn, Mn, Pb, Fe, Hg, Ca and Mg leached from the Pering tailings using distilled water and deoxygenated distilled water (bar lines represent ±SD, n = 3; 1 pore volume = 91.3 cm^3).

3.5 Conclusions

A number of leaching column experiments were undertaken to assess the movement of contaminants within the Pering tailings and to predict the possibility of groundwater contamination which may arise from water percolation through the impoundment. The column studies found that Mg, Mn, Hg, S and Zn will most likely pose the greatest threat to groundwater quality. In many instances the concentration of these elements in the column effluent was significantly greater than recommended South African water quality guidelines.

Solute transport modelling with *CXTFIT* predicted that contamination from SO_4^{2-} and Mn could persist for a very long period of time (±700 years), whereas elevated levels of Mg and Zn will most likely be released for a shorter duration (< 300 years). In comparison to field based observations, Malmström *et al.* (2006) found that their laboratory based leaching columns overestimated the rate of SO_4^{2-} release (i.e. sulfide oxidation) by a factor of approximately 10. In light of this and the lack of continuous leaching in the field it is expected that these predictions underestimate the actual time span over which contamination is likely to be released in the field.

CHAPTER 4

FIELD BASED INVESTIGATION OF THE PERING MINE TAILINGS IMPOUNDMENT

4.1 Introduction

It is widely accepted that the disposal of sulfide containing mine tailings may be a precursor to a wide array of both local and regional environmental problems (Dudka and Adriano, 1997; Rösner and van Schalkwyk, 2000; Naicker *et al.*, 2003; Heyden and New, 2004; España *et al.*, 2005). Incomplete extraction of galena, sphalerite and pyrite from the ore mined at Pering has resulted in traces of these minerals being present within the tailings material deposited onsite. As a result of this metal sulfide load in the tailings, concerns about groundwater contamination have been raised. This is of concern because of the arid environment in which Pering is located, where local inhabitants and livestock are almost solely dependent on groundwater reserves for their survival. In light of this, it was necessary to accurately quantify the extent to which the tailings impoundment may be affecting groundwater quality. The previous laboratory studies have helped to identify the scope of the problem, however, in order to gain full insight into its complexity and the actual field based risks it is necessary to relate these studies to field observations.

Drill-rigs have been widely used to collect samples from multiple depths within abandoned tailings impoundments (Lin, 1997; Blowes *et al.*, 1998; McGregor *et al.*, 1998; Ljungberg and Öhlander, 2001; Moncur *et al.*, 2005). By this means it is possible to study the internal geochemical and mineralogical properties and to ascertain the nature of the drainage water leaching out of the impoundment. Tailings and pore-water samples were gathered from various locations within the Pering Mine tailings impoundment during July 2005. It is the objective of this chapter to provide a basic hydrophysical and geochemical overview of the impoundment, and to highlight any potential risks for groundwater contamination based on measured pore-water concentrations.

4.2 Sample collection and field analyses

Samples were collected from within the tailings impoundment by means of a portable drill-rig. The drill shaft was contained inside a rigid steel sleeve (Figure 4.1), which enabled samples to be brought up from multiple depths within the impoundment with minimal

cross contamination. Samples were collected from eight boreholes (Figure 4.2), which were strategically positioned to best represent the entire width, depth and breadth of the impoundment.

Figure 4.1 Steel cased coring system used to collect samples from the Pering tailings impoundment. The insertion of the shaft into the tailings using a drill-rig is also shown.

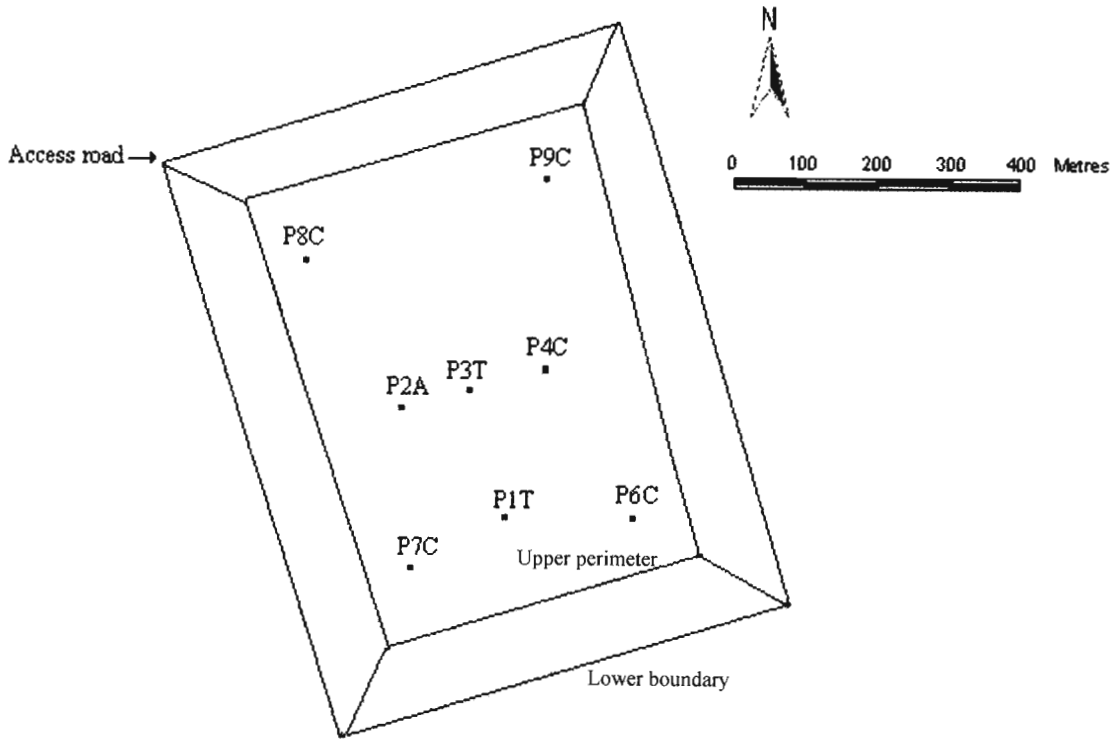

Figure 4.2 Aerial view of the Pering tailings impoundment, showing the location of the eight boreholes (P1T; P2A; P3T; P4C; P6C; P7C; P8C; P9C) sampled in July 2005. The horizontal dimensions of the tailings dam and all borehole positions were determined with a Garmin Etrex Vista GPS (Appendix 4).

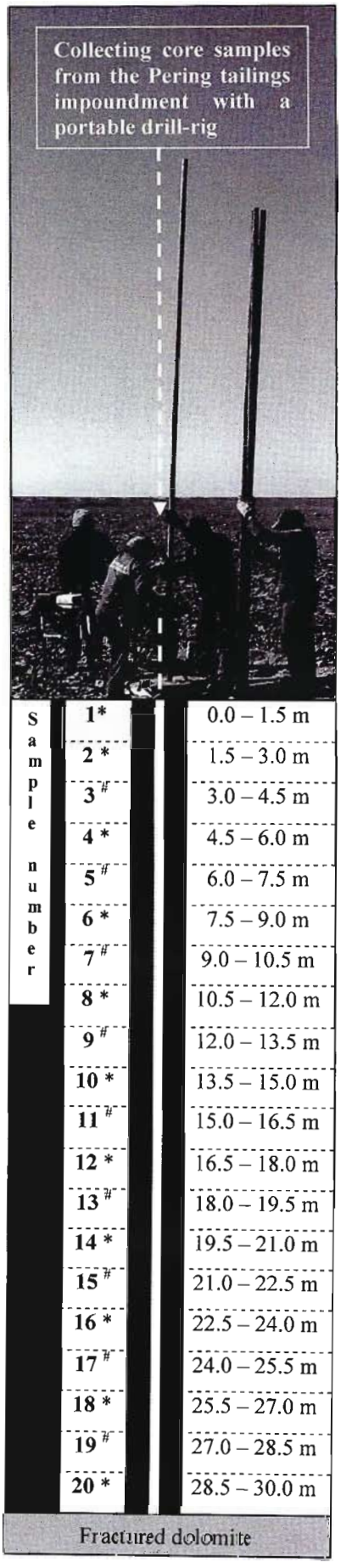

Figure 4.3 Borehole drilling.

The drilling setup is demonstrated in Figure 4.3. The long steel shafts, in which the rotating drill bit was contained, were pushed manually into the tailings. The combined downward force and drilling action caused the tailings to be forced into the steel sleeve shown in Figure 4.1. The entire 30 m depth of the impoundment was sampled by drilling successive increments of 1.5 m. After each increment the steel shafts were brought to the surface and the tailings removed, this material was combined and treated as a single sample.

A total of 20 samples were collected to represent the depth of the impoundment. All samples are thus described by the borehole and depth from which they were taken. For example a notation of P1T-3 indicates that the sample was taken from borehole P1T (Figure 4.2) and included the tailings material collected from a depth of 3.0 to 4.5 m below the surface of the impoundment (Figure 4.3).

All 20 samples were collected from boreholes P1T and P3T, while only samples 2, 8, 15 and 19 were taken back from the field to represent the remaining boreholes. While drilling boreholes P1T and P3T the first sample and all even numbered samples were packaged immediately as they were brought up from the borehole (see samples designated with * in Figure 4.3). These samples were stored in double lined plastic bags, from which the oxygen had been removed by displacement with nitrogen gas. The sealed samples were then transported to the University of KwaZulu-Natal for analysis.

The remaining odd numbered samples, designated by # in Figure 4.3, collected from boreholes P1T and P3T

were treated in the following way: small sub-samples were taken immediately as the tailings was brought to the surface for the measurement of pH and redox (E_h). This was done using a battery powered Radiometer PHM210 pH meter and a Radiometer CDM83 redox meter with a Ag/AgCl redox probe. Measurements were made in deoxygenated distilled water using a 1:2.5 soil to solution ratio, which was corrected for the water content of the tailings, assumed to be 0.25 g g^{-1} at saturation (this estimate was based on prior water content analysis of the TT material). The pore-water in equilibrium with these samples was extracted at the same time by vacuum suction (Sposito, 1989). This consisted of placing the moist tailings in a Büchner funnel, to which a 100 m*l* glass bottle had been tightly sealed and a suction applied to an outlet tube. The tailings were placed on top of Whatman no. 41 filter paper and firmly compacted to minimise the ingress of air. The vacuum caused the pore-water to be drawn through the filter paper, from where it was able to drip down into the glass bottle below. Approximately 100 m*l* of liquid was gathered from each sample, which was then stored at 4 °C for later analysis by ICP (Varian Liberty X150). After vacuum extraction the remaining unutilised wet bulk samples were stored under nitrogen gas in the same manner as mentioned above. All pore-water solutions were analysed for Al, Ca, Cd, Cu, Fe, Hg, K, Mg, Mn, Na, Ni, Pb, S, Sr and Zn. Chloride concentrations were determined by titration with 0.005 *N* $AgNO_3$, using a 5% potassium chromate solution as an indicator (Soil Salinity Laboratory Staff, 1954).

By the same means the changes in pH and E_h down boreholes P2A, P4C, P6C, P7C, P8C and P9C were determined, only this time by analysis of samples 3, 4, 9, 10, 11, 16, 17 and 20. The equilibrium pore-water of these tailings samples was also separated off. This, however, was not possible for those samples taken from the two boreholes located in the extreme southwest and northwest corners of the impoundment, P7C and P8C, respectively, as these profiles contained insufficient moisture for vacuum extraction. Analysis of these dry profiles was completed by means of saturated pastes.

4.3 Laboratory analyses

The samples collected in the field were packaged in water and airtight bags, which allowed for the water content of the tailings material to be measured once back in the laboratory. The water content of all samples was determined gravimetrically before any other analyses

were undertaken. This was done in triplicate by taking sub-samples of approximately 10 g each and measuring the gravimetric water loss after 24 hours of drying at 105 °C.

Element availability under saturated conditions was determined for all borehole samples by means of saturated pastes (Soil Salinity Laboratory Staff, 1954). In each case this was done by weighing out approximately 600 g of field moist tailings material into a glass mixing jar, and then slowly adding distilled water while stirring vigorously until a smooth paste was formed. Following this, the glass jar was covered with a plastic lid and allowed to stand for 24 hours at an ambient air temperature of 23 °C. After this equilibration period, the paste was re-stirred and two sub-samples were taken for the measurement of the gravimetric water content. The liquid was extracted from the paste by vacuum extraction through Whatman no. 41 filter paper. The pH and electrical conductivity (EC) of the solution was measured and then stored at 4 °C for analysis of Al, Ca, Cd, Cu, Fe, Hg, K, Mg, Mn, Na, Ni, Pb, S, Sr and Zn by ICP (Varian Liberty X150).

4.4 Results and discussion

4.4.1 Hydrophysical properties of the tailings

Milling of the ore for froth flotation has produced very fine tailings. Particle size analysis of tailings collected from all boreholes identified the material as having a silt loam texture (Soil Classification Working Group, 1991; Appendix 5). Slight variations in particle size were observed across the impoundment. This is due to coarser particles settling out of the tailings slurry first, close to the point of discharge, while finer particles were transported further away (Sidle *et al.*, 1991; Blowes *et al.*, 1998; McGregor *et al.*, 1998). The tailings in boreholes P2A, P7C and P8C on the western side of the impoundment tended to be slightly coarser than the material in the central and eastern part of the impoundment (boreholes P1T, P3T, P4C, P6C and P9C). This variation in particle size through the impoundment is expected to be associated with differences in bulk density, saturated hydraulic conductivity and water retention characteristics (Wu *et al.*, 1990; Crawford *et al.*, 1995; Kern, 1995; Blowes *et al.*, 1998; McGregor *et al.*, 1998). This was substantiated for the surface of the impoundment by measuring the hydrophysical properties of five undisturbed cores (see Appendix 6). The tailings were shown to have a higher hydraulic

conductivity, lower bulk density and greater water storage capacity in the vicinity of the more coarsely grained P8C borehole in comparison to the finer grained P3T borehole.

The bulk density at the surface of borehole P8C was measured to be 1444 kg m^{-3}, while around borehole P3T the average of three cores was 1708 kg m^{-3}. This difference caused a range in the calculated porosities of between 0.388 and 0.499 m^3 m^{-3} (Appendix 6). According to the limits given by Klute and Dirksen (1986), the saturated hydraulic conductivity ranged from low (3.712 cm $hour^{-1}$, Core 1 taken from P8C) to highly impermeable (0.018 cm $hour^{-1}$, Core 5 taken from P3T; Appendix 6). This range is consistent with those reported for other abandoned tailings impoundments (Blowes *et al.*, 1998; Moncur *et al.*, 2005; Malmström *et al.*, 2006).

The low hydraulic conductivity and fineness of the tailings would promote surface runoff and evaporation. However, since modification of the impoundment in September 2004, lateral runoff of water is prevented by the retainer walls and it is highly likely that surface evaporation has been substantially reduced by the rock cladding (Hanks and Woodruff, 1958; Adams, 1966; Jury and Bellantuoni, 1976; Groenevelt *et al.*, 1989; Kemper *et al.*, 1994). Thus, it is expected that greater volumes of water will now be infiltrating into the impoundment. This will have an impact on the geochemistry of the tailings, but since sampling occurred only 10 months after the modifications the full effects of this are not expected to be visible within the current data. Future observations will have to be undertaken to elucidate possible changes.

4.4.2 Borehole profile analysis

The quantitative geochemical data presented here provides a 'snapshot in time', an insight into the chemical nature of the tailings two and a half years after closure. It does not provide a final definitive answer, as weathering and oxidation will continue for decades and thus the nature of the leaching pore-water will most likely change. Based on the data presented here and in the previous chapter an attempt will be made to predict these potential changes. Particular focus, however, will be given to the possible risk of groundwater contamination which may arise as a result of water percolation through the metal-rich tailings.

Field observations of the prevailing chemical conditions within the tailings impoundment and subsequent analysis of the pore-water has allowed the current geochemical conditions to be accurately determined. Vacuum extraction was only able to remove pore-water from depths below 1.5 m and from the wetter borehole (i.e. P1T, P2A, P3T, P4C, P6C and P9C), thus discussions in this section are limited to these profiles. Boreholes P1T and P3T were sampled most intensely and they therefore provide the best detailed overview of the conditions down the depth of the tailings impoundment. These two profiles were also found to be representative of the central region of the impoundment. The remaining boreholes were more sparsely sampled, but they nevertheless also provide valuable data for other sections of the impoundment.

A number of general trends, some more strongly expressed than others, were found to extend across the length and breadth of the impoundment. Trends in pH, E_h and EC have been detailed for the individual boreholes in Figure 4.4.

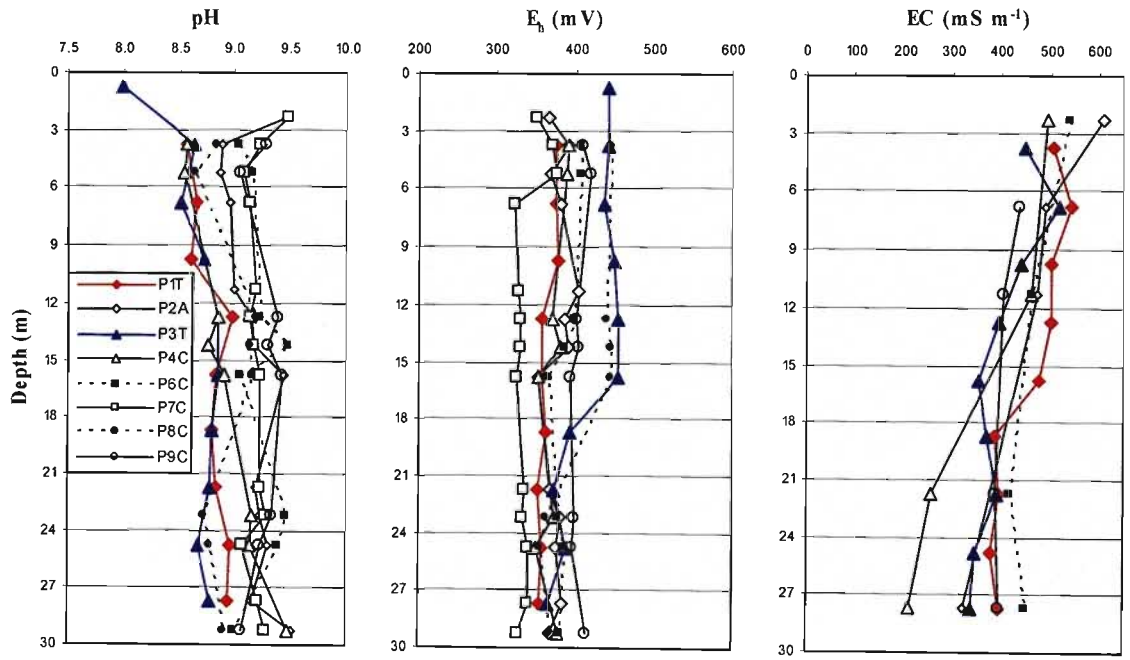

Figure 4.4 Changes in pH, redox potential (E_h) and electrical conductivity (EC) with increasing depth below the surface of the Pering tailings impoundment.

4.4.2.1 pH trends

It is not uncommon for the upper layers of abandoned mine tailings to be highly acidic, especially in tailings which contain limited carbonate minerals (e.g. Lin, 1997; McGregor *et al.*, 1998; Bain *et al.*, 2000; Moncur *et al.*, 2005). At the time of sampling no obviously defined low pH zone had developed in the tailings at Pering Mine (Figure 4.4). The pH recorded in the field ranged between 8.50 and 9.50, with only sample P3T-1 falling outside of this range at pH 7.98 (Appendix 9). Given the proportion of dolomite in relation to sulfide minerals (Section 2.5.5) and the proven long-term buffering capacity of the tailings (Section 3.4.2.1), it is expected that the pH of the impoundment will remain alkaline. Neutral pH favours precipitation and sorption of metal cations (Alloway, 1990; McBride, 1994; Badawy *et al.*, 2002; Dorronsoro *et al.*, 2002; Rouff *et al.*, 2005), thus it is likely that the long term immobilisation of metals will be favoured.

4.4.2.2 E_h trends

Field based measurements of E_h found that most of the impoundment was within aerobic limits. Redox measurements fell within a narrow range of +323 to +454 mV (Figure 4.4; Appendix 9). It must be noted that the measurement of soil redox potential in the field can have quite considerable errors, which makes interpretation of absolute values difficult (see McBride, 1994 for a detailed description on possible errors in measuring E_h with an electrode). Nevertheless the values obtained are sufficiently accurate to enable general interpretations about the stability of sulfide minerals to be made (see Section 4.4.2.5).

Lower redox potentials were generally found at the base of the profile where conditions would be expected to be somewhat reduced in relation to the upper layers. According to McBride (1994), an E_h of about 350 mV typically defines the lower end of aerobic conditions in soil solutions. It would therefore appear that oxygen was trapped within the tailings during deposition. This oxygen will act as an electron acceptor that will fuel sulfide oxidation until such time as it is completely utilised. After this point, if present, Mn^{3+} or Fe^{3+} may begin to function as the oxidising agents.

Scanning electron microscopy (SEM) revealed that sulfide minerals were still present at the base of the impoundment (Appendix 1). There is some uncertainty as to whether the

oxidising potential of the tailings impoundment is sufficient to oxidise all available sulfide minerals or if, at some point, the availability of aqueous oxidising species will become a limiting factor. If this occurs it is likely that oxidation within the impoundment will be greatly reduced, because the low air-permeability and air-filled porosity of the material will severely limit the penetration of atmospheric oxygen to any significant depth (Appendix 6). It is expected, however, that the depletion of the oxygen and other oxidising species already in the tailings will be very slow. Even at the base of the impoundment, which had been isolated from the atmosphere for approximately 19 years at the time of sampling, the E_h was aerobic (average of 369 mV for the last sample in all boreholes).

4.4.2.3 EC trends

The electrical conductivity (EC) of the pore-water decreased with depth in all profiles. A maximum of 607 mS m^{-1} was recorded near the surface of the tailings (P2A-2) and a minimum of 212 mS m^{-1} at the base of borehole P4C (Figure 4.4; Appendix 9). This decrease is directly linked to the simultaneous decrease in the concentration of all or a few of the base cations (Ca, K, Mg and Na) in each of the boreholes (Appendix 9). Salinisation has most likely been the cause of the higher elemental concentrations in the upper layers of the impoundment.

Salinisation frequently occurs in arid environments where a net upward movement of water occurs in soils due to high evaporative demand. Water lost from the surface of the soil is replaced by capillary water fed from lower in the profile. This water generally brings with it dissolved salts and metals which precipitate out as evaporation occurs. Shu *et al.* (2001) observed this phenomenon occurring on Pb/Zn mine tailings in China. Salt precipitates on the bare surfaces of the Pering tailings impoundment suggested that this process was also occurring at Pering Mine (Appendix 1). Precipitates, however, were only found in very localised areas where the rock cladding was very thin or absent (no precipitates were observed under the rock cladding). This is of some significance as it indicates that prior to the rock cladding there must have been a net upward movement of water across the entire surface of the impoundment. This would explain the increase in the EC of the pore-water towards the surface in all boreholes. With the current rock cladding this trend may begin to be reversed as increased infiltration and reduced evaporation cause the salts to be washed downwards.

4.4.2.4 Moisture regime

Despite the arid environment, and the fact that Pering Mine had been out of operation for two and a half years at the time of sampling, much of the impoundment was found to be at or close to saturation. The gravimetric water content of all borehole samples is shown in Figure 4.5. At saturation the gravimetric water content of the tailings was found to range from a low of 0.227 kg kg^{-1} in the very fine grained material around borehole P3T to a high of 0.365 kg kg^{-1} in the more coarsely grained material from borehole P8C (Appendix 6). Based on this it can be seen that boreholes P1T, P3T and P4C located in the central region of the impoundment were at or very close to saturation, while the boreholes closer to the outer edges were somewhat drier.

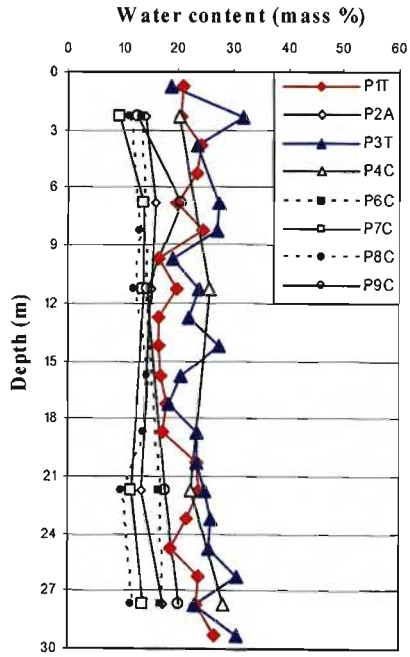

Figure 4.5 Changes in the gravimetric water content of the tailings with increasing depth below the surface of the impoundment.

A number of changes were observed in the water content of the tailings from layer to layer in profiles P1T and P3T (Figure 4.5). This is less evident in the other boreholes as fewer samples were gathered from these profiles. The marked changes in water content are in accordance with field observations made while drilling and are probably the result of differences in the water holding capacity of each layer based on variations in particle size (Appendix 5) and bulk density. These zones of increased moisture may also be the result of

water accumulating above highly compacted impervious layers. Field based investigations, using for example piezometer-response tests or tracer tests, will have to be undertaken in order to identify such layers. The presence of impervious layers could control the rate at which infiltrating water may be lost from the base of the impoundment and thereby could act to protect groundwater reserves if they were found to be extensive.

4.4.2.5 Sulfur oxidation and speciation

The oxidation of the metal sulfide minerals within the Pering tailings has released high concentrations of S into the pore-water of the impoundment, especially in the upper layers. Changes in the concentration of S and various heavy metals down the individual boreholes can be seen in Figure 4.6. A maximum S concentration of 1221 mg l^{-1} was recorded in borehole P2A at a depth of 2.25 m (Appendix 9). Concentrations were found to decrease with increasing depth below the surface of the tailings, declining to an average of 558 mg l^{-1} in the last sample taken from each borehole (sample 19). No sudden decrease in the sulfur content of the pore-water was observed, as has been reported for tailings systems in more advanced stages of weathering (e.g. McGregor *et al.*, 1998; Moncur *et al.*, 2005). This lack of a clearly defined oxidation zone is most likely due to the youthfulness of the tailings (sampling occurred only two and a half years after mine closure). During operation the formation of this zone would have been prevented by the continuous leaching of water through the impoundment. Given time, increased oxidation closer to the surface could release greater concentrations of S into the pore-water of the upper layers. Based on the elevated redox conditions throughout the impoundment it is also possible that sulfide oxidation is occurring at all depths and therefore preventing the formation of an obvious oxidation zone.

The sulfur content of the pore-water was analysed by ICP for total S. In order to assess the environmental significance of the recorded total sulfur it is necessary to understand its speciation within the tailings. E_h – pH diagrams have been used to assess the stability of minerals in mine tailings (Mihaljevič *et al.*, 2004; Bednar *et al.*, 2005). They offer a useful means whereby, according to the prevailing E_h and pH conditions, the stability of certain aqueous species or solid phases can be determined.

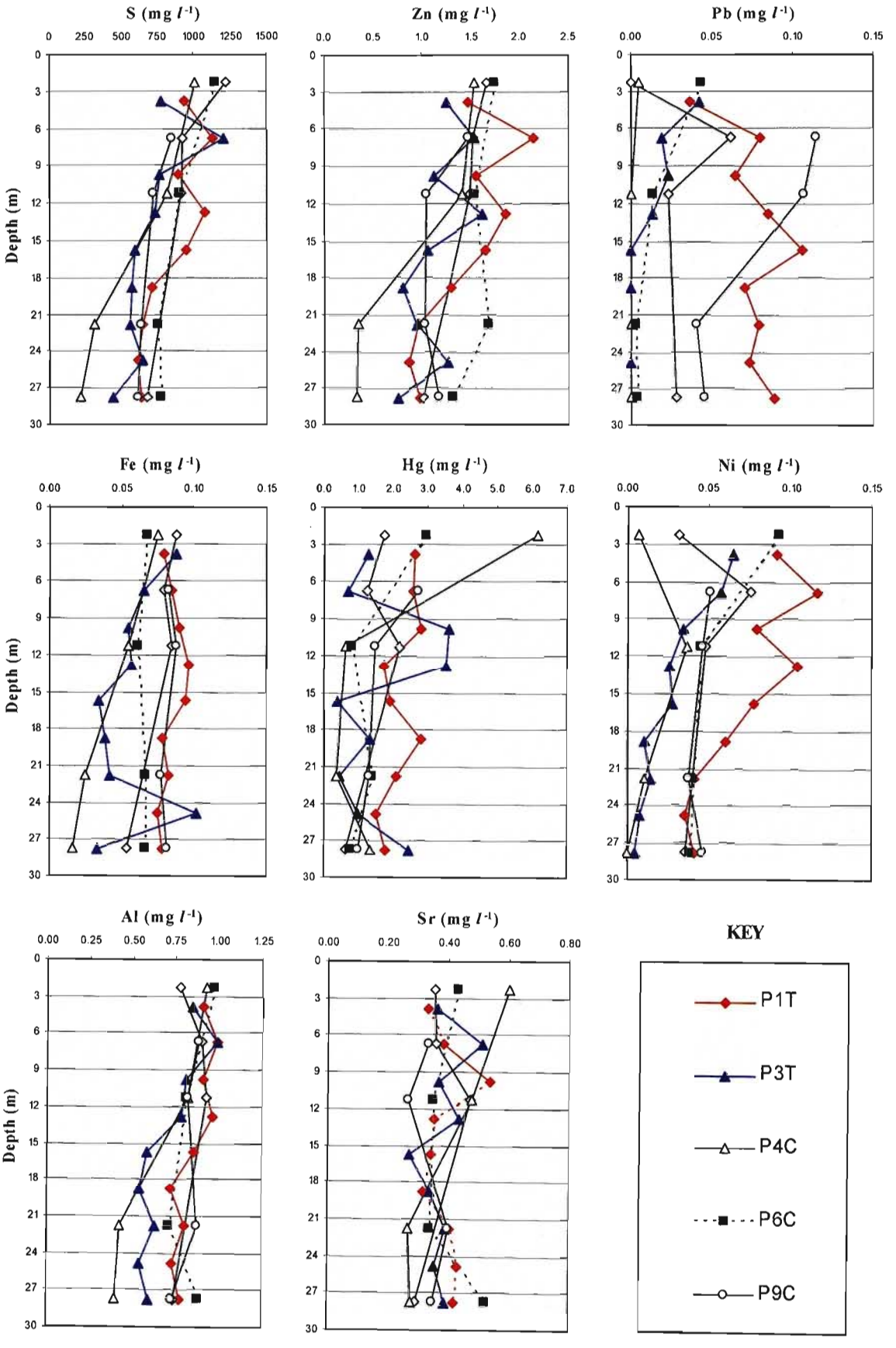

Figure 4.6 Concentrations of S, Zn, Pb, Fe, Hg, Ni, Al and Sr in pore-water samples extracted from various depths within boreholes P1T, P2A, P3T, P4C, P6C and P9C.

The redox diagram of the sulfur, oxygen, hydrogen system is given in Figure 4.7. The area defined by circle A encompasses all E_h and pH measurements which were made in the field (Figure 4.4). This suggests that SO_4^{2-} is the stable phase throughout the impoundment. Thus, provided a suitable oxidant is available (e.g. O_2, Mn^{3+}, Fe^{3+}) to accept electrons, all S contained in the sulfide form should be transformed to SO_4^{2-}. This also means that SO_4^{2-} ions and metal cations in solution will not be immobilised in the lower regions of the impoundment by the re-precipitation of metal sulfides.

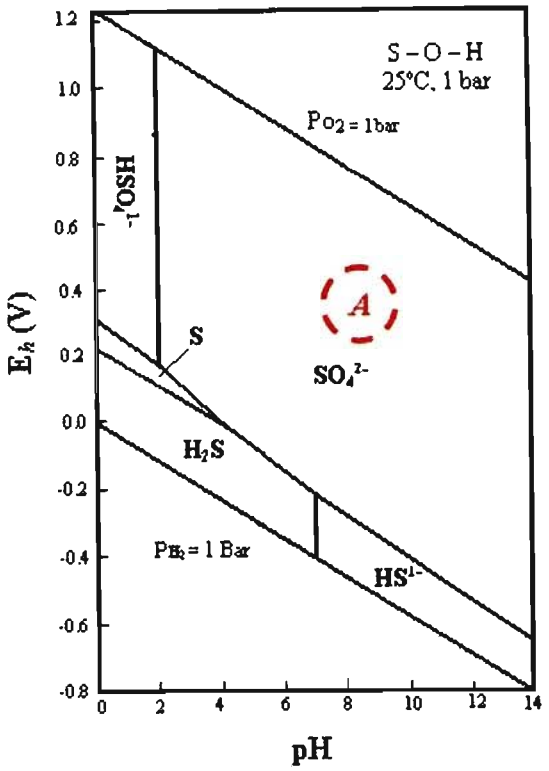

Figure 4.7 E_h – pH diagram showing the relative stabilities of important naturally occurring sulfur species (after Brookins, 1988). All E_h and pH measurements taken within the Pering tailings impoundment are contained within circle *A*.

Based on Figure 4.7 it can be assumed that all S in the pore-water of the Pering Mine tailings impoundment is present as SO_4^{2-}. One third of the total molar mass of SO_4^{2-} is S. Thus the SO_4^{2-} concentrations within the impoundment would be three times greater than the concentrations of total S measured by ICP and shown in Figure 4.6. It is therefore expected that the SO_4^{2-} concentrations leaching from the tailings impoundment could be between 633 mg l^{-1} (P4C-19) and 2323 mg l^{-1} (P6C-19). These concentrations are in excess of South African guidelines for drinking water, which state that a limit of 200 mg l^{-1}

(DWAF, 1996a) to 400 mg l^{-1} (SABS 241, 1999) is the maximum acceptable concentration for long-term consumption (Appendix 2). Thus, in accordance with the leaching column work, it would appear that the local groundwater may be at risk from SO_4^{2-} contamination.

4.4.2.6 Heavy metals

The high sulfate concentration in the pore-water of the impoundment is a direct consequence of metal sulfide oxidation. The release of heavy metals is synonymous with this oxidation, and thus at Pering elevated concentrations of Fe, Zn and Pb would be expected in response to the oxidation of pyrite, sphalerite and galena, respectively (Table 1.1).

Within the pore-water of the tailings impoundment a total sulfur concentration of 1000 mg l^{-1} was common in the upper layers (Figure 4.6). In an isolated system the complete oxidation of 1.87 g of FeS_2, 3.04 g of ZnS and 7.46 g of PbS would each stochiometricly (see Table 1.1) release 1000 mg of S into solution and 870 mg of Fe, 2040 mg of Zn, and 6640 mg of Pb, respectively. Sulfide reactivity is highly varied (Rimstidt and Vaughan, 2003) and it is therefore difficult to quantify to what degree each of the above sulfide minerals are contributing to this observed sulfur concentration. Nevertheless, a minimum total combined metal concentration of 870 mg l^{-1} would be expected to be associated with 1000 mg l^{-1} of S in solution if only FeS_2 were undergoing oxidation. If ZnS and PbS were also being oxidised this hypothetical combined concentration would be even greater. The concentration profiles of Pb and Fe in Figure 4.6 show that these elements occur in very low concentrations (< 0.12 mg l^{-1}). Even Zn did not reach concentrations in excess of 2.13 mg l^{-1}. Based on the sulfur concentrations in the pore-water these concentrations are significantly less than would theoretically be expected by the above calculations. This provides an indication that precipitation and/or extensive sorption onto the tailings is occurring, which is effectively immobilising a vast proportion of the metals released into solution after sulfide oxidation. This sorption will help to protect the groundwater from what would otherwise be severe Fe, Pb and Zn contamination.

In comparison to the total concentrations of Fe (19083 mg kg^{-1}), Al (9152 mg kg^{-1}), Mn (29102 mg kg^{-1}), Pb (398 mg kg^{-1}) and Zn (5481 mg kg^{-1}) in the TT material (Table 2.2), very little has entered into solution. Very low concentrations of Fe, Ni and Pb (< 0.12

mg l^{-1}) were recorded in the pore-water of the tailings impoundment. Strontium and Al reached maximum concentrations of 0.38 mg l^{-1} (sample P1T-5) and 0.99 mg l^{-1} (P3T-5), respectively (Appendix 9). In the leaching column experiments high concentrations of Mn were mobilised (Figures 3.5, 3.9 and 3.11); this, however, was not found within the tailings where Mn levels were below detection. The only identified heavy metal of immediate concern in the impoundment was Hg, with a maximum recorded concentration of 6.17 mg l^{-1} in sample P4C-2. In all boreholes the Hg levels exceeded the SABS 241 (1999) drinking water guideline by as much as 100 to a 1000 times (Appendix 2).

The environmental chemistry of mercury is complex. Mercury, as Hg^{2+}, is reported to be strongly held in soils (Alloway, 1990; McBride, 1994). However, in the presence of high concentrations of Cl^-, SO_4^{2-} and OH^- ions it is likely to form negatively charged aqueous species (Rytuba, 2000). Under such conditions Hg is more effectively immobilised at pH < 7, because these complexes may then be sorbed onto iron hydroxides and other positively charged colloidal material (Rytuba, 2000). The alkaline conditions of the Pering tailings, combined with the presence of high concentrations of SO_4^{2-} and Cl^- (±300 mg l^{-1}, Figure 4.8), will not favour the immobilisation of Hg. It is therefore expected that Hg will be relatively mobile in the impoundment and could potentially pose a severe risk to the local groundwater.

Accurate analysis of environmental mercury contamination is difficult as it is quickly lost from soils and solutions. Newton and Ellis (1974) studied mercury losses from different solutions. They looked at how concentration, chemical composition of the carrier solution and the material of the storage containers affected Hg losses. It was found that solutions with a Hg^{2+} concentration of 0.2 mg l^{-1} or lower experienced severe losses as a result of volatilisation. When stored in a carrier solution of 0.01 *M* $CaCl_2$ these losses were accentuated. At a concentration of 0.002 mg l^{-1} in a 0.01 *M* $CaCl_2$ carrier solution losses of 50% in a day were recorded. It was also noted that storage in plastic, as opposed to glass, resulted in greater losses of Hg due to surface adsorption. The relative moisture content of a soil and the ambient temperature has also been reported to affect Hg losses (Landa, 1978). Considering the high ionic strength of the pore-water and the time delay before analysis occurred (2 weeks), the reported mercury levels (Figure 4.6) may be an underestimation of actual concentrations in the field.

4.4.2.7 Base cations and chloride

The acid produced from sulfide oxidation is being buffered by the dissolution of dolomite. This is releasing high concentrations of Ca and Mg into the pore-water of the impoundment (Figure 4.8). Calcium concentrations ranged between 62.6 and 247 mg l^{-1}, with an average of 161 mg l^{-1}. The average Mg concentration in the pore-water was 589 mg l^{-1} with a range from 175 to 917 mg l^{-1}. The concentration of these elements typically decreased with depth. This trend, as previously mentioned, is most likely due to surface evaporation prior to the rock cladding, which would have drawn salt laden waters towards the surface of the impoundment.

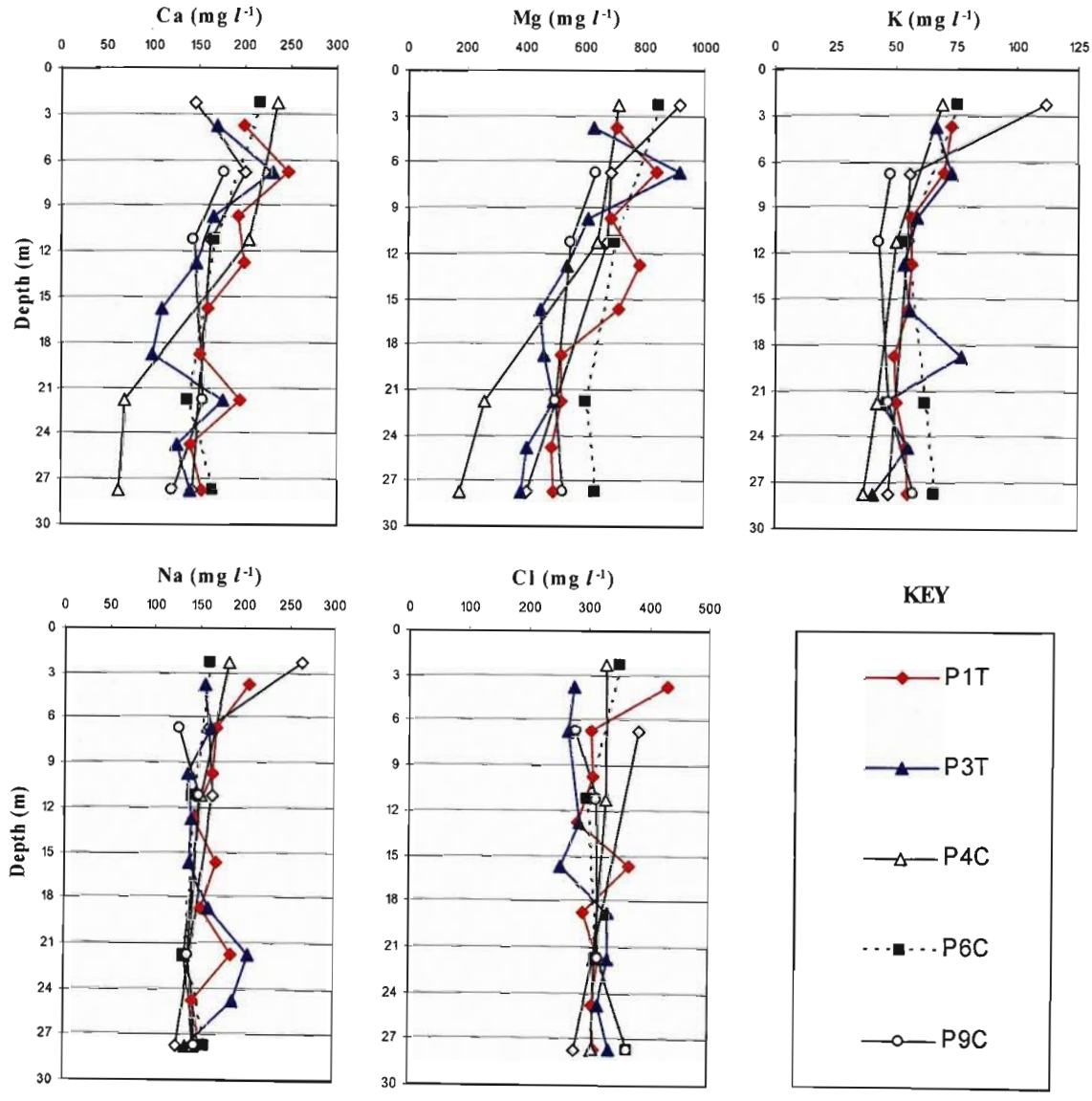

Figure 4.8 Concentrations of Ca, Mg, K, Na and Cl in pore-water samples extracted from boreholes P1T, P2A, P3T, P4C, P6C and P9C.

The measured Mg concentrations at the base of the tailings were 2.5 to 9.0 times greater than the SABS 241 (1999) guideline of 70 mg l^{-1} (Appendix 2). Magnesium sulfate is a known saline laxative (DWAF, 1996a; WHO, 1996), which induces diarrhoea by setting up an osmotic gradient across the bowel wall. This gradient causes fluid to be drawn into the gut lumen. According to DWAF (1996a) Mg concentrations of between 200 and 400 mg l^{-1} in drinking water will cause diarrhoea in all new users, if it occurs in conjunction with SO_4^{2-}. Based on the high concentrations of both Mg^{2+} and SO_4^{2-} at the base of the tailings it would appear that this could pose one of the most severe risks to groundwater at Pering Mine.

Prior to the reduction and solidification of the ore body at Pering, it is thought that saline ore-bearing fluids flowed upwards through fractures in the Earth's crust (du Toit, 1998). It is this saline origin that is speculated to be the source of Cl^- and Na in the pore-water. An average Cl^- concentration of 317 mg l^{-1} was recorded, with Na averaging 158 mg l^{-1} (Figure 4.8). The concentrations of both elements are currently relatively constant down most of the profiles. The presence of K in the pore-water is most likely linked to the dissolution of potassium feldspar, which was identified in the XRD analysis (Section 2.5.2). Concentrations of this element ranged from about 75 mg l^{-1} in the upper impoundment to about 50 mg l^{-1} at the base. This is at the limit of concentrations considered to be acceptable for drinking water. Sodium concentrations were within recommended limits, while Cl^- concentrations were above what is considered an acceptable limit for environmental and human exposure (DWAF, 1996a; 1996b; DWAF, 2005; Appendix 2).

4.4.2.8 Geochemical modelling

The pore-water geochemistry was assessed with the help of the equilibrium geochemical speciation model *visual MINTEQ* (after *MINTEQ-A2*; Allison *et al.*, 1991). The pore-water composition and pH of each sample collected from boreholes P1T and P3T were inputted into *MINTEQ* (S concentrations were given as SO_4^{2-}, see Section 4.4.2.5). Analyses were all run using the default database of mineral equilibrium constants provided by this program. No redox calculations were taken into account, because the redox conditions down both boreholes were consistently aerobic and showed little variation (Figure 4.4).

Geochemical modelling predicted that the mineral phases controlling the pore-water chemistry were similar in both boreholes P1T and P3T; this is not surprising considering their similar chemistry (see Figures 4.4 to 4.6, and 4.8). The analysis revealed that the pore-water throughout these boreholes was undersaturated with respect to dolomite (Table 4.1 gives examples for borehole P1T). This could be expected as dolomite is relatively insoluble especially at neutral to alkaline pH. It is also likely that pore-water flow rates were too fast to allow equilibrium to be achieved. Field based studies conducted by Al *et al.* (2000), and subsequent laboratory investigations by (Jurjovec *et al.*, 2002), found that dolomite minerals in tailings typically undergo incongruent dissolution.

Table 4.1 Saturation indices of some important mineral phases in the pore-water extracted from borehole P1T. Minerals which have reached points of supersaturation with respect to the pore-water are highlighted.

Sample number		***3***	***5***	***7***	***9***	***11***	***13***	***15***	***17***	***19***
Average Depth (m)		***3.75***	***6.75***	***9.75***	***12.75***	***15.75***	***18.75***	***21.75***	***24.75***	***27.75***
Mineral		***Saturation Index (SI)***								
Anhydrite	$CaSO_4$	-0.74	-0.62	-0.75	-0.71	-0.83	-0.88	-0.80	-0.94	-0.90
Bianchite	$ZnSO_4$	-5.76	-5.60	-5.75	-5.78	-5.78	-5.91	-6.09	-6.20	-6.12
Boehmite	$Al(OH)_2$	**0.97**	**0.92**	**0.95**	**0.58**	**0.68**	**0.65**	**0.66**	**0.49**	**0.54**
Brucite	MgO	-1.85	-1.62	-1.80	-0.99	-1.31	-1.48	-1.39	-1.15	-1.21
Calcite	$CaCO_3$	-12.42	-12.29	-12.40	-12.11	-12.29	-12.27	-12.12	-12.14	-12.14
Cerrusite	$PbCO_3$	-12.81	-12.49	-12.55	-12.48	-12.34	-12.47	-12.43	-12.47	-12.39
Cotunnite	$PbCl_2$	-7.34	-7.39	-7.39	-7.71	-7.23	-7.54	-7.45	-7.62	-7.51
Diaspore	AlOH	**2.68**	**2.62**	**2.65**	**2.28**	**2.38**	**2.36**	**2.36**	**2.19**	**2.25**
Dolomite	$CaMg(CO_3)_2$	-23.91	-23.67	-23.86	-23.24	-23.55	-23.63	-23.44	-23.37	-23.39
Epsomite	$MgSO_4$	-2.18	-2.07	-2.19	-2.10	-2.16	-2.33	-2.37	-2.39	-2.38
$Fe(OH)_2$		-2.94	-2.77	-2.82	-2.07	-2.35	-2.46	-2.34	-2.13	-2.17
Gibbsite	$Al(OH)_3$	**1.81**	**1.75**	**1.78**	**1.41**	**1.51**	**1.49**	**1.50**	**1.33**	**1.38**
Goslarite	$ZnSO_4{\cdot}7H_2O$	-5.52	-5.35	-5.50	-5.53	-5.54	-5.66	-5.85	-5.96	-5.88
Gypsum	$CaSO_4{\cdot}2H_2O$	-0.49	-0.37	-0.50	-0.46	-0.58	-0.63	-0.55	-0.69	-0.65
Halite	NaCl	-5.82	-6.06	-6.05	-6.16	-5.96	-6.10	-5.97	-6.09	-6.06
Hercynite	$FeAl_2O_4$	**6.83**	**6.89**	**6.90**	**6.91**	**6.84**	**6.67**	**6.80**	**6.68**	**6.75**
Larnakite	$PbSO_4O$	-0.70	**0.06**	-0.19	**0.19**	**0.34**	-0.07	-0.01	-0.06	**0.12**
$Pb(OH)_2$		**0.93**	**1.37**	**1.22**	**1.76**	**1.71**	**1.51**	**1.60**	**1.71**	**1.76**
Smithsonite	$ZnCO_3$	-12.43	-12.25	-12.37	-12.16	-12.23	-12.29	-12.39	-12.39	-12.35
Wustite	FeO	-0.72	-0.55	-0.60	**0.15**	-0.13	-0.24	-0.12	**0.09**	**0.05**
Zincite	ZnO	**0.43**	**0.73**	**0.52**	**1.20**	**0.94**	**0.81**	**0.76**	**0.91**	**0.92**

The pore-water in the central impoundment (i.e. boreholes P1T and P3T) was supersaturated with respect to various aluminium hydroxide species as well as hercynite ($FeAl_2O_4$), lead hydroxide ($Pb(OH)_2$) and zincite (ZnO, Table 4.1). It is therefore possible that these minerals could precipitate in the tailings. Lead and Fe in solution appear to be controlled by Larnakite ($PbSO_4O$) and Wusite (FeO), respectively. Both of these minerals

were close to equilibrium with respect to the pore-water (Table 4.1). Smithsonite ($ZnCO_3$), Bianchite ($ZnSO_4$) and cerrusite ($PbCO_3$) were all undersaturated, and therefore are unlikely to be found in the tailings.

The pore-water samples collected from boreholes P1T and P3T were close to equilibrium with respect to gypsum ($CaSO_4 \cdot 2H_2O$, Table 4.1). It is therefore possible that Ca^{2+} and SO_4^{2-} in solution were being controlled by the precipitation and dissolution of this mineral. The presence of gypsum was confirmed by SEM observations of tailings samples taken from borehole P1T (Appendix 1). Precipitation within mine tailings can play an important role in preventing potential contaminants from leaching into groundwater systems (Lin, 1997; Johnson *et al.*, 2000; McGregor and Blowes, 2002; Gieré *et al.*, 2003; Martin-Garin *et al.*, 2003; Cave and Talens-Alesson, 2005). According to *MINTEQ* modelling it is possible that Al, Fe, Pb, SO_4^{2-} and Zn could be partially immobilised within the Pering tailings through precipitation.

Geochemical speciation calculations suggested that metal cations in solution were forming sulfate, carbonate and hydroxide complexes (Appendix 9, Table A9.10). Chloride ions do not form ion pairs with cations to any significant degree (Garrels and Christ, 1965; Tan, 1998). It was therefore found that just over 96% of all Cl^- ions remained free in solution. Sulfate is the predominant anion in solution which is forming neutral and negatively charged complexes with the metal cations (Ca, Mg, Fe, Ni, Pb and Zn). Due to the high pH of the tailings anionic sorption is not favoured and therefore the mobility of metals in the tailings may be slightly enhanced by the formation of this complex. The extent to which mobility will be enhanced depends on the strength of ion pairing versus the affinity for sorption, as this will determine in which direction the equilibrium will ultimately lie.

4.4.3 Element release from aerated saturated tailings

In order to achieve complete profile descriptions, and to reassess element availability under slightly more reactive conditions than found in the field, saturated pastes were completed on all borehole samples. In order to simulate field conditions as closely as possible the saturated pastes were made up directly from the moist tailings which had been packaged in the field. The chemistry of the tailings has already been discussed in some detail; thus, this

section will only mention the observed changes in pH, EC and elemental composition of the paste solutions in comparison to the field extracted samples.

The pH of the extracted solutions were marginally lower than those found in the field, ranging between pH 7.11 and 8.77 (Figure 4.9; Appendix 10). This was most likely due to the addition of slightly acidic distilled water (pH ±5.5) and the possible release of acidity from sulfide oxidation, which could have been promoted by increased aeration and temperature. The EC was higher than that recorded in the field (Figure 4.6), most likely due to increased mineral dissolution as a result of higher water contents and the vigorous stirring of the saturated pastes. Once again EC showed trends of decreasing with increasing depth below the surface of the tailings.

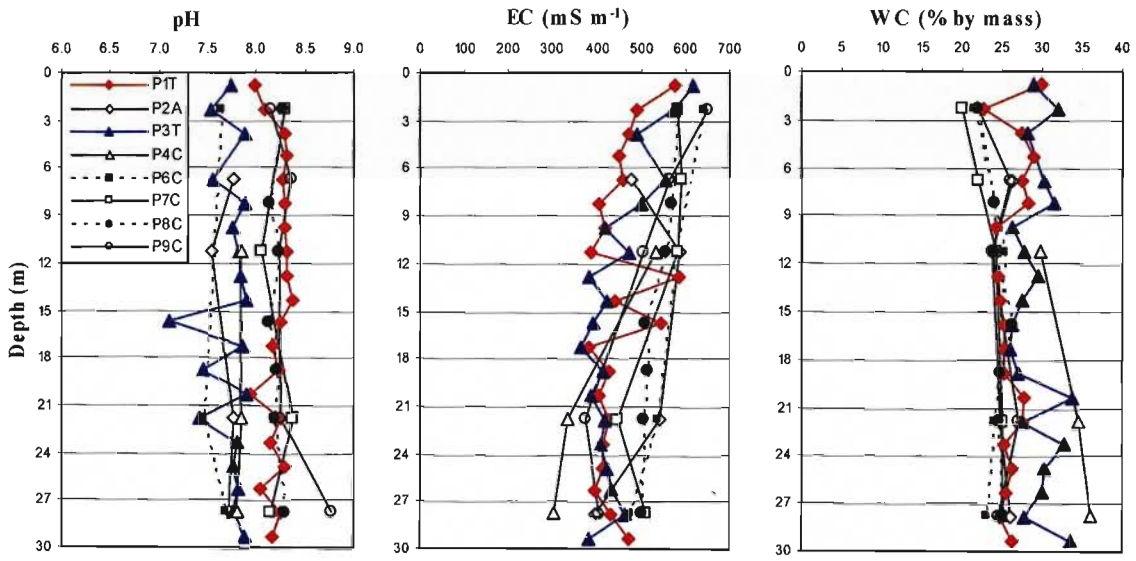

Figure 4.9 pH, electrical conductivity (EC) and water content (WC) of saturated pastes.

Noticeable increases in the concentrations of S and Zn were observed (Figure 4.10; Appendix 10) in comparison to the field equilibrated pore-water (Figure 4.6). A maximum S concentration of 2177 mg l^{-1} was recorded in sample P9C-2 with the average across all samples being 1292 mg l^{-1}. Substantially more Zn was also found to be free in solution. A maximum of 27.4 mg l^{-1} (P7C-8) was recorded, with a calculated average of 5.0 mg l^{-1}. Increased concentrations, in relation to the borehole pore-water, are most likely the result of mechanical stirring together with greater dissolution under the saturated and warmer conditions. Under this treatment much lower Hg concentrations would be expected, due to

increased volatilisation as a result of stirring, higher temperatures and time delays (Newton and Ellis, 1974; Landa, 1978). This is reflected in the results, which show that Hg concentrations were all below 0.34 mg l^{-1}, except for sample P3T-19 at 0.71 mg l^{-1}.

Concentrations of Cu, Fe and Pb were all lower than 0.30 mg l^{-1}. Despite this low concentration, Pb was above the recommended limit of 0.05 mg l^{-1} (SABS 241, 1999). Likewise Al was above the 0.30 mg l^{-1} limit, having an average concentration of 1.52 mg l^{-1} (SABS 24, 1999; Appendix 2). The release of Mn into solution varied considerably from borehole to borehole; from 0 mg l^{-1} in boreholes P1T and P3T to a maximum of 3.17 mg l^{-1} in borehole P7C. All marked variations in concentrations were confirmed by duplicate extractions.

Magnesium and Ca concentrations in the saturated pastes (Figure 4.10) were significantly greater than those measured in the pore-water, while those of K and Na were similar. Calcium ranged between 133 and 622 mg l^{-1} and Mg between 347 and 1202 mg l^{-1}, having averages of 377 and 727 mg l^{-1}, respectively. The more saturated borehole profiles, in particular P1T, P3T and P4C, tended to have lower concentrations of all elements. The reason for this is uncertain, but it may have to do with greater leaching in the wetter profiles.

Based on the saturated pastes it is evident that in many instances the available concentrations of Al, Ca, K, Mg, Mn, Pb, S and Zn are in excess of South African guidelines (Appendix 2). From this it would appear that there is potential for groundwater contamination, even if this is not currently expressed within the actual pore-water of the tailings impoundment.

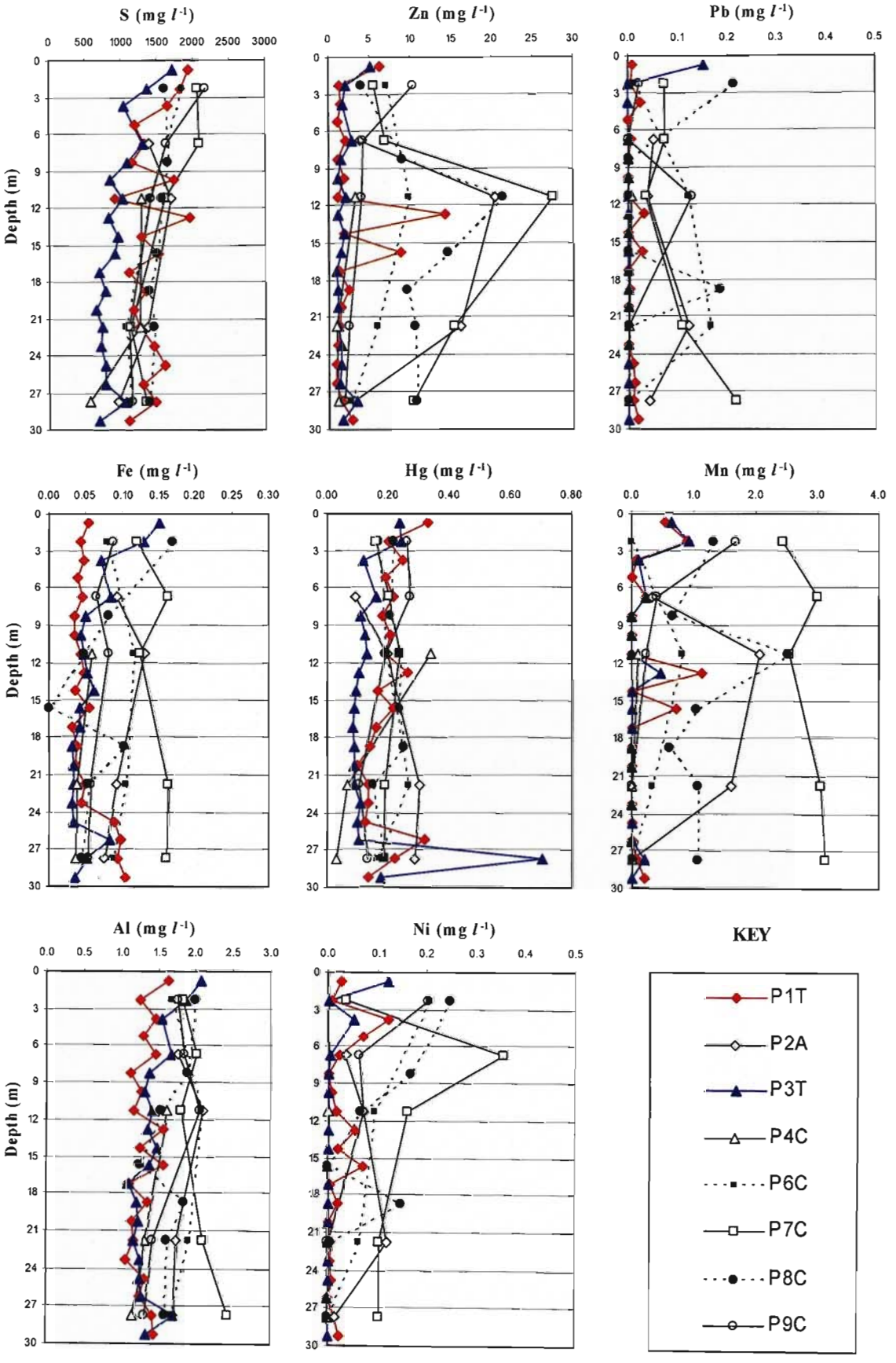

Figure 4.10 Elemental chemistry of the saturated paste extractions done on tailings samples collected from the eight boreholes.

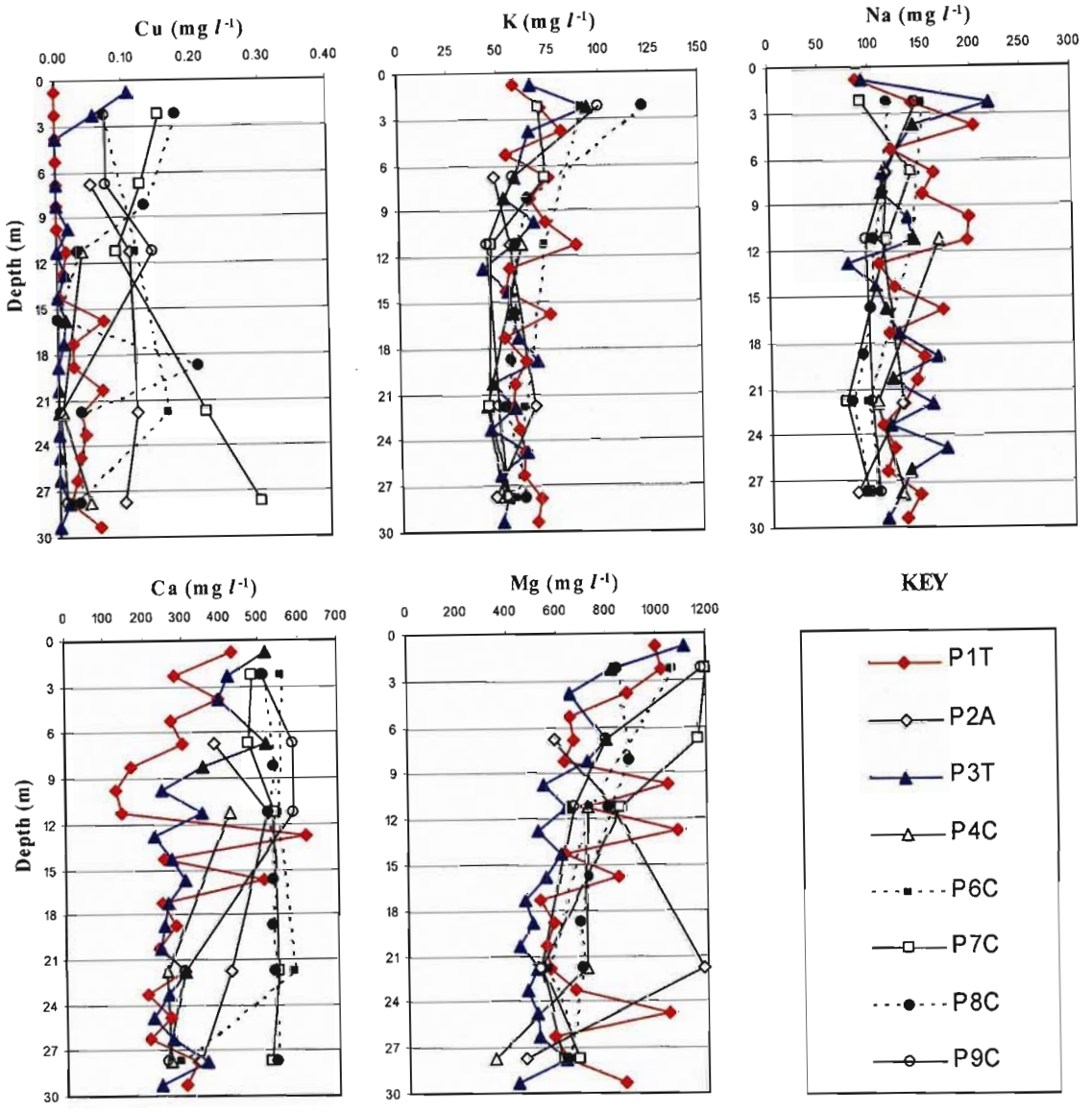

Figure 4.10*(cont)* Elemental chemistry of the saturated paste extractions done on tailings samples collected from the eight boreholes.

4.5 Conclusions

The main aim of this investigation was a field based assessment of the discarded Pb/Zn tailings at the Pering Mine. Particular focus was given to assessing the potential for groundwater contamination. It was found that the oxidation of metal sulfides has released sulfate and metal cations into the pore-water of the tailings. This oxidation is thought to be occurring throughout the impoundment. The release of acidity is being buffered by carbonate dissolution which is effectively maintaining the pH of the tailings above pH 8.

Based on pore-water samples and subsequent saturated paste extracts the greatest threat to groundwater will most likely come from Al, Cl, Hg, Mg, Mn, SO_4^{2-} and Zn. Even though other potentially toxic metals are present in the tailings, and may potentially pose a risk to groundwater, they are currently unavailable within the impoundment.

The trends in the measured EC of the pore-water suggested that significant amounts of water had at some point been evaporated from the surface of the impoundment. Field observations in July 2005 found that evaporation was now limited by the newly installed rock cladding. It is speculated that as a result of this greater volumes of water may now pass into the lower parts of the impoundment. This will ultimately result in increased seepage losses from the base of the impoundment, which in light of the pore-water chemistry may further exacerbate groundwater contamination. In order substantiate these speculations the water balance of the impoundment was modelled. This forms the subject of the next chapter.

CHAPTER 5

MODELING THE WATER BALANCE OF THE PERING MINE TAILINGS IMPOUNDMENT USING *HYDRUS-2D*

5.1 Introduction

The main concerns associated with mine tailings are mine drainage and dust blow off (Salmons, 1995). In order to eradicate the latter problem, the tailings impoundment at Pering Mine was covered with a layer of rocks. Surface mulches consisting of sand, rocks or gravel are often used in arid environments to help increase infiltration and reduce evaporative losses from soil surfaces (Hanks and Woodruff, 1958; Adams, 1966; Kemper *et al.*, 1994). It is therefore expected that the rock cladding has significant implications in terms of the water balance of the Pering Mine tailings impoundment.

The use of numerical models to describe water flow and solute transport in porous media are becoming increasingly popular. Models are often used for predictive purposes and scenario testing, and thereby play an important role in decision making processes. At larger scales solute mobility is controlled by the mass flow of water through a profile. Therefore by modelling water movement it is possible to assess the overall driving force for contaminant leaching. The borehole analyses, saturated pastes and leaching column work have already provided some indication of which elements may cause groundwater contamination if they are leached from the tailings impoundment. It is therefore the objective of this chapter to use a numerical model to provide an understanding of water flow within the impoundment, so that changes in drainage volumes can be identified over an extended period of time.

Prior to cladding the impoundment in September 2004 the tailings were uncovered. In order to determine how the water balance has subsequently been modified, a model simulation was run using both the bare tailings and the rock cladding as the upper boundary conditions. It was also deemed necessary to provide information on alternative cover scenarios, which may potentially be used as remediation strategies. Ideally, any remediation strategy should aim to reduce leaching losses to groundwater and protect the impoundment from wind erosion. Plants provide an effective means by which water can be drawn upwards and can therefore help to slow down or even prevent the downward

leaching of contaminants (Peters, 1988; Gee *et al.*, 1994; Sellers, 1998; Ward and Gee, 1997). Plants also intercept rainfall and help protect tailings against wind and water erosion. In order to examine the effect of growing plants in the tailings, two additional model simulations were undertaken to account for plant growth in a bare and a rock covered surface.

The commercially available computer model *HYDRUS-2D* (Šimůnek *et al.*, 1999) was chosen for assessing the effect of the various surface covers on the water balance of the Pering tailings impoundment. This model has been successfully used for a number of applications, such as modelling the movement of water and reactive/nonreactive chemicals in various soils (Ventrella *et al.*, 2000; Rassam and Cook, 2002; de Vos *et al.*, 2002; Abbasi *et al.*, 2004; Phillips, 2006), evaluating nitrogen fertiliser transformations and transport (Hanson *et al.*, 2006), and describing the degradation and transport of pesticides (Pang *et al.*, 2000; Close *et al.*, 2003). The *HYDRUS-2D* software package has a number of flexible applications. It was developed as a numerical model to simulate the two-dimensional (2D) flow of water, root water uptake, heat transport and movement of reactive solutes in variably saturated porous media. The logical manipulation of input parameters, describing the flow domain, soil properties and boundary conditions enables the user to model a wide variety of mass and energy transport problems.

5.2 Simulated runs

The only way in which the water balance of the tailings impoundment can be altered is by increasing or decreasing infiltration, and/or by modifying the rate at which water can be lost via evapotranspiration. Both infiltration and evaporation can be manipulated by altering the surface covering of the tailings. This chapter will give particular focus to modelling the water balance of the impoundment under four different surface covers, each of which is expected to have varying effects on mine drainage.

5.2.1 Water balance with bare surface

The first *HYDRUS-2D* simulation was aimed at describing the loss and gain of water from the impoundment prior to the rock cladding. In this simulation, *HYDRUS-2D* calculated the

surface evaporation from the potential evaporation rates, assuming that there was no suppression of evaporation by a surface cover or plant shading.

5.2.2 Water balance with rock cladding

Evaporation from a soil surface is dependent on, among other things, the availability of water at the soil surface, soil texture, temperature, atmospheric humidity, wind velocity and surface roughness (Hide, 1954; Hanks and Woodruff, 1958). Surface mulches reduce evaporation by reducing the temperature, wind velocity and humidity gradient at the soil surface and also by preventing the capillary rise of water. Lemon (1956), Unger (1971), Modaihsh *et al.* (1985) and Groenevelt *et al.* (1989) have all reported that, in comparison to unmulched wet soil surfaces, relatively thin surface layers of gravel and coarse sands can reduce evaporation by as much as 80 to 90%. In a field based study, Jury and Bellantuoni (1976) found that surface rocks helped to accumulate and retain water in the underlying soil. Soil surfaces composed of sands or gravels, have also been shown to promote groundwater recharge in arid regions by increasing infiltration and decreasing evaporation (Gee *et al.*, 1994; Kemper *et al.*, 1994). With particular reference to tailings systems, Tordoff *et al.* (2000) warn that one of the drawbacks associated with using coarse materials as surface covers is that they tend to increase downward and lateral leaching of metal-rich waters. These authors mention one instance in which the use of these types of material resulted in a neighbouring water course becoming contaminated.

In light of the above mentioned literature, it is apparent that the rock cladding (Figure 5.1) will have a major suppressive effect on evaporation rates. There is some uncertainty as to how much surface evaporation is being reduced as a result of the rock cladding, which in most places is between 30 and 50 cm thick. This is a substantially thicker than the mulches reported on in the above research, which ranged between 1 and 6 cm. It is therefore expected that in most areas evaporation from the tailings surface has been almost completely inhibited. The dark grey colour of the rocks, however, may promote evaporation directly after rainfall, as they often become very hot during the summer months. In order to account for a range of evaporation rates, three model simulations were run. The first and second simulations assumed that the rock cladding only reduced the potential evaporation by 50% and 65%, respectively. In accordance with the above mentioned literature, the third run assumed an 80% reduction in the potential evaporation.

Figure 5.1 Rock cladding on the surface of the Pering Mine tailings impoundment and (inset) a view of the retainer walls.

5.2.3 Water balance with plant growth

In tailings systems, plants have been reported to be of benefit because they intercept precipitation, transpire water and help to form an oxygen-consuming barrier (Peters, 1988; Tordoff *et al.*, 2000). Thus, if the Pering tailings were successfully revegetated with local vegetation, a change in the water balance would be expected. Two scenarios were modelled to test this. The first run modelled the effect of growing plants in bare tailings and the second, growing plants in amongst a rock covering. In the former some potential exists for surface evaporation and in the latter zero surface evaporation was assumed.

5.3 Theoretical background: modelling water movement in porous media

Most process-based models, including *HYDRUS-2D*, describe water flow through variably saturated porous media by means of the Richards equation (Richards, 1931). *HYDRUS-2D* uses the standard Galerkin linear finite element method (Pinder and Gray, 1977; Celia *et al.*, 1990) to solve the water and solute transport equations at each nodal point. These nodes are arranged in a predefined mesh, which represents the problem area being modelled.

5.3.1 Governing flow equation

Water movement through a saturated soil is commonly described by Darcy's Law, which states that the rate of water movement through a profile occurs at a rate Q, where:

$$Q = \frac{V}{At} = K_s \frac{\Delta h}{Z} \tag{5.1}$$

V is the volume of water (L^3; L = length) passing through a defined area A (L^2) over a given time span (t). K_s is the saturated hydraulic conductivity ($L\ t^{-1}$); Δh is the difference in pressure head (L) across the profile and Z is the distance between these two pressure boundaries (L). When describing water movement in unsaturated soils the simplified scheme of the above equation does not hold, because the hydraulic conductivity decreases with decreasing water content.

The Richards equation (Richards, 1931) is a modified and differentiated version of the Darcian equation, which enables changes in water content over time and space to be described mathematically for unsaturated soils. This equation is used as the governing flow equation in *HYDRUS-2D* and is defined by:

$$\frac{\partial \theta(z,t)}{\partial t} = \frac{\partial}{\partial z}\left[K\left(\frac{\partial h}{\partial z} - 1\right)\right] - S(z,t) \tag{5.2}$$

where θ is the volumetric water content ($L^3\ L^{-3}$); h is the pressure head (L); K is the unsaturated hydraulic conductivity in $L\ t^{-1}$ at a given water content θ; S is a sink term accounting for water uptake by plants; z is depth (L) and t is time.

5.3.2 Plant water uptake

For plant water uptake Feddes *et al.* (1978) defined S in Equation 5.2 as:

$$S(h) = \alpha(h)S_p \tag{5.3}$$

α is a prescribed water stress response function, which is dependent on the soil water pressure head (Figure 5.2). S_p is the potential water uptake rate or transpiration rate, which drops to zero under saturated conditions or when the pressure head falls below the wilting point of the plant. As a saturated soil drains and the pressure head drops below some predefined value, P0, transpiration begins, but at a reduced rate (Figure 5.2). Under ideal conditions, between P0pt and P2H, water uptake by plants will be at a maximum ($\alpha = 1$), after which uptake declines until the wilting point is reached. *HYDRUS-2D* includes a database which gives values for P0, P0pt, P2H and P3 for various crops.

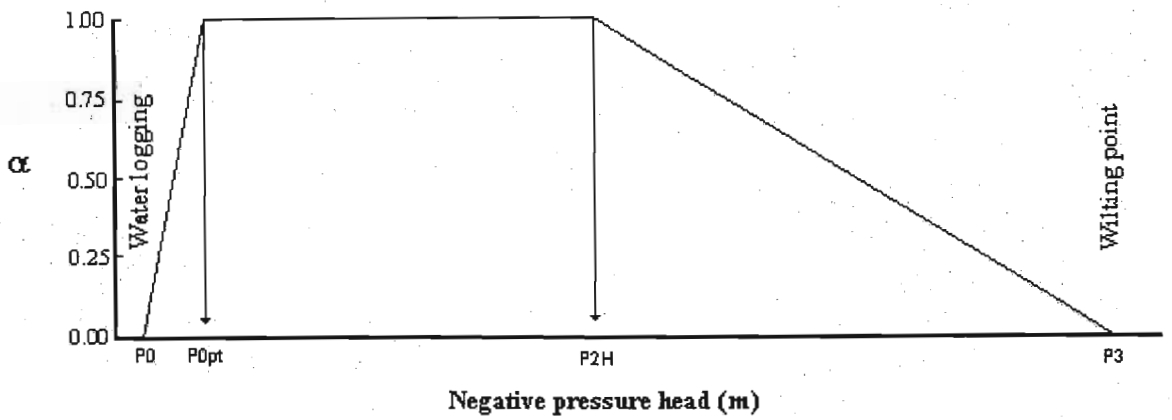

Figure 5.2 Schematic diagram of the plant water stress response function, α, of Feddes *et al.* (1978). When α equals 1 then transpiration is at a maximum, α values less than unity indicate water stress and designate a fractional reduction in potential transpiration.

Transpiration, given as S_p in Equation 5.3, can be calculated from A-pan evaporation. This is done by multiplying the A-pan reference or potential evaporation by a given crop coefficient (Schulze, 1995). The crop coefficient varies from plant to plant and is dependent on its stage of growth and the time of year. On a larger scale, Schulze (2006) has given monthly crop coefficients for all of South Africa's vegetative land types. By combining this information with A-pan evaporation rates it is possible to estimate monthly transpiration rates for the different vegetative biomes.

5.3.3 Water retention and unsaturated hydraulic conductivity

The measurement of water content (θ) and the hydraulic conductivity (K) of unsaturated soils in the field, is a complex and often impractical exercise. Due to this impracticality a number of numerical equations have been developed which relate the more easily determined water retention curve (WRC) to the unsaturated hydraulic conductivity of the soil (Brooks and Corey, 1964; Mualem, 1976; van Genuchten, 1980; Carsel and Parrish, 1988; Vogel and Císlerová, 1988; Vogel *et al.*, 1991). Reasonable correlation has been found between actual and numerically predicted values of K (Green and Corey, 1971; Bruce, 1972; van Genuchten, 1980). *HYDRUS-2D* gives a choice between the Brooks and Corey (1964), van Genuchten (1980) and Vogel and Císlerová (1988) equations. By inputting a numerical code into *HYDRUS-2D* which describes the WRC of the porous media to be modelled, it is possible to describe both the water storage capacity of the material and its hydraulic conductivity at varying pressure heads.

Brooks and Corey (1964) defined the water content (θ) and hydraulic conductivity (K), at different pressure heads, by the following two formulas:

$$S_e = \begin{cases} |\alpha h|^{-n} & if \quad h < -1/\alpha \\ 1 & if \quad h \geq -1/\alpha \end{cases} \tag{5.4}$$

$$K = K_s S_e^{2/n+l+2} \tag{5.5}$$

where S_e is the effective water content, defined as:

$$S_e = \frac{\theta - \theta_r}{\theta_s - \theta_r} \tag{5.6}$$

θ_r and θ_s designate the residual and saturated water contents, respectively. K_s is the saturated hydraulic conductivity; α is the inverse of the air-entry value (or bubbling pressure); n is a pore-size distribution index; and l is a pore connectivity parameter, assumed to be 2 in the original study. In *HYDRUS-2D* the parameters α, n and l are considered to be empirical coefficients which can be manipulated in Equation 5.4 in order to achieve the best fitting curve to a laboratory determined WRC (Figure 5.3A). Once a close fit has been achieved the coefficients α, n and l, which define the WRC of a given

porous media, are substituted into Equation 5.5. This allows an estimation of K to be made at any given water content or pressure head (Figure 5.3B).

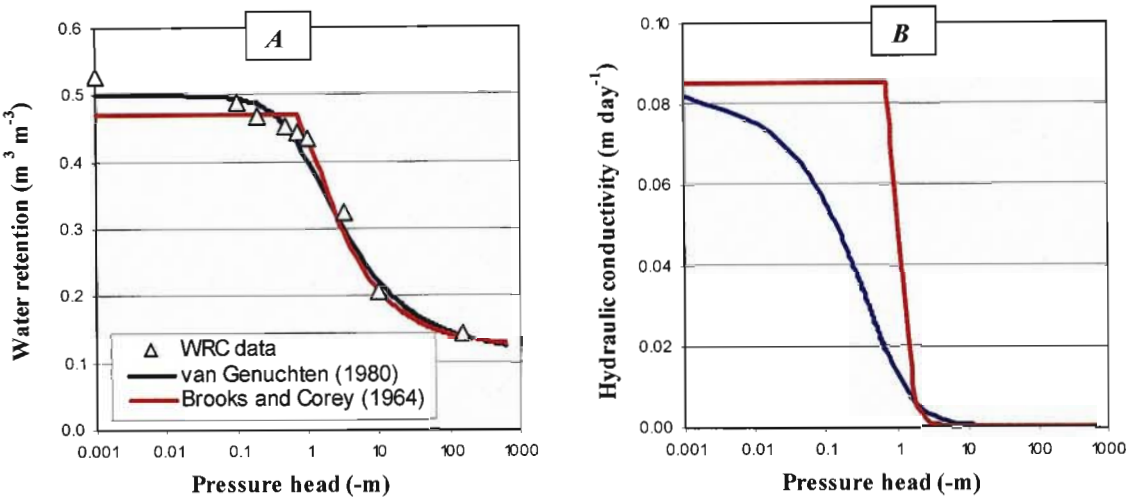

Figure 5.3 Image *A* shows an experimentally determined water retention curve (black triangles), with best fitting curves as defined by the van Genuchten (1980) and Brooks and Corey (1964) numerical models (Equations 5.4 and 5.7, respectively). The curves in *A* are defined by the empirical coefficients α, n, and l. These parameters are substituted into Equations 5.5 and 5.8 to determine the hydraulic conductivity at varying pressure heads shown in *B*.

The use of van Genuchten's (1980) numerical code in *HYDRUS-2D* provides an alternative method whereby the unsaturated hydraulic conductivity can be determined from the WRC. Equation 5.7 below was developed to define the water retention curve. By manipulating the parameters α, n and l it is possible to derive a curve that closely matches the experimentally determined WRC. Figure 5.3A shows the best fit of Equations 5.4 and 5.7 to an experimental data set. In the same way as mentioned above, the empirical coefficients defining the WRC are substituted into Equation 5.8, which allows K to be estimated for various pressure heads.

$$\theta(h) = \begin{cases} \theta_r + \dfrac{\theta_s - \theta_r}{\left[1+|\alpha h|^n\right]^m} & h < 0 \\ \theta_s & h \geq 0 \end{cases} \qquad (5.7)$$

$$K(h) = K_s\left[\frac{1-(\alpha h)^{n-1}\left[1+(\alpha h)^n\right]^{-m}}{\left[1+(\alpha h)^n\right]^{m/2}}\right]^2 \quad \text{where } m = 1 - 1/n \quad n > 1 \qquad (5.8)$$

The five parameters θ_r, θ_s, α, *n and* K_s are identical to those defined for Equations 5.4 to 5.6. van Genuchten (1980) based his model on that of Mualem (1976) who proposed a value of 0.5 for the pore connectivity parameter *l*, which appears to be an average for many soils (Šimůnek *et al.*, 1999).

The above mentioned equations have the dual benefit of describing both the water retention characteristics and the unsaturated hydraulic conductivity of the material with just three parameters, α, *n,* and *l*. By inputting these parameters into *HYDRUS-2D* and defining the initial water content of the porous media it is possible to model the flow of water through the material. In order to model natural environments, however, a number of additional defining factors or components need to be taken into account.

5.3.4 HYDRUS-2D input components

There are a number of qualitative and quantitative input components which need to be defined and decided upon before *HYDRUS-2D* can be run. For modelling water movement and calculating mass balances these inputs include:

1. Constructing the flow domain or problem area to be modelled with the *HYDRUS-2D* finite element mesh (FEM) editor. This defines the shape of the boundaries and the number of nodes at which iterative calculations will be made during the modelling process.
2. Stipulating boundary conditions which describe how water is transferred across the outer edges of the flow domain.
3. Giving mathematical definitions for the hydrophysical properties of the porous media which is to be modelled. These are known as the material inputs and include a description of the WRC and quantification of *K*.
4. Atmospheric inputs are also required. These include rainfall and evaporation data.
5. Vegetation inputs require that the transpiration rates, water stress response functions and rooting depths of the plants are defined.

5.4 Model setup: defining the input parameters

This section describes how *HYDRUS-2D* was set up and which data were used for the different input components.

5.4.1 Flow domain and boundary conditions

The finite element mesh editor in *HYDRUS-2D* was used to define the flow domain or the 'problem area' which was to be modelled. Due to the homogeneity of the tailings, only a small section of the impoundment was chosen for modelling. Smaller flow domains are preferable, in that they help to reduce the model run time and increase numerical stability. Figure 5.4 shows the element mesh generated for the chosen flow domain, which was set to cover the depth of the tailings impoundment and 60 m horizontally. The mesh was constructed to consist of 3411 mesh triangles, or elements, and 1781 nodal points.

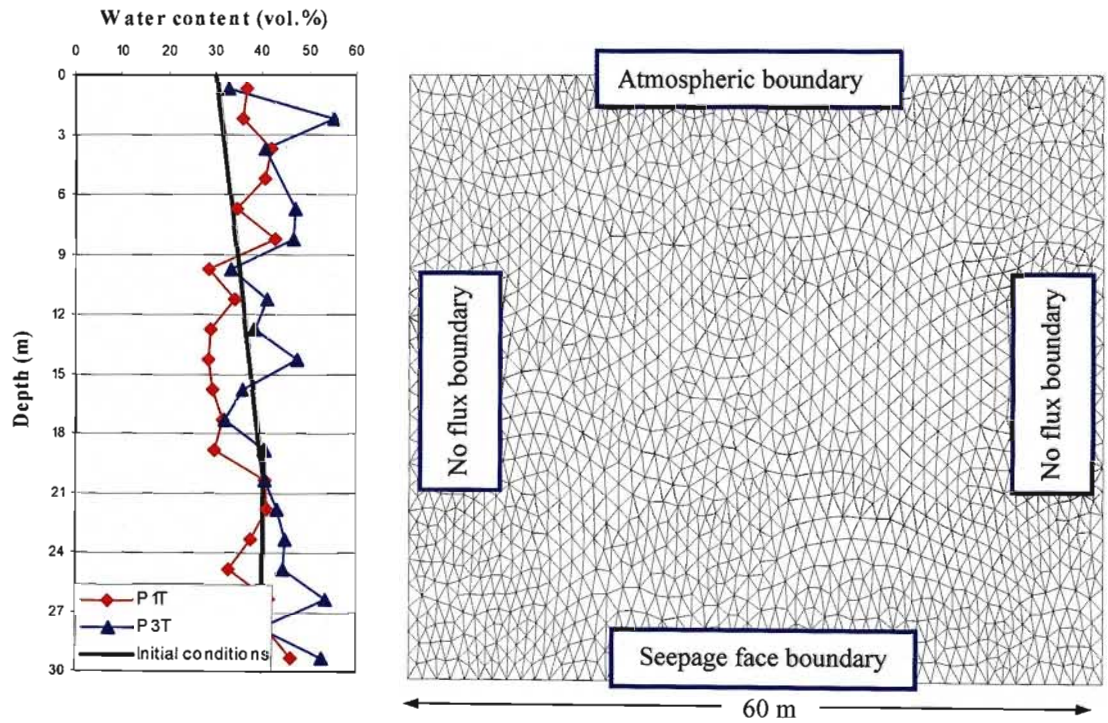

Figure 5.4 Finite element mesh and boundary conditions defining the flow domain used for modelling the Pering Mine tailings impoundment. The graph shows the initial starting conditions (black line) in comparison to the measured water contents of boreholes P1T and P3T.

Boreholes P1T and P3T were identified as being representative of the bulk of the tailings in the central parts of the impoundment. For this reason model simulations were based on field data gathered from these two profiles. *HYDRUS-2D* requires the user to input the initial volumetric water content of the profile. The volumetric water content was calculated from the gravimetric water content (Figure 4.5) using the density of water at 20 °C and the average bulk density of the tailings (1.71 g cm^{-3}, Appendix 6). Based on this the water content of the flow domain was set to increase from 30% saturation at the surface to complete saturation at a depth of 20 m (Figure 5.4).

The upper surface of the tailings was defined as an atmospheric boundary to allow surface fluxes of evaporation and daily rainfall to be included in the model. Zero transfer was assumed to occur across the vertical boundaries of the flow domain, because in reality the domain would be surrounded on all sides by the same material and thus negligible horizontal transfers would be expected (Abbasi *et al.*, 2004). The base of the tailings is underlain by fractured dolomite and thus water was assumed to drain from the base of the tailings only under a positive pressure head (i.e. seepage face boundary condition).

5.4.2 Material inputs

Modelling water movement through porous media requires that both the water holding capacity and the hydraulic conductivity of the material be defined for different pressure heads. The water holding capacity and saturated hydraulic conductivity of the Pering tailings was determined in the laboratory from five undisturbed cores collected in the field (Appendix 6). Four of these cores, collected in the vicinity of boreholes P3T and P7C, had similar water retention characteristics. The WRCs of these cores are expected to be representative of most of the upper impoundment, other than in the extreme northwest corner where the tailings are somewhat coarser. The hydraulic properties in this area were defined by Core 1 (Figure 5.5).

As described in the theoretical section of this chapter, the unsaturated hydraulic conductivity of a porous medium can be approximated from its WRC. The average WRC of cores 2 to 5 is shown by the green line in Figure 5.5. The best fitting curves, as described by the van Genuchten (1980) and the Brooks and Corey (1964) numerical codes are also shown. These curves were optimised visually, using the equations presented in

Section 5.3.3, with the help of the *RETC* program (van Genuchten *et al.*, 1999). The parameters θ_s, θ_r, α, n and m which define these curves are given in Table 5.1. From these parameters *HYDRUS-2D* was able to determine the unsaturated hydraulic conductivity of the material (Figure 5.6).

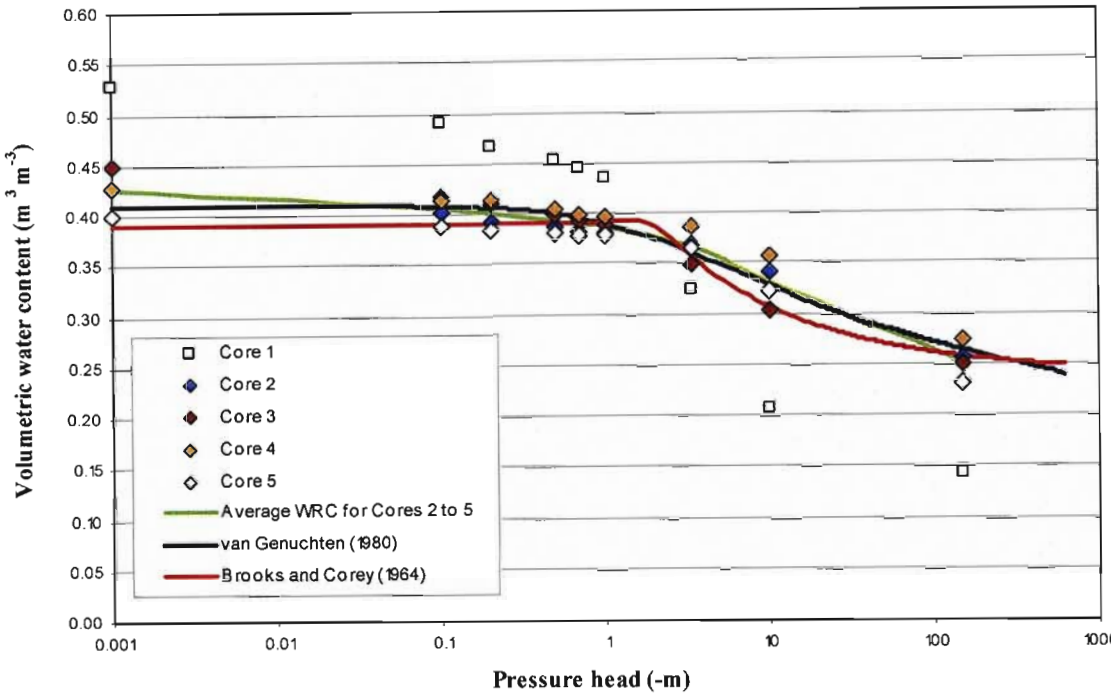

Figure 5.5 Water retention characteristics of the Pering tailings, with the best fitting water retention curves (WRC) as defined by the van Genuchten (1980) and Brooks and Corey (1964) numerical codes.

The water retention data of the four cores was best described by van Genuchten's (1980) equation. The predicted unsaturated hydraulic conductivity provided by this equation also appeared to be more realistic than that provided by the Brooks and Corey (1964) equation (Figure 5.6). For this reason the parameters defining the van Genuchten (1980) curve were used for all modelling procedures (Table 5.1). Currently the only available data on the hydraulic properties of the tailings come from these undisturbed surface cores. It was therefore necessary to assume that the hydrophysical properties of the tailings impoundment were consistent throughout its entire depth. This may not be altogether correct as compaction of the tailings can cause reductions in the hydraulic conductivity, a trend which was observed by Blowes *et al.* (1998) and McGregor *et al.* (1998). For future modelling it may be necessary to determine the hydraulic properties at different depths

within the impoundment so that impervious layers can be identified (e.g. using piezometer-response tests or tracer tests).

Table 5.1 Parameters defining the average WRC of cores 2 to 5 shown in Figure 5.4.

Parameter	*van Genuchten (1980)*	*Brooks and Corey (1964)*
θ_s (m^3 m^{-3})	0.41	0.40
θ_r (m^3 m^{-3})	0.17	0.23
α	0.75	0.30
n	1.20	0.55
m	0.17	
l	0.50	2.00
K_s (m day^{-1})	0.085*	0.085*

* Average K_s of Cores 2 to 5 (see Appendix 6)

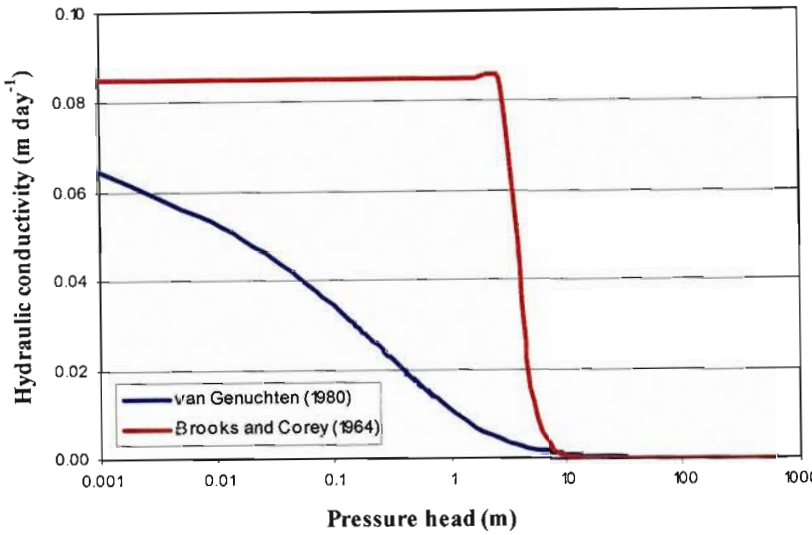

Figure 5.6 Unsaturated hydraulic conductivity of the Pering tailings material as predicted by the van Genuchten (1980) and Brooks and Corey (1964) numerical codes. The curves are based on the parameters θ_s, θ_r, α, n, m, l and K_s given in Table 5.1.

Another important defining character of soils or tailings is their ability to lose water as a result of surface evaporation. *HYDRUS-2D* uses a scheme whereby the actual evaporation remains equal to the potential evaporation until some user defined pressure head called "hCritA" is reached. Rassam *et al.* (2004) used *HYDRUS-2D* to model evaporation losses from sand, silt and clay soils and report that sandy soils typically have an hCritA value of about 500 m, silty soils 1000 m and clayey soils 3000 m. Due to the fineness of the Pering tailings (Appendix 5) an intermediate value of 2000 m was decided upon for all model simulations.

5.4.3 Atmospheric inputs

Atmospheric inputs required by *HYDRUS-2D* include precipitation and potential evaporation rates. Daily rainfall data were obtained from the Reivilo weather station (weather station No. 359304 W) for the period 1885 to 2000. Analysis of this data set showed that the mean annual precipitation for this region is 413 mm. Model simulations were run for a total of 15 years using daily rainfall data from the period 1st of January 1985 to 31st of December 1999. The total precipitation in each of these years is given in Table 5.2. The average yearly rainfall for this period is 416.3 mm, which is very close to the long term average of 413 mm. Uncharacteristically high rainfall occurred in 1988 (788.6 mm) and a few years later, from 1992 to 1994, severe droughts were experienced. This data range provides a good starting point for modelling, as overall it is very close to the long term average and also offers the opportunity to model, and thus observe, the effects of high and low rainfall years on the water balance of the tailings.

Most rainfall at Pering Mine occurs in the form of thundershowers, with short duration and high intensity. Under normal circumstances, given the low hydraulic conductivity of the tailings, some degree of surface runoff would be expected. However, the retainer walls surrounding the edge of the impoundment and the rock cladding will now prevent lateral runoff and promote infiltration. In order to model the situation with zero runoff all rainfall was allowed to infiltrate. This was ensured by modelling at a daily rather than hourly timescale as no daily rainfall event over the entire simulation exceeded the saturated hydraulic conductivity of the material (0.085 m day^{-1}).

The A-pan evaporation reported for Pering Mine is 1476 mm (Table 5.3). Based on this it is evident that there is a substantial water deficit in the region. This deficit plays a significant role in evaporative losses from the tailings and therefore forms an important component of the mass balance. The mean daily potential evaporation for each month is given in Table 5.3. Maximum evaporation occurs in December (6.2 mm day^{-1}), after which rates tend to decline to a minimum in June (1.9 mm day^{-1}). The daily averages reported for Pering were inputted into *HYDRUS-2D* for the 15 year simulation. These values are lower than those reported for the regional climate zone (Table 5.3) and thus are expected to provide a conservative estimate of evaporation.

Table 5.2 Rainfall of modelled years and corresponding time period in days.

Year	*Rainfall*	*Time*
	mm	*days*
1985	407.1	0 to 365
1986	333.7	365 to 731
1987	384.4	731 to 1096
1988	788.6	1096 to 1493
1989	529.6	1493 to1827
1990	331.4	1827 to 2192
1991	579.8	2192 to 2556
1992	189.0	2556 to 2892
1993	313.2	2892 to 3288
1994	212.0	3288to 3653
1995	461.0	3653 to 4018
1996	352.1	4018 to 4384
1997	523.4	4384 to 4749
1998	413.3	4749 to 5114
1999	426.6	5114 to 5479
Total	*6245.2*	
Average	*416.3*	
SD	*150.0*	

Table 5.3 Potential (A-pan) evaporation data for Pering Mine and the regional climate zone.

Month	*Pering Mine*[1]	*Climate zone*[2]
	mm day^{-1}	
January	6.0	8.2
February	5.2	6.8
March	3.9	5.2
April	3.0	4.1
May	2.4	3.4
June	1.9	2.9
July	2.3	3.4
August	3.0	4.5
September	4.1	6.5
October	4.9	7.6
November	5.9	8.0
December	6.2	8.6
Annual total	1476.0	2099.9

1: Information supplied by bhpbilliton (personal communication Ms S. Raja).
2: Land Type Survey Staff (1986)

5.4.4 Vegetation inputs

The Pering tailings impoundment is currently unvegetated and will in most likelihood remain so unless some major changes are instigated. The most limiting factors are the rock cladding and the poor nutrient status of the tailings. However, should vegetative remediation be undertaken, it is important that its effect on the water balance be known.

When modelling evapotranspiration losses it is necessary to distinguish between transpiration from plants (E_T) and evaporation from the soil surface (E_S). If vegetation has a full canopy cover and ground shading is at a maximum it may be assumed that 95% of potential evaporation (E_P) is the result of plant transpiration and the remaining 5% the result of soil surface evaporation (Childs and Hanks, 1975; Schulze, 1995). As the canopy cover decreases so does the transpiration rate, and when no canopy cover exists all evapotranspiration is the result of soil surface evaporation. The crop coefficient, C_c, defines the extent of canopy cover. Full cover is assumed to occur when C_c equals 1.0 and

decreases to zero cover as C_c approaches 0.2 (Schulze, 1995). The fraction of potential evaporation which is made up by transpiration has been defined by the following equation (Schulze, 1995):

$$F_t = 0.95\frac{(C_c \times 0.2)}{0.8} \quad \text{when } C_c > 0.2 \qquad (5.9)$$

$$F_t = 0 \quad \text{when } C_c < 0.2$$

F_t is the fraction of the potential evaporation lost as transpiration, thus $E_T = F_t \times E_P$. The maximum amount of water that can be lost from the soil surface is then equal to the difference between potential evaporation and transpiration (i.e. $E_S = E_P - E_T$). By this means, the daily potential evaporation rates can be separated into transpiration and soil surface evaporation. These are the two main inputs requirements for modelling water losses from vegetated surfaces.

It is assumed that if revegetation of the tailings were to occur it would have similar qualities to the surrounding vegetation. Schulze (2006) has given hydrological attributes to South Africa's vegetation based on the different veld types outlined by Acocks (1988). His suggested monthly crop coefficients for the local Kalahari Thornveld type vegetation are given in Table 5.4. Based on these values, the potential transpiration and the potential soil evaporation rates were calculated from $E_T = F_t \times E_P$ and $E_S = E_P - E_T$, respectively. The calculated daily values of E_T and E_S for each month are given in Table 5.4. These values were used to define the potential evapotransportation rates over the duration of the simulations.

Table 5.4 Monthly crop coefficients (C_c) for Acocks's Kalahari Thornveld and calculated daily transpiration ($E_T = F_t \times E_P$) and soil surface evaporation ($E_S = E_P - E_T$) rates for each month (all evaporation rates are given in mm day^{-1}).

	Jan	*Feb*	*Mar*	*Apr*	*May*	*Jun*	*Jul*	*Aug*	*Sep*	*Oct*	*Nov*	*Dec*
C_c	0.65	0.75	0.70	0.60	0.45	0.20	0.20	0.20	0.40	0.50	0.55	0.65
E_P	5.97	5.18	3.87	2.97	2.42	1.87	2.27	2.97	4.10	4.94	5.90	6.23
F_t	0.53	0.65	0.59	0.48	0.30	0.00	0.00	0.00	0.24	0.36	0.42	0.53
E_T	3.19	3.38	2.30	1.41	0.72	0.00	0.00	0.00	0.97	1.76	2.45	3.33
E_S	2.78	1.80	1.57	1.56	1.70	1.87	2.27	2.97	3.13	3.18	3.45	2.90

The response of the vegetation to water stress was described by means of the Feddes *et al.* (1978) equation (Equation 5.3). The parameters defining the shape of the water stress response curve (shown in Figure 5.1) were taken from the default parameters offered for

grass in the *HYDRUS-2D* library. Based on this, transpiration was assumed to start at a pressure head of -0.1 m (P0) and achieving maximum soil water extraction by -0.25 m (P0pt). Between pressure heads of -0.25 and -3.00 m (P0pt) transpiration was equal to the maximum potential transpiration (E_T). After this point, transpiration declined until the wilting point was reached at -160 m (P3). These parameters seemed to be well suited to describing the hardy veld species which are found around the Pering Mine.

When modelling plant water uptake it is also necessary to define the rooting depth of the plants in the flow domain. According to Schulze (2006) between 80 and 100% of the water extracting roots in the Kalahari Thornveld are located in the topsoil. The rooting zone was therefore described as being exclusively contained within the top 50 cm of the tailings.

5.5 Results and discussion

Increased infiltration of oxygenated rainwater water into the Pering tailings is likely to increase the rate of sulfide oxidation and at the same time increase the potential for leaching. Thus if infiltration is enhanced, greater contamination of groundwater reserves could be expected. Computer simulations with *HYDRUS-2D* were used to quantify how the rock cladding would affect the water balance of the impoundment, assuming various levels of evaporation suppression. The model simulations also focused on assessing other potential approaches which may favour the drying of the Pering tailings impoundment, while at the same time minimising seepage from the lower boundary. Table 5.5 outlines the six model simulations which were described in Section 5.2, for ease of reference in this discussion each simulation has been assigned a run number.

Table 5.5 A brief description of the six model simulations with their run number.

Run No.	*Defining criteria*
Run 1	Model simulation of bare tailings with no limitation to evaporation
Run 2	Model simulation of tailings covered in rocks – 50% reduction in potential evaporation assumed
Run 3	Model simulation of tailings covered in rocks – 65% reduction in potential evaporation assumed
Run 4	Model simulation of tailings covered in rocks – 80% reduction in potential evaporation assumed
Run 5	Model simulation of plants grown in rocky covering – transpiration with zero soil evaporation
Run 6	Model simulation of plants grown in bare tailing – transpiration and soil evaporation

5.5.1 Mass balance information

The predicted annual change in the volumetric water content of the flow domain in each of the individual runs is shown in Figure 5.7 (information was extracted from yearly mass balance data; Appendix 11). All simulations underwent an initial phase of rapid drying, due to seepage losses from the lower boundary. The fact that this trend was followed almost equally in all runs suggests that the model overestimated the permeability of the underlying dolomite. A seepage face boundary condition stipulates that water will pass through the boundary as soon as a positive pressure head builds up (Rassam *et al.*, 2004). In reality water probably only passes into the rock once a pressure head well above unity is achieved. Thus it is likely that reported seepage rates are overestimated. However, after stabilisation at about 1000 days, the effects of each surface covering become evident. It is therefore still possible to compare scenarios and make interpretations about how each of them will likely affect the water balance of the impoundment in the future.

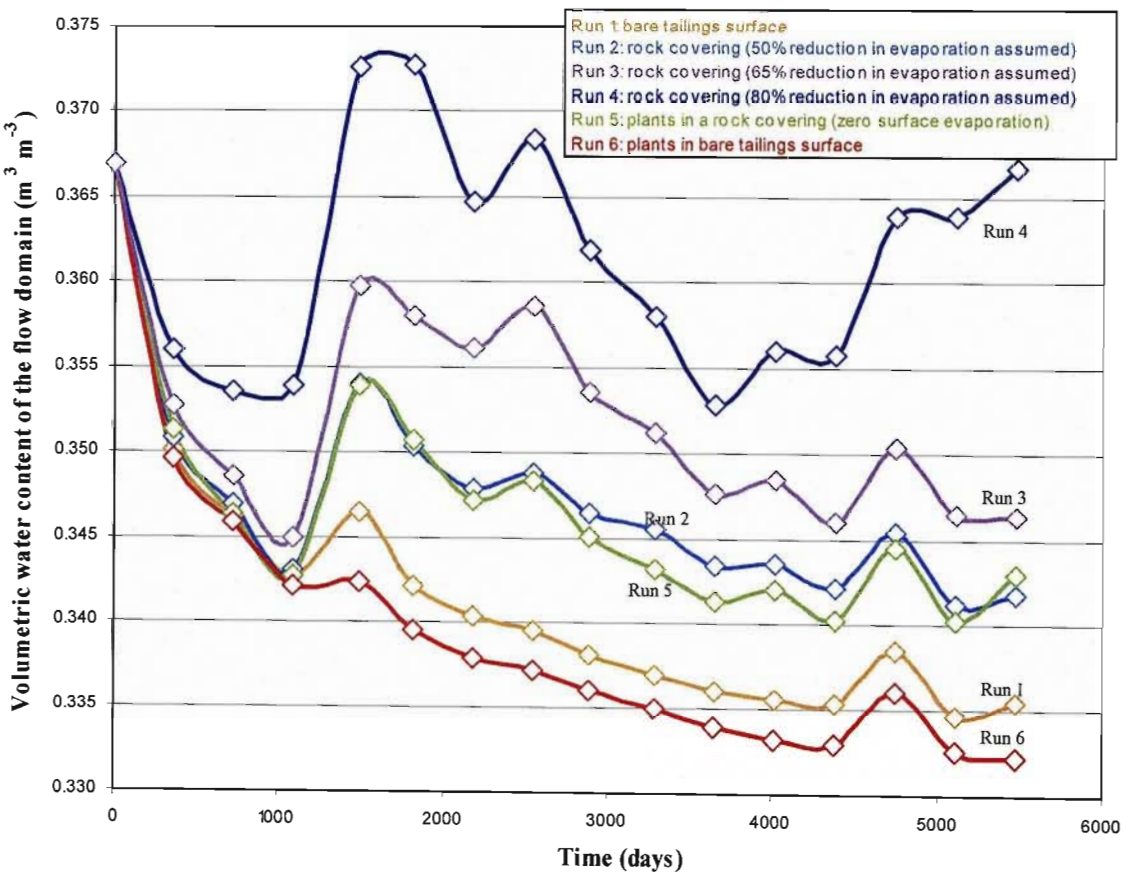

Figure 5.7 The effect of various surface covers on the average volumetric water content of the entire flow domain.

The arid environment, combined with the fine texture and low hydraulic conductivity of the tailings provides an ideal combination for promoting surface evaporation. The low hydraulic conductivity of the tailings would help to ensure that rainwater remains close to the surface after each rainfall event, thus allowing time for the water to be removed by plant roots and/or surface evaporation. With no rock covering, (Figure 5.7, Run 1) *HYDRUS-2D* predicted that the tailings would dry out consistently over time, with slight increases occurring only after the heavy rainfall years (years 4, 5 and 13). In the runs in which evaporation had been suppressed by rock coverings (i.e. Runs 2, 3, 4 and 5), drying of the profile was inhibited. By the end of the simulation period it was found that Run 4 contained approximately 0.031 m^3 more water per 1 m^3 of tailings than Run 1. At first this appears insignificant, but given the 12.5 million m^3 volume of the impoundment, this adds up to a difference in the region of 390 000 m^3 of water. This difference is a final net value, based on mass balance outputs, which does not take into account the greater seepage losses which occurred in Run 3 throughout the 15 year simulation. Thus, much greater volumes of water pass through the impoundment under mulched surfaces than can initially be identified from the mass balance information.

As surface evaporation is reduced, the response of the profile to wetting becomes more pronounced. For example, in both Runs 1 and 6 in which there was no limitation to surface evaporation, there was only a slight recharge of the profile as a result of the heavy rains in the 4^{th} and 13^{th} year of the simulations. During these years the flow domain in Run 4 experienced a marked increase in the volume of water stored. Even in years of lower rainfall, which had no effect on Runs 1 and 6, the profile in Run 4 was unable to lose sufficient water as evaporation and thus ended up gaining water. Increased moisture will most likely result in greater drainage volumes and could potentially also extend the length of time over which leaching will occur.

According to *HYDRUS-2D* predictions, the greatest degree of drying would have occurred if the tailings had been left bare and planted with Kalahari Thornveld vegetation (Figure 5.7, Run 6). This is because evaporation can occur from both the tailings surface and from the plants, the roots of which extend into the tailings. It must be noted however, that a uniform and continuous plant cover was assumed in both Runs 5 and 6. In reality it is likely that this will not be the case, particularly if the plants are grown in a rock covering. Thus, water losses attributed to transpiration are probably somewhat overestimated and

therefore the drying of the profiles in Runs 5 and 6 may not be as marked as suggested in Figure 5.7.

5.5.2 Cumulative boundary fluxes

The mass balance data described above showed that the various surface covers cause the tailings material to undergo different cycles of wetting and drying. This information, however, gives little indication as to whether water was lost from the system by means of evapotranspiration or basal seepage. Covers which reduced the amount of seepage from the tailings are naturally favourable, in that they will help to reduce the risk of groundwater contamination. It is therefore necessary to examine the predicted flow of water across the upper and lower boundaries of the flow domain so that the full effects of the different surface covers can be assessed.

The cumulative movement of water across both the lower seepage face and the upper atmospheric boundary for the six runs are given in Figure 5.8. All fluxes are given as depth measurements. Positive values indicate that water was being lost from the system, while negative values indicate that water moved into the profile. For a bare surface *HYDRUS-2D* predicted that overall more water was lost from the tailings surface than was gained through precipitation (Figure 5.8A, Run 1). After the 15 year simulation it was predicted that cumulatively 0.295 m of water was lost from the atmospheric boundary. It is therefore expected that prior to the rock cladding the impoundment was drying from the surface and downward leaching was being minimised as a result. The process of surface drying is supported by the fact that salt precipitates were observed on the surface of the impoundment where the tailings were exposed.

If evaporative losses are reduced by as little as 50%, a net movement of water into the flow domain is predicted (Figure 5.8A, Run 2). If a more realistic 80% reduction in evaporation is assumed (Run 4), the net infiltration is significantly higher, ending at -1.752 m. Given that the total rainfall depth for the simulation was 6.245 m (Table 5.2), this equates to a net infiltration of 28%. Thus the rock cladding is causing a net inflow of water into the impoundment and will most likely exacerbate the problem of mine drainage.

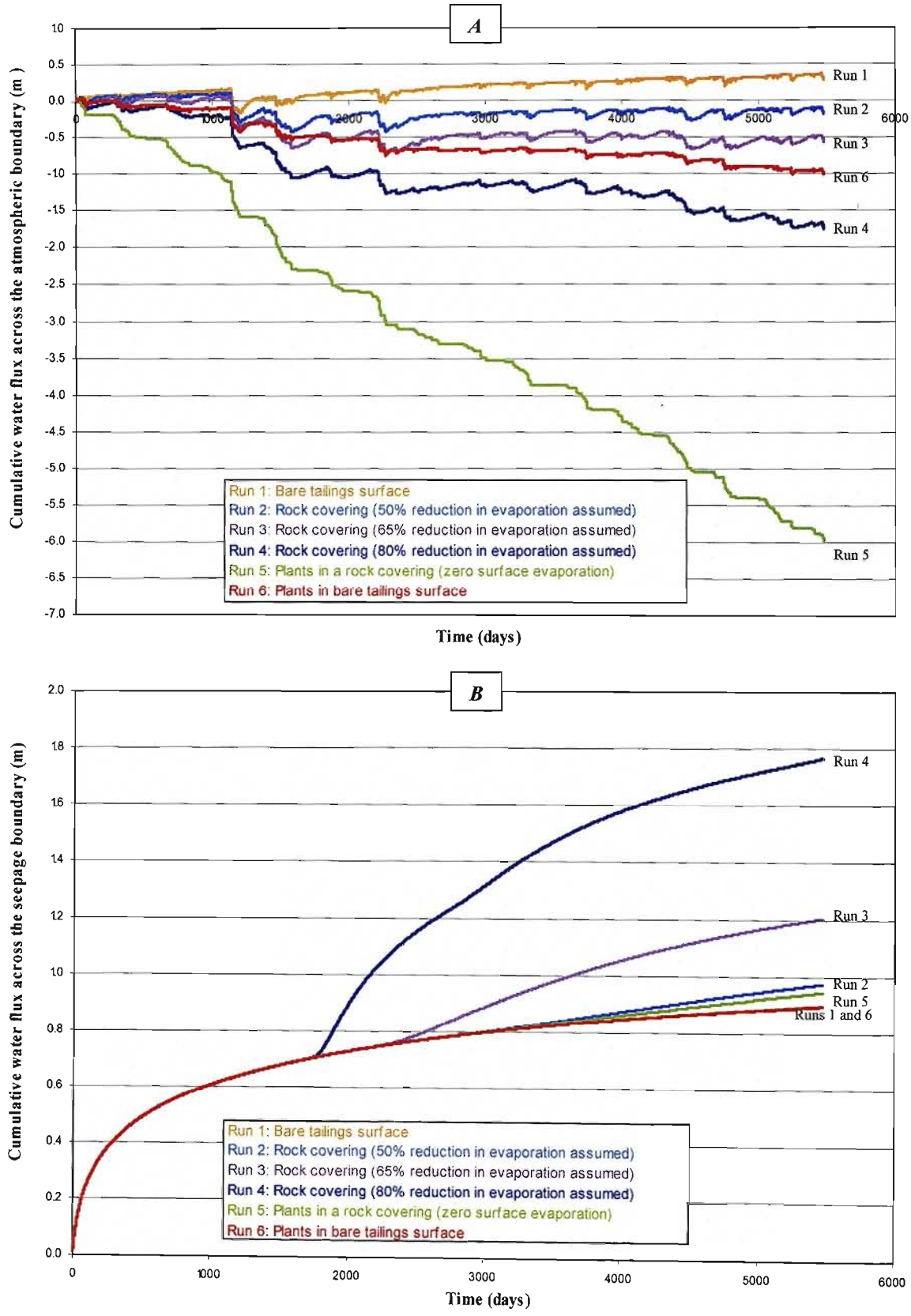

Figure 5.8 Predicted cumulative fluxes across (A) the atmospheric and (B) seepage face boundaries.

Over the 15 year simulation a depth of 6.067 m (or 6.067 m^3 per m^2 of surface area) of water was transpired from the vegetative cover in Run 5 and 1.431 m from Run 6 (Figure 5.9). The vegetation in Run 5 was able to extract more water because the tailings were consistently wetter as a result of the rock mulch. In this run the rock mulch was assumed to suppress surface evaporation completely and as a result infiltration was significantly higher than all other runs (96% of total rainfall, see Figure 5.8A). Despite this significant infiltration, transpiration ensured that seepage from the profile was kept to a minimum (0.948 m, Figure 5.8B). In Run 6, where surface evaporation could still occur, the vegetation experienced periods of water stress during the winter months and drought years and as a result transpired less water. This is evident in Figure 5.9, in which it can be seen that the cumulative uptake of water by plant roots was staggered in Run 6, while almost continuous in Run 5.

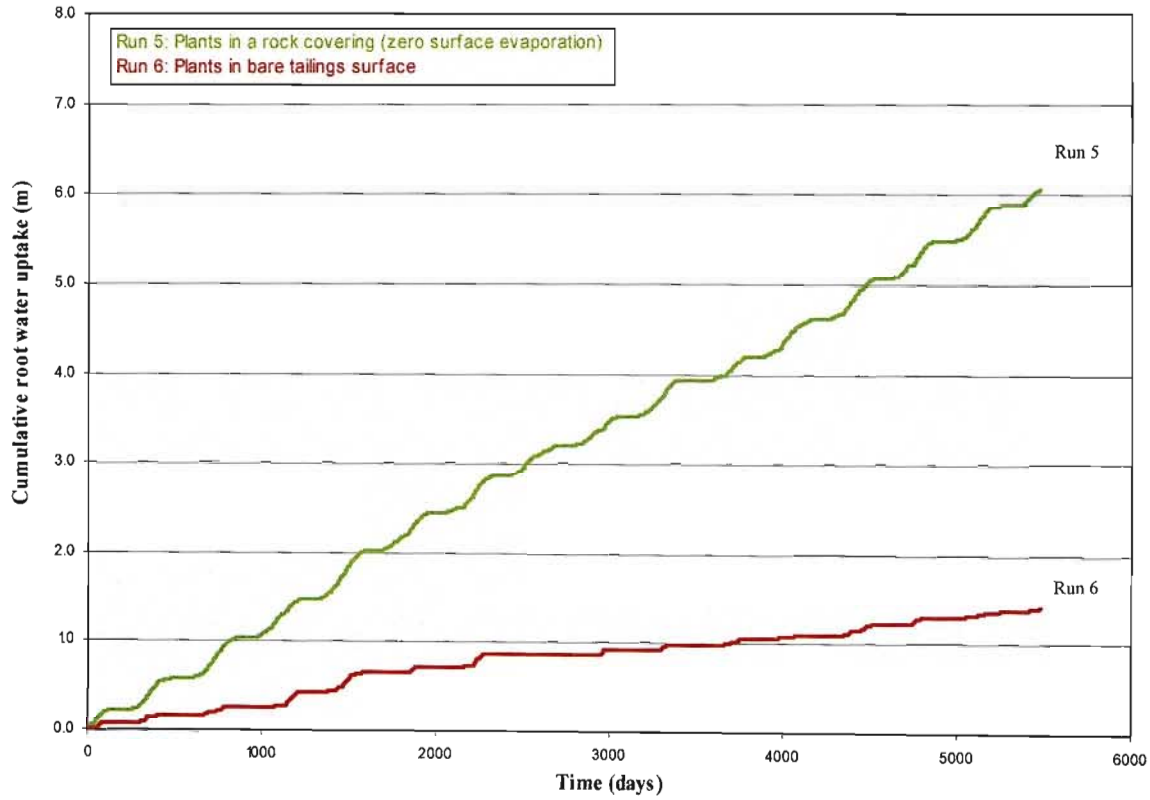

Figure 5.9 Predicted cumulative uptake of water by plants grown in a rock covered (Run 5) and bare tailings surface (Run 6).

The combined effect of surface evaporation and plant growth seems to provide the best option for reducing seepage. In Run 6 the predicted cumulative seepage was the lowest out of all runs at 0.899 m. Run 5 demonstrated that unstressed vegetation can extract

significant volumes of water, thus if rainfall had to increase in the future a vegetated surface would also seem to provide a much more responsive mechanism to reducing seepage than a bare surface.

The initial rate of seepage in all simulations was rapid; only after approximately 1700 days did the trends of the individual runs becoming evident (Figure 5.8B). This initial drainage, as already discussed, was the result of free water in the profile being allowed to pass too easily through the seepage face. The initial conditions inputted into *HYDRUS-2D* stipulated that the lower 10 m of the flow domain, in accordance with field observations, were saturated. Thus the initial loss of water can be attributed to the fact that excess water in this zone drained freely from the profiles (Figure 5.8B). After this point however, seepage was controlled by the volume of water infiltrating at the surface.

These simulations show that there is an increase in the seepage volume as surface evaporation is suppressed. Run 1 experienced a net loss of water from the atmospheric boundary and as a result it had minimal seepage losses. Over the 15 years 0.902 m of water was lost from the seepage face in Run 1, in comparison to 0.977 m, 1.207 m and 1.767 m for Runs 2, 3 and 4, respectively (Figure 5.8B). It is thus evident that surface evaporation significantly affects infiltration and plays a major role in controlling the amount of drainage water lost from the base of the tailings. These trends are highlighted in Figure 5.10, which shows how the predicted 15 year cumulative seepage is increased as evaporation rates are decreased.

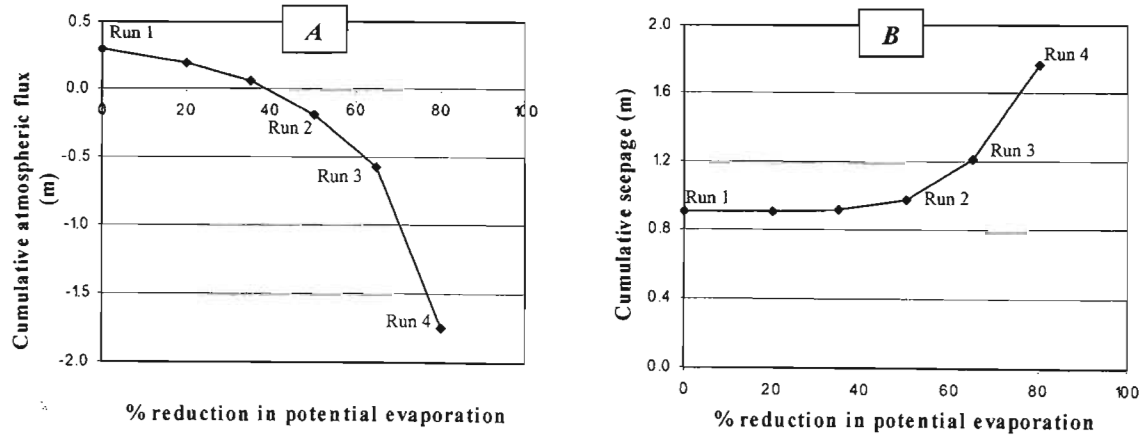

Figure 5.10 The effect of reducing surface evaporation on (A) the 15 year cumulative atmospheric flux and (B) on the cumulative volume of seepage water lost from the base of the tailings.

If evaporation is suppressed by no more than about 40% it is predicted that over extended periods of time more water will be lost via evaporation than gained by infiltration (Figure 5.10A; Appendix 11). Any further suppression of evaporation will cause an exponential increase in infiltration and seepage. At 65% reduction, 9% of the total simulated rainfall was predicted to infiltrate. Given the footprint area of the tailings (522 000 m^2) this amounts to a cumulative volume of about 296 000 m^3 for the simulation period (Appendix 11). An 80% reduction will cause about 28% infiltration, which equates to a net volume of approximately 914 000 m^3 across the entire impoundment. As a result of this infiltration the amount of water lost as seepage undergoes a similar exponential increase. The simulations predicted that compared to bare tailings the rock cladding increased drainage by between 159 000 m^3 (Run 3) and 452 000 m^3 (Run 4) for the 15 years.

5.6 Conclusions

The *HYDRUS-2D* simulations have shown that the rock cladding is increasing the volume of drainage water leaving the base of the impoundment. In order to quantify this more accurately, further investigations will have to be undertaken to investigate the extent to which the rock cladding suppress evaporation from the tailings surface. Based on literature values it is expected to be in the region of 80%. At this level, infiltration and seepage were shown to be greatly enhanced and thus the impoundment is expected to remain saturated and leach greater volumes of contaminated water if no remediation strategy is implemented.

According to the model simulations, a vegetated surface with no mulching will provide the best opportunity for maximising water losses from the surface of the impoundment. However, due to the arid environment it may be very difficult to establish and maintain a good vegetative cover without some form of mulching. The rock mulch was shown to increase the moisture content of the tailings; this could help to promote the establishment and vigour of a vegetation cover. This latter option may then provide the most suitable and practical alternative for effective remediation of the Pering tailings impoundment. The rock mulch would also be of further benefit in that it would help to prevent dust blow off during drought years, when the vegetation cover may be sparse.

CHAPTER 6

GENERAL CONCLUSIONS

The main objective of this investigation was to quantify the potential risk for groundwater contamination that may arise as a result of water percolation through the metal-rich tailings impoundment at the Pering Mine.

Mineralogical analysis (XRD) and investigations with SEM/EDAX identified that the tailings consists predominantly of dolomite with traces of potassium feldspar, quartz, pyrite, sphalerite and galena. Acid-base accounting (ABA) showed that the buffering capacity of the material exceeds its capacity to produce acidity through sulfide oxidation. It is therefore expected that the pH of the mine drainage at Pering will remain alkaline. This will favour the immobilisation of heavy metals and thereby help to protect the groundwater from excessive heavy metal contamination.

In comparison to the total metal load in the tailings, only a small fraction was solublised under saturated conditions. Of the four extraction methods which were tested, the TCLP gave the highest estimate of element availability. This method extracted 1873 mg kg^{-1} of Zn and 249 mg kg^{-1} of Pb. DTPA extractable Zn and Pb were somewhat lower than this at 1056 and 27.3 mg kg^{-1}, respectively. In comparison to other Pb/Zn mine tailings around the World, the available Zn concentrations are very high, whereas those of Pb are moderate.

Leaching the tailings with distilled water caused substantial mobilisation of contaminants. In many instances high concentrations of S, Mg, Mn, Hg and Zn were observed. It was therefore concluded that infiltrating water could cause groundwater contamination, if sufficient volumes were lost from the base of the impoundment. Due to the underlying fractured dolomite and minimal soil cover, it was assumed that limited sorption of contaminants was occurring. This study, however, did not look into the mechanisms of solute transport below the impoundment and thus this assumption will require further investigation.

No strongly developed oxidation zone was found in the tailings impoundment at Pering Mine. This was most likely due to the fact that the impoundment had only been

decommissioned two years prior to sampling. The elevated redox conditions and alkaline pH throughout the impoundment would have also promoted sulfide oxidation at all depths and thereby preventing the formation of such a zone (E_h ranged from +323 to +454 mV). The oxidation of sulfide minerals has caused high concentrations of S to be released into solution (an average of 772 mg S l^{-1} or 2317 mg SO_4^{2-} l^{-1}). The corresponding release of high concentrations of metals is mitigated by the strong sorbing capacity of the tailings and possible secondary precipitation. The acidity produced from sulfide oxidation is being buffered by the dissolution of dolomite, which is releasing Ca and Mg into solution.

The average Mg concentration (589 mg l^{-1}) in all pore-water samples was just over 8 times the recommended South African guideline for drinking water (SABS 241: 70 mg l^{-1}). This, in combination with the high SO_4^{2-} concentrations, which on average were just under 6 times the recommended limit of 400 mg l^{-1}, will pose one of the more severe threats to groundwater quality. The $MgSO_4$ aqueous complex is a known laxative and therefore may cause problems for local farmers who depend on good quality groundwater for themselves and their livestock. Analysis of the pore-water also identified a significant mercury problem. Concentrations exceeded recommended limits by between 100 and a 1000 times. It is thought that Hg mobility will be enhanced by forming negatively charged aqueous complexes with anions in solution and therefore it may be leached relatively easily into the groundwater.

Modelling using *HYDRUS-2D* showed that suppressing surface evaporation by more than 40% began to cause exponential increases in the volume of seepage being released from the base of the tailings. In line with the literature, the rock cladding is thought to reduce evaporation by about 80%, although this may be a conservative estimate considering the thickness of the rock layer in many areas. Further investigation will be required in order to quantify the actual extent to which the rock cladding is suppressing evaporation. Future investigations could also be extended to modelling solute transport in both the impoundment and the underlying rock structures. This could allow for the development and progression of a pollution plume to be more accurately assessed. If this were undertaken, however, it would first be necessary to quantify the groundwater hydrology more accurately and the hydrophysical properties of the dolomite.

From this investigation of the Pering Mine tailings impoundment it can be concluded that water percolating through the tailings will become contaminated. From batch extractions, saturated pastes, leaching columns and field sampling of the impoundment pore-water it was identified that Hg, Mg, Mn, Pb, S and Zn were the elements of concern. In many instances the concentrations of these elements released into solution exceeded those considered safe for drinking water (DWAF, 1996a; 1996c; SABS 241, 1999) or the environment (DWAF, 2005). Based on this it is evident that there is a significant possibility of groundwater contamination around the Pering Mine, which has likely been exacerbated by increased infiltration brought about by the rock cladding.

REFERENCES

Abbasi, F., J. Feyen, and M.T. van Genuchten. 2004. Two-dimensional simulation of water flow and solute transport below furrows: Model calibration and validation. Journal of Hydrology 290:63-79.

Abraitis, P., M. Kendrick, R.A.D. Pattrick, and D.J. Vaghan. 2004. Variations in the compositional, textural and electrical properties of natural pyrite: A review. International Journal of Mineral Processes 74:41-59.

Acocks, J.P.H. 1988. Veld types of South Africa, 3rd Edition. Department of Agriculture and Water Supply, Pretoria.

Adams, J.E. 1966. Influence of mulches on runoff, erosion, and soil moisture depletion. Soil Science of America proceedings 30:110-114.

Adriano, D.C. 1986. Trace elements in the terrestrial environment. Springer-Verlag, New York.

Al, T.A., C.J. Martin, and D.W. Blowes. 2000. Carbonate-mineral/water interactions in sulphide-rich tailings. Geochemica et Cosmochimica Acta 64:3933-3948.

Al-Abadleh, A., and V.H. Grassian. 2003. Oxide surfaces as environmental interfaces. Surface Science Reports 52:63-161.

Al-Abadleh, A., H.A. Al-Hosney, and V.H. Grassian. 2005. Oxide and carbonate surfaces as environmental interfaces: The importance of water in surface composition and surface reactivity. Journal of Molecular Catalysis A: Chemical 228:47-54.

Allison, J.D., D.S. Brown, and K.J. Novo-Gradac. 1991. MINTEQ-A2/PRODEF-A2 A geochemical assessment model for environmental systems: Version 3.0 User's Manual. Environmental Research Laboratory, USEPA, Athens, GA.

Alloway, B.J. 1990. Heavy metals in soils. Blackie and Son Ltd, London.

Almås, A., B.R. Singh, and B. Salbu. 1999. Mobility of cadmium-109 and zinc-65 in soil influenced by equilibration time, temperature, and organic matter. Journal of Environmental Quality 28:1742-1750.

Álvarez-Benedi, J., R. Munoz-Carpena, and M. Vanclooster. 2005. Modelling as a tool for the characterization of soil water and chemical fate and transport. p 87-121. *In* Benedi, J.A., and R.M. Carpena (eds.) Soil-water-solute process characterization: An integrated approach. CRC Press, Boca Raton, FL.

Aucamp, P., and A. van Schalkwyk. 2003. Trace element pollution of soils by abandoned gold mine tailings, near Potchefstroom, South Africa. Bulletin of Engineering, Geology and the Environment 62:123-134.

Badawy, S.H., M.I.D. Helal, A.M. Chaudri, K. Lawlor, and S.P. McGrath. 2002. Soil solid-phase controls lead activity in soil solution. Journal of Environmental Quality 31:162-167.

Bain, J.G., D.W. Blowes, W.D. Robertson, and E.O. Frind. 2000. Modelling of sulfide oxidation with reactive transport at a mine drainage site. Journal of Contaminant Hydrology 41:23-47.

Baksi, S.N. 1982. Physiological effects of lead dusts. p 281-310. *In* McGrath, J.J., and C.D. Barnes (eds.) Air pollution: Physiological effects. Academic Press, New York.

Banwart, S.A., and M.E. Malmström. 2001. Hydrochemical modelling for preliminary assessment of minewater pollution. Journal of Geochemical Exploration 74:73-97.

Bartlett, R.J. 1999. Characterizing soil redox behaviour. p 371-397. *In* Sparks, D.L. (ed.) Soil physical chemistry, 2nd Edition. CRC Press, Boca Raton, FL.

Bartlett, R.J., and B.R. James. 1993. Redox chemistry of soils. Advances in Agrononomy 50:151-208.

Bednar, A.J., J.R. Garbarino, J.F. Ranville, and T.R. Wildeman. 2005. Effects of iron on arsenic speciation and redox chemistry in acid mine water. Journal of Geochemical Exploration 85:55-62.

Bellir, K., M. Bencheikh-Lehocine, A.H. Meniai, and N. Gherbi. 2005. Study of the retention of heavy metals by natural material used as liners in landfills. Desalination 185:111-119.

Belzile, N., Y. Chen, M. Cai, and L. Li. 2004. A review on pyrrhotite oxidation. Journal of Geochemical Exploration 84:65-76.

Blake, G.R., and K.H. Hartge. 1986. Particle density. p 377-382. *In* Klute, A. (ed.) Methods of soil analysis: Part 1: Physical and mineralogical methods, 2nd Edition. ASA, CSSA and SSSA, Madison, WI.

Blodau, C. 2006. A review of acidity generation and consumption in acidic coal mine lakes and their watersheds. Science of the Total Environment 369:307-332.

Blowes, D.W., J.L. Jambor, and C.J. Hanton-Fong. 1998. Geochemical, mineralogical and microbiological characterization of a sulphide-bearing carbonate-rich gold-mine tailings impoundment, Joutel, Québec. Applied Geochemistry 13:687-705.

Booth, J., Q. Hong, R.G. Compton, K. Prout, and R.M. Payne. 1997. Gypsum overgrowths passivate calcite to acid attack. Journal of Colloid and Interface Science 192:207-214.

Bradl, H.B. 2004. Adsorption of heavy metal ions on soil and soil constituents. Journal of Colloid and Interface Science 277:1-18.

Brady, P.V., H.W. Papenguth, and J.W. Kelly. 1999. Metal sorption to dolomite surfaces. Applied Geochemistry 14:569-579.

Brookins, D.G. 1988. Eh – pH diagrams for geochemistry. Springer-Verlag, Berlin.

Brooks, R.H., and A.T. Corey. 1964. Hydraulic properties of porous media. Hydrology paper No. 3. Civil Engineering Dept., Colorado State University, Fort Collins, Colorado.

Brown, A.D., and J.J. Jurinak. 1989. Mechanisms of pyrite oxidation in aqueous mixtures. Journal of Environmental Quality 18:545-550.

Bruce, R.R. 1972. Hydraulic conductivity evaluation of the soil profile from soil water retention relations. Soil Science Society of America Proceedings 36:555-561.

Bruno, J., L. Duro, J. de Pablo, I. Casa, C. Ayora, J. Delgado, M.J. Gimeno, J. Pena, C. Linklater, L.P. Pérez del Villar, and P. Gómez. 1998. Estimation of the concentrations of trace metals in natural systems: The application of codissolution and coprecipitation approaches to El Berrocal (Spain) and Pocos de Caldas (Brazil). Chemical Geology 151:277-291.

Cameron, D.R., and A. Klute. 1977. Convective-dispersive solute transport with combined equilibrium and kinetic adsorption model. Water Resources Research 13:183-188.

Carlsson, E., J. Thunberg, B. Öhlander, and H. Holmström. 2002. Sequential extraction of sulfide-rich tailings remediated by the application of till cover, Kristineberg mine, northern Sweden. The Science of the Total Environment 299:207-226.

Carsel, R.F., and R.S. Parrish. 1988. Developing joint probability distributions of soil water retention characteristics. Water Resources Research 24:755-769.

Cave, K., and F.I. Talens-Alesson. 2005. Comparative effect of Mn(II) and Fe(III) as activators and inhibitors of the adsorption of other heavy metals on calcite. Colloids and Surfaces 268:19-23.

Celia, M.A., E.T. Bouloutas, and R.L. Zarba. 1990. A general mass-conservative numerical solution for the unsaturated flow equation. Water Resources Research 26:1483-1496.

Chamber of Mines. 2006. Information obtained from www.bullion.org.za on the 18th of November 2006.

Chernyshova, I.V. 2003. An in situ FTIR study of galena and pyrite oxidation in aqueous solution. Journal of Electroanalytical Chemistry 558:83-98.

Childs, S.W., and J.R. Hanks. 1975. Model of soil salinity effects on crop growth. Soil Science Society of America Journal 39:617-622.

Close, M.E., L. Pang, G.N. Magesan, R. Lee, and S.R. Green. 2003. Field study of pesticide leaching in an allophanic soil in New Zealand. 2: Comparison of simulations from four leaching models. Australian Journal of Soil Research 41:825-846.

Corey, A.T. 1986. Air permeability. p 1121-1136. *In* Klute, A. (ed.) Methods of soil analysis: Part 1: Physical and mineralogical methods, 2nd Edition. ASA, CSSA and SSSA, Madison, WI.

Costigan, P.A., A.D. Bradshaw, and R.P. Gemmell. 1981. The reclamation of acidic colliery spoil: I. Acid production potential. Journal of Applied Ecology 18:865-878.

Cowey, A. 1998. Mineral processing and extractive metallurgy. p 21-31. *In* Wilson, M.G.C., and C.R. Anhaeusser (eds.) The mineral resources of South Africa: Handbook. Council for Geoscience.

Cravotta, C.A., and M.K. Trahan. 1999. Limestone drains to increase pH and remove dissolved metals from acidic mine drainage. Applied Geochemistry 14:581-606.

Crawford, J.W., N. Matsui, and I.M. Young. 1995. The relation between the moisture release curve and the structure of soil. European Journal of Soil Science 46:369-375.

Cukrowska, E.M., K. Govender, and M. Viljoen. 2004. Ion mobility based on column leaching of South African gold tailings dam with chemometric evaluation. Chemosphere 56:39-50.

da Silva, G. 2004. Kinetics and mechanism of the bacterial and ferric sulphate oxidation of galena. Hydrometallurgy 75:99-110.

Dane, J.H., and J.W. Hopmans. 2002. Water retention and storage. p 671-691. *In* Dane, J.H. (ed.) Methods of soil analysis: Part 4: Physical and mineralogical methods. ASA, CSSA and SSSA, Madison, WI.

de Matos, A.T., M.P.F. Fontes, L.M. da Costa, and M.A. Martinez. 2001. Mobility of heavy metals as related to soil chemical and mineralogical characteristics of Brazilian soils. Environmental Pollution 111:429-435.

de Vos, J.A., P.A.C. Raats, and R.A. Feddes. 2002. Chloride transport in a recently reclaimed Dutch polder. Journal of Hydrology 257:59-77.

Dorronsoro, C., F. Martin, I. Ortiz, I. Garcia, M. Simon, E. Fernandez, J. Aguilar, and J. Fernandez. 2002. Migration of trace elements from pyrite tailings in carbonate soils. Journal of Environmental Quality 31:829-835.

Dudka, S., and D.C. Adriano. 1997. Environmental impacts of metal ore mining and processing: A review. Journal of Environmental Quality 26:590-602.

du Toit, C.M. 1998. Zinc. p 676-681. *In* Wilson, M.G.C., and C.R. Anhaeusser (eds.) The mineral resources of South Africa: Handbook. Council for Geoscience.

DWAF. 1996a. South African water quality guidelines, 2nd Edition. Volume 1: Domestic water use. Department of Water Affairs and Forestry, Pretoria.

DWAF. 1996b. South African water quality guidelines, 2nd Edition. Volume 4: Agricultural water use - Irrigation. Department of Water Affairs and Forestry, Pretoria.

DWAF. 1996c. South African water quality guidelines, 2nd Edition. Volume 5: Agricultural water use - Livestock watering. Department of Water Affairs and Forestry, Pretoria.

DWAF. 2005. Waste management series. Minimum requirements for the handling, classification and disposal of hazardous waste, 3rd Edition. Department of Water Affairs and Forestry, Pretoria.

Elberling, B., R.V. Nicholson, and J.M. Scharer. 1994. A combined kinetic and diffusion model for pyrite oxidation in tailings: A change in controls with time. Journal of Hydrology 157:47-60.

Elzahabi, M., and R.N. Yong. 2001. pH influence on the sorption characteristics of heavy metals in the vadose zone. Engineering Geology 60:61-68.

España, J.S., E.L. Pamo, E. Santofimia, O. Aduvire, J. Reyes, and D. Barettino. 2005. Acid mine drainage in the Iberian Pyrite Belt (Odiel river watershed, Huelva, SW Spain): Geochemistry, mineralogy and environmental implications. Applied Geochemistry 15:1-35.

Feddes, R.A., P.J. Kowalik, and H. Zaradny. 1978. Simulation of field water use and crop yield. Simulation monographs. Pudoc, Wageningen, Netherlands.

Ferguson, K.D., and P.M. Erickson. 1988. Pre-mine prediction of acid mine drainage. p 24-33. *In* Salmons, W., and U. Förstner (eds.) Environmental management of solid wastes. Springer-Verlag, Berlin.

Fergusson, J.E. 1990. The heavy elements: Chemistry, environmental impact and health effects. Pergamon Press, Oxford.

Frimmel, F.H., and L. Hube. 1996. Influence of humic substances on the aquatic adsorption of heavy metals on defined mineral phases. Environment International 22:507-517.

Garrels, R.M., and C.L. Christ. 1965. Solutions, minerals, and equilibria. Harper and Row, New York.

Gazea, B., K. Adam, and A. Kontopoulos. 1996. A review of passive systems for the treatment of acid mine drainage. Minerals Engineering 9:23-42.

Gee, G.W., and J.W. Bauder. 1986. Particle size analysis. p 312-383. *In* Klute, A. (ed.) Methods of soil analysis: Part 1: Physical and mineralogical methods, 2nd Edition. ASA, CSSA and SSSA, Madison, WI.

Gee, G.W., P.J. Wierenga, B.J. Andraski, M.H. Young, M.J. Fayer, and M.L. Rockhold. 1994. Variations in water balance and recharge potential at three western desert sites. Soil Science Society of America Journal 58:63-72.

Gerke, H.H., and M.T. van Genuchten. 1993. A duel-porosity model for simulating the preferential movement of water and solutes in structured porous media. Water Resources Research 29:305-319.

Gerson, A.R., and A.R. O'Dea. 2003. A quantum chemical investigation of the oxidation and dissolution mechanisms of galena. Geochemica et Cosmochimica Acta 67:813-822.

Gieré, R., N.V. Sidenko, and E.V. Lazareva. 2003. The role of secondary minerals in controlling the migration of arsenic and metals from high-sulfide wastes (Berikul gold mine, Siberia). Applied Geochemistry 18:1347-1359.

Gleisner, M., and R.B. Herbert. 2002. Sulfide mineral oxidation in freshly processed tailings: Batch experiments. Journal of Geochemical Exploration 76:139-153.

Gómez del Río, J.A., P.J. Morando, and D.S. Cicerone. 2004. Natural materials for the treatment of industrial effluents: Comparative study of the retention of Cd, Zn and Co by calcite and hydroxyapatite. Part 1: Batch experiments. Journal of Environmental Management 71:169-177.

Green, R.E., and J.C. Corey. 1971. Calculation of hydraulic conductivity: A further evaluation of some predictive methods. Soil Science Society of America Proceedings 35:3-8.

Groenevelt, PH., P. van Straaten, V. Rasiah, and J. Simpson. 1989. Modification in evaporation parameters by rock mulches. Soil Technology 2:279-285.

Gulson, B.L., J.J. Davis, K.J. Mizon, M.J. Korsch, A.J. Law, and D. Howarth. 1994. Lead bioavailability in the environment of children: Blood lead levels in children could be elevated in a mining community. Archives of Environmental Health 49:326-331.

Gupta, S.K. 1992. Mobilizable metal in anthropogenic soils and its ecological significance. p 299-310. *In* Vernet, J.P (ed.) Impact of heavy metals on the environment. Elsevier Science Publishers, Amsterdam.

Gupta, S.K., M.K. Vollmer, and R. Krebs. 1996. The importance of mobile, mobilisable and pseudo total heavy metal fractions in soil for three-level risk assessment and risk management. The Science of the Total Environment 178:11-20.

Hall, J.R., B. Reynolds, T. Sparks, A. Colgan, I. Thornton, and S.P. McGrath. 2001. The relationship between topsoil, soil and stream sediment heavy metal concentrations and acidification. Water, Air, and Soil Pollution 130:1067-1072.

Hallberg, R.O., J.R. Granhagen, and A. Liljemark. 2005. A fly ash/biosludge dry cover for mitigation of AMD at the Falun mine. Chemie der Erde Geochemistry 65:S1,43-63.

Hanks, R.J., and N.P. Woodruff. 1958. Influence of wind on water vapour transfer through soil, gravel, and straw mulches. Soil Science 86:160-164.

Hanson, B.R., J. Šimůnek, and J.W. Hopmans. 2006. Evaluation of urea-ammonium-nitrate fertigation with drip irrigation using numerical modelling. Agricultural Water Management 86:102-113.

Heyden, C.J., and M.G. New. 2004. Groundwater pollution on the Zambian Copperbelt: Deciphering the source and the risk. Science of the Total Environment 327:17-30.

Hide, J.C. 1954. Observations on factors influencing the evaporation of soil moisture. Soil Science Society Proceedings 18:234-238.

Hiroyoshi, N., H. Miki, T. Hirajima, and M. Tsunekawa. 2001. Enhancement of chalcopyrite leaching by ferrous ions in acidic ferric sulfate solutions. Hydrometallurgy 60:185-197.

Hutson, J.L. 2001. Leaching estimation and chemistry model - LEACHM: Model description and users guide. The Flinders University of South Australia, School of Chemistry, Physics and Earth Sciences.

Jackson, M.L. 1958. Soil chemical analysis. Constable Company Limited, London.

Janzen, M.P., R.V. Nicholson, J.M. Scharer. 2000. Pyrrhotite reaction kinetics: Reaction rates for oxidation by oxygen, ferric iron, and for nonoxidative dissolution. Geochemica et Cosmochimica Acta 64:1511-1522.

Jaynes, D.B., A.S. Rogowski, and H.B. Pionke. 1984. Acid mine drainage from reclaimed coal strip mines: 1 Model description. Water Resources Research 2:233-242.

Johnson, R.H., D.W. Blowes, W.D. Robertson, and J.L. Jambor. 2000. The hydrogeochemistry of the Nickel Rim mine tailings impoundment, Sudbury, Ontario. Journal of Contaminant Hydrology 41:49-80.

Jurjovec, J., C.J. Ptacek, and D.W. Blowes. 2002. Acid neutralization mechanisms and metal release in mine tailings: A laboratory column experiment. Geochemica et Cosmochimica Acta 66:1511-1523.

Jury, W.A., and B. Bellantuoni. 1976. Heat and water movement under surface rocks in a field soil: II. Moisture effects. Soil Science Society of America Journal 40:509-513.

Kemper, W.D., A.D. Nicks, and A.T. Corey. 1994. Accumulation of water in soils under gravel and sand mulches. Soil Science Society of America Journal 58:56-63.

Kern, J.S. 1995. Evaluation of soil water retention models based on basic soil properties. Soil Science Society of America Journal 59:1134-1141.

Klute, A., and C. Dirksen. 1986. Hydraulic conductivity and diffusivity: Laboratory methods. p 687-770. *In* Klute, A. (ed.) Methods of soil analysis: Part 1: Physical and mineralogical methods, 2nd Edition. ASA, CSSA and SSSA, Madison, WI.

Koschinsky, A., A. Winkler, and U. Fritsche. 2003. Importance of different types of marine particles for the scavenging of heavy metals in the deep-sea bottom water. Applied Geochemistry 18:693-710.

Kovács, E., W.E. Dubbin, and J. Tamás. 2006. Influence of hydrology on heavy metal speciation and mobility in a Pb-Zn mine tailing. Environmental Pollution 141:310-320.

Lan, C.Y., W.S. Shu, and M.H. Wong. 1998. Reclamation of Pb/Zn Mine tailings at Shaoguan, Guangdong Province, People's Republic of China: The role of river sediment and domestic refuse. Bioresources Technology 65:117-124.

Land Type Survey Staff. 1986. Land types of the maps SE27/20 Witdraai, 2720 Noenieput, 2722 Kuruman, 2724 Christana, 2820 Upington, 2822 Postmasburg. Memoirs on the Agricultural Natural Resources of South Africa No. 3.

Landa, E.R. 1978. Soil water content and temperature as factors in the volatile loss of applied mercury (II) from soils. Soil Science 126:44-48.

Lee, S., J.A. Dyer, D.L. Sparks, N.C. Scrivner, and E.J. Elzinga. 2006. A multi-scale assessment of Pb(II) sorption on dolomite. Journal of Colloid and Interface Science 298:20-30.

Lei, L., and R. Watkins. 2005. Acid drainage reassessment of mine tailings, Black Swan Nickel Mine, Kalgoorlie, Western Australia. Applied Geochemistry 20:661-667.

Lemon, E.R. 1956. The potentialities for decreasing soil moisture evaporation loss. Soil Science Society of America Proceedings 20:120-125.

Liang, J., and R.E. Karamanos. 1993. DTPA-extractable Cu, Fe, Mn and Zn. p 87-90. *In* Carter, M.R. (ed.) Soil sampling and methods of analysis. Lewis Publishers, Boca Raton, FL.

Lin, Z. 1997. Mobilization and retention of heavy metals in mill-tailings from Garpenberg sulfide mines, Sweden. The Science of the Total Environment 198:13-31.

Lindsay, W.L. 1979. Chemical equilibria in soils. John Wiley and Sons, New York.

Ljungberg, J., and B. Öhlander. 2001. The geochemical dynamics of oxidising mine tailings at Laver, northern Sweden. Journal of Geochemical Exploration 74:57-72.

Lorentz, S.A., P. Goba, and J. Pretorius. 2001. Experiments and measurements of soil hydraulic characteristics. Report to the Water Research Commission on the project: Experimentation and laboratory measurement for hydrological process research. WRC Report 744/0/01.

Louise, S., and S. Stipp. 1998. Surface analytical techniques applied to calcite: Evidence of solid-state diffusion and implications for isotope methods. Palaeogeography, Palaeoclimatology, Palaeoecology 140:441-457.

Low, A.B., and A.G. Rebelo. 1996. Vegetation of South Africa, Lesotho and Swaziland. Department of Environmental Affairs and Tourism, Pretoria.

Lu, J., D.B. Dreisinger, and W.C. Cooper. 1997. Cobalt precipitation by reduction with sodium borohydride. Hydrometallurgy 45:305-322.

Malmström, M.E., M. Gleisner, and R.B. Herbert. 2006. Element discharge from pyretic mine tailings at limited oxygen availability in column experiments. Applied Geochemistry 21:184-202.

Manz, M., and L.J. Castro. 1997. The environmental hazard caused by smelter slags from the Sta. Maria De La Paz mining district in Mexico. Environmental Pollution 98:7-13.

Martin-Garin, A., P. Van Cappellen, and L. Charlet. 2003. Aqueous cadmium uptake by calcite: A stirred flow-through reactor study. Geochemica et Cosmochimica Acta 67:2763-2774.

Maynard, D.G., and Y.P. Kalra. 1993. Nitrate and exchangeable ammonium nitrogen. p 25-38. *In* Carter, M.R. (ed.) Soil sampling and methods of analysis. Lewis Publishers, Boca Raton, FL.

McBride, M.B. 1989. Reactions controlling heavy metal solubility. Advances in Soil Science 10:1-53.

McBride, M.B. 1994. Environmental chemistry of soils. Oxford University Press, New York.

McGowen, S.L., and N.T. Basta. 2001. Heavy metal solubility and transport in soil contaminated by mining and smelting. p 89-107. *In* Selim, H.M., and D.L. Sparks (eds.) Heavy metals release in soils. Lewis Publishers, London.

McGregor, R.G., and D.W. Blowes. 2002. The physical, chemical and mineralogical properties of three cemented layers within sulfide-bearing mine tailings. Journal of Geochemical Exploration 76:195-207.

McGregor, R.G., D.W. Blowes, and J.L. Jambor. 1998. The solid phase controls on the mobility of heavy metals at the Copper Cliff tailings area, Sudbury, Ontario, Canada. Journal of Contaminant Hydrology 33:247-271.

McIntyre, D.S. 1974. Procuring undisturbed cores for soil physical measurements. p 12-20. *In* Loveday, J. (ed.) Methods for analysis of irrigated soils. Teck. Comm. 54. Commonwealth Bureau of Soils. Farnham Royal, Bucks, England.

Mihaljevič, M., L. Sisr, V. Ettler, O. Šebek, and J. Průša. 2004. Oxidation of As-bearing gold ore – a comparison of batch and leaching experiments. Journal of Geochemical Exploration 81:59-70.

Milton, A., M.S. Johnson, and J.A. Cooke. 2002. Lead within ecosystems on metalliferous mine tailings in Wales and Ireland. The Science of the Total Environment 299:177-190.

Modaihsh, A.S., R. Horton, and D. Kirkham. 1985. Soil water evaporation suppression by sand mulches. Soil Science 139:357-361.

Moncur, M.C., C.J. Ptacek, D.W. Blowes, and J.L. Jambor. 2005. Release, transport and attenuation of metals from an old tailings impoundment. Applied Geochemistry 20:639-659.

Moodley, M. 2001. Effects of the land disposal of water treatment sludge on soil physical quality. Ph.D. diss. University of Natal, Pietermaritzburg, South Africa.

Moreno, L., and I. Neretnieks. 2006. Long-term environmental impact of tailings deposits. Hydrometallurgy 83:176-183.

Mualem, Y. 1976. A new model for predicting the hydraulic conductivity of unsaturated porous media. Water Resources Research 12:513-522.

Naicker, K., E. Cukrowska, and T.S. McCarthy. 2003. Acid mine drainage arising from gold mining activity in Johannesburg, South Africa and environs. Environmental Pollution 122:29-40.

Nekedi-Kizza, P., J.W. Biggar, H.M. Selim, M.T. van Genuchten, P.J. Wierenga, J.M. Davidson, and D.R. Nielsen. 1984. On the equivalence of two conceptual models for describing ion exchange during transport through an aggregated Oxisol. Water Resources Research 20:1123-1130.

Newton, D.W., and R. Ellis. 1974. Loss of mercury (II) from solution. Journal of Environmental Quality 3:20-23.

Nielsen, D.R., and J.W. Biggar. 1961. Miscible displacement: 1. Experiment information. Soil Science Society of America Proceedings 25:1-5.

Palmer, K.T., and C.L. Kucera. 1980. Lead contamination of sycamore and soil from lead mining and smelting operations in Eastern Missouri. Journal of Environmental Quality 9:106-110.

Pang, L., M.E. Close, J.P.C. Watt, and K.W. Vincent. 2000. Simulation of picloram, atrazine, and simazine leaching through two New Zealand soils and into groundwater using HYDRUS-2D. Journal of Contaminant Hydrology 44:19-46.

Peters, T.H. 1988. Mine tailings reclamation. Inco Limited's Experience with the reclaiming of sulphide tailings in the Sudbury Area, Ontario, Canada. *In* Salmons, W., and U. Förstner (eds.) Environmental management of solid wastes. Springer-Verlag, Berlin.

Phillips, I.R. 2006. Modelling water and chemical transport in large undisturbed soil cores using HYDRUS-2D. Australian Journal of Soil Research 44:27-34.

Pinder, G.F., and W.G. Gray. 1977. Finite element simulation in surface and subsurface hydrology. Academic Press, New York.

Potgieter, J.H., S.S. Potgieter-Vermaak, and P.D. Kalibantonga. 2006. Heavy metal removal from solution by palygorskite clay. Minerals Engineering 19:463-470.

Potgieter-Vermaak, S.S., J.H. Potgieter, P. Monama, and R. van Grieken. 2006. Comparison of limestone, dolomite and fly ash as pre-treatment agents for acid mine drainage. Minerals Engineering 19:454-462.

Rassam, D.W., and F.J. Cook. 2002. Numerical simulations of water flow and solute transport applied to acid sulfate soils. Journal of Irrigation and Drainage Engineering 128:107-115.

Rassam, D.W., J. Šimůnek, and T.M. van Genuchten. 2004. Modelling variably saturated flow with HYDRUS-2D, 2nd Edition. ND Consult, Brisbane.

Richards, L.A. 1931. Capillary conduction of liquids in porous media. Physics 1:318-333.

Rimstidt, J., and D.J. Vaughan. 2003. Pyrite oxidation: A state-of-the-art assessment of the reaction mechanism. Geochemica et Cosmochimica Acta 67:873-880.

Romano, C.G., K.U. Mayer, D.R. Jones, D.A. Ellerbroek, and D.W. Blowes. 2003. Effectiveness of various cover scenarios on the rate of sulfide oxidation of mine tailings. Journal of Hydrology 271:171-187.

Romero, E., E. Benítez, and R. Nogales. 2005. Suitability of wastes from olive-oil industry for initial reclamation of a Pb/Zn mine tailing. Water, Air, and Soil Pollution 165:153-165.

Rösner, T., and A. van Schalkwyk. 2000. The environmental impact of mine tailings footprints in the Johannesburg region, South Africa. Bulletin of Engineering, Geology and the Environment 59:137-148.

Ross, S.M. 1994. Sources and forms of potentially toxic metals in soil-plant systems. p 3-26. *In* Ross, S.M. (ed.) Toxic metals in soil-plant systems. John Wiley and Sons Ltd, Chichester.

Rosso, K.M., U. Becker, and M.F. Hochella. 1999. The interaction of pyrite {001} surfaces with O_2 and H_2O: Fundamental oxidation mechanisms. American Mineralogist 84:1549-1561.

Rouff, A.A., R.J. Reeder, and N.S. Fisher. 2005. Electrolyte and pH effects on Pb(II)–calcite sorption processes: The role of the $PbCO_3^0{}_{(aq)}$ complex. Journal of Colloid and Interface Science 286:61-67.

Rytuba, J.J. 2000. Mercury mine drainage and process that control its environmental impact. The Science of the Total Environment 260:57-71.

SABS 241. 1999. Drinking Water, 4th Edition. South African Bureau of Standards, Pretoria.

Salmon, S.U., and M.E. Malmström. 2006. Quantification of mineral dissolution rates and applicability of rate laws: Laboratory studies of mill tailings. Applied Geochemistry 21:269-288.

Salmons, W. 1995. Environmental impact of metals derived from mining activities: Processes, predictions, prevention. Journal of Geochemical Exploration 52:5-23.

Sandström, A., A. Shchukarev, and J. Paul. 2005. XPS characterisation of chalcopyrite chemically and bio-leached at high and low redox potential. Minerals Engineering 18:505-515.

Saxena, S., and S.F. D'Souza. 2006. Heavy metal pollution abatement using rock phosphate mineral. Environment International 32:199-202.

Schosseler, P.M., B. Wehrli, and A. Schweiger. 1999. Uptake of Cu^{2+} by the calcium carbonates vaterite and calcite as studied by continuous wave (CW) and pulse electron paramagnetic resonance. Geochemica et Cosmochimica Acta 63:1955-1999.

Schulze, R.E. 1995. Hydrology and agrohydrology: A text to accompany the *ACRU 3.00* agrohydrological modelling system. University of Natal, Pietermaritzburg.

Schulze, R.E. 2006. Baseline land cover. *In* Schulze, R.E. (ed.) South African atlas of climatology and agrohydrology. Water Research Commission, Pretoria. WRC Report 1489/1/06.

Sellers, K. 1998. Fundamentals of hazardous waste site remediation. Lewis Publishers, Florida.

Sharma, R.S., and T.S. Al-Busaidi. 2001. Groundwater pollution due to a tailings dam. Engineering Geology 60:235-244.

Shi, W.S., Z. Fang, and J. Ni. 2006. Comparative study on the bioleaching of zinc sulphides. Process Biochemistry 41:438-446.

Shu, W.S., H.P. Xia, Z.Q. Zhang, C.Y. Lan, and M.H. Wong. 2002. Use of *Vetiver* and three other grasses for revegetation of Pb/Zn mine tailings: Field experiment. International Journal of Phytoremediation 4:47-57.

Shu, W.S., Z.H. Ye, C.Y. Lan, Z.Q. Zhang, and M.H. Wong. 2001. Acidification of lead/zinc mine tailings and its effect on heavy metal mobility. Environment International 26:389-394.

Shuman, L.M. 1999. Effect of organic waste amendments on Zn adsorption by two soils. Soil Science 164:197-205.

Sidle, R.C., J.C. Chambers, and M.C. Amacher. 1991. Fate of heavy metals in an abandoned lead-zinc tailings pond: II. Sediment. Journal of Environmental Quality 20:752-758.

Sims, J.T. 1996. Lime requirement. p 491-515. *In* Sparks, D.L. (ed.) Methods of soil analysis: Part 3. Chemical methods. ASA, CSSA and SSSA, Madison, WI.

Šimůnek, J., M. Šejna, and M.T. van Genuchten. 1999. The HYDRUS-2D software package for simulating the two-dimensional movement of water, heat, and multiple solutes in variably-saturated media: Version 2.0. U.S. Salinity Laboratory, USDA, Riverside, California.

Sinha, V., and K. Li. 2000. Alternative methods for dissolved oxygen removal from water: A comparative study. Desalination 127:155-164.

Soil Classification Working Group. 1991. Soil classification: A taxonomic system for South Africa. The Department of Agricultural Development, Pretoria.

Soil Salinity Laboratory Staff. 1954. Diagnosis and improvement of saline and alkali soils. USDA, Washington DC.

Sposito, G. 1989. The chemistry of soils. Oxford University Press, New York.

Strömberg, B., and S. Banwart. 1999. Weathering kinetics of waste rock from the Aitic copper mine, Sweden: Scale dependent rate factors and pH controls in large column experiments. Journal of Contaminant Hydrology 39:59-89.

Tan, K.H. 1998. Principals of soil chemistry, 3rd Edition. Marcel and Dekker, Inc., New York.

The Non-Affiliated Soil Analysis Work Committee. 1990. Handbook of standard soil testing methods for advisory purposes. Soil Science Society of South Africa, Pretoria.

Tordoff, G.M., A.J.M. Baker, and A.J. Willis. 2000. Current approaches to the revegetation and reclamation of metalliferous mine wastes. Chemosphere 41:219-228.

Toride, N., F.J. Leij, and M.T. van Genuchten. 1999. The CXTFIT code for estimating transport parameters from laboratory or field tracer experiments: Version 2.1. U.S. Salinity Laboratory Agricultural Research Service, Riverside, California.

Travis, C.C., and E.L. Etnier. 1981. A survey of sorption relationships for reactive solutes in soil. Journal of Environmental Quality 10:8-17.

Unger, P.W. 1971. Soil profile gravel layers effect on water storage distribution and evaporation. Soil Science of America Proceedings 35:631-634.

van Genuchten, M.T. 1980. A closed-form equation for predicting the hydraulic conductivity of unsaturated soils. Soil Science Society of America Journal 44:892-898.

van Genuchten, M.T., and P.J. Wierenga. 1977. Mass transfer studies in sorbing porous media: I. Analytical solutions. Soil Science Society of America Journal 41:272-277.

van Genuchten, M.T., and R.J. Wagenet. 1989. Two-site/two-region models for pesticide transport and degradation: Theoretical development and analytical solutions. Soil Science Society of America Journal 53:1303-1310.

van Genuchten, M.T., J. Šimůnek, F.J. Leij, and M. Šejna. 1999. Code for quantifying the hydraulic functions of unsaturated soils. U.S. Salinity Laboratory, Riverside, California.

Vaughan, D.J., U. Becker, and K. Wright. 1997. Sulfide mineral surfaces: Theory and experiment. International Journal of Mineral Processes 51:1-14.

Ventrella, D., B.P. Mohanty, J. Šimůnek, N. Losavio, and M.T. van Genuchten. 2000. Water and chloride transport in fine-textured soil: Field experiment and modelling. Soil Science 165:624-631.

Vigneault, B., P.G. Campbell, A. Tessier, and R. De Vitre. 2001. Geochemical changes in sulfidic mine tailings stored under a shallow water cover. Water Research 35:1066-1076.

Voegelin, A., K. Barmettler, and R. Kretzschmar. 2003. Heavy metal release from contaminated soils: Comparison of column leaching and batch extraction results. Journal of Environmental Quality 32:865-875.

Vogel, T., and M. Císlerová. 1988. On the reliability of unsaturated hydraulic conductivity calculated from the moisture retention curve. Transport in Porous Media 3:1-15.

Vogel, T., M. Cislerova, and J.W. Hopmans. 1991. Porous media with linearly variable hydraulic properties. Water Resources Research 27:2735-2741.

Walkley, A. 1947. A critical examination of a rapid method for determining organic carbon in soils: Effect of variations in digestion conditions and of organic soil constituents. Soil Science 63:251-263.

Ward, A., and G. Gee. 1997. Performance evaluation of a field-scale surface barrier. Journal of Environmental Quality 26:694-705.

Weisner, C.G., R.C. Smart, and A.R. Gerson. 2004. A comparison of the kinetics and mechanism of acid leaching of sphalerite containing low and high concentrations of iron. International Journal of Mineral Processes 74:239-249.

WHO. 1996. Guidelines for drinking-water quality, 2nd Edition. Volume 2: Health criteria and other supporting information. World Health Organization, Geneva.

WHO. 2001. Air quality guidelines, 2nd Edition. World Health Organization, Copenhagen.

WHO. 2004. Guidelines for drinking-water quality, 3rd Edition. Volume 1: Recommendations. World Health Organization, Geneva.

Wilson, M.G.C. 1998. Mining in South Africa: Legislation and environmental considerations. p 11-20. *In* Wilson, M.G.C., and C.R. Anhaeusser (eds.) The mineral resources of South Africa: Handbook. Council for Geoscience.

Wu, L., J.A. Vomocil, and S.W. Childs. 1990. Pore size, particle size, aggregate size and water retention. Soil Science Society of America Journal 54:952-956.

Wunderly, M.D., D.W. Blowes, E.O. Frind, and C.J. Ptacek. 1996. Sulfide mineral oxidation and subsequent reactive transport of oxidation products in mine tailings impoundments: A numerical model. Water Resources Research 32:3173-3187.

Xenidis, A., N. Papassiopi, and K. Kominitsas. 2003. Carbonate-rich mining tailings in Lavrion: Risk assessment and proposed rehabilitation schemes. Advances in Environmental Research 7:479-494.

Ye, Z.H., J.W. Wong, M.H. Wong, A.J. Baker, W.S. Shu, and G.Y. Lan. 2000. Revegetation of Pb/Zn mine tailings, Guangdong Province, China. Restoration Ecology 8:87-92.

Ye, Z.H., W.S. Shu, Z.Q. Zhang, C.Y. Lan, and M.H. Wong. 2002. Evaluation of major constraints to revegetation of lead/zinc mine tailings using bioassay techniques. Chemosphere 47:1103-1111.

Yin, Q., G.H. Kelsall, D.J. Vaughan, and K.E.R. England. 1995. Atmospheric and electrochemical oxidation of the surface of chalcopyrite ($CuFeS_2$). Geochemica et Cosmochimica Acta 59:1091-1100.

Yong, R.N., W.Z.W. Yaacob, S.P. Bentley, C. Harris, and B.K. Tan. 2001. Partitioning of heavy metals on soil samples from column tests. Engineering Geology 60:307-322.

Zachara, J.M., J.A. Kittrick, L.S. Dake, and J.B. Harsh. 1989. Solubility and surface spectroscopy of zinc precipitates on calcite. Geochemica et Cosmochimica Acta 53:9-19.

LIST OF APPENDICES

APPENDIX 1

Microscopy investigations

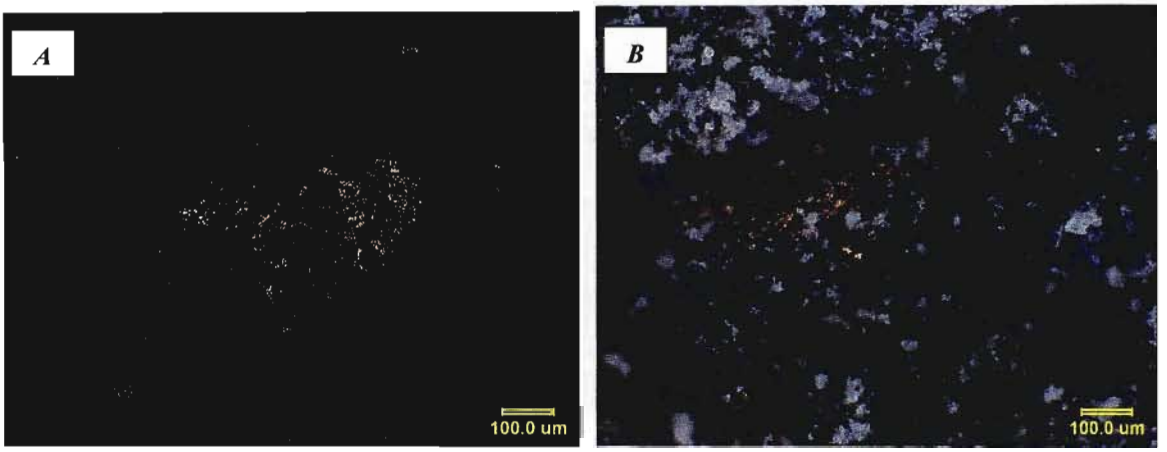

Figure A1.1 Images of Pering's tailings material (TT sample) under a light microscope. Sulfide minerals can be seen to occur as discreet particles (*A*) or associated directly with the dolomite granules (*B*).

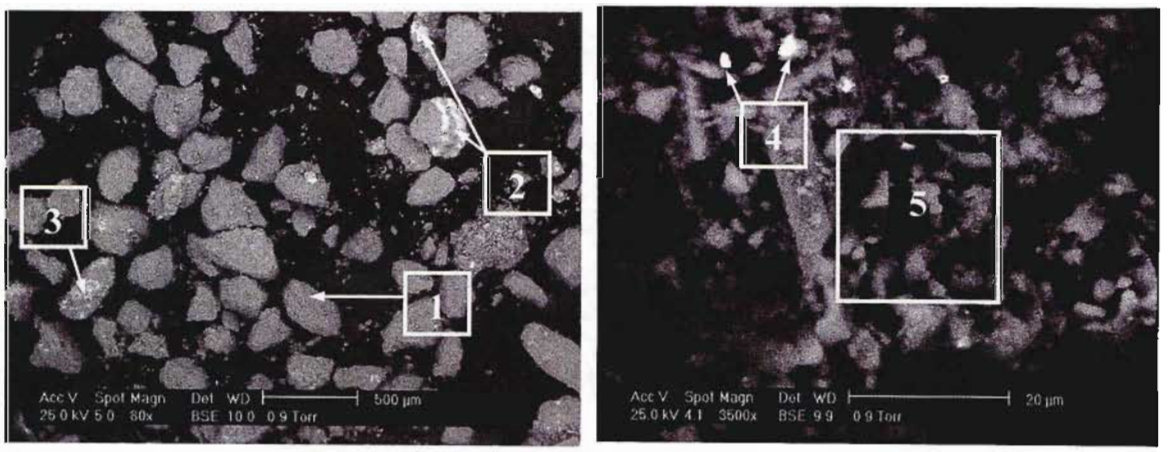

Figure A1.2 SEM images of Pering's tailings material (TT sample) showing the background dolomitic matrix (1), sphalerite (2), pyrite (3), galena (4) and surface precipitates (5), most likely calcite ($CaCO_3$) with possible traces of gypsum ($CaSO_4$).

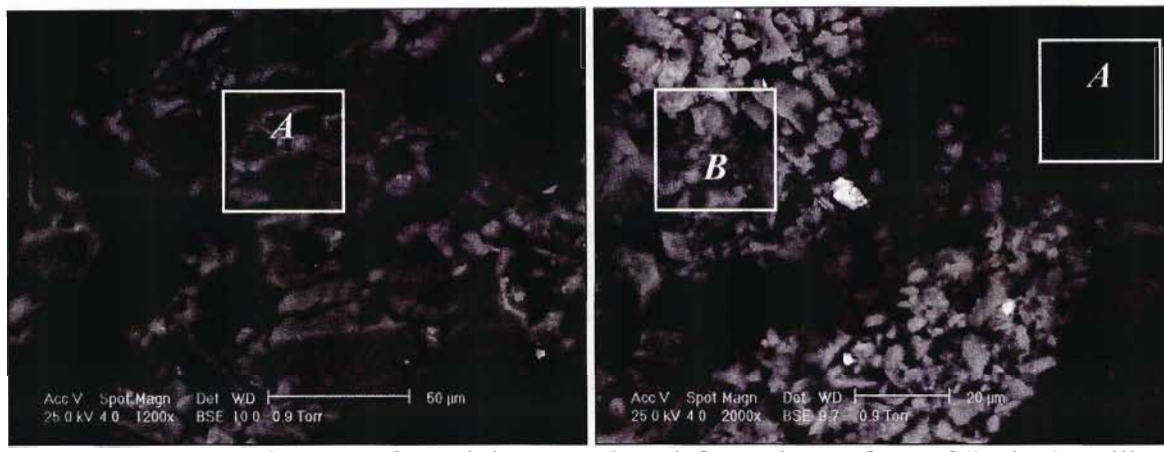

Figure A1.3 SEM images of precipitates gathered from the surface of Pering's tailings impoundment. Simultaneous EDAX scans identified the mineral in the blocks labelled *A* as consisting exclusively of Mg, O and S, most likely as $MgSO_4$. The block labelled *B* contained traces of Pb, Zn and Fe as impurities in what was most likely NaCl, $CaCO_3$ and $CaSO_4$ precipitates, which cover the background $MgSO_4$ mineral (*A*).

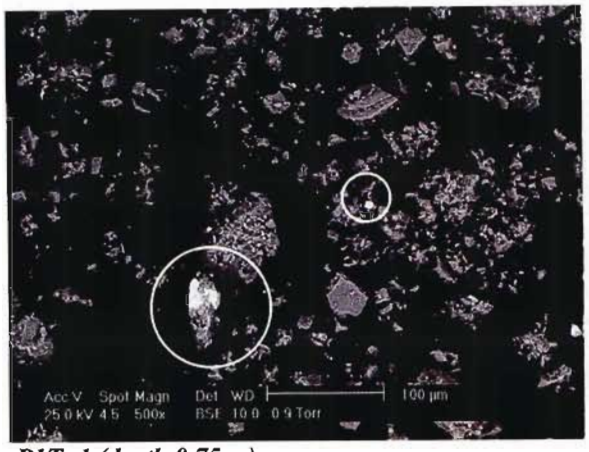

P1T -1 (depth 0.75 m)

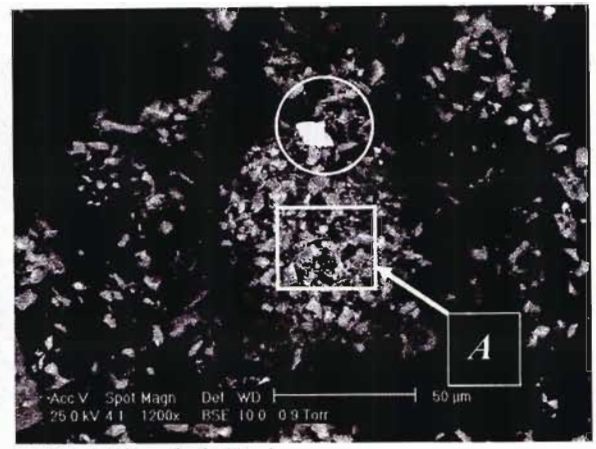

P1T – 5 (depth 6.75 m)

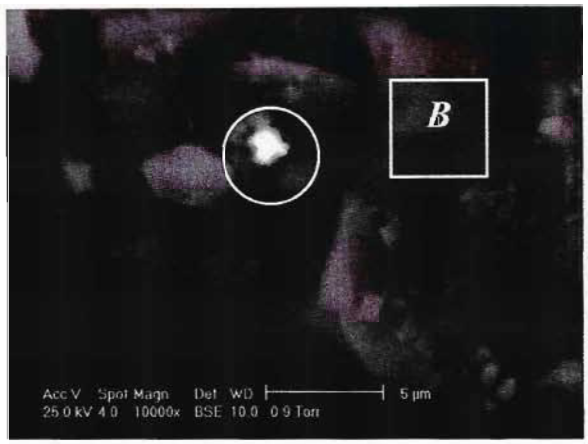

P1T-15 (depth 21.75m)

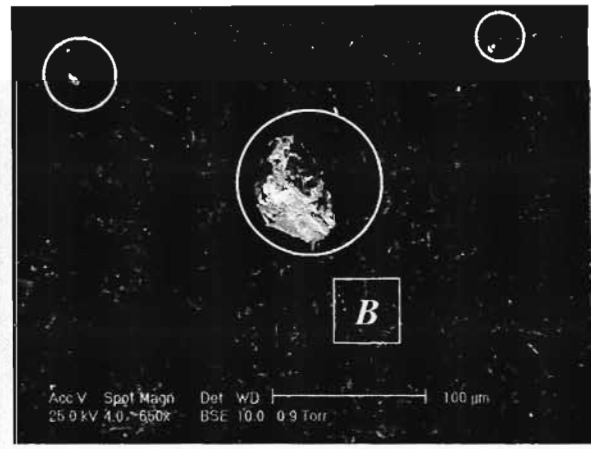

P1T-19 (depth 27.75 m)

Figure A1.4 SEM images of Pering's tailings at four different depths within borehole P1T. The square block designated as *A* shows what would appear to be a combination of gypsum and calcite precipitates. The blocks *B* highlight pure dolomite grains ($CaMg(CO_3)_2$) with no surface precipitates. The circles highlight a number of sulfides (appear as white specs), identified by EDAX point scans to be those of Zn, Pb and most commonly Fe. From this it can also be seen that sulfide minerals were still present close to the base of the tailings, which had been deposited some 17 years prior to analysis.

APPENDIX 2

Element concentrations in borehole pore-water, saturated pastes and distilled water leaching columns in comparison to South African water quality guidelines.

Table A2.1 Average, and maximum and minim element concentrations (in parenthesis) of continuous leaching column experiment, in relation to South African Bureau of Standards (SABS) drinking water guidelines and Department of Water Affairs and Forestry (DWAF) target water quality guidelines for domestic water use, livestock watering, irrigation and environmental exposure.

Species	*Continuous leaching (1089 hours)*[1]	*SABS Class 1*[2]	*DWAF*			
			Domestic water use[3]	*Agriculture water use*		*Acceptable environmental exposure*[6]
				Livestock[4]	*Irrigation*[5]	
	mg l^{-1}					
Al^{3+}	0 (0 – 0)	0.3	0.15	5	5	0.7
Ca^{2+}	598.47 (692.96 – 496.21)	150	32	1000	L.N.G	150
Cd^{2+}	0.01 (0.03 – 0)	0.005	0.005	0.01	0.01	0.031
Cu^{2+}	0.02 (0.08 – 0)	1	1	varied	0.2	0.13
Fe^{2+}	0.15 (0.18 – 0.13)	0.2	0.1	10	5	9
Hg^{2+}	0.03 (0.75 – 0)	0.002	0.001	0.001	L.N.G	0.024
K^{+}	34.49 (90.41 – 2.14)	50	50	L.N.G	L.N.G	200
Mg^{2+}	412.06 (1515.29 – 8.10)	70	30	500	L.N.G	70
Mn^{2+}	0.9 (1.74 – 0.31)	0.1	0.05	10	0.02	0.3
Na^{+}	33.62 (122.03 – 0.30)	200	100	2000	L.N.G	148
Ni^{2+}	0 (0.04 – 0)	0.15	L.N.G	1	0.2	0.75
Pb^{2+}	0 (0.49 – 0)	0.05	0.01	0.1	0.2	0.12
SO_4^{2-}	1127.86 as S[7] (2945.68 – 549.54)	400	200	1000	L.N.G	L.N.G
Se^{2+}	0.22 (0.41 – 0)	L.N.G	0.02	0.05	0.02	1.2
Zn^{2+}	2.86 (5.35 – 1.39)	4	3	20	1	L.N.G
EC mS/m	312.08 (655.70 – 224.60)	150	L.N.G	L.N.G	L.N.G	L.N.G
pH	7.42 (7.58 – 7.24)	5.0 – 9.5	6.0 – 9.0	L.N.G	6.5 – 8.4	L.N.G

1: leaching with untreated distilled water, average and range is given for the entire experiment; see Chapter 3 for details and Appendix 7 for raw data
2: SABS 241 (1999), Class I guideline: Water that is known to be acceptable for whole lifetime consumption
3: DWAF (1996a)
4: DWAF (1996c)
5: DWAF (1996b)
6: DWAF (2005). ***Acceptable environmental exposure, "indicates*** the $LC_{50} \times 0.1$ of the contaminant, which will result in a concentration that would cause mortality incidence of one in three hundred thousand in the aquatic environment."
7: to obtain SO_4^{2-} concentrations multiply by 3
L.N.G.: limit not given

Table A2.2 Average, and maximum and minim element concentrations (in parenthesis) of intermittent leaching column experiment, in relation to South African Bureau of Standards (SABS) drinking water guidelines and Department of Water Affairs and Forestry (DWAF) target water quality guidelines for domestic water use, livestock watering, irrigation and environmental exposure.

Species	*Intermittent leaching (10 weeks)*[1]	*SABS Class 1*[2]	*DWAF*			
			Domestic water use[3]	*Agriculture water use*		*Acceptable environmental exposure*[6]
				Livestock[4]	*Irrigation*[5]	
	mg l^{-1}					
Al^{3+}	nd	0.3	0.15	5	5	0.7
Ca^{2+}	307.25 (593.93 - 28.17)	150	32	1000	L.N.G	150
Cu^{2+}	0 (0 – 0)	1	1	varied	0.2	0.13
Fe^{2+}	0.29 (0.41 – 0.15)	0.2	0.1	10	5	9
Hg^{2+}	0.3 (0.53 – 0.11)	0.002	0.001	0.001	L.N.G	0.024
K^{+}	9.79 (23.78 – 2.35)	50	50	L.N.G	L.N.G	200
Mg^{2+}	30.46 (209.70 – 5.01)	70	30	500	L.N.G	70
Mn^{2+}	1.22 (2.91 – 0.22)	0.1	0.05	10	0.02	0.3
Na^{+}	1.94 (6.00 – 0.67)	200	100	2000	L.N.G	148
Ni^{2+}	0.01 (0.05 - 0)	0.15	L.N.G	1	0.2	0.75
Pb^{2+}	0.06 (0.10 – 0.01)	0.05	0.01	0.1	0.2	0.12
SO_4^{2-}	320.33 as S[7] (713.63 – 8.46)	400	200	1000	L.N.G	L.N.G
Zn^{2+}	4.48 (8.72 – 0.58)	4	3	20	1	L.N.G
EC mS/m	160.12 (275.17 – 24.63)	150	L.N.G	L.N.G	L.N.G	L.N.G
pH	7.34 (7.44 – 7.26)	5.0 – 9.5	6.0 – 9.0	L.N.G	6.5 – 8.4	L.N.G

1: leaching with untreated distilled water, average and range is given for the entire experiment (n = 3); see Chapter 3 for details and Appendix 7 for raw data
2: SABS 241 (1999), Class I guideline: Water that is known to be acceptable for whole lifetime consumption
3: DWAF (1996a)
4: DWAF (1996c)
5: DWAF (1996b)
6: DWAF (2005). ***Acceptable environmental exposure, "indicates*** the $LC_{50} \times 0.1$ of the contaminant, which will result in a concentration that would cause mortality incidence of one in three hundred thousand in the aquatic environment."
7: to obtain SO_4^{2-} concentrations multiply by 3
L.N.G.: limit not given

Table A2.3 Average, and maximum and minim element concentrations (in parenthesis) of borehole pore-water samples, in relation to South African Bureau of Standards (SABS) drinking water guidelines and Department of Water Affairs and Forestry (DWAF) target water quality guidelines for domestic water use, livestock watering, irrigation and environmental exposure.

Species	*Borehole Pore-water*[1]	*SABS Class 1*[2]	*DWAF*			
			Domestic water use[3]	*Agriculture water use*		*Acceptable environmental exposure*[6]
				Livestock[4]	*Irrigation*[5]	
			mg l^{-1}			
Al^{3+}	0.78 (0.99 – 0.39)	0.3	0.15	5	5	0.7
Ca^{2+}	161.33 (246.70 – 62.60)	150	32	1000	L.N.G	150
Cd^{2+}	0 (0 – 0)	0.005	0.005	0.01	0.01	0.031
Cl^{-}	316.83 (429.57 – 250.53)	L.N.G	100	varied	100	250
Cu^{2+}	0 (0 – 0)	1	1	varied	0.2	0.13
Fe^{2+}	0.07 (0.10 – 0.02)	0.2	0.1	10	5	9
Hg^{2+}	1.8 (6.17 – 0.38)	0.002	0.001	0.001	L.N.G	0.024
K^{+}	57.44 (111.50 – 36.40)	50	50	L.N.G	L.N.G	200
Mg^{2+}	588.81 (917.30 – 174.50)	70	30	500	L.N.G	70
Mn^{2+}	0 (0 – 0)	0.1	0.05	10	0.02	0.3
Na^{+}	158.03 (263.10 – 124.60)	200	100	2000	L.N.G	148
Ni^{2+}	0.05 (0.12 - 0)	0.15	L.N.G	1	0.2	0.75
Pb^{2+}	0.04 (0.11 - 0)	0.05	0.01	0.1	0.2	0.12
SO_4^{2-}	772.3 as S[7] (1221.00 – 211.10)	400	200	1000	L.N.G	L.N.G
Zn^{2+}	1.28 (2.13 – 0.34)	4	3	20	1	L.N.G
EC mS/m	425.88 (608.80 – 211.18)	150	L.N.G	L.N.G	L.N.G	L.N.G
pH	9.03 (9.52 – 7.98)	5.0 – 9.5	6.0 – 9.0	L.N.G	6.5 – 8.4	L.N.G

1: average and range of all pore-water samples extracted in the field from six boreholes; see Chapter 4 for details and Appendix 9 for raw data

2: SABS 241 (1999), Class I guideline: Water that is known to be acceptable for whole lifetime consumption

3: DWAF (1996a)

4: DWAF (1996c)

5: DWAF (1996b)

6: DWAF (2005). ***Acceptable environmental exposure,*** *"indicates* the $LC_{50} \times 0.1$ of the contaminant, which will result in a concentration that would cause mortality incidence of one in three hundred thousand in the aquatic environment."

7: to obtain SO_4^{2-} concentrations multiply by 3

L.N.G.: limit not given

Table A2.4 Average, and maximum and minim element concentrations (in parenthesis) of saturated paste extracts, in relation to South African Bureau of Standards (SABS) drinking water guidelines and Department of Water Affairs and Forestry (DWAF) target water quality guidelines for domestic water use, livestock watering, irrigation and environmental exposure.

Species	*Saturated pastes of borehole tailings samples*[1]	*SABS Class I*[2]	*DWAF*			
			Domestic water use[3]	*Agriculture water use*		*Acceptable environmental exposure*[6]
				Livestock[4]	*Irrigation*[5]	
			mg l^{-1}			
Al^{3+}	1.52 (2.43 – 1.04)	0.3	0.15	5	5	0.7
Ca^{2+}	376.74 (622.20 – 133.40)	150	32	1000	L.N.G	150
Cd^{2+}	0 (0 – 0)	0.005	0.005	0.01	0.01	0.031
Cu^{2+}	0.05 (0.30 – 0)	1	1	varied	0.2	0.13
Fe^{2+}	0.07 (0.17 – 0)	0.2	0.1	10	5	9
Hg^{2+}	0.18 (0.71 – 0.03)	0.002	0.001	0.001	L.N.G	0.024
K^{+}	61.68 (122.70 – 42.39)	50	50	L.N.G	L.N.G	200
Mg^{2+}	724.4 (1202.00 – 347.00)	70	30	500	L.N.G	70
Mn^{2+}	0.54 (3.12 – 0)	0.1	0.05	10	0.02	0.3
Na^{+}	126.64 (219.40 – 75.02)	200	100	2000	L.N.G	148
Ni^{2+}	0.04 (0.35 – 0)	0.15	L.N.G	1	0.2	0.75
Pb^{2+}	0.03 (0.22 – 0)	0.05	0.01	0.1	0.2	0.12
SO_4^{2-}	1291.76 as S[7] (2177.00 – 554.40)	400	200	1000	L.N.G	L.N.G
Zn^{2+}	5 (27.42 – 0.97)	4	3	20	1	L.N.G
EC mS/m	476.64 (650.30 – 303.60)	150	L.N.G	L.N.G	L.N.G	L.N.G
pH	8.01 (8.77 – 7.11)	5.0 – 9.5	6.0 – 9.0	L.N.G	6.5 – 8.4	L.N.G

1: average and range of all tailings samples collected from 8 boreholes; see Chapter 4 for details and Appendix 10 for raw data
2: SABS 241 (1999), Class I guideline: Water that is known to be acceptable for whole lifetime consumption
3: DWAF (1996a)
4: DWAF (1996c)
5: DWAF (1996b)
6: DWAF (2005). ***Acceptable environmental exposure, "indicates*** the $LC_{50} \times 0.1$ of the contaminant, which will result in a concentration that would cause mortality incidence of one in three hundred thousand in the aquatic environment."
7: to obtain SO_4^{2-} concentrations multiply by 3
L.N.G.: limit not given

APPENDIX 3

Raw data for sorption isotherms and batch extractions presented in Chapter 2

Table A3.1 Sorption of Cu and Ni onto the TT material. Data used to construct the sorption isotherms presented in Chapter 2 (Figure 2.2).

Rep	*Cu added*	*Sample mass*	*Equilibrium concentration*	*Cu sorbed*	*Ni added*	*Sample mass*	*Equilibrium concentration*	*Ni sorbed*
	mg l^{-1}	*g*	*mg l^{-1}*	*mg kg^{-1}*	*mg l^{-1}*	*g*	*mg l^{-1}*	*mg kg^{-1}*
1	0	1.021	0.000	0.000	0	1.026	0.393	0.000
2	0	1.004	0.000	0.000	0	1.026	0.333	0.000
3	0	1.008	0.000	0.000	0	1.012	0.338	0.000
1	2	1.020	0.000	49.020	2	1.011	0.396	39.664
2	2	1.008	0.000	49.603	2	1.006	0.518	36.829
3	2	1.014	0.000	49.310	2	1.004	0.492	37.550
1	4	1.025	0.000	97.561	4	1.018	0.515	85.584
2	4	1.021	0.000	97.943	4	1.025	0.407	87.634
3	4	1.021	0.000	97.943	4	1.016	0.456	87.205
1	8	1.008	0.000	198.413	8	1.015	1.273	165.690
2	8	1.002	0.000	199.601	8	1.016	1.200	167.323
3	8	1.002	0.000	199.601	8	1.019	1.469	160.231
1	16	1.008	0.000	396.825	16	1.000	6.744	231.400
2	16	1.008	0.000	396.825	16	1.005	7.151	220.124
3	16	1.010	0.000	396.040	16	1.003	7.428	213.659
1	32	1.012	0.000	790.514	32	1.004	18.600	333.665
2	32	1.009	0.000	792.864	32	1.006	19.214	317.744
3	32	1.002	0.000	798.403	32	1.003	18.963	324.950
1	64	1.006	0.000	1590.457	64	1.018	43.020	515.226
2	64	1.014	0.000	1577.909	64	1.011	44.670	477.992
3	64	1.018	0.000	1571.709	64	1.005	41.330	563.930
1	125	1.014	0.512	3069.231	125	1.007	88.890	896.475
2	125	1.004	0.769	3093.401	125	1.024	89.560	865.234
3	125	1.006	0.294	3099.056	125	1.014	92.560	799.803
1	250	1.004	6.710	6058.018	250	1.009	190.490	1474.480
2	250	1.002	4.921	6114.746	250	1.011	195.620	1344.708
3	250	1.004	5.367	6091.459	250	1.004	197.760	1300.797
1	500	1.012	29.220	11629.941	500	1.012	223.900	6820.652
2	500	1.018	41.770	11253.193	500	1.020	235.600	6480.392
3	500	1.007	36.330	11511.172	500	1.006	259.500	5976.640
1	1000	1.005	16.770	24458.458	1000	1.005	741.600	6427.861
2	1000	1.003	33.070	24100.947	1000	1.003	761.700	5939.681
3	1000	1.005	39.660	23889.055	1000	1.003	760.500	5969.591

Table A3.2 Sorption of Pb and Zn onto the TT material. Data used to construct the sorption isotherms presented in Chapter 2 (Figure 2.2).

Rep	*Pb added*	*Sample mass*	*Equilibrium concentration*	*Pb sorbed*	*Zn added*	*Sample mass*	*Equilibrium concentration*	*Zn sorbed*
	mg l^{-1}	*g*	*mg l^{-1}*	*mg kg^{-1}*	*mg l^{-1}*	*g*	*mg l^{-1}*	*mg kg^{-1}*
1	0	1.003	0.158	3.938	0	1.010	0.000	0.000
2	0	1.026	0.148	3.606	0	1.012	0.000	0.000
3	0	1.038	0.167	4.022	0	1.004	0.000	0.000
1	2	1.013	0.153	45.582	2	1.022	0.000	48.924
2	2	1.036	0.140	44.884	2	1.022	0.000	48.924
3	2	1.017	0.143	45.649	2	1.018	0.000	49.116
1	4	1.021	0.135	94.638	4	1.009	0.000	99.108
2	4	1.006	0.119	96.446	4	1.019	0.000	98.135
3	4	1.015	0.121	95.542	4	1.021	0.000	97.943
1	8	1.041	0.050	190.922	8	1.020	0.000	196.078
2	8	1.035	0.032	192.464	8	1.005	0.000	199.005
3	8	1.035	0.038	192.319	8	1.000	0.000	200.000
1	16	1.023	0.030	390.274	16	1.015	0.340	385.714
2	16	1.011	0.057	394.238	16	1.020	0.234	386.422
3	16	1.020	0.064	390.588	16	1.014	0.322	386.538
1	32	1.018	0.039	776.277	32	1.019	2.696	718.940
2	32	1.031	0.058	761.882	32	1.016	2.779	719.021
3	32	1.010	0.071	774.505	32	1.003	2.682	730.758
1	64	1.018	0.104	1546.169	64	1.008	16.507	1177.902
2	64	1.009	0.076	1566.898	64	1.012	15.958	1186.808
3	64	1.029	0.087	1533.771	64	1.010	16.228	1182.475
1	125	1.044	0.127	2962.883	125	1.015	41.530	2055.911
2	125	1.023	0.136	3021.505	125	1.018	44.590	1974.705
3	125	1.015	0.077	3059.852	125	1.006	43.420	2027.336
1	250	1.014	0.076	5976.331	250	1.009	149.640	2486.620
2	250	1.036	0.026	5970.077	250	1.009	145.220	2596.135
3	250	1.027	0.076	5900.682	250	1.013	143.730	2622.655
1	500	1.017	0.064	12133.727	500	1.002	272.800	5668.663
2	500	1.018	0.069	12109.528	500	1.005	256.000	6069.652
3	500	1.030	0.104	11883.495	500	1.004	275.800	5582.669
1	1000	1.014	0.088	24437.870	1000	1.003	652.800	8654.038
2	1000	1.017	0.108	24316.618	1000	1.008	672.700	8117.560
3	1000	1.010	0.135	24418.317	1000	1.007	667.400	8257.200

Table A3.3 Element release from Pering's tailings by the TCLP, acid rain and DTPA extraction methods.

	TCLP[1]			*Acid Rain*[2]			*DTPA*[3]		
	Rep-1	***Rep-2***	***Rep-3***	***Rep-1***	***Rep-2***	***Rep-3***	***Rep-1***	***Rep-2***	***Rep-3***
					***mg l*$^{-1}$**				
Ca	533.700	546.600	532.300	28.62	28.95	31.22			
Cd	bd	bd	bd	0.288	0.050	0.039	bd	bd	bd
Co	0.036	bd	bd	0.019	0.016	0.004			
Cr	bd	bd	bd	bd	bd	bd	bd	bd	bd
Cu	1.158	0.935	0.919	0.002	0.005	0.010	6.030	6.160	5.840
Fe	4.821	5.926	5.595	0.033	0.060	0.026	2.920	2.600	2.470
K	0.464	0.335	0.440	0.072	0.066	0.121			
Mg	292.860	297.720	288.190	6.993	6.723	6.721			
Mn	60.440	59.300	59.810	1.193	1.157	1.203	4.090	4.120	3.990
Na				0.933	1.091	1.155			
Ni	0.114	0.052	0.017	0.035	0.027	0.015	0.850	bd	bd
Pb	12.840	12.020	12.530	0.181	0.196	0.196	26.890	27.490	27.490
Zn	93.511	93.442	93.933	23.820	28.653	28.109	1042.52	1055.52	1069.22
pH	5.11	5.12	5.11	6.98	6.97	7.05			

1: TCLP-2 solution - 5.7 m*l* acetic acid in 1 *l* of water with pH of 2.88 (DWAF, 2005)
2: saturated solution of carbonic acid, pH 3.80 (DWAF, 2005)
3: DTPA-TEA extraction method, pH 7.30 (Liang and Karamanos, 1993)

APPENDIX 4

GPS waypoints of the Pering Mine tailings impoundment and the eight boreholes

Table A4.1 GPS waypoints (in decimal degrees) for the eight boreholes and the lower and upper corner points of Pering Mine's tailings impoundment.

Boreholes	*South*	*East*
Borehole P1T	-27.4257696	24.2850120
Borehole P2A	-27.4244724	24.2835671
Borehole P3T	-27.4242770	24.2845265
Borehole P4C	-27.4240213	24.2855775
Borehole P6C	-27.4257849	24.2868037
Borehole P7C	-27.4263868	24.2837071
Borehole P8C	-27.4227535	24.2822288
Borehole P9C	-27.4218005	24.2856115

Corner points	*South*	*East*
SW corner - BOTTOM	-27.4283130	24.2827099
SW corner - TOP	-27.4272958	24.2833989
SE corner - BOTTOM	-27.4268160	24.2889613
SE corner - TOP	-27.4262093	24.2876952
NE corner - BOTTOM	-27.4199912	24.2866879
NE corner - TOP	-27.4209099	24.2861186
NW corner - BOTTOM	-27.4215716	24.2802357
NW corner - TOP	-27.4220571	24.2813735

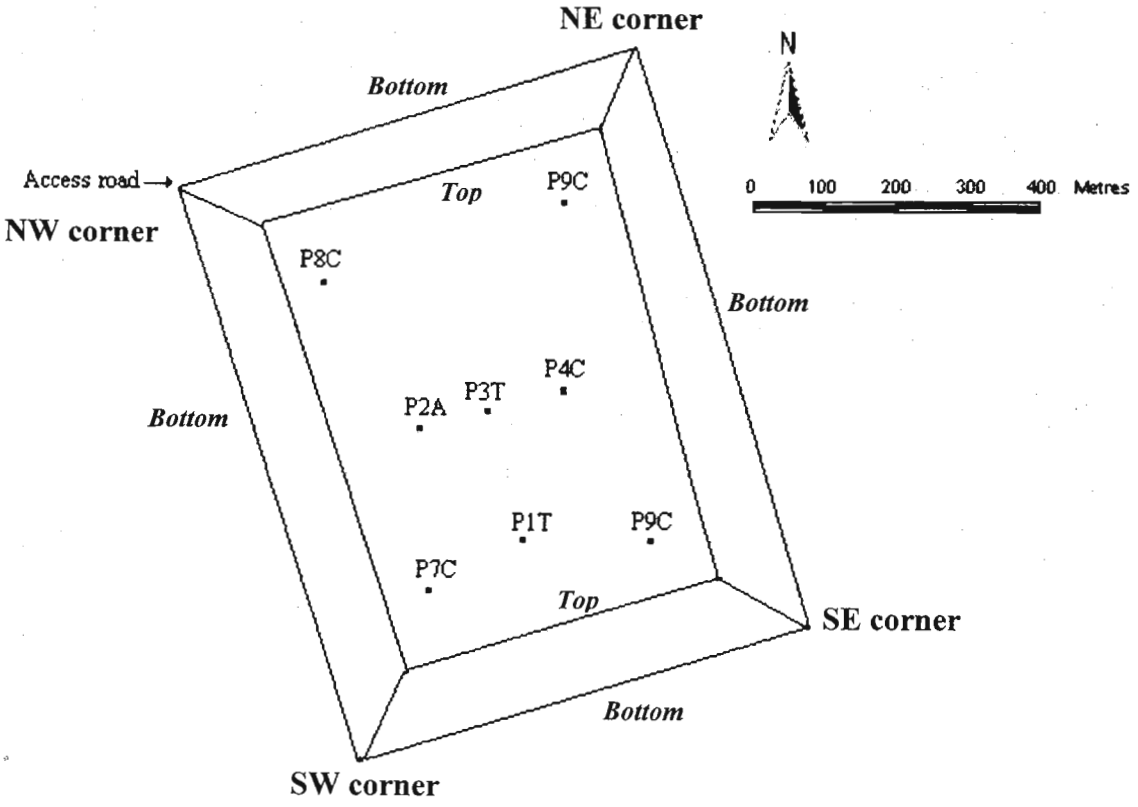

Figure A4.1 Aerial view of Pering's tailings dam plotted from GPS waypoints given in Table A4.1.

APPENDIX 5

Particle size distribution across the Pering Mine tailings impoundment

Variation in the particle size distribution across the tailings dam was determined by a modified version of the Gee and Bauder (1986) pipette method (see below). Analyses were done for all odd numbered samples in boreholes P1T and P3T and for samples 2, 8, 15 and 19 in the remaining boreholes (i.e. P2A, P4C, P6C, P7C, P8C and P9C).

A.5.1 Materials and methods

Air-dried samples were used for all analyses. In order to compensate for residual water their gravimetric moisture contents were measured by drying two sub-samples at 105 °C.

Samples of 20 g each were weighed out into glass beakers and dispersed with 10.0 m*l* calgon solution (35.7 g of sodium hexametaphosphate and 7.9 g sodium carbonate in 1 *l* of distilled water). In addition 20.0 m*l* of distilled water was added prior to a three minute treatment with an ultrasound probe (Labsonic 2000; output 350 to 400 W). The dispersed tailings was then passed through a 0.053 mm sieve into a 1 *l* sedimentation cylinder and made up to the mark with distilled water. The fraction < 0.053 mm, which had been washed into the sedimentation cylinder was dispersed by rapid mixing using a steel plunger. The rate of sedimentation is defined by Stokes Law (Gee and Bauder, 1986) and enables the amount of coarse silt (0.02 to 0.05 mm), fine silt (0.002 to 0.02 mm) and clay (< 0.002 mm) to be determined by accurate pipette sampling at stipulated time intervals in accordance with the ambient water temperature.

The sand fraction remaining in the sieve (i.e. particles > 0.053 mm) was placed in a glass beaker and dried over night at 105 °C. The relative proportions of course, medium and fine sand were determined by sieving through a sieve stack of 0.500 mm, 0.250 mm and 0.106 mm, respectively. Very fine sand passed through the 0.106 mm sieve. All particles size fractions were calculated as a mass percentage of oven-dry tailings.

A.5.2 Results

The results are tabulated in Table A5.1.

Table A5.1 Particle size distribution of tailings samples collected from eight boreholes positioned across the Pering tailings impoundment (see Chapter 4 for details).

Sample	*Depth*	*clay*[1]	*c. silt*[2]	*f. silt*[3]	*c. sand*[4]	*m. sand*[5]	*f. sand*[6]	*v. f. sand*[7]
	m				*Mass %*			
P1T - 1	0.0 – 1.5	15.5	18.1	56.7	0	0.1	0.2	9.4
P1T - 3	3.0 – 4.5	13.9	18.8	52.6	0	0.1	2	12.6
P1T - 5	6.0 – 7.5	15.6	19.1	57	0	0.1	1.5	6.7
P1T - 7	9.0 – 10.5	12.7	22.6	52.7	0	0.1	1.7	10.2
P1T - 9	12.0 – 13.5	16.2	17.7	54.3	0	0	2.4	9.4
P1T - 11	15.0 – 16.5	13.1	17.2	49.9	0	0	3.6	16.2
P1T - 13	18.0 – 19.5	13.9	17.7	52.5	0	0.4	4.5	11
P1T - 15	21.0 – 22.5	18.8	15.2	61.9	0	0	0.3	3.8
P1T - 17	24.0 – 25.5	15.9	21.1	52.5	0	0	0.8	9.7
P1T - 19	27.0 – 28.5	11.3	21.9	36.2	0	0.1	4.8	25.7
P2A - 2	1.5 – 3.0	10	25.6	30.9	0	0.5	13.4	19.6
P2A - 8	10.5 – 12.0	10.5	25.6	31.9	0	0.4	13.2	18.4
P2A - 15	21.0 – 22.5	5.9	28.7	29.7	0	0.3	11.4	24
P2A - 19	27.0 – 28.5	10.4	31.6	32.1	0	0.1	6	19.8
P3T - 1	0.0 – 1.5	16.3	18.6	57.2	0	0	0.6	7.3
P3T - 3	3.0 – 4.5	18.3	18.8	55.1	0.1	0.3	1.8	5.6
P3T - 5	6.0 – 7.5	20.7	13.2	62.3	0	0	0.5	3.3
P3T - 7	9.0 – 10.5	19.5	17.4	50.9	0	0.5	2.7	9
P3T - 9	12.0 – 13.5	17.4	16.7	56.4	0	0.3	2.8	6.4
P3T - 11	15.0 – 16.5	15.5	20.5	49.9	0	0.3	2.7	11.1
P3T - 13	18.0 – 19.5	15.3	24.4	45.8	0	0	2.5	12
P3T - 15	21.0 – 22.5	16	20.7	46.9	0	0.2	3.6	12.6
P3T - 17	24.0 – 25.5	17.6	18.8	51.6	0.1	0.1	2.2	9.6
P3T - 19	27.0 – 28.5	14.8	21.1	51.5	0	0	2.1	10.5
P4C - 2	1.5 – 3.0	18.9	17.7	47.1	0	0.6	7.1	8.6
P4C - 8	10.5 – 12.0	23.4	12.3	61.3	0	0.1	1.1	1.8
P4C - 15	21.0 – 22.5	27.6	6.8	64.1	0	0.1	0.4	1
P4C - 19	27.0 – 28.5	26	9.7	61.2	0	0	0.6	2.5
P6C - 2	1.5 – 3.0	11.1	23.4	34.1	0	0.5	11.8	19.1
P6C - 8	10.5 – 12.0	14.9	23.8	46.3	0	0.1	3.5	11.4
P6C - 15	21.0 – 22.5	12.7	26.8	41.3	0	0.1	3.1	16
P6C - 19	27.0 – 28.5	12.2	29.2	32.8	0	0.8	8.8	16.2
P7C - 2	1.5 – 3.0	4.7	17.6	9.4	0.1	6.6	38.7	22.9
P7C - 8	10.5 – 12.0	7.1	29.9	25.5	0	0.4	13.2	23.9
P7C - 15	21.0 – 22.5	6.1	28	20.1	0	0.2	18	27.6
P7C - 19	27.0 – 28.5	6.6	28	20.3	0	0.3	15.1	29.7
P8C - 2	1.5 – 3.0	6.3	21.6	24.7	0	1.6	17.9	27.9
P8C - 8	10.5 – 12.0	6.1	27	25.1	0	0.4	14.8	26.6
P8C - 15	21.0 – 22.5	6.1	23.7	17.3	0	0.3	19.8	32.8
P8C - 19	27.0 – 28.5	5.9	25.4	15.3	0	1.1	22.6	29.7
P9C - 2	1.5 – 3.0	7.8	22.8	21.5	0	1.7	21	25.2
P9C - 8	10.5 – 12.0	9.7	14.7	48.8	0	0.3	9.1	17.4
P9C - 15	21.0 – 22.5	15.8	24	48.5	0	0.1	2.3	9.3
P9C - 19	27.0 – 28.5	11.3	28.7	38.6	0	0.1	5.2	16.1

[1]Clay (<0.002 mm); [2]Coarse silt (0.02-0.05 mm); [3]Fine silt (0.002-0.02 mm); [4]Coarse sand (0.50-2.00 mm); [5]Medium sand (0.25-0.50 mm); [6]Fine sand (0.10-0.25 mm); [7]Very fine sand (0.05-0.10 mm)

APPENDIX 6

Hydrophysical properties of the Pering Mine tailings material

A6.1 Sample collection

Five undisturbed cores were collected from the surface of the Pering Mine tailings impoundment, by means of a core sampler and steel sleeve (McIntyre, 1974; Moodley, 2001). This was done by removing the rock cladding and digging a hole to an approximate depth of 30 cm. A stainless steel sleeve (internal diameter 75 mm, 50 mm long) was then driven vertically into the profile using the core sampler. The tailings were cut away from around the steel sleeve, before being tightly sealed in plastic to prevent drying and cracking. The cores were carefully padded for transport back to the laboratory, where their water retention characteristics, air-permeability and saturated hydraulic conductivities were determined.

A6.2 Materials and methods

The tailings material held within the cores was neatly cut away in line with the top and bottom of the steel sleeves. Losses from the bottom of the cores were prevented by placing a mesh cloth, held in place with an elastic band, over the base of the sleeves. The cores were brought up to saturation by placing them in a 4 cm deep water bath for 72 hours.

A6.2.1 Water retention characteristics

The saturated cores were removed from the water bath and their weight recorded accurately to two decimal places. Thereafter they were placed on a porous bed under tension from a hanging water column (Dane and Hopmans, 2002). The cores were equilibrated at tension intervals of -1, -2, -5 and -7 kPa. Equilibrium was assumed when the mass of the cores no longer changed (an equilibration period of approximately 3 days was normal). For the higher tensions, -10, -33, - 100 and – 1500 kPa, the cores were equilibrated using pressure plate extractors (Dane and Hopmans, 2002). After the final equilibration at -1500 kPa the cores were re-saturated to allow for the measurement of saturated hydraulic conductivity (K_s). Following this the cores were oven dried at 105 °C

for four days, which enabled the bulk density of the material to be determined. According to Moodley (2001) this is an acceptable practice due to insignificant sample losses during the measurement of K_s.

The water content at a given matric pressure (θ_k) was calculated as follows:

$$\theta_k = \frac{M_{ws} - M_{ods}}{\rho_w \times V_s}$$

where M_{ws} is the mass of the moist sample; M_{ods} is the mass of the sample after oven drying; ρ_w is the density of water (998.23 kg m^{-3} at 20 °C); and V_s is the volume of the core (m^3).

A6.2.2 Saturated hydraulic conductivity

In this study K_s was measured by means of the constant head method (Klute and Dirksen, 1986).

Prior to resaturation of the cores a second steel sleeve was securely strapped onto each sample core to allow for surface ponding. This enabled the formation of a constant head boundary at the top of the core, which was maintained by way of a mariott bottle system. The positive water head caused water to pass through the core. Once a steady flow rate had been reached Darcy's Law for saturated flow was applied:

$$K_s = \frac{V \times L}{A \times t \times \Delta H}$$

where K_s is the saturated hydraulic conductivity (m s^{-1}); V is the volume of water that passes through the sample (m^3); L is the length of the core (m); A is the cross sectional area of the core (m^2); t is time (s); and ΔH is the difference in hydraulic head between the inflow and outflow boundaries of the sample core (m).

A6.2.3 Air-permeability

The permeability of the undisturbed cores to air was measured after equilibration at -10, -33, and -100 kPa. This was done using the method described by Moodley (2001), which

was adapted from Corey (1986). The method entails forcing air through an undisturbed sample core and measuring the pressure drop across the sample by means of a water manometer. For each core a low flow rate and a high flow rate were passed through the core, the average of the two was reported as the air permeability (K_a). K_a (in m^2) was calculated by the following formula (after Corey, 1986):

$$K_a = \frac{\eta_a \times Q \times L}{A \times H_1 \times \rho_w \times g}$$

where η_a is the air viscosity at the measured temperature (1.832×10^{-5} Pa s at 20 °C); Q is the flow rate in ($m^3\ s^{-1}$); L is the length of the steel sleeve/core (m); A is the cross sectional area of the soil core (m^2); H_1 is the height of water in the manometer (m); ρ_w is the density of the fluid in the manometer (998.23 kg m^{-3} for water at 20 °C), g is the acceleration due to gravity (9.81 m s^{-1}).

A6.3 Results

The results for the different methods discussed above are presented in tabular and graphical form.

A6.3.1 Saturated hydraulic conductivity and bulk density

Table A6.1 Location, saturated hydraulic conductivity (K_s), bulk density (BD) and particle size distribution of five undisturbed cores collected from the surface of the Pering tailings impoundment.

	Location	K_s	*BD*	*Particle size distribution* (mass %)*						
		cm hour^{-1}	*kg m^{-3}*	*clay*[1]	*c. silt*[2]	*f. silt*[3]	*c. sand*[4]	*m. sand*[5]	*f. sand*[6]	*v. f. sand*[7]
Core 1	P8C	3.712	1444.171	5.9	44.1	34.7	0.0	0.2	1.0	14.1
Core 2	P7C	0.045	1731.663	12.7	17.1	68.7	0.2	0.6	0.2	0.5
Core 3	P3T	0.838	1649.880	15.5	23.9	53.0	0.3	0.2	0.6	6.5
Core 4	P3T	0.101	1711.327	15.3	13.8	58.7	0.2	3.1	6.4	2.5
Core 5	P3T	0.018	1762.040	11.0	30.5	57.0	0.1	0.1	0.3	1.0

* Determined by a modified method of the Gee and Bauder (1986) pipette method, see Appendix 5 for details
[1]Clay (<0.002 mm); [2]Coarse silt (0.02-0.05 mm); [3]Fine silt (0.002-0.02 mm); [4]Coarse sand (0.50-2.00 mm); [5]Medium sand (0.25-0.50 mm); [6]Fine sand (0.10-0.25 mm); [7]Very fine sand (0.05-0.10 mm).

A6.3.2 Water retention curves

Table A6.2 Gravimetric water content of the five undisturbed cores at various matric potentials/suctions.

Suction		*Core 1*	*Core 2*	*Core 3*	*Core 4*	*Core 5*
-kPa	*-m*	*Gravimetric water content (kg^{1} kg^{-1})*				
0	0	0.3654	0.2459	0.2713	0.2497	0.2271
1	0.1	0.3387	0.2315	0.2529	0.2418	0.2203
2	0.2	0.3227	0.2264	0.2480	0.2412	0.2180
5	0.5	0.3132	0.2227	0.2413	0.2357	0.2157
7	0.7	0.3075	0.2206	0.2376	0.2323	0.2142
10	1	0.3007	0.2193	0.2347	0.2309	0.2140
33	3.3	0.2242	0.2121	0.2103	0.2247	0.2059
100	10	0.1433	0.1961	0.1837	0.2082	0.1823
1500	150	0.0996	0.1472	0.1513	0.1592	0.1309

Table A6.3 Volumetric water content of the five undisturbed cores at various matric potentials/suctions.

Suction		*Core 1*	*Core 2*	*Core 3*	*Core 4*	*Core 5*
-kPa	*-m*	*Volumetric water content (m^{3} m^{-3})*				
0	0	0.5288	0.4267	0.4485	0.4281	0.4010
1	0.1	0.4901	0.4017	0.4181	0.4145	0.3890
2	0.2	0.4669	0.3929	0.4099	0.4136	0.3850
5	0.5	0.4532	0.3864	0.3988	0.4042	0.3808
7	0.7	0.4450	0.3827	0.3928	0.3983	0.3782
10	1	0.4352	0.3805	0.3881	0.3959	0.3778
33	3.3	0.3244	0.3680	0.3476	0.3854	0.3635
100	10	0.2073	0.3402	0.3038	0.3569	0.3219
1500	150	0.1441	0.2555	0.2501	0.2730	0.2311

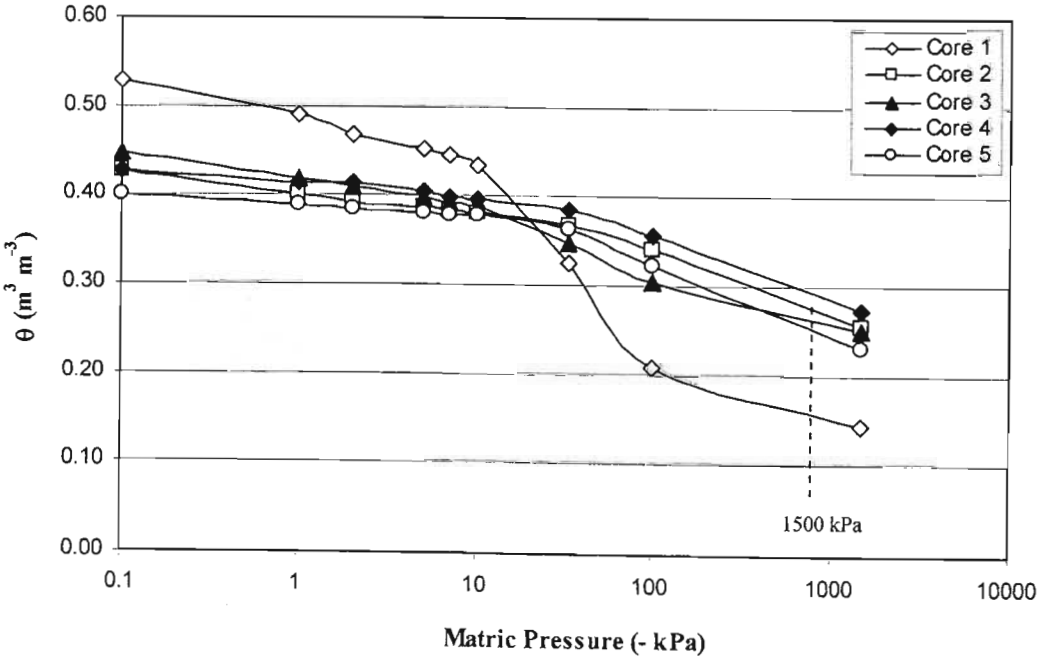

Figure A6.1 Graphical display of the change in volumetric water content (θ) of the five cores with increasing matric pressure (raw data is presented in Table A6.3).

A6.3.3 Air-filled porosity

The particle density of the tailings was determined by the pycnometer method to be 2.8801 g cm^{-3} (Blake and Hartge, 1986). The particle density was used to calculate the total porosity and air-filled porosity of the undisturbed cores (FigureA6.2).

Table A6.4 Air-filled porosity of the five cores at various matric potentials/suctions.

Suction		*Core 1*	*Core 2*	*Core 3*	*Core 4*	*Core 5*
-kPa	*-m*	*Air-filled porosity (m^3 m^{-3})*				
0	0	0	0	0	0	0
1	0.1	0.0084	0	0.0091	0	0
2	0.2	0.0316	0.0059	0.0172	0	0.0032
5	0.5	0.0454	0.0123	0.0283	0.0016	0.0074
7	0.7	0.0535	0.0160	0.0343	0.0075	0.0100
10	1	0.0634	0.0183	0.0391	0.0099	0.0104
33	3.3	0.1742	0.0308	0.0796	0.0204	0.0247
100	10	0.2912	0.0585	0.1234	0.0489	0.0663
1500	150	0.3545	0.1433	0.1771	0.1328	0.1571

Table A6.5 Total porosity of the five undisturbed cores.

	Total porosity m^3 m^{-3}
Core 1	0.499
Core 2	0.399
Core 3	0.427
Core 4	0.406
Core 5	0.388

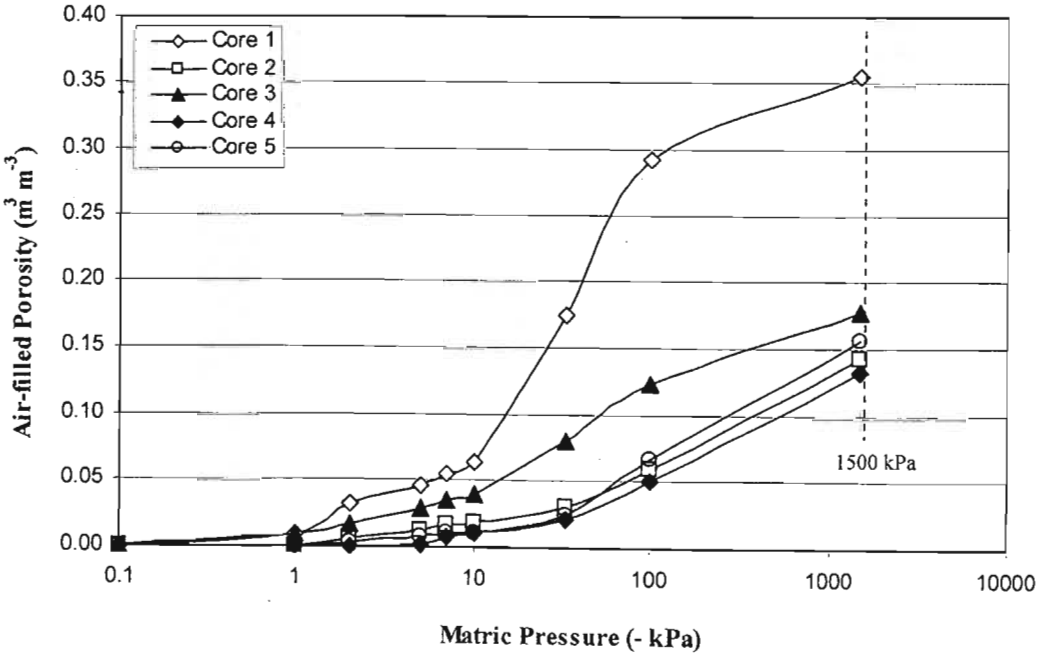

Figure A6.2 Increase in air-filled porosity of the five undisturbed cores with decreasing matric potential (raw data is presented in Table A6.4).

A6.3.4 Air-permeability

Table A6.6 The permeability of the five undisturbed cores to air at three matric potentials.

	-10 kPa	*-33 kPa*	*-100kPa*
		K_a (μm^2)	
Core 1	0.0338	0.0248	0.0547
Core 2	0.0133	0.0287	0.0472
Core 3	0.0250	0.0358	0.0849
Core 4	0.0107	0.0246	0.0231
Core 5	0.0137	0.0243	0.0233

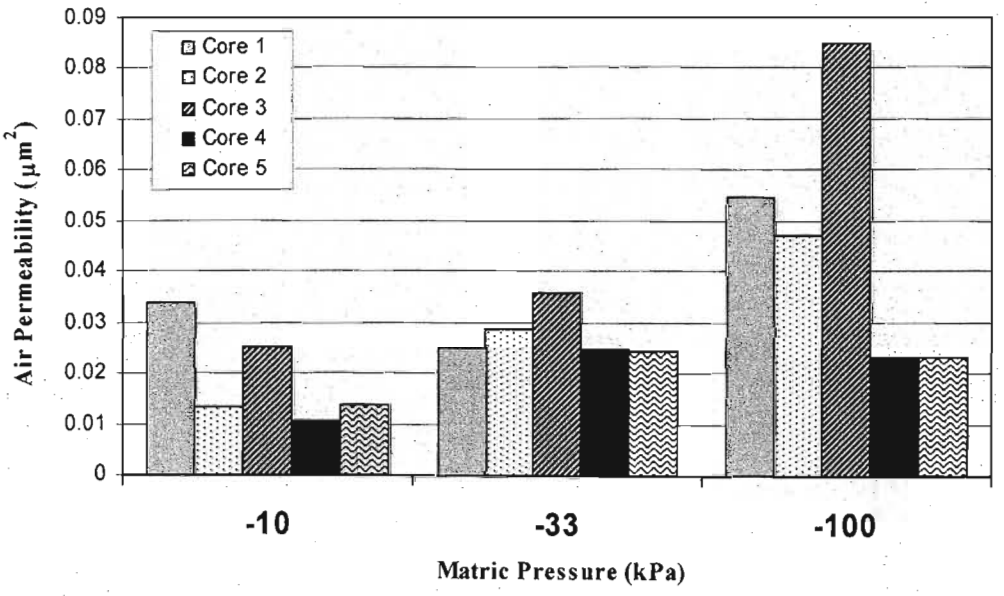

Figure A6.3 Air-permeability of the five undisturbed cores at -10 kPa, -33 kPa and -100 kPa (raw data is presented in Table A6.6).

APPENDIX 7

Leaching column experiments: experimental setup, raw data and results of geochemical modelling to supplement Chapter 3

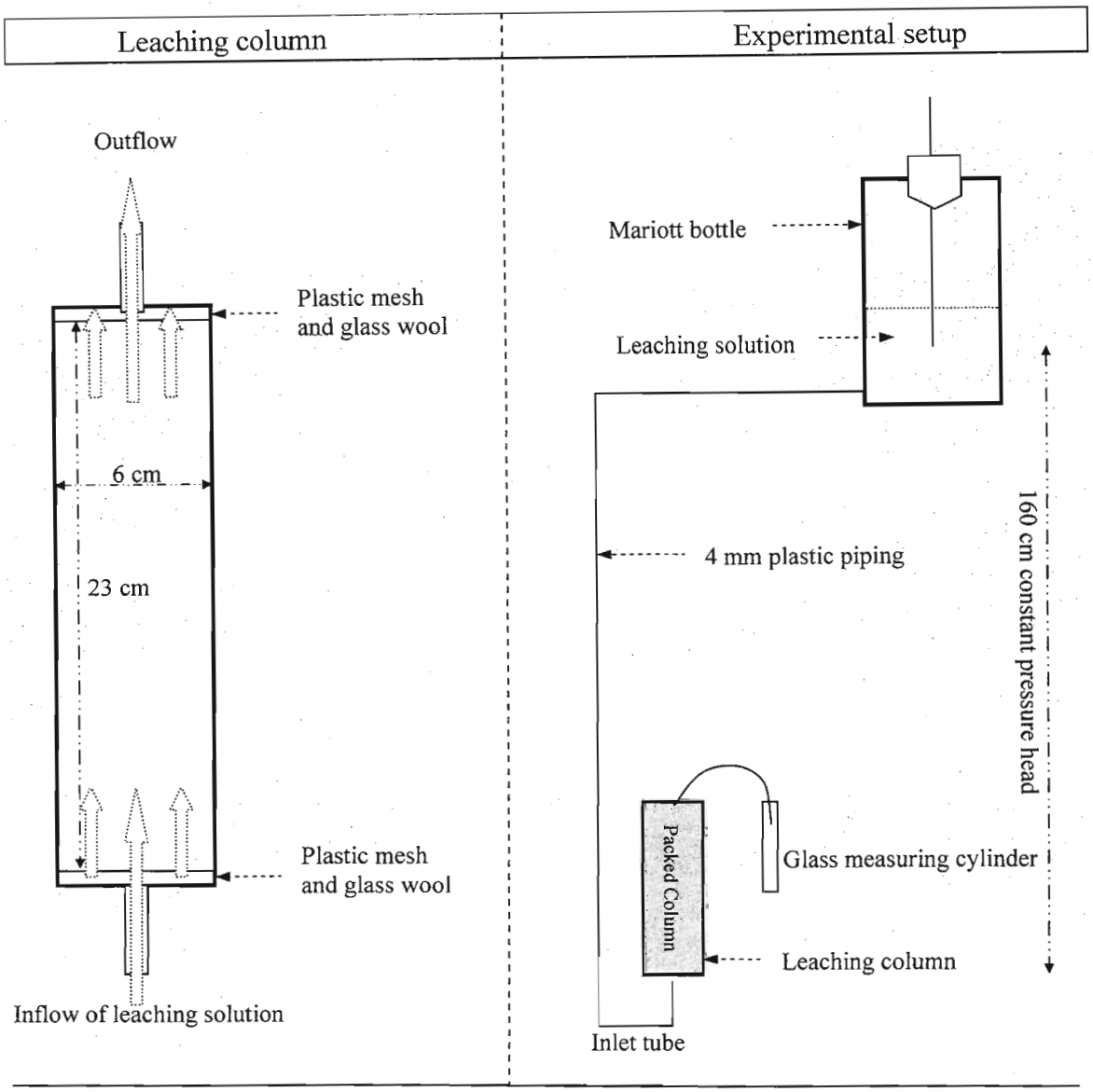

Figure A7.1 Experimental setup used to determine the chloride breakthrough curve (BTC) and the release of various potential contaminants from the Pering tailings material (The TN bulk sample was leached under continuous saturated flow, see Chapter 3 for details).

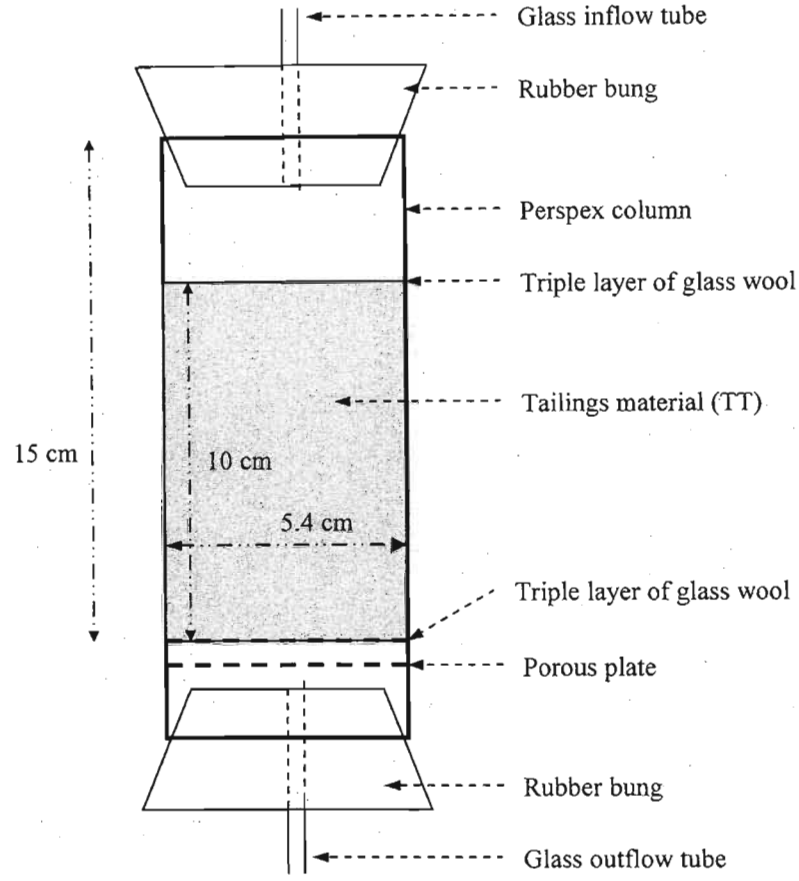

Figure A7.2 A diagram of the leaching column used for weekly intermittent leaching of the TT tailings sample. This column setup was used in Treatments 1 to 3 (i.e. leaching with TCLP-2 solution, distilled water and deoxygenated distilled water, see Chapter 3 for details).

Table A7.1 Chloride concentrations and EC of effluent samples collected from Column 1 and EC and pH of Column 2. Both columns were packed with the TN tailings sample and leached continuously (see Chapter 3 for details).

	Column 1					Column 2			
Sample	*Time*	*PVD**	*Cl*	*Cl*	*EC*	*Time*	*PVD*	*EC*	*pH*
No.	*hours*	*V/V_0*	*mg l^{-1}*	*C/Co*	*uS cm^{-1}*	*hours*	*V/V_0*	*uS cm^{-1}*	
1	2.575	0.022	253.489	0.259		3.267	0.016		
2	7.675	0.060	267.670	0.273		12.250	0.061		
3	18.675	0.121	264.125	0.270	6390	22.158	0.111	6049	7.33
4	30.783	0.187	262.352	0.268		33.483	0.159	6557	7.34
5	40.117	0.239	265.898	0.271	5962	44.733	0.207		
6	50.008	0.294	265.898	0.271		51.833	0.244		
7	61.333	0.356	269.443	0.275	6345	61.633	0.293	6451	7.26
8	72.575	0.417	269.443	0.275		72.150	0.347		
9	79.675	0.457	276.533	0.282		82.417	0.399	6431	7.49
10	89.483	0.511	278.306	0.284	6036	92.925	0.453		
11	100.017	0.570	283.624	0.290		99.975	0.491		
12	110.292	0.627	290.715	0.297	6266	107.608	0.532		
13	120.792	0.684	303.123	0.309		116.125	0.576		
14	128.342	0.726	311.986	0.318		123.567	0.615		
15	136.458	0.769	352.757	0.360	5786	132.683	0.663		
16	144.967	0.815	413.027	0.422		143.375	0.721	6723	7.47
17	152.925	0.857	471.525	0.481		153.958	0.780	5353	7.54
18	162.542	0.906	563.703	0.575	5740	163.467	0.829		
19	173.225	0.965	652.335	0.666		170.867	0.866		
20	183.808	1.024	726.787	0.742	5371	179.208	0.906		
21	193.350	1.075	813.646	0.831		188.208	0.950		
22	200.758	1.114	861.508	0.879		195.608	0.986		
23	209.075	1.157	877.462	0.896	4948	204.575	1.029	5092	7.58
24	218.075	1.204	884.552	0.903		215.700	1.083		
25	225.467	1.243	900.506	0.919		226.825	1.137	4315	7.56
26	234.425	1.288	930.641	0.950	4319	236.325	1.181		
27	245.567	1.345	930.641	0.950		248.167	1.237	3892	7.55
28	256.692	1.402	934.187	0.954	4300	260.675	1.295		
29	266.208	1.450	948.368	0.968		272.792	1.352	3372	7.51
30	278.083	1.509	951.913	0.972	4386	284.892	1.417		
31	290.592	1.570	946.595	0.966		292.017	1.464		
32	302.708	1.630	951.913	0.972	4515	301.358	1.517	2912	7.52
33	314.825	1.697	960.776	0.981		311.158	1.569		
34	321.950	1.744	959.004	0.979		321.425	1.621	2769	7.47
35	331.283	1.797	960.776	0.981	4312	332.942	1.682		
36	341.083	1.850	955.458	0.975		344.883	1.747	2728	7.47
37	351.250	1.906	960.776	0.981	4329	357.475	1.814		
38	362.683	1.972	962.549	0.983		370.208	1.880	2541	7.48
39	374.633	2.042	966.094	0.986	4371	381.458	1.940		
40	387.225	2.115	960.776	0.981		392.742	1.999	2339	7.49
41	399.958	2.189	959.004	0.979	4196	404.317	2.059		
42	411.208	2.253	960.776	0.981		416.383	2.122	2438	7.52
43	422.492	2.318	955.458	0.975	4163	428.325	2.185		
44	434.067	2.384	955.458	0.975		440.233	2.250	2521	7.47
45	446.133	2.452	955.458	0.975	4154	451.258	2.316		
46	458.058	2.520	960.776	0.981		456.458	2.354		
47	469.967	2.590	960.776	0.981	4347	466.392	2.414	2500	7.51
48	480.958	2.659	966.094	0.986		477.575	2.479		
49	End of initial Cl breakthrough curve					488.858	2.545	2466	7.45

* *PVD*: pore volume displacement = volume of leachate divided by pore volume of packed tailings

Table A7.1*(cont)* Chloride concentrations and EC of effluent samples collected from Column 1 and EC and pH of Column 2. Both columns were packed with the TN tailings sample and leached continuously (see Chapter 3 for details).

	Column 1					Column 2			
Sample	Time	PVD*	Cl	Cl	EC	Time	PVD	EC	pH
No.	hours	V/V_0	mg l^{-1}	C/Co	uS cm^{-1}	hours	V/V_0	uS cm^{-1}	
50	Start of column flushing with distilled water					500.008	2.607		
51	7.475	0.049	967.867	0.988	4373	506.533	2.644		
52	18.583	0.123	967.867	0.988		515.083	2.690	2137	7.43
53	29.858	0.196	962.549	0.983	4348	524.042	2.737		
54	41.025	0.266	971.412	0.992		530.425	2.771		
55	47.558	0.307	969.640	0.990		539.283	2.816	2198	7.37
56	56.108	0.358	960.776	0.981	4049	549.092	2.866		
57	65.075	0.411	957.231	0.977		560.950	2.926	2281	7.41
58	71.458	0.449	959.004	0.979		572.567	2.983		
59	80.317	0.500	957.231	0.977	4107	584.383	3.040		
60	90.125	0.557	950.140	0.970		595.883	3.097		
61	101.983	0.623	944.822	0.964	4162	602.525	3.135		
62	113.592	0.687	939.505	0.959		611.192	3.183	2020	7.47
63	119.733	0.721	918.233	0.937		619.550	3.227		
64	127.892	0.766	859.735	0.878	3625	625.942	3.265		
65	136.917	0.817	806.556	0.823		633.817	3.311	1474	7.37
66	143.550	0.857	755.149	0.771		641.342	3.353		
67	152.217	0.908	673.607	0.688	3248	648.158	3.393		
68	160.575	0.956	574.339	0.586		658.225	3.450	2187	7.4
69	166.958	0.994	494.569	0.505		682.425	3.589		
70	174.833	1.042	409.482	0.418	2697	706.542	3.733	2279	7.39
71	182.417	1.085	320.850	0.328		715.300	3.786		
72	189.233	1.124	260.580	0.266		728.833	3.852	2365	7.45
73	199.233	1.182	186.128	0.190	2521	743.242	3.924		
74	208.733	1.236	132.949	0.136		753.617	3.984	2273	7.45
75	215.092	1.274	104.586	0.107		764.283	4.048		
76	223.883	1.327	76.224	0.078	2268	776.458	4.125	2335	7.39
77	232.792	1.381	47.862	0.049		789.442	4.206		
78	238.708	1.419	35.453	0.036		801.733	4.279	2331	7.42
79	247.575	1.476	23.044	0.024	2331	813.633	4.350		
80	256.317	1.530	5.318	0.005		825.517	4.421	2318	7.38
81	269.850	1.609	3.545	0.004	2394	837.075	4.493		
82	284.275	1.694	0.000	0.000		848.767	4.570	2326	7.32
83	294.642	1.755	1.773	0.002	2288	859.183	4.640		
84	305.308	1.820	3.545	0.004		872.750	4.739		
85	317.475	1.897	0.000	0.000	2342	896.433	4.911	2338	7.34
86	330.450	1.978	0.000	0.000		911.508	5.019		
87	342.758	2.052	0.000	0.000	2322	922.692	5.095	2313	7.27
88	354.667	2.123	0.000	0.000		934.717	5.177		
89	366.550	2.194	0.000	0.000	2313	947.367	5.260	2246	7.38
90	378.100	2.265	1.773	0.002		960.025	5.341		
91	389.792	2.338	0.000	0.000	2322	972.217	5.415	2296	7.3
92						983.733	5.485		
93						995.242	5.556	2269	7.24
94						1007.483	5.632		
95						1018.467	5.704	2262	7.27
96						1029.067	5.774		
97						1042.500	5.865	2296	7.32
98						1055.525	5.954		
99						1069.925	6.046		
100						1089.025	6.167		

* *PVD*: pore volume displacement = volume of leachate divided by pore volume of packed tailings

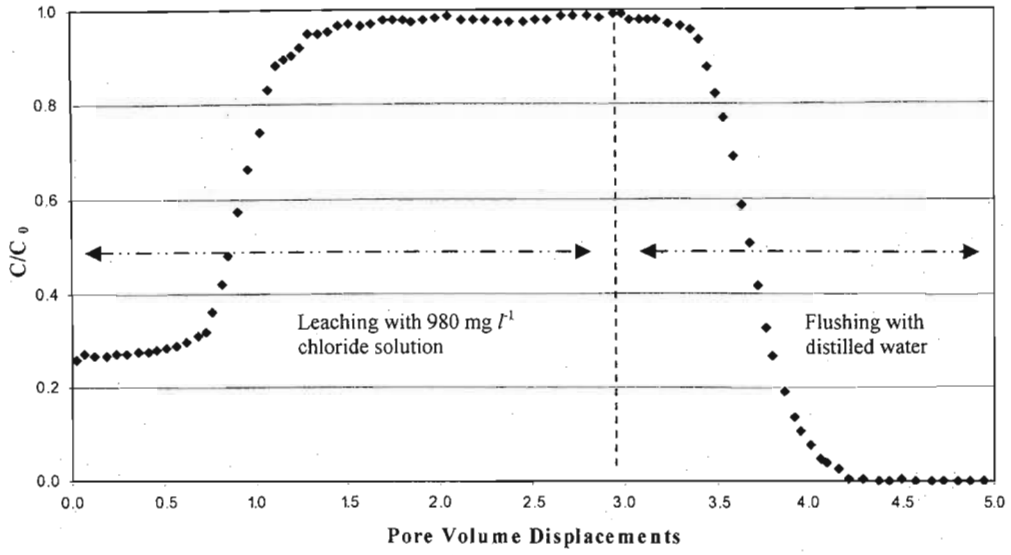

Figure A7.3 Chloride breakthrough curve determined by initial leaching with 980 mg l^{-1} chloride solution and then subsequent leaching with distilled water. From this it can be seen that the initial breakthrough curve was incomplete due to Cl^- being present within the tailings (graph drawn from data contained in Table A7.1, see Chapter 3 for details).

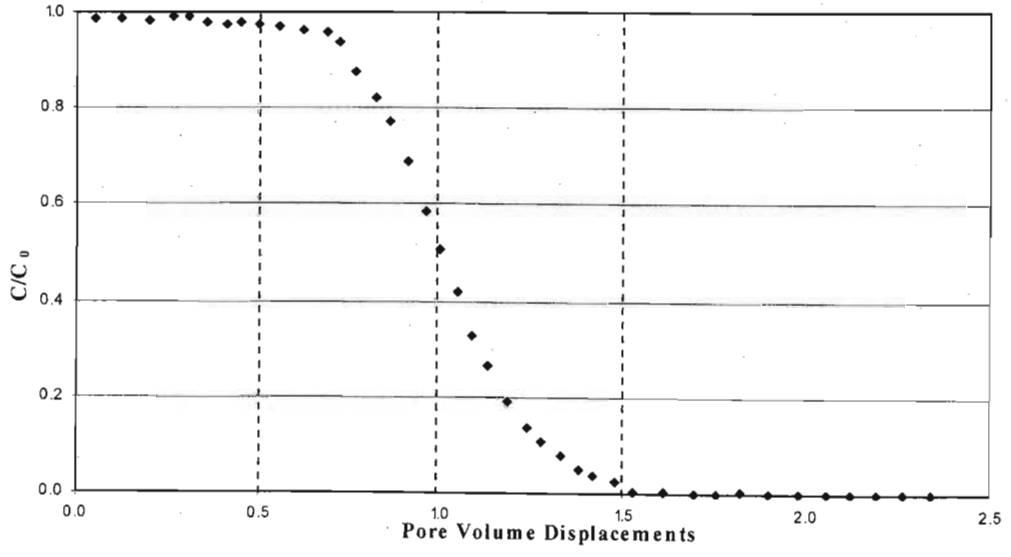

Figure A7.4 Chloride breakthrough curve determined by continuous leaching with distilled water after pre saturation with 980 mg l^{-1} chloride solution (graph drawn from data contained in Table A7.1, see Chapter 3 for details).

Table A7.2 Element concentrations in the effluent collected from Column 2 (TN sample), which was continuously leached with distilled water (see Chapter 3 for details).

Sample	*PVD**	*Time*	*Al*	*Ba*	*Ca*	*Cd*	*Co*	*Cu*	*Cr*
No.	V/V_0	*hours*				*mg* l^{-1}			
1	0.017	3.267	bd	0.071	692.963	0.033	0.027	0.055	bd
2	0.063	12.250	bd	0.059	588.450	0.026	0.023	0.020	bd
4	0.162	33.483	bd	0.052	554.861	0.026	0.026	0.026	bd
5	0.212	44.733	bd	0.049	526.831	0.030	0.024	0.034	bd
7	0.300	61.633	bd	0.047	513.862	0.026	0.027	0.050	bd
8	0.355	72.150	bd	0.046	507.602	0.026	0.024	0.041	bd
9	0.408	82.417	bd	0.046	518.746	0.028	0.027	0.055	bd
10	0.463	92.925	bd	0.044	500.312	0.025	0.024	0.067	bd
11	0.502	99.975	bd	0.046	522.881	0.026	0.023	0.059	bd
12	0.545	107.608	bd	0.042	496.214	0.028	0.022	0.070	bd
13	0.589	116.125	bd	0.045	496.801	0.027	0.027	0.066	bd
15	0.679	132.683	bd	0.027	512.846	0.006	bd	bd	bd
18	0.848	163.467	bd	0.028	544.795	0.006	bd	0.034	bd
20	0.927	179.208	bd	0.024	548.062	0.005	bd	0.031	bd
22	1.009	195.608	bd	0.017	566.115	0.009	bd	0.046	bd
24	1.108	215.700	bd	0.023	518.410	0.007	bd	0.066	bd
26	1.209	236.325	bd	0.022	533.855	0.005	bd	0.032	bd
28	1.325	260.675	bd	0.023	557.171	0.003	bd	0.075	bd
31	1.498	292.017	bd	0.028	582.000	0.006	bd	0.035	bd
33	1.606	311.158	bd	0.027	582.636	0.006	bd	0.024	bd
35	1.721	332.942	bd	0.025	581.414	0.006	bd	bd	bd
37	1.856	357.475	bd	0.030	602.536	0.005	bd	bd	bd
39	1.985	381.458	bd	0.024	597.102	0.004	bd	bd	bd
41	2.107	404.317	bd	0.024	610.928	0.005	bd	bd	bd
43	2.236	428.325	bd	0.023	617.040	0.007	bd	0.003	bd
46	2.409	456.458	bd	0.031	629.168	0.004	bd	0.050	bd
48	2.537	477.575	bd	0.028	624.543	0.006	bd	0.016	bd
50	2.668	500.008	bd	0.026	627.580	0.005	bd	0.015	bd
53	2.801	524.042	bd	0.027	633.311	0.005	bd	0.023	bd
56	2.933	549.092	bd	0.025	621.840	0.006	bd	bd	bd
58	3.052	572.567	bd	0.024	623.474	0.004	bd	bd	bd
60	3.169	595.883	bd	0.025	616.914	0.006	bd	bd	bd
63	3.302	619.550	bd	0.024	609.434	0.005	bd	bd	bd
65	3.388	633.817	bd	bd	629.002	bd	bd	bd	0.031
67	3.472	648.158	bd	bd	641.858	bd	bd	bd	0.031
70	3.820	706.542	bd	bd	646.761	bd	bd	bd	0.027
71	3.874	715.300	bd	bd	646.440	bd	bd	bd	0.029
73	4.015	743.242	bd	bd	634.319	bd	bd	bd	0.028
75	4.142	764.283	bd	bd	647.010	bd	bd	bd	0.027
77	4.304	789.442	bd	bd	651.278	bd	bd	bd	0.026
79	4.451	813.633	bd	bd	650.614	bd	bd	bd	0.026
81	4.598	837.075	bd	bd	640.960	bd	bd	bd	0.027
83	4.748	859.183	bd	bd	658.339	bd	bd	bd	0.026
86	5.135	911.508	bd	bd	665.159	bd	bd	bd	0.026
88	5.298	934.717	bd	bd	646.062	bd	bd	bd	0.027
90	5.465	960.025	bd	bd	663.059	bd	bd	bd	0.026
92	5.613	983.733	bd	bd	655.558	bd	bd	bd	0.027
94	5.763	1007.483	bd	bd	647.459	bd	bd	bd	0.026
96	5.908	1029.067	bd	bd	645.369	bd	bd	bd	0.027
98	6.092	1055.525	bd	bd	663.178	bd	bd	bd	0.025
100	6.310	1089.025	bd	bd	628.603	bd	bd	bd	0.026

* *PVD*: pore volume displacement = volume of leachate divided by pore volume of packed tailings
bd: below detection

Table A7.3 Element concentrations in the effluent collected from Column 2 (TN sample), which was continuously leached with distilled water (see Chapter 3 for details).

Sample	*PVD**	*Time*	*Fe*	*Hg*	*K*	*Mg*	*Mn*	*Na*	*Ni*
No.	V/V_0	*hours*				$mg\ l^{-1}$			
1	0.017	3.267	0.177	bd	82.754	1515.285	1.740	122.029	0.041
2	0.063	12.250	0.148	bd	82.459	1106.923	1.656	114.709	0.012
4	0.162	33.483	0.157	bd	77.175	1216.081	1.627	103.647	0.009
5	0.212	44.733	0.149	bd	75.823	1129.811	1.591	98.416	0.011
7	0.300	61.633	0.146	0.746	76.801	1142.028	1.602	96.564	0.016
8	0.355	72.150	0.155	bd	76.881	1154.931	1.583	105.765	bd
9	0.408	82.417	0.154	bd	76.759	1160.584	1.599	103.332	bd
10	0.463	92.925	0.145	bd	76.429	1134.497	1.575	110.108	0.000
11	0.502	99.975	0.151	bd	76.482	1174.662	1.569	100.422	bd
12	0.545	107.608	0.147	bd	75.304	1151.786	1.546	98.475	0.018
13	0.589	116.125	0.157	bd	77.036	1144.812	1.576	98.781	bd
15	0.679	132.683	0.127	0.018	80.685	1165.436	1.707	120.110	0.003
18	0.848	163.467	0.144	0.038	82.048	1134.968	1.652	117.525	bd
20	0.927	179.208	0.127	0.010	90.414	1130.350	1.603	103.308	bd
22	1.009	195.608	0.133	0.009	76.309	904.307	1.499	82.052	bd
24	1.108	215.700	0.130	0.009	64.695	686.531	1.339	59.280	bd
26	1.209	236.325	0.139	0.012	56.730	525.586	1.216	37.268	0.006
28	1.325	260.675	0.132	bd	48.539	389.814	1.097	13.845	bd
31	1.498	292.017	0.143	bd	41.519	254.359	1.030	3.801	0.005
33	1.606	311.158	0.151	0.016	35.847	208.134	0.960	2.613	bd
35	1.721	332.942	0.148	bd	33.479	186.004	0.879	1.973	bd
37	1.856	357.475	0.147	0.005	27.654	136.305	0.941	1.639	bd
39	1.985	381.458	0.150	0.022	23.862	117.589	0.822	1.462	bd
41	2.107	404.317	0.147	0.016	21.143	103.691	0.790	1.265	0.002
43	2.236	428.325	0.145	0.008	18.812	91.551	0.767	1.139	bd
46	2.409	456.458	0.153	0.022	18.279	79.717	0.789	1.140	bd
48	2.537	477.575	0.149	0.008	15.970	73.735	0.774	1.066	0.004
50	2.668	500.008	0.156	0.020	14.597	67.854	0.743	0.999	0.028
53	2.801	524.042	0.151	bd	13.111	63.531	0.749	0.948	bd
56	2.933	549.092	0.149	0.018	12.387	59.457	0.720	0.939	bd
58	3.052	572.567	0.149	0.027	11.818	55.007	0.715	0.843	bd
60	3.169	595.883	0.156	0.015	10.916	51.511	0.704	0.875	bd
63	3.302	619.550	0.148	0.044	10.512	48.156	0.711	0.802	bd
65	3.388	633.817	0.155	0.060	8.873	46.716	0.752	0.574	bd
67	3.472	648.158	0.153	0.020	8.432	45.019	0.784	0.547	0.003
70	3.820	706.542	0.149	0.019	7.510	37.412	0.738	0.449	bd
71	3.874	715.300	0.148	0.016	7.148	36.750	0.808	0.577	bd
73	4.015	743.242	0.144	0.022	6.765	33.075	0.714	0.522	bd
75	4.142	764.283	0.154	bd	6.363	31.843	0.710	0.436	0.006
77	4.304	789.442	0.140	0.042	5.929	30.040	0.694	0.405	bd
79	4.451	813.633	0.144	bd	6.063	28.048	0.702	0.657	bd
81	4.598	837.075	0.151	bd	5.469	25.632	0.678	0.403	bd
83	4.748	859.183	0.158	bd	5.162	24.454	0.712	0.397	bd
86	5.135	911.508	0.162	0.003	4.751	19.759	0.704	0.385	0.029
88	5.298	934.717	0.157	bd	4.173	17.328	0.642	0.378	0.018
90	5.465	960.025	0.155	0.010	3.999	16.419	0.644	0.337	bd
92	5.613	983.733	0.159	0.010	3.644	14.741	0.712	0.344	0.001
94	5.763	1007.483	0.145	0.014	3.384	13.129	0.634	0.319	0.006
96	5.908	1029.067	0.149	0.033	3.200	11.664	0.640	0.331	bd
98	6.092	1055.525	0.160	bd	2.753	9.987	0.614	0.369	bd
100	6.310	1089.025	0.154	bd	2.138	8.097	0.616	0.296	bd

* *PVD*: pore volume displacement = volume of leachate divided by pore volume of packed tailings
bd: below detection

Table A7.4 Element concentrations in the effluent collected from Column 2 (TN sample), which was continuously leached with distilled water (see Chapter 3 for details).

Sample	*PVD**	*Time*	*P*	*Pb*	*S*	*Se*	*Sr*	*Zn*
No.	V/V_0	*hours*			*mg* l^{-1}			
1	0.017	3.267	0.012	0.487	2945.679	0.237	0.939	4.921
2	0.063	12.250	0.029	0.113	2882.837	0.246	0.873	5.168
4	0.162	33.483	bd	0.077	2282.271	bd	0.832	5.350
5	0.212	44.733	bd	0.114	2117.140	0.108	0.813	5.224
7	0.300	61.633	bd	0.113	2122.299	0.309	0.771	5.280
8	0.355	72.150	bd	0.129	2154.101	0.310	0.763	5.205
9	0.408	82.417	bd	0.129	2108.210	0.135	0.757	5.229
10	0.463	92.925	bd	0.152	2128.029	0.234	0.737	5.205
11	0.502	99.975	bd	0.129	2153.225	0.167	0.706	5.165
12	0.545	107.608	bd	0.138	2104.082	0.394	0.721	5.106
13	0.589	116.125	bd	0.174	2091.594	0.154	0.686	5.222
15	0.679	132.683	bd	0.060	2058.754	0.265	0.607	5.006
18	0.848	163.467	bd	0.094	2054.428	0.263	0.637	4.928
20	0.927	179.208	bd	0.142	2089.885	0.233	0.613	4.752
22	1.009	195.608	bd	0.071	1763.130	0.179	0.559	4.386
24	1.108	215.700	bd	0.116	1464.079	0.116	0.535	3.894
26	1.209	236.325	bd	0.103	1244.869	0.235	0.510	3.510
28	1.325	260.675	bd	0.102	1053.705	0.149	0.502	3.153
31	1.498	292.017	bd	0.096	876.853	0.156	0.470	2.866
33	1.606	311.158	0.002	0.082	807.802	0.166	0.433	2.662
35	1.721	332.942	bd	0.079	768.105	0.140	0.418	2.409
37	1.856	357.475	bd	0.045	732.173	0.194	0.483	2.293
39	1.985	381.458	bd	0.064	688.256	0.156	0.480	2.180
41	2.107	404.317	bd	bd	668.837	0.142	0.471	2.000
43	2.236	428.325	bd	0.050	664.230	0.145	0.470	2.011
46	2.409	456.458	bd	0.043	656.348	0.181	0.484	2.012
48	2.537	477.575	bd	0.065	640.279	0.171	0.429	1.964
50	2.668	500.008	bd	0.093	617.214	0.077	0.427	1.959
53	2.801	524.042	bd	0.037	617.039	0.024	0.402	1.929
56	2.933	549.092	bd	0.092	603.315	0.163	0.355	1.852
58	3.052	572.567	bd	0.093	600.924	0.108	0.356	1.838
60	3.169	595.883	bd	0.058	586.711	0.180	0.278	1.755
63	3.302	619.550	bd	0.099	588.099	0.197	0.327	1.752
65	3.388	633.817	bd	0.030	608.855	0.275	0.451	1.600
67	3.472	648.158	bd	bd	609.295	0.390	0.305	1.661
70	3.820	706.542	bd	0.024	602.540	0.405	0.335	1.581
71	3.874	715.300	bd	0.002	616.213	0.360	0.440	1.601
73	4.015	743.242	bd	0.027	594.845	0.334	0.265	1.591
75	4.142	764.283	bd	0.045	579.001	0.342	0.339	1.572
77	4.304	789.442	bd	0.073	588.206	0.252	0.348	1.530
79	4.451	813.633	bd	0.072	587.776	0.240	0.372	1.572
81	4.598	837.075	bd	0.043	584.611	0.331	0.342	1.523
83	4.748	859.183	bd	0.055	602.148	0.345	0.240	1.561
86	5.135	911.508	bd	0.078	580.078	0.216	0.407	1.566
88	5.298	934.717	bd	0.079	583.190	0.391	0.385	1.490
90	5.465	960.025	bd	0.095	577.275	0.348	0.370	1.490
92	5.613	983.733	bd	0.087	594.693	0.242	0.418	1.531
94	5.763	1007.483	bd	0.092	575.809	0.312	0.419	1.457
96	5.908	1029.067	bd	0.063	585.138	0.173	0.262	1.478
98	6.092	1055.525	bd	0.052	567.232	0.235	0.316	1.388
100	6.310	1089.025	bd	0.077	549.543	0.193	0.411	1.510

* *PVD*: pore volume displacement = volume of leachate divided by pore volume of packed tailings
bd: below detection

Table A7.5 Predicted (*MINTEQ* modelling) species distribution in the first and last sample collected from the continuous flow leaching column (Tables A7.1 to A7.4).

		Sample 1	*Sample 100*
Element	***Species name***	***% of total element concentration***	***% of total element concentration***
Ca^{+2}	Ca^{+2}	50.95	63.49
	$CaSO_{4\,(aq)}$	49.06	36.51
CO_3^{-2}	CO_3^{-2}	0.28	0.15
	$MnCO_{3\,(aq)}$	0.03	
	$Mg_2CO_3^{+2}$	0.08	
	HCO^{3-}	83.92	86.32
	$H_2CO3^*_{\,(aq)}$	4.49	7.63
	$PbCO_{3\,(aq)}$	0.01	0.01
	$ZnCO_{3\,(aq)}$	0.06	0.03
	$ZnHCO^{3+}$	0.03	0.02
	$CuCO_{3\,(aq)}$	0.04	
	$MgCO_{3\,(aq)}$	0.65	
	$MgHCO^{3+}$	7.57	0.10
	$CaHCO^{3+}$	2.39	5.18
	$CaCO_{3\,(aq)}$	0.33	0.54
	$NaHCO_{3\,(aq)}$	0.11	
Cu^{+2}	Cu^{+2}	41.37	
	$CuOH^{+}$	17.84	
	$Cu(OH)_{2\,(aq)}$	0.81	
	$Cu_2(OH)_2^{+2}$	0.15	
	$CuSO_{4\,(aq)}$	39.83	
Fe^{+2}	Fe^{+2}	49.09	61.69
	$FeOH^{+}$	0.27	0.30
	$FeSO_{4\,(aq)}$	50.65	38.02
K^{+1}	K^{+1}	91.56	96.35
	KSO_4^{-}	8.44	3.65
Mg^{+2}	Mg^{+2}	56.66	68.64
	$MgSO_{4\,(aq)}$	43.34	31.36
Mn^{+2}	Mn^{+2}	57.21	69.12
	$MnOH^{+}$	0.02	0.02
	$MnSO_{4\,(aq)}$	42.76	30.86
Na^{+1}	Na^{+1}	93.46	97.20
	$NaSO4^{-}$	6.54	2.80
Ni^{+2}	Ni^{+2}	54.30	
	$NiOH^{+}$	0.09	
	$NiSO_{4\,(aq)}$	45.54	
Pb^{+2}	Pb^{+2}	25.61	38.21
	$PbOH^{+}$	8.77	11.52
	$Pb(OH)_{2\,(aq)}$	0.06	0.06
	$PbSO_{4\,(aq)}$	52.73	46.98
	$Pb(SO_4)_2^{-2}$	12.82	3.24
SO_4^{-2}	SO_4^{-2}	59.01	65.94
	$ZnSO_{4\,(aq)}$	0.05	0.05
	$Zn(SO_4)_2^{-2}$	0.04	
	$MnSO_{4\,(aq)}$	0.02	0.01
	$MgSO_{4\,(aq)}$	30.46	0.61
	$CaSO_{4\,(aq)}$	9.75	33.37
	$NaSO_4^{-}$	0.42	
	KSO_4^{-}	0.25	0.01
Zn^{+2}	Zn^{+2}	44.31	61.87
	$ZnOH^{+}$	0.60	0.74
	$Zn(OH)_{2\,(aq)}$	0.02	0.02
	$ZnSO_{4\,(aq)}$	40.74	33.98
	$Zn(SO_4)_2^{-2}$	14.32	3.38

Table A7.6 Predicted (*MINTEQ* modelling) saturation indices (SI) of various minerals in the first effluent sample collected from the continuous leaching column experiment (Column 2; see Chapter 3 for details). This is the most concentrated sample, it therefore provides an indication of which minerals may have precipitated in this experiment.

Mineral	*SI*	*Stoichiometry*							
Anglesite	-0.77	1	Pb+2	1	SO4-2				
Anhydrite	-0.02	1	Ca+2	1	SO4-2				
Antlerite	-2.12	3	Cu+2	4	H2O	-4	H+1	1	SO4-2
Aragonite	-13.47	1	Ca+2	1	CO3-2				
Artinite	-18.14	-2	H+1	2	Mg+2	1	CO3-2	5	H2O
Azurite	-27.23	3	Cu+2	2	H2O	-2	H+1	2	CO3-2
Bianchite	-5.07	1	Zn+2	1	SO4-2	6	H2O		
Brochantite	-0.85	4	Cu+2	6	H2O	-6	H+1	1	SO4-2
Brucite	-4.18	1	Mg+2	2	H2O	-2	H+1		
Bunsenite	-4.75	-2	H+1	1	Ni+2	1	H2O		
$CaCO_3$:H_2O	-14.67	1	Ca+2	1	CO3-2	1	H2O		
Calcite	**-13.33**	1	Ca+2	1	CO3-2				
Cerrusite	-12.80	1	Pb+2	1	CO3-2				
Chalcanthite	-6.10	1	Cu+2	1	SO4-2	5	H2O		
$Cu(OH)_2$	-0.97	1	Cu+2	2	H2O	-2	H+1		
$CuCO_3$	-14.67	1	Cu+2	1	CO3-2				
$CuOCuSO_4$	-11.34	-2	H+1	2	Cu+2	1	H2O	1	SO4-2
$CuSO_4$	-11.68	1	Cu+2	1	SO4-2				
Dolomite (disordered)	**-26.47**	1	Ca+2	1	Mg+2	2	CO3-2		
Dolomite (ordered)	**-25.92**	1	Ca+2	1	Mg+2	2	CO3-2		
Epsomite	-1.65	1	Mg+2	1	SO4-2	7	H2O		
$Fe(OH)_2$	-5.26	1	Fe+2	2	H2O	-2	H+1		
Goslarite	-4.83	1	Zn+2	1	SO4-2	7	H2O		
Gypsum	**0.23**	1	Ca+2	1	SO4-2	2	H2O		
Huntite	-55.45	3	Mg+2	1	Ca+2	4	CO3-2		
Hydrocerrusite	-25.36	3	Pb+2	2	H2O	-2	H+1	2	CO3-2
Hydromagnesite	-63.38	5	Mg+2	4	CO3-2	-2	H+1	6	H2O
Hydrozincite	-28.38	5	Zn+2	2	CO3-2	-6	H+1	6	H2O
Langite	-3.12	-6	H+1	4	Cu+2	7	H2O	1	SO4-2
Larnakite	-0.25	-2	H+1	2	Pb+2	1	SO4-2	1	H2O
Lime	-20.64	-2	H+1	1	Ca+2	1	H2O		
Litharge	-4.82	1	Pb+2	1	H2O	-2	H+1		
Magnesite	-13.74	1	Mg+2	1	CO3-2				
Malachite	-13.00	2	Cu+2	2	H2O	-2	H+1	1	CO3-2
Massicot	-5.02	1	Pb+2	1	H2O	-2	H+1		
Melanterite	-5.93	1	Fe+2	1	SO4-2	7	H2O		
$Mg(OH)_{2\ (active)}$	-6.13	1	Mg+2	2	H2O	-2	H+1		
Mirabilite	-5.56	2	Na+1	1	SO4-2	10	H2O		
$MnCO_{3\ (am)}$	-13.99	1	Mn+2	1	CO3-2				
$MnSO_4$	-9.64	1	Mn+2	1	SO4-2				
Morenosite	-6.61	1	Ni+2	1	SO4-2	7	H2O		
Natron	-22.79	2	Na+1	1	CO3-2	10	H2O		
Nesquehonite	-16.54	1	Mg+2	1	CO3-2	3	H2O		
$Ni(OH)_2$	-5.10	1	Ni+2	2	H2O	-2	H+1		
$Ni4(OH)_6SO_4$	-17.65	-6	H+1	4	Ni+2	1	SO4-2	6	H2O
$NiCO_3$	-14.98	1	Ni+2	1	CO3-2				
$Pb(OH)_2$	-0.27	-2	H+1	1	Pb+2	2	H2O		
$Pb10(OH)_6O(CO_3)_6$	-115.71	10	Pb+2	6	CO3-2	7	H2O	#	H+1
$Pb_2O(OH)_2$	-10.43	2	Pb+2	3	H2O	-4	H+1		
Pb_2OCO_3	-17.56	-2	H+1	2	Pb+2	1	H2O	1	CO3-2
$Pb_3O_2CO_3$	-21.26	-4	H+1	3	Pb+2	1	CO3-2	2	H2O
$Pb_3O_2SO_4$	-3.50	-4	H+1	3	Pb+2	1	SO4-2	2	H2O

Table A7.6*(cont)* Predicted (*MINTEQ* modelling) saturation index (SI) of various minerals in the first effluent sample collected from the continuous leaching column experiment (Column 2; see Chapter 3 for details). This is the most concentrated sample, it therefore provides an indication of which minerals may have precipitated in this experiment.

Mineral	*SI*	*Stoichiometry*							
$PbO{:}0.3H_2O$	-5.10	-2	H+1	1	Pb+2	1	H2O		
Periclase	-8.91	-2	H+1	1	Mg+2	1	H2O		
Portlandite	-10.74	1	Ca+2	2	H2O	-2	H+1		
Pyrochroite	-5.81	1	Mn+2	2	H2O	-2	H+1		
Retgersite	-6.71	1	Ni+2	1	SO4-2	6	H2O		
Rhodochrosite	-13.49	1	Mn+2	1	CO3-2				
Siderite	-14.97	1	Fe+2	1	CO3-2				
Smithsonite	-13.36	1	Zn+2	1	CO3-2				
Tenorite	**0.06**	1	Cu+2	1	H2O	-2	H+1		
Thenardite	-6.98	2	Na+1	1	SO4-2				
Thermonatrite	-24.73	2	Na+1	1	CO3-2	1	H2O		
Vaterite	-13.90	1	Ca+2	1	CO3-2				
Wustite	-3.04	-2	H+1	1	Fe+2	1	H2O		
Zincite	-1.72	1	Zn+2	1	H2O	-2	H+1		
Zincosite	-10.76	1	Zn+2	1	SO4-2				
$Zn(OH)_{2\ (am)}$	-2.86	1	Zn+2	2	H2O	-2	H+1		
$Zn(OH)_{2\ (beta)}$	-2.14	1	Zn+2	2	H2O	-2	H+1		
$Zn(OH)_{2\ (epsilon)}$	-1.92	1	Zn+2	2	H2O	-2	H+1		
$Zn(OH)_{2\ (gamma)}$	-2.12	1	Zn+2	2	H2O	-2	H+1		
$Zn_2(OH)_2SO_4$	-4.71	-2	H+1	2	Zn+2	2	H2O	1	SO4-2
$Zn_3O(SO_4)_2$	-22.95	-2	H+1	3	Zn+2	2	SO4-2	1	H2O
$Zn_4(OH)_6SO_4$	-6.39	-6	H+1	4	Zn+2	6	H2O	1	SO4-2
$ZnCO_3$	-13.46	1	Zn+2	1	CO3-2				
$ZnCO_3{:}1H_2O$	-14.00	1	Zn+2	1	CO3-2	1	H2O		
$ZnO_{\ (active)}$	-1.57	-2	H+1	1	Zn+2	1	H2O		
$ZnSO_4{:}1H_2O$	-6.19	1	Zn+2	1	SO4-2	1	H2O		

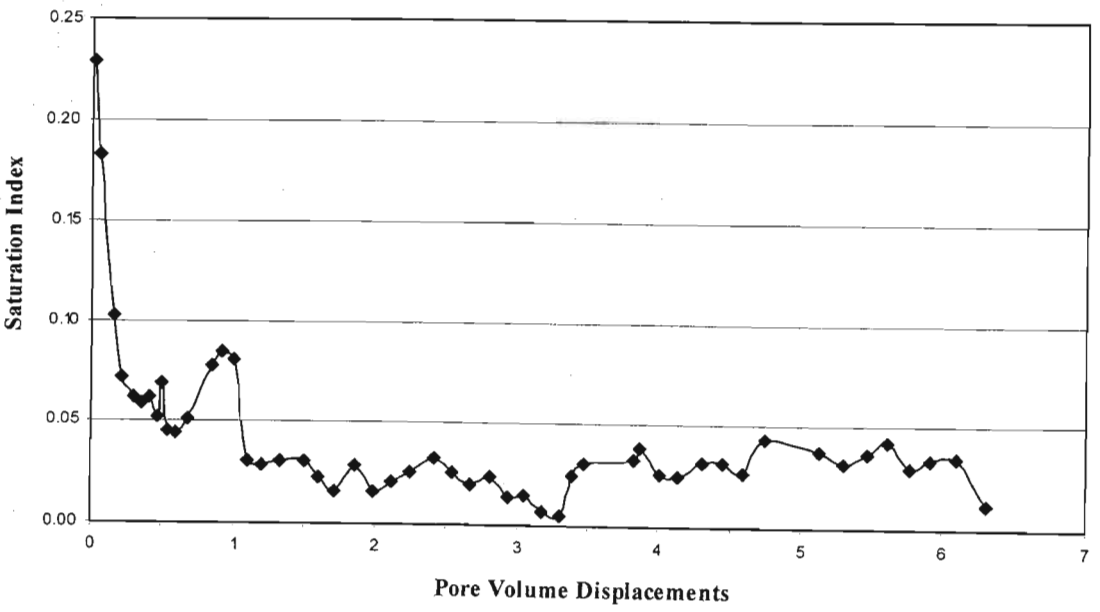

Figure A7.5 *MINTEQ* predicted saturation indices for gypsum ($CaSO_4{\cdot}2H_2O$) in the effluent samples of Column 2 (TN sample), which was continuously leached with distilled water (see Chapter 3 for details). This graph suggests initial precipitation, followed by equilibrium between the solid and liquid phase.

Table A7.7 Element concentrations in the effluent collected from three columns which were leached with 1 pore volume of TCLP-2 solution on a weekly basis (TT tailings sample was used; see Chapter 3 for details). PVD = pore volume displacements.

PVD	*Al*			*Ba*			*Ca*		
	Rep 1	*Rep 2*	*Rep 3*	*Rep 1*	*Rep 2*	*Rep 3*	*Rep 1*	*Rep 2*	*Rep 3*
					mg l^{-1}				
1	0.02	0.01	0.01	0.06	0.06	0.06	1271	1287	1262
2	bd	bd	bd	0.01	0.01	0.01	1526	1583	1572
3	bd	bd	bd	0.05	0.05	0.05	1705	1710	1749
4	0.03	0.01	0.01	0.05	0.06	0.06	1672	1653	1610
5	bd	0.01	0.02	0.08	0.09	0.1	1547	1489	1479
6	0.01	bd	0.02	0.12	0.16	0.17	1210	1219	1212
7	bd	bd	bd	0.19	0.23	0.24	1164	1106	1104
8	0.01	0.01	bd	0.32	0.38	0.36	783.4	1017.2	1034.4
9	1.87	1.86	1.83	0.17	0.1	0.06	955.6	951.5	934.5
11	bd	0	bd	0.13	0.11	0.1	1054	1056	1067
14	1.65	1.63	1.63	0.1	0.09	0.07	876.3	870.6	870.5
17	bd	bd	bd	0.06	0.06	0.05	2156.5	1371	984.5
20	bd	bd	bd	0.05	0.05	0.05	2091.5	994	989
23	bd	bd	bd	0.05	0.05	0.05	1477	1341	968
26	1.83	1.84	1.85	bd	bd	bd	887	890.8	894.6
29	1.82	1.73	1.66	bd	bd	bd	913.5	916.5	916.5
32	2.14	2.16	2.18	0.12	0.08	0.05	911.5	1083	913.5
35	2.01	2.13	1.98	bd	bd	bd	899.5	882	883.5
38	2.26	2.23	2.23	bd	bd	bd	770.7	835.09	940.89
41	2.06	2.01	2.04	bd	bd	bd	831.66	840.71	837.69
44	1.62	1.56	1.81	bd	bd	bd	911.74	878.66	1237.44

bd: below detection

Table A7.8 Element concentrations in the effluent collected from three columns which were leached with 1 pore volume of TCLP-2 solution on a weekly basis (TT tailings sample was used; see Chapter 3 for details). PVD = pore volume displacements.

PVD	*Cd*			*Co*			*Cr*		
	Rep 1	*Rep 2*	*Rep 3*	*Rep 1*	*Rep 2*	*Rep 3*	*Rep 1*	*Rep 2*	*Rep 3*
					mg l^{-1}				
1	bd	bd	bd	0.02	0.02	0.02	0.01	0.01	0.01
2	bd	bd	bd	0.01	0.01	0.01	bd	bd	0.01
3	bd	bd	bd	bd	bd	bd	0.01	0.02	0.01
4	0.01	0.01	0.01	bd	bd	bd	0.01	bd	bd
5	0.01	0.01	0.00	0.01	0.01	0.01	bd	bd	bd
6	0.02	0.03	0.02	bd	bd	bd	0.00	bd	bd
7	0.03	0.04	0.03	0.01	0.01	0.01	0.01	0.01	0.01
8	bd	0.02	0.04	bd	bd	bd	bd	bd	0.00
11	0.03	0.03	0.03	0.19	0.17	0.17	bd	bd	bd
17	0.04	0.04	0.03	0.00	bd	bd	0.02	0.02	0.02
20	0.04	0.04	0.04	0.16	0.15	0.15	0.02	0.02	0.02
23	0.03	0.04	0.05	bd	bd	bd	0.02	0.02	0.02
20				bd	bd	bd			
23				bd	bd	bd			
26				0.02	0.04	0.05			
29				0.13	0.15	0.17			
32				0.22	0.25	0.23			
35				0.12	0.12	0.12			
38				0.21	0.21	0.22			
41				0.15	0.15	0.16	0.10	0.10	0.10
44				0.04	bd	0.02	0.17	0.15	0.14

bd: below detection

Table A7.9 Element concentrations in the effluent collected from three columns which were leached with 1 pore volume of TCLP-2 solution on a weekly basis (TT tailings sample was used; see Chapter 3 for details). PVD = pore volume displacements.

PVD	*Cu*			*Fe*			*Hg*		
	Rep 1	*Rep 2*	*Rep 3*	*Rep 1*	*Rep 2*	*Rep 3*	*Rep 1*	*Rep 2*	*Rep 3*
					mg l^{-1}				
1	0.13	0.18	0.19	bd	bd	bd	0.64	0.54	0.60
2	0.08	0.07	0.05	bd	bd	bd	0.83	0.59	0.66
3	0.05	0.08	0.05	bd	bd	bd	0.51	0.50	0.58
4	0.02	0.03	0.03	bd	bd	bd	0.54	0.44	0.50
5	0.04	0.05	0.05	bd	bd	bd	0.41	0.41	0.46
6	0.02	0.02	0.02	bd	bd	bd	0.34	0.42	0.41
7	0.03	0.04	0.04	0.01	bd	bd	0.29	0.36	0.37
8	0.04	0.04	0.03	0.01	bd	bd	0.26	0.40	0.48
9	0.09	0.09	0.10	0.09	0.09	0.09	0.54	0.65	0.74
11	0.01	0.01	bd	bd	bd	bd	0.24	0.35	0.45
14	0.16	0.14	0.17	0.09	0.08	0.08	0.58	0.61	0.69
17	0.00	0.09	0.01	bd	bd	bd	0.31	0.34	0.32
20	0.14	0.17	0.05	bd	bd	bd	0.32	0.36	0.37
23	0.13	0.16	0.12	bd	bd	bd	0.22	0.32	0.35
26	0.19	0.23	0.22	0.11	0.10	0.11	0.99	0.67	0.83
29	0.13	0.38	0.32	0.11	0.11	0.11	0.63	0.63	0.68
32	0.08	0.13	0.25	0.09	0.10	0.09	0.64	0.64	0.66
35	0.05	0.06	0.14	0.07	0.06	0.06	0.70	0.85	0.76
38	0.11	0.13	0.16	0.12	0.11	0.11	0.65	0.64	0.68
41	0.04	0.05	0.05	0.06	0.06	0.06	0.55	0.54	0.60
44	bd	bd	bd	bd	bd	bd	0.56	0.58	0.51

bd: below detection

Table A7.10 Element concentrations in the effluent collected from three columns which were leached with 1 pore volume of TCLP-2 solution on a weekly basis (TT tailings sample was used; see Chapter 3 for details). PVD = pore volume displacements.

PVD	*K*			*Mg*			*Mn*		
	Rep 1	*Rep 2*	*Rep 3*	*Rep 1*	*Rep 2*	*Rep 3*	*Rep 1*	*Rep 2*	*Rep 3*
					mg l^{-1}				
1	26.72	28.92	30.63	609.00	581.00	627.00	41.32	39.16	41.44
2	10.38	7.92	7.57	466.00	472.00	461.00	41.95	43.12	43.15
3	4.00	3.43	3.40	510.00	508.00	506.00	58.98	48.95	55.31
4	2.49	2.26	2.30	519.00	506.00	498.00	48.66	52.46	58.06
5	2.15	2.08	2.00	559.00	533.00	551.00	49.03	67.70	48.81
6	1.69	1.64	1.62	535.50	670.00	530.00	47.18	55.80	58.47
7	1.46	1.41	1.46	533.00	527.00	539.00	53.34	57.51	56.06
8	1.23	1.21	1.25	533.90	548.80	550.00	49.16	53.48	58.52
9	2.06	2.08	2.04	492.50	489.40	482.00	63.08	71.95	66.45
11	1.16	1.12	1.16	53.35	53.45	54.70	63.30	63.35	63.39
14	1.61	1.61	1.63	587.10	597.60	607.80	72.55	70.08	70.50
17	1.16	1.13	1.15	1345.00	830.00	585.00	176.50	108.00	68.00
20	1.13	1.13	1.12	1257.50	587.00	588.50	97.30	72.00	70.50
23	0.93	1.03	1.08	911.50	815.00	594.00	125.00	111.00	75.00
26	1.58	1.56	1.59	29.58	29.71	29.68	83.93	83.44	84.16
29	1.61	1.54	1.57	34.78	29.46	31.31	98.08	84.50	92.42
32	2.22	2.24	2.22	31.92	28.91	21.27	95.82	87.23	64.24
35	1.44	1.37	1.40	581.00	581.50	582.50	63.82	96.78	121.70
38	2.19	2.18	2.25	34.74	39.43	29.39	88.92	102.42	76.97
41	2.07	2.05	1.88	30.63	31.11	31.06	79.10	79.77	79.63
44	1.63	1.55	1.61	30.55	26.63	30.62	80.35	71.51	80.60

Table A7.11 Element concentrations in the effluent collected from three columns which were leached with 1 pore volume of TCLP-2 solution on a weekly basis (TT tailings sample was used; see Chapter 3 for details). PVD = pore volume displacements.

PVD	*Na*			*Ni*			*P*		
	Rep 1	*Rep 2*	*Rep 3*	*Rep 1*	*Rep 2*	*Rep 3*	*Rep 1*	*Rep 2*	*Rep 3*
					mg l^{-1}				
1	15.47	15.99	19.09	0.63	0.72	0.73	0.01	0.01	0.03
2	2.18	1.89	2.11	0.23	0.17	0.16	0.01	bd	0.08
3	1.14	0.92	1.02	0.12	0.15	0.10	0.04	0.05	0.02
4	0.67	0.77	0.78	0.11	0.10	0.10	0.02	0.06	0.05
5	1.01	0.74	0.91	0.08	0.09	0.08	0.04	0.04	0.04
6	0.72	0.77	0.87	0.07	0.06	0.07	0.03	0.04	bd
7	0.75	0.74	0.95	0.07	0.07	0.07	0.02	0.02	bd
8	0.94	0.91	1.14	0.07	0.06	0.05	0.01	bd	0.01
9	1.89	2.08	1.96	0.02	0.02	0.01	0.37	0.41	0.43
11	1.01	1.10	1.03	0.03	0.04	0.02	bd	bd	0.00
14	2.32	2.26	2.37	0.01	0.01	0.00	0.36	0.37	0.37
17	1.87	1.87	1.89	0.03	0.03	0.03	bd	bd	bd
20	1.78	1.80	1.81	0.03	0.02	0.02	bd	bd	bd
23	1.52	1.75	1.78	0.01	0.02	0.02	bd	bd	bd
26	2.75	2.58	2.73	bd	bd	bd	0.35	0.37	0.35
29	2.52	2.30	2.35	bd	bd	bd	0.21	0.32	0.34
32	1.68	1.73	2.03	bd	0.01	0.01	0.27	0.32	0.34
35	1.39	1.73	1.60	bd	bd	bd	0.26	0.27	0.33
38	1.57	1.58	1.68	0.05	0.05	0.06	0.25	0.25	0.26
41	2.24	2.45	2.14	bd	bd	bd	0.25	0.25	0.26
44	1.07	0.69	1.08	bd	bd	bd	0.22	0.20	0.17

bd: below detection

Table A7.12 Element concentrations in the effluent collected from three columns which were leached with 1 pore volume of TCLP-2 solution on a weekly basis (TT tailings sample was used; see Chapter 3 for details). PVD = pore volume displacements.

PVD	*Pb*			*S*			*Se*		
	Rep 1	*Rep 2*	*Rep 3*	*Rep 1*	*Rep 2*	*Rep 3*	*Rep 1*	*Rep 2*	*Rep 3*
					mg l^{-1}				
1	6.93	7.08	6.98	763.50	788.30	853.00	0.06	0.05	0.06
2	5.91	6.12	6.84	566.00	556.00	552.00	0.08	0.05	0.09
3	6.76	6.54	7.00	576.30	565.00	532.80	0.11	0.07	0.08
4	5.71	5.38	6.56	756.60	749.00	636.30	0.11	0.09	0.10
5	5.41	5.73	5.84	763.10	552.10	369.30	0.08	0.07	0.07
6	4.16	5.29	5.65	306.10	299.40	235.50	0.07	0.08	0.08
7	4.08	4.53	4.61	166.20	122.70	96.10	0.09	0.09	0.08
8	3.04	3.63	4.15	38.70	26.69	37.03	0.08	0.06	0.08
9	1.25	2.19	2.40	28.34	32.84	42.46	0.08	0.07	0.07
11	1.13	2.04	1.39	17.31	20.80	32.84			
14	0.92	0.53	1.05	16.74	21.06	28.68			
17	1.57	2.49	1.04	13.15	15.26	23.55			
20	4.56	4.37	2.25	10.31	15.69	22.09	0.14	0.13	0.15
23	5.98	6.22	2.54	8.80	15.04	21.50			
26	10.97	9.49	2.20	11.89	17.05	25.40			
29	14.27	10.11	6.52	14.42	18.10	22.20			
32	10.29	10.03	5.50	13.28	18.53	23.90	0.14	0.11	0.12
35	10.17	10.06	11.31	14.66	23.68	27.92			
38	15.08	15.52	8.41	13.66	18.37	23.94			
41	12.84	13.74	11.22	15.15	19.20	24.70	0.15	0.17	0.14
44	15.20	11.67	12.42	14.46	19.56	18.33			

Table A7.13 Element concentrations in the effluent collected from three columns which were leached with 1 pore volume of TCLP-2 solution on a weekly basis (TT tailings sample was used; see Chapter 3 for details). PVD = pore volume displacements.

PVD	*Sr*			*V*			*Zn*		
	Rep 1	*Rep 2*	*Rep 3*	*Rep 1*	*Rep 2*	*Rep 3*	*Rep 1*	*Rep 2*	*Rep 3*
					mg l^{-1}				
1	0.33	0.31	0.32	0.01	0.01	0.01	1049.00	1181.00	1228.00
2	0.21	0.21	0.21	0.01	0.01	0.01	691.00	566.00	552.00
3	0.20	0.19	0.20	0.02	0.02	0.02	468.00	546.00	390.00
4	0.18	0.19	0.18	bd	bd	bd	390.00	399.00	371.00
5	0.17	0.16	0.16	0.01	0.01	0.01	339.00	390.00	362.00
6	0.14	0.13	0.13	bd	bd	bd	343.30	389.00	301.00
7	0.09	0.08	0.70	bd	bd	bd	301.00	314.00	309.00
8	bd	bd	bd	bd	bd	bd	231.30	288.00	250.00
9							192.60	178.90	225.50
11	0.03	0.02	0.02	bd	bd	bd	290.00	302.00	285.00
14	bd	bd	bd				264.20	260.70	242.30
17	bd	bd	bd	0.02	0.02	0.02	452.50	367.00	241.00
20	bd	bd	bd	0.02	0.02	0.02	425.00	194.00	221.00
23	bd	bd	bd	0.02	0.02	0.02	215.00	197.00	204.00
26	bd	bd	bd				93.38	108.80	158.10
29	bd	bd	bd				56.81	72.91	151.75
32	bd	bd	bd				36.38	44.37	71.35
35	bd	bd	bd				34.15	53.12	78.45
38	bd	bd	bd				31.56	41.23	39.46
41	bd	bd	bd	0.15	0.16	0.16	28.62	34.50	39.48
44	bd	bd	bd	0.12	0.12	0.10	25.71	27.22	34.54

bd: below detection

Table A7.14 pH of the effluent collected from three columns leached on a weekly basis with 1 pore volume of distilled water (DW) and from three columns leached with deoxygenated distilled water (DDW) (TT tailings sample; see Chapter 3 for details).

pH	*Pore volume displacements*									
Treatment	*1*	*2*	*3*	*4*	*5*	*6*	*7*	*8*	*9*	*10*
DW (1)	7.29	7.24	7.38	7.30	7.43	7.39	7.46	7.39	7.18	7.14
DW (2)	7.29	7.25	7.44	7.36	7.41	7.38	7.39	7.29	7.32	7.33
DW (3)	7.31	7.33	7.44	7.36	7.47	7.38	7.39	7.34	7.34	7.30
DDW (1)	7.14	7.41	7.43	7.49	7.40	7.32	7.30	7.38	7.40	7.13
DDW (2)	7.19	7.45	7.49	7.50	7.43	7.37	7.39	7.43	7.41	7.35
DDW (3)	7.21	7.49	7.45	7.53	7.46	7.35	7.41	7.44	7.46	7.36

Table A7.15 EC (in mS m^{-1}) of the effluent collected from three columns leached on a weekly basis with 1 pore volume of distilled water (DW) and from three columns leached with deoxygenated distilled water (DDW) (TT tailings sample; see Chapter 3 for details).

EC	*Pore volume displacements*									
Treatment	*1*	*2*	*3*	*4*	*5*	*6*	*7*	*8*	*9*	*10*
DW (1)	270.1	218.8	232.5	211.2	179.3	157.6	99.8	123.7	36.6	25.4
DW (2)	289.1	219.4	236.1	216.4	188.6	151.9	158.4	118.3	35.4	24.5
DW (3)	266.3	218.7	235.1	211.9	182.4	156.1	162.8	117.9	35.2	24.0
DDW (1)	295.4	211.7	220.4	190.2	206.8	147.0	105.5	62.8	28.0	17.3
DDW (2)	274.2	208.9	220.8	195.7	173.0	145.0	116.2	66.1	32.7	17.7
DDW (3)	286.1	214.3	225.7	202.4	185.9	151.0	126.0	81.7	54.8	27.2

Table A7.16 E_h (in mV) of the effluent collected from three columns leached on a weekly basis with 1 pore volume of distilled water (DW) and from three columns leached with deoxygenated distilled water (DDW) (TT tailings sample; see Chapter 3 for details).

E_h	*Pore volume displacements*									
Treatment	*1*	*2*	*3*	*4*	*5*	*6*	*7*	*8*	*9*	*10*
DW (1)	673	540	460	481	542	473	701	650	694	680
DW (2)	675	525	454	414	523	477	685	613	689	668
DW (3)	671	533	458	440	483	481	663	586	676	633
DDW (1)	414	384	399	454	540	449	668	465	484	656
DDW (2)	408	377	400	464	462	443	613	455	455	626
DDW (3)	411	385	405	427	514	442	611	453	446	619

Table A7.17 Calcium concentration (mg l^{-1}) of the effluent collected from three columns leached on a weekly basis with 1 pore volume of distilled water (DW) and from three columns leached with deoxygenated distilled water (DDW) (see Chapter 3 for details).

Ca	*Pore volume displacements*										
Treatment	*1*	*2*	*3*	*4*	*5*	*6*	*7*	*8*	*9*	*10*	*11*
W (1)	491.10	569.20	687.30	526.40	537.40	345.80	237.25	82.18	33.24	25.49	28.06
DW (2)	448.50	585.00	598.70	504.90	417.10	382.10	302.20	83.90	36.35	25.01	28.88
DW (3)	448.80	575.30	495.80	515.20	320.20	355.90	286.30	75.78	34.31	28.13	27.58
DDW (1)	501.40	563.60	551.80	518.80	277.20	482.60	396.60	382.30	141.40	23.29	28.16
DDW (2)	516.10	587.70	571.90	507.50	300.50	451.80	339.50	392.70	156.60	27.31	25.60
DDW (3)	528.00	589.90	590.60	645.90	423.00	431.00	393.10	451.50	186.70	40.41	23.16

Table A7.18 Copper concentration (mg l^{-1}) in the effluent collected from three columns leached on a weekly basis with 1 pore volume of distilled water (DW) and from three columns leached with deoxygenated distilled water (DDW) (see Chapter 3 for details).

Cu	*Pore volume displacements*									
Treatment	*1*	*2*	*3*	*4*	*5*	*6*	*7*	*8*	*9*	*10*
DW (1)	bd	bd	bd	bd	bd	bd	bd	bd	bd	bd
DW (2)	bd	bd	bd	bd	bd	bd	bd	bd	bd	bd
DW (3)	bd	bd	bd	bd	bd	bd	bd	bd	bd	bd
DDW (1)	0.021	bd	bd	bd	bd	bd	bd	bd	bd	bd
DDW (2)	0.021	bd	bd	bd	bd	bd	bd	bd	bd	bd
DDW (3)	0.020	bd	bd	bd	bd	bd	bd	bd	bd	bd

bd: below detection

Table A7.19 Iron concentration (mg l^{-1}) in the effluent collected from three columns leached on a weekly basis with 1 pore volume of distilled water (DW) and from three columns leached with deoxygenated distilled water (DDW) (see Chapter 3 for details).

Fe	*Pore volume displacements*									
Treatment	*1*	*2*	*3*	*4*	*5*	*6*	*7*	*8*	*9*	*10*
DW (1)	0.441	0.369	0.275	0.225	0.438	0.491	0.151	0.133	0.244	0.315
DW (2)	0.423	0.330	0.130	0.301	0.476	0.602	0.171	0.206	0.229	0.222
DW (3)	0.356	0.266	0.177	0.299	0.441	0.340	0.203	0.102	0.271	0.206
DDW (1)	0.492	0.304	0.263	0.419	0.505	0.397	0.230	0.092	0.186	0.305
DDW (2)	0.812	0.347	0.301	0.374	0.336	0.376	0.211	0.138	0.178	0.391
DDW (3)	0.521	0.343	0.222	0.427	0.586	0.402	0.352	0.299	0.184	0.231

Table A7.20 Mercury concentration (mg l^{-1}) in the effluent collected from three columns leached on a weekly basis with 1 pore volume of distilled water (DW) and from three columns leached with deoxygenated distilled water (DDW) (see Chapter 3 for details).

Hg	***Pore volume displacements***									
Treatment	*1*	*2*	*3*	*4*	*5*	*6*	*7*	*8*	*9*	*10*
DW (1)	0.551	0.307	0.195	0.463	0.483	0.311	0.489	0.278	0.207	0.268
DW (2)	0.490	0.244	0.086	0.487	0.321	0.200	0.311	0.200	0.266	0.330
DW (3)	0.534	0.201	0.041	0.408	0.267	0.206	0.351	0.079	0.228	0.293
DDW (1)	0.546	0.341	0.283	0.235	0.207	0.221	0.218	0.133	0.131	0.171
DDW (2)	0.698	0.227	0.190	0.352	0.181	0.169	0.212	0.101	0.120	0.127
DDW (3)	0.642	0.274	0.201	0.366	0.155	0.169	0.219	0.148	0.107	0.136

Table A7.21 Potassium concentration (mg l^{-1}) in the effluent collected from three columns leached on a weekly basis with 1 pore volume of distilled water (DW) and from three columns leached with deoxygenated distilled water (DDW) (see Chapter 3 for details).

K	***Pore volume displacements***									
Treatment	*1*	*2*	*3*	*4*	*5*	*6*	*7*	*8*	*9*	*10*
DW (1)	24.430	19.370	17.050	12.410	12.091	3.214	3.186	2.337	2.269	2.634
DW (2)	24.650	19.211	16.163	12.604	12.166	3.272	2.913	2.369	2.529	2.327
DW (3)	22.250	19.704	16.910	12.540	11.981	3.298	2.791	2.415	2.253	2.367
DDW (1)	25.180	18.140	12.655	12.445	12.419	3.954	3.210	2.624	2.522	2.346
DDW (2)	26.510	17.550	12.570	12.770	12.809	4.200	3.396	2.675	2.540	2.391
DDW (3)	28.650	18.870	13.550	13.483	12.864	4.440	3.770	2.825	2.815	2.469

Table A7.22 Magnesium concentration (mg l^{-1}) in the effluent collected from three columns leached on a weekly basis with 1 pore volume of distilled water (DW) and from three columns leached with deoxygenated distilled water (DDW) (see Chapter 3 for details).

Mg	***Pore volume displacements***									
Treatment	*1*	*2*	*3*	*4*	*5*	*6*	*7*	*8*	*9*	*10*
DW (1)	193.200	33.910	21.410	10.810	7.440	6.350	5.782	4.920	6.072	6.900
DW (2)	198.700	30.200	16.630	9.823	6.521	6.196	5.736	5.258	7.034	7.242
DW (3)	237.200	25.730	14.670	9.550	5.786	6.104	5.724	4.866	6.710	7.410
DDW (1)	257.600	48.620	12.816	9.360	7.858	5.360	5.112	4.408	4.748	4.462
DDW (2)	393.000	45.000	8.842	9.591	7.270	5.500	5.066	4.584	4.448	4.144
DDW (3)	313.300	40.070	14.956	9.530	7.869	5.862	5.454	4.758	4.532	4.522

Table A7.23 Manganese concentration (mg l^{-1}) in the effluent collected from three columns leached on a weekly basis with 1 pore volume of distilled water (DW) and from three columns leached with deoxygenated distilled water (DDW) (see Chapter 3 for details).

Mn	***Pore volume displacements***									
Treatment	*1*	*2*	*3*	*4*	*5*	*6*	*7*	*8*	*9*	*10*
DW (1)	2.960	1.874	1.915	1.726	1.155	0.995	0.929	0.552	0.349	0.217
DW (2)	2.736	1.805	1.545	1.693	1.298	0.965	0.768	0.513	0.362	0.230
DW (3)	3.046	1.853	1.657	1.509	0.890	0.999	0.858	0.783	0.279	0.205
DDW (1)	2.948	2.128	1.597	1.359	1.168	1.147	1.016	0.824	0.550	0.203
DDW (2)	4.578	2.104	1.492	1.729	1.201	1.700	1.822	1.159	0.782	0.234
DDW (3)	3.492	2.204	1.724	1.411	1.249	1.235	1.074	0.939	0.721	0.266

Table A7.24 Sodium concentration (mg l^{-1}) in the effluent collected from three columns leached on a weekly basis with 1 pore volume of distilled water (DW) and from three columns leached with deoxygenated distilled water (DDW) (see Chapter 3 for details).

Na	*Pore volume displacements*									
Treatment	*1*	*2*	*3*	*4*	*5*	*6*	*7*	*8*	*9*	*10*
DW(1)	6.106	3.272	3.121	1.726	1.158	1.478	0.623	1.538	0.601	0.816
DW (2)	5.564	2.834	3.099	1.693	1.298	0.897	0.720	1.162	0.594	0.721
DW (3)	6.344	2.853	2.888	1.684	1.239	1.200	0.731	1.005	0.810	0.545
DDW (1)	6.458	3.926	2.310	1.359	1.393	2.714	1.016	1.501	1.304	0.917
DDW (2)	10.882	3.582	2.144	1.824	1.723	1.851	2.952	1.537	1.443	1.159
DDW (3)	9.096	3.432	2.870	1.411	1.624	1.920	1.138	1.530	1.635	1.072

Table A7.25 Nickel concentration (mg l^{-1}) in the effluent collected from three columns leached on a weekly basis with 1 pore volume of distilled water (DW) and from three columns leached with deoxygenated distilled water (DDW) (see Chapter 3 for details).

Ni	*Pore volume displacements*									
Treatment	*1*	*2*	*3*	*4*	*5*	*6*	*7*	*8*	*9*	*10*
DW(1)	0.044	bd	bd	bd	bd	bd	bd	bd	bd	bd
DW (2)	0.052	bd	bd	bd	bd	bd	bd	bd	bd	bd
DW (3)	0.055	bd	bd	bd	bd	bd	bd	bd	bd	bd
DDW (1)	0.057	bd	bd	bd	bd	bd	bd	bd	bd	bd
DDW (2)	0.060	bd	bd	bd	bd	bd	bd	bd	bd	bd
DDW (3)	0.044	bd	bd	bd	bd	bd	bd	bd	bd	bd

bd: below detection

Table A7.26 Lead concentration (mg l^{-1}) in the effluent collected from three columns leached on a weekly basis with 1 pore volume of distilled water (DW) and from three columns leached with deoxygenated distilled water (DDW) (see Chapter 3 for details).

Pb	*Pore volume displacements*									
Treatment	*1*	*2*	*3*	*4*	*5*	*6*	*7*	*8*	*9*	*10*
DW(1)	0.100	0.005	0.061	0.030	0.067	bd	0.069	bd	0.100	0.005
DW (2)	0.066	0.011	0.076	0.052	0.040	0.033	0.107	bd	0.066	0.011
DW (3)	0.124	0.025	0.072	0.072	0.100	0.067	0.082	bd	0.124	0.025
DDW (1)	0.173	0.029	bd	0.094	0.051	0.092	0.100	bd	0.173	0.029
DDW (2)	0.194	bd	bd	0.028	0.020	bd	0.044	0.023	0.194	bd
DDW (3)	0.180	0.034	bd	0.101	0.056	0.114	0.161	bd	0.180	0.034

bd: below detection

Table A7.27 Sulfur concentration (mg l^{-1}) in the effluent collected from three columns leached on a weekly basis with 1 pore volume of distilled water (DW) and from three columns leached with deoxygenated distilled water (DDW) (see Chapter 3 for details).

S	*Pore volume displacements*										
Treatment	*1*	*2*	*3*	*4*	*5*	*6*	*7*	*8*	*9*	*10*	*11*
DW(1)	737.90	465.70	458.50	527.70	564.60	441.60	205.51	70.76	16.95	12.71	11.68
DW (2)	670.00	437.20	428.00	523.10	507.30	471.90	245.00	73.86	23.00	12.83	13.71
DW (3)	733.00	477.30	460.90	528.30	614.70	469.40	259.90	64.50	19.54	12.67	11.13
DDW (1)	625.70	561.00	446.50	482.00	535.70	376.60	390.80	224.80	76.68	11.56	7.42
DDW (2)	927.30	512.60	439.50	490.70	541.40	373.90	333.60	253.20	89.92	12.44	8.44
DDW (3)	744.40	542.40	495.00	513.60	527.30	408.60	299.30	272.80	138.16	24.32	6.50

Table A7.28 Zinc concentration (mg l^{-1}) in the effluent collected from three columns leached on a weekly basis with 1 pore volume of distilled water (DW) and from three columns leached with deoxygenated distilled water (DDW) (see Chapter 3 for details).

Zn	***Pore volume displacements***										
Treatment	*1*	*2*	*3*	*4*	*5*	*6*	*7*	*8*	*9*	*10*	*11*
DW(1)	8.34	6.58	6.97	7.35	7.07	4.57	4.12	2.74	1.71	0.68	0.42
DW (2)	8.74	6.45	5.97	5.78	5.35	4.84	3.73	2.08	0.67	0.44	0.36
DW (3)	9.09	6.68	7.24	7.70	7.02	4.93	4.57	2.96	1.00	0.61	1.14
DDW (1)	5.46	3.74	3.52	3.51	2.51	3.83	2.77	2.52	1.20	0.29	0.20
DDW (2)	5.69	3.15	2.81	2.84	2.53	2.38	2.34	2.32	0.96	0.25	0.25
DDW (3)	6.45	3.38	2.96	3.05	2.89	3.20	2.78	2.47	2.04	0.76	0.12

APPENDIX 8

Example of *CXTFIT* input and output files for parameter optimisation in the convection-dispersion equation and graphs of predicted long-term release of Mg, Mn, Zn and SO_4^{2-} from the Pering tailings impoundment

Table A8.1 Example of *CXTFIT* input file used for inverse parameter optimisation to define the Mg breakthrough curve.

```
1
*** BLOCK A: MODEL DESCRIPTION*********************************************
Mg displacement from Pering's tailings material- chemical non-equilibrium
  Relative concentration (mg/L) vs. time (hours)
INVERSE     MODE       NREDU
   1          2          1
 MODC        ZL(BLANK IF MODE=NREDU=1)
   1         23
*** BLOCK B: INVERSE PROBLEM***********************************************
  MIT        ILMT     MASS
  100         0         0
  MNEQ       MDEG
   2          0
*** BLOCK C: TRANSPORT PARAMETERS*************************************
    V          D          R       Beta   Omega   Mu1 Mu2
  0.1302     0.0685      2.0      0.5     0.6     0   0
    0          0          1        1       1      0   0
*** BLOCK D: BVP; MODB=0 ZERO; =1 Dirac ; =2 STEP; =3 A PULSE ***********
  MODB                 =4 MULTIPLE; =5 EXPONENTIAL; =6 ARBITRARY
   0
*** BLOCK E: IVP; MODI=0 ZERO; =1 CONSTANT; =2 STEPWISE; =3 EXPONENTIAL**
  MODI
    1
    1
*** BLOCK F: PVP; MODP=0 ZERO; =1 CONSTANT; =2 STEPWISE; =3 EXPONENTIAL*
   MODP
    0
*** BLOCK G: DATA FOR INVERSE PROBLEM **********************************
INPUTM =0; Z,T,C  =1; T,C FOR SAME Z  =2; Z,C FOR SAME T
   1
  23.0
  TIME       CONC      (Give "0 0 0" after last data set.)
44.73333333 0.961818042
61.63333333 0.972218348
    ↓          ↓
1055.525    0.008501816
1089.025    0.006893272
0.0         0.0
```

Table A8.2 Example of *CXTFIT* output file for the Mg breakthrough curve and the parameters which define it.

```
*********************************************************************
*                                                                   *
*     CXTFIT VERSION 2.1 (4/17/99)                                  *
*     ANALYTICAL SOLUTIONS FOR ONE-DIMENSIONAL CDE                  *
*     NON-LINEAR LEAST-SQUARES ANALYSIS                             *
*                                                                   *
*     Mg displacement from Pering's tailings material               *
*     Relative concentration (mg/L) vs. time (hours)                *
*                                                                   *
*     DATA INPUT FILE:  mg1.in                                      *
*                                                                   *
*********************************************************************


MODEL DESCRIPTION
=================
   DETERMINISTIC NONEQUILIBRIUM CDE (MODE=2)
   FLUX-AVERAGED CONCENTRATION
   REAL TIME (t), POSITION(x)
   D AND V ARE DIMENSIONAL; R,beta,omega,mu,gamma are dimensionless
   CHARACTERISTIC LENGTH =   23.0000
   FOR DIMENSIONLESS PARAMETERS


INITIAL VALUES OF COEFFICIENTS
==============================
NAME         INITIAL VALUE    FITTING
 V........      .1302E+00        N
 D........      .6850E-01        N
 R........      .2000E+01        Y
 beta.....      .5000E+00        Y
 omega....      .6000E+00        Y
 mu1......      .0000E+00        N
 mu2......      .0000E+00        N


BOUNDARY, INITIAL, AND PRODUCTION CONDITIONS
============================================
  SOLUTE FREE INPUT
  CONSTANT INITIAL CONC. =     1.0000
  NO PRODUCTION TERM


PARAMETER ESTIMATION MODE
=========================
  MAXIMUM NUMBER OF ITERATIONS =  100
  TWO-SITE CHEMICAL NONEQUILIBRIUM MODEL

ITER      SSQ          R....       beta.       omega
 0     .6285E+00   .200E+01   .500E+00   .600E+00
 1     .9119E-01   .148E+01   .790E+00   .268E+00
 2     .1772E-01   .155E+01   .843E+00   .181E+00
 3     .1692E-01   .155E+01   .840E+00   .165E+00
 4     .1692E-01   .155E+01   .839E+00   .165E+00
 5     .1692E-01   .155E+01   .839E+00   .165E+00
```

COVARIANCE MATRIX FOR FITTED PARAMETERS

	R....	beta.	omega
R....	1.000		
beta.	-.825	1.000	
omega	-.288	-.103	1.000

RSQUARE FOR REGRESSION OF OBSERVED VS PREDICTED = .99773368
(COEFFICIENT OF DETERMINATION)

MEAN SQUARE FOR ERROR (MSE) = .3759E-03

NON-LINEAR LEAST SQUARES ANALYSIS, FINAL RESULTS

NAME	VALUE	S.E.COEFF.	T-VALUE	95% CONFIDENCE LIMITS LOWER	UPPER
R....	.1551E+01	.2105E-01	.7370E+02	.1509E+01	.1594E+01
beta.	.8392E+00	.1106E-01	.7589E+02	.8169E+00	.8615E+00
omega	.1650E+00	.2198E-01	.7506E+01	.1207E+00	.2093E+00

----------ORDERED BY COMPUTER INPUT----------

$	NO	DISTANCE	TIME	OBS	CONCENTRATION FITTED	RESI-DUAL
	1	23.0000	44.7333	.9618	1.0000	-.0382
	2	23.0000	61.6333	.9722	1.0000	-.0278
			↓		↓	
	47	23.0000	1055.5250	.0085	.0093	-.0008
	48	23.0000	1089.0250	.0069	.0083	-.0014

Table A8.3 Example of *CXTFIT* input file used for direct modelling to determine the long-term release of Mg from Pering's tailings impoundment.

```
1
*** BLOCK A: MODEL DESCRIPTION
*****************************************
Mg displacement from Pering's tailings impoundment - direct problem
Conc vs. Time
INVERSE     MODE        NREDU
   0         2           1
 MODC        ZL(BLANK IF MODE=NREDU=1)
   1         30
*** BLOCK C: TRANSPORT PARAMETERS*****************************************
     V           D           R        Beta    Omega   Mu1 Mu2
  0.007942  0.000685     1.551    0.8392    27.72   0    0
*** BLOCK D: BVP; MODB=0 ZERO; =1 Dirac ; =2 STEP; =3 A PULSE ***********
  MODB                =4 MULTIPLE; =5 EXPONENTIAL; =6 ARBITRARY
   0
*** BLOCK E: IVP; MODI=0 ZERO; =1 CONSTANT; =2 STEPWISE; =3 EXPONENTIAL**
  MODI
    1
    1
*** BLOCK F: PVP; MODP=0 ZERO; =1 CONSTANT; =2 STEPWISE; =3 EXPONENTIAL**
   MODP
    0
*** BLOCK H: POSITION AND TIME FOR DIRECT PROBLEM************************
    NZ        DZ        ZI        NT        DT        TI        MPRINT
     1        1         30       400        52        0           1
```

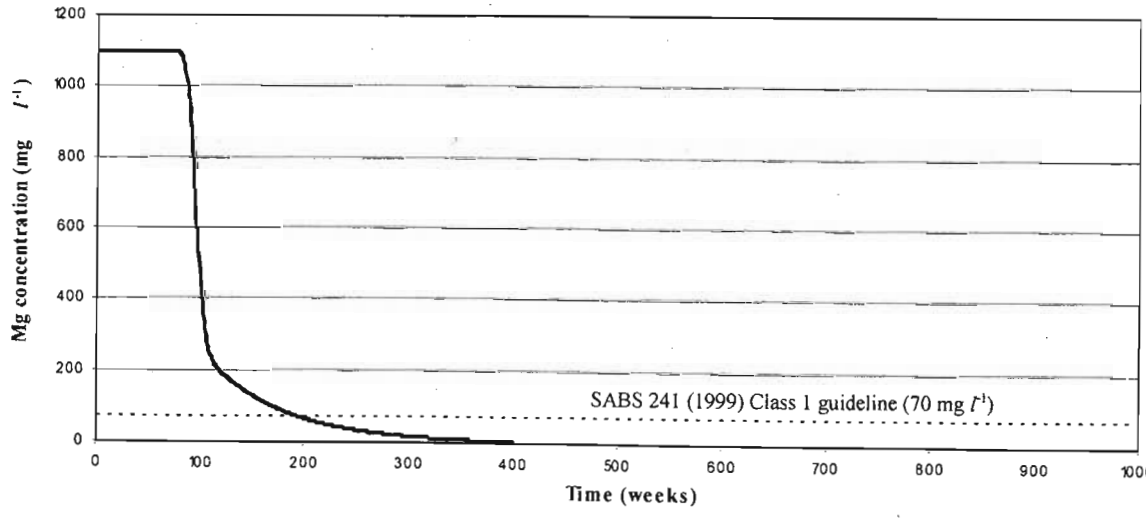

Figure A8.1 Predicted release of Mg from the base of Pering's tailings impoundment in relation to the SABS 241 drinking water guideline. Predictions based on BTC and modelling with *CXTFIT* (see Tables A8.1 to A8.3 above in conjunction with Chapter 3 for details).

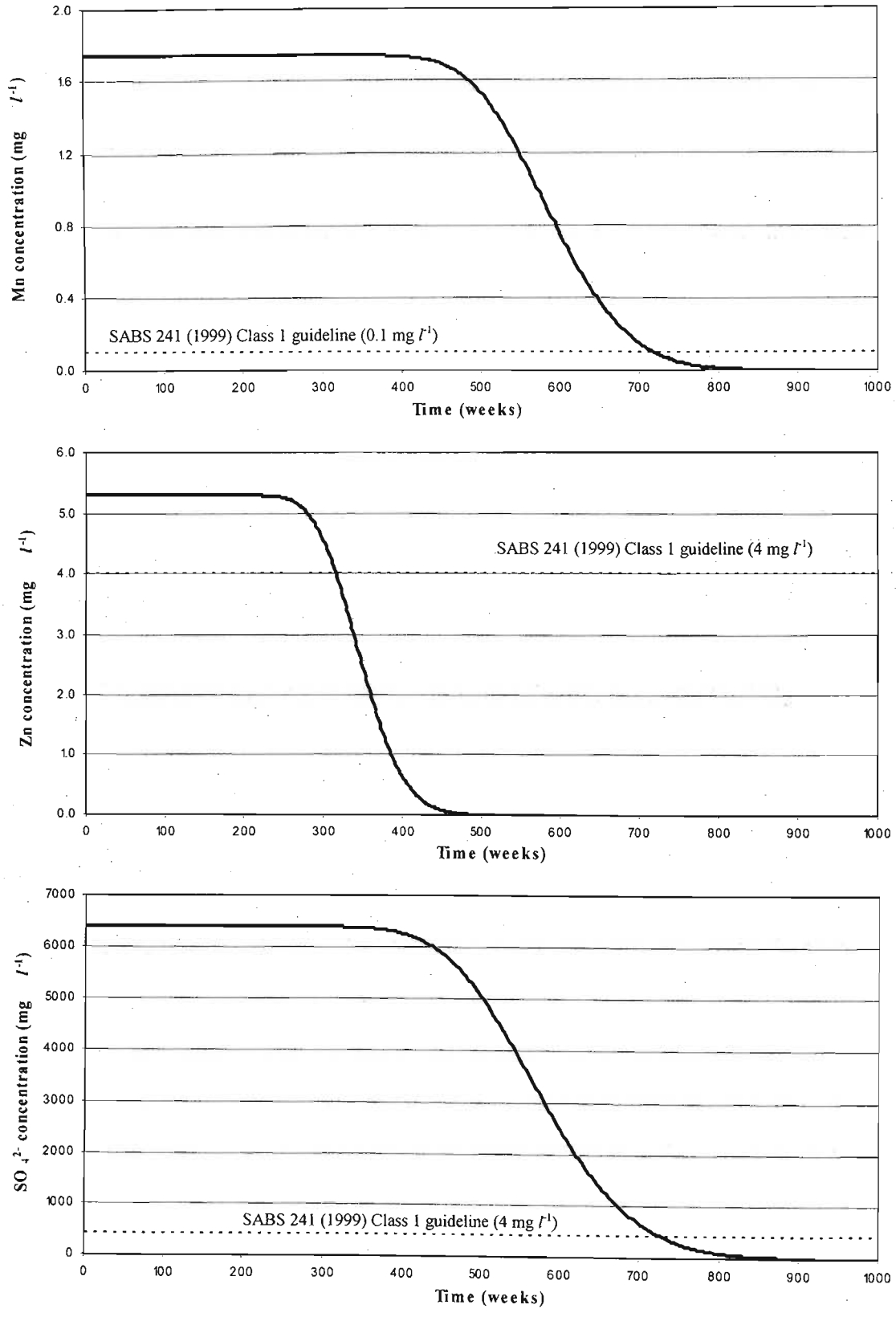

Figure A8.2 Predicted release of Mn, Zn and SO_4^{2-} from the base of Pering's tailings impoundment in relation to the SABS 241 drinking water guidelines. Predictions based on BTCs and modelling with *CXTFIT* (BTCs determined under continuous saturated flow; see Chapter 3 for details).

APPENDIX 9

Borehole chemistry: raw data and results of geochemical modelling to supplement Chapter 4

Table A9.1 pH of tailings samples taken from multiple depths within eight boreholes located across Pering's tailings impoundment (pH measured onsite in 1:2.5 tailings to deoxygenated distilled water solution; see Chapter 4 for details).

Sample depth	*P1T*	*P2A*	*P3T*	*P4C*	*P6C*	*P7C*	*P8C*	*P9C*
m								
0 – 1.5			7.98					
1.5 – 3.0		9.47				9.48		
3.0 – 4.5	8.56	8.89	8.64	8.57	9.03	9.22	8.83	9.28
4.5 – 6.0		8.87		8.55	9.15	9.08	8.64	9.04
6.0 – 7.5	8.65	8.96	8.5			9.13		
7.5 – 9.0								
9.0 – 10.5	8.59		8.72					
10.5 – 12.0		8.99				9.19		
12.0 – 13.5	8.98	9.16	8.84	8.84	9.23	9.14	9.19	9.38
13.5 – 15.0		9.17		8.75	9.47	9.18	9.14	9.29
15.0 – 16.5	8.83	9.45	8.85	8.9	9.04	9.22	9.15	9.43
16.5 – 18.0								
18.0 – 19.5	8.79		8.79					
19.5 – 21.0								
21.0 – 22.5	8.83	9.19	8.78			9.22		
22.5 – 24.0		9.22		9.15	9.46	9.28	8.73	9.34
24.0 – 25.5	8.96	9.3	8.67	9.14	9.38	9.07	8.78	9.22
25.5 – 27.0								
27.0 – 28.5	8.93	9.16	8.78			9.21		
28.5 – 30.0		9.52		9.48	8.99	9.28	8.9	9.07

Table A9.2 E_h of tailings samples taken from multiple depths within eight boreholes located across Pering's tailings impoundment (measurements taken onsite with a Ag/AgCl redox probe in a 1:2.5 tailings to deoxygenated distilled water solution; see Chapter 4 for details).

Sample depth	*P1T*	*P2A*	*P3T*	*P4C*	*P6C*	*P7C*	*P8C*	*P9C*
m				*E_h (mV)*				
0 – 1.5			441					
1.5 – 3.0		366				350		
3.0 – 4.5	376	390	442	392	407	370	445	410
4.5 – 6.0		369		388	407	376		418
6.0 – 7.5	376	381	438			323		
7.5 – 9.0								
9.0 – 10.5	378		450					
10.5 – 12.0		403				328		
12.0 – 13.5	359	386	454	370	398	329	440	402
13.5 – 15.0		391		380	386	331	445	404
15.0 – 16.5	357	353	454	352	365	326	444	394
16.5 – 18.0								
18.0 – 19.5	362		393					
19.5 – 21.0								
21.0 – 22.5	354	368	373			335		
22.5 – 24.0		380		372	379	333	362	398
24.0 – 25.5	358	375	389	350	385	340	356	396
25.5 – 27.0								
27.0 – 28.5	355	383	366			341		
28.5 – 30.0		367		378	381	328	367	413

Table A9.3 Gravimetric water content of tailings samples taken from multiple depths within eight boreholes located across Pering's tailings impoundment (see Chapter 4 for details).

Sample depth	*P1T*	*P2A*	*P3T*	*P4C*	*P6C*	*P7C*	*P8C*	*P9C*
m	*gravimetric water content (wt.%)*							
0 – 1.5	21.127		18.883					
1.5 – 3.0	20.671	13.917	31.901	20.211	13.449	9.345	11.053	12.767
3.0 – 4.5	24.122		23.521					
4.5 – 6.0	23.530							
6.0 – 7.5	19.985	15.953	27.300			13.684		20.612
7.5 – 9.0	24.641		27.010				13.017	
9.0 – 10.5	16.588		19.140					
10.5 – 12.0	19.704	15.333	23.833	25.800	13.985	13.888	11.834	14.574
12.0 – 13.5	16.801		22.114					
13.5 – 15.0	16.503		27.527					
15.0 – 16.5	16.953		20.716				14.607	
16.5 – 18.0	18.163		18.476					
18.0 – 19.5	17.210		23.350				13.744	
19.5 – 21.0	23.577		23.492					
21.0 – 22.5	23.825	13.239	24.877	22.576	16.556	11.400	9.793	17.835
22.5 – 24.0	21.605		25.876					
24.0 – 25.5	18.931		25.675					
25.5 – 27.0	24.016		30.864					
27.0 – 28.5	23.633	17.387	23.071	28.136	17.101	13.771	11.648	20.245
28.5 – 30.0	26.666		30.551					

Table A9.4 pH and E_h of sub-samples taken from borehole P1T as well as elemental composition and EC of the pore-water (see Chapter 4 for details).

Sample	*Sample depth*	*pH*	*EC*	E_h	*Al*	*Ca*	*Cd*	*Cu*	*Fe*
	m		*mS m^{-1}*	*mV*			*mg l^{-1}*		
P1T - 3	3.0 – 4.5	8.56	505.4	376	0.905	197.300	bd	bd	0.079
P1T - 5	6.0 – 7.5	8.65	543.8	376	0.985	246.700	bd	bd	0.085
P1T - 7	9.0 – 10.5	8.59	501.4	378	0.910	192.100	bd	bd	0.090
P1T - 9	12.0 – 13.5	8.98	500.8	359	0.959	197.000	bd	bd	0.097
P1T - 11	15.0 – 16.5	8.83	477.7	357	0.853	157.400	bd	bd	0.094
P1T - 13	18.0 – 19.5	8.79	386.7	362	0.721	150.000	bd	bd	0.078
P1T - 15	21.0 – 22.5	8.83	395.3	354	0.803	194.300	bd	bd	0.083
P1T - 17	24.0 – 25.5	8.96	376.7	358	0.729	140.400	bd	bd	0.075
P1T - 19	27.0 – 28.5	8.93	395.3	355	0.776	152.500	bd	bd	0.079

Sample	*Hg*	*K*	*Mg*	*Mn*	*Na*	*Ni*	*Pb*	*S*	*Sr*	*Zn*
	mg l^{-1}									
P1T - 3	2.619	72.690	705.000	bd	203.200	0.091	0.037	927.100	0.334	1.477
P1T - 5	2.579	69.620	839.900	bd	167.500	0.117	0.080	1122.000	0.382	2.130
P1T - 7	2.805	56.340	684.000	bd	163.900	0.079	0.064	892.600	0.540	1.546
P1T - 9	1.756	56.310	779.700	bd	142.600	0.104	0.084	1076.000	0.356	1.847
P1T - 11	1.910	54.380	712.000	bd	167.700	0.077	0.106	941.200	0.345	1.643
P1T - 13	2.795	48.720	516.800	bd	150.300	0.060	0.070	702.500	0.318	1.295
P1T - 15	2.103	49.510	516.800	bd	184.500	0.041	0.078	643.800	0.406	0.970
P1T - 17	1.510	53.420	481.100	bd	141.700	0.035	0.073	608.000	0.430	0.877
P1T - 19	1.769	54.590	490.200	bd	150.900	0.041	0.088	635.900	0.420	0.988

bd: below detection

Table A9.5 pH and E_h of sub-samples taken from borehole P2A as well as elemental composition and EC of the pore-water (see Chapter 4 for details).

Sample	*Sample depth*	*pH*	*EC*	*Redox*	*Al*	*Ca*	*Cd*	*Cu*	*Fe*
	m		*mS m^{-1}*	*mV*			*mg l^{-1}*		
P2A - 2	1.5 – 3.0	9.47	608.8	366	0.773	145.100	bd	bd	0.088
P2A - 5	6.0 – 7.5	8.96	488.0	381	0.898	201.000	bd	bd	0.079
P2A - 8	10.5 – 12.0	8.99	471.7	403	0.924	161.900	bd	bd	0.085
P2A - 19	27.0 – 28.5	9.16	322.2	383	0.739	142.700	bd	bd	0.054

Sample	*Hg*	*K*	*Mg*	*Mn*	*Na*	*Ni*	*Pb*	*S*	*Sr*	*Zn*
					mg l^{-1}					
P2A - 2	1.742	111.500	915.600	bd	263.100	0.031	bd	1221.000	0.354	1.659
P2A - 5	1.265	55.600	687.000	bd	160.500	0.075	0.061	921.100	0.361	1.514
P2A - 8	2.189	54.690	673.900	bd	163.200	0.048	0.023	912.900	0.471	1.482
P2A - 19	0.619	46.440	398.800	bd	124.600	0.035	0.028	674.100	0.292	1.018

note: Sample P2A-15 contained insufficient moisture for vacuum extraction
bd: below detection

Table A9.6 pH and E_h of sub-samples taken from borehole P3T as well as elemental composition and EC of the pore-water (see Chapter 4 for details).

Sample	*Sample depth*	*pH*	*EC*	*Redox*	*Al*	*Ca*	*Cd*	*Cu*	*Fe*
	m		*mS m^{-1}*	*mV*			*mg l^{-1}*		
P3T - 3	3.0 – 4.5	8.64	449.2	442	0.844	168.100	bd	bd	0.088
P3T - 5	6.0 – 7.5	8.50	520.0	438	0.991	229.000	bd	bd	0.065
P3T - 7	9.0 – 10.5	8.72	439.1	450	0.807	165.300	bd	bd	0.055
P3T - 9	12.0 – 13.5	8.84	396.3	454	0.780	145.600	bd	bd	0.057
P3T - 11	15.0 – 16.5	8.85	353.9	454	0.587	108.400	bd	bd	0.035
P3T - 13	18.0 – 19.5	8.79	371.1	393	0.541	98.050	bd	bd	0.038
P3T - 15	21.0 – 22.5	8.78	389.1	373	0.626	175.700	bd	bd	0.042
P3T - 17	24.0 – 25.5	8.67	345.7	389	0.536	125.000	bd	bd	0.102
P3T - 19	27.0 – 28.5	8.78	335.9	366	0.592	139.100	bd	bd	0.033

Sample	*Hg*	*K*	*Mg*	*Mn*	*Na*	*Ni*	*Pb*	*S*	*Sr*	*Zn*
					mg l^{-1}					
P3T - 3	1.312	66.740	624.500	bd	155.400	0.065	0.042	770.800	0.3618	1.2564
P3T - 5	0.716	72.820	917.300	bd	161.000	0.057	0.019	1195.000	0.5126	1.5284
P3T - 7	3.622	58.350	608.200	bd	136.700	0.034	0.023	765.300	0.3694	1.1248
P3T - 9	3.543	52.870	535.300	bd	141.000	0.026	0.014	725.800	0.4342	1.608
P3T - 11	0.385	55.150	446.700	bd	138.400	0.028	bd	587.200	0.2724	1.0622
P3T - 13	1.335	76.790	455.600	bd	160.400	0.010	bd	571.500	0.3384	0.8036
P3T - 15	0.446	44.200	491.600	bd	204.900	0.014	bd	561.900	0.3914	0.9502
P3T - 17	0.982	54.620	402.400	bd	186.300	0.008	bd	642.100	0.3550	1.26
P3T - 19	2.461	40.190	379.900	bd	135.700	0.005	bd	439.700	0.3876	0.753

bd: below detection

Table A9.7 Elemental composition and EC of the pore-water extracted from borehole P4C (see Chapter 4 for details).

Sample	*Sample depth*	*EC*	*Al*	*Ca*	*Cd*	*Cu*	*Fe*	*Hg*
	m	*mS m^{-1}*		*mg l^{-1}*				
P4C - 2	1.5 – 3.0	491.8	0.930	236.000	0.000	bd	0.075	6.172
P4C - 8	10.5 – 12.0	459.9	0.815	205.200	0.000	bd	0.055	0.637
P4C - 15	21.0 – 22.5	255.6	0.419	69.480	0.000	bd	0.025	0.378
P4C - 19	27.0 – 28.5	211.8	0.392	62.600	0.000	bd	0.016	1.316

Sample	*K*	*Mg*	*Mn*	*Na*	*Ni*	*Pb*	*S*	*Sr*	*Zn*
					mg l^{-1}				
P4C - 2	68.530	712.800	bd	183.500	0.007	0.005	1004.000	0.602	1.539
P4C - 8	49.620	637.800	bd	150.900	0.036	bd	812.100	0.476	1.415
P4C - 15	42.260	257.800	bd	133.900	0.011	bd	309.400	0.267	0.342
P4C - 19	36.400	174.500	bd	144.700	0.000	bd	211.100	0.275	0.338

bd: below detection

Table A9.8 Elemental composition and EC of the pore-water extracted from borehole P6C (see Chapter 4 for details).

Sample	*Sample depth*	*EC*	*Al*	*Ca*	*Cd*	*Cu*	*Fe*	*Hg*
	m	*mS m^{-1}*		*mg l^{-1}*				
P6C - 2	1.5 – 3.0	539.8	0.971	216.200	bd	bd	0.067	2.958
P6C - 8	10.5 – 12.0	462.2	0.808	166.400	bd	bd	0.061	0.813
P6C - 15	21.0 – 22.5	413.9	0.713	136.700	bd	bd	0.066	1.3884
P6C - 19	27.0 – 28.5	447.9	0.879	164.600	bd	bd	0.067	0.7612

Sample	*K*	*Mg*	*Mn*	*Na*	*Ni*	*Pb*	*S*	*Sr*	*Zn*
					mg l^{-1}				
P6C - 2	75.060	846.500	bd	162.200	0.092	0.043	1149.000	0.430	1.738
P6C - 8	53.880	697.700	bd	141.900	0.045	0.014	901.800	0.351	1.542
P6C - 15	61.370	600.200	bd	134.400	0.040	0.003	745.900	0.3400	1.675
P6C - 19	65.820	634.400	bd	156.700	0.038	0.004	774.300	0.5246	1.316

bd: below detection

Table A9.9 Elemental composition and EC of the pore-water extracted from borehole P9C (see Chapter 4 for details).

Sample	*Sample depth*	*EC*	*Al*	*Ca*	*Cd*	*Cu*	*Fe*	*Hg*
	m	*mS m^{-1}*		*mg l^{-1}*				
P9C - 5	6.0 – 7.5	437.1	0.885	177.300	bd	bd	0.082	2.726
P9C - 8	10.5 – 12.0	402.5	0.816	144.100	bd	bd	0.088	1.454
P9C - 15	21.0 – 22.5	387.2	0.874	153.900	bd	bd	0.078	1.280
P9C - 19	27.0 – 28.5	396.2	0.726	120.000	bd	bd	0.082	0.969

Sample	*K*	*Mg*	*Mn*	*Na*	*Ni*	*Pb*	*S*	*Sr*	*Zn*
					mg l^{-1}				
P9C - 5	47.600	631.600	bd	127.900	0.051	0.115	845.600	0.336	1.475
P9C - 8	42.620	546.800	bd	148.000	0.046	0.107	722.900	0.269	1.046
P9C - 15	47.030	494.300	bd	137.800	0.038	0.040	633.200	0.399	1.025
P9C - 19	57.060	522.800	bd	147.500	0.046	0.045	611.300	0.348	1.174

bd: below detection

Table A9.10 Predicted (*MINTEQ* modelling) species distribution in the pore-water extracted from borehole P1T.

Sample number		*3*	*5*	*7*	*9*	*11*	*13*	*15*	*17*	*19*
Average Depth (m)		*3.75*	*6.75*	*9.75*	*12.75*	*15.75*	*18.75*	*21.75*	*24.75*	*27.75*
	Species name	*% of total element concentration*								
Al^{+3}	$Al(OH)_{3\,(aq)}$	0.17	0.13	0.16	0.06	0.09	0.10	0.09	0.07	0.07
	$Al(OH)_4^-$	99.83	99.86	99.84	99.94	99.91	99.90	99.91	99.93	99.93
Ca^{+2}	Ca^{+2}	62.66	60.81	62.96	60.21	61.83	64.44	67.08	66.59	66.06
	$CaCl^+$	1.19	0.79	0.87	0.74	1.01	0.90	1.01	1.01	1.00
	$CaSO_{4\,(aq)}$	36.15	38.40	36.17	39.05	37.16	34.66	31.91	32.40	32.94
Cl^{-1}	Cl^-	96.45	96.06	96.51	96.38	96.57	97.09	96.86	97.15	97.11
	$CaCl^+$	0.48	0.56	0.48	0.46	0.38	0.41	0.55	0.41	0.43
	$MgCl^+$	2.87	3.21	2.85	3.02	2.89	2.35	2.41	2.30	2.30
	$KCl_{\,(aq)}$	0.03	0.03	0.03	0.03	0.02	0.02	0.02	0.03	0.03
	$NaCl_{\,(aq)}$	0.16	0.13	0.13	0.11	0.13	0.12	0.15	0.12	0.12
CO_3^{-2}	CO_3^{-2}	2.80	3.35	2.94	6.16	4.74	4.31	4.57	5.84	5.54
	$Mg_2CO_3^{+2}$	0.61	0.92	0.63	1.49	1.04	0.62	0.70	0.80	0.77
	HCO_3^-	79.68	75.61	79.14	66.00	72.77	76.59	73.97	71.31	72.09
	$H_2CO_3^*{}_{(aq)}$	0.38	0.29	0.35	0.12	0.19	0.22	0.19	0.14	0.15
	$PbCO_{3\,(aq)}$	0.03	0.06	0.05	0.06	0.08	0.06	0.07	0.06	0.08
	$ZnCO_{3\,(aq)}$	0.27	0.40	0.30	0.49	0.42	0.37	0.29	0.29	0.32
	$ZnHCO_3^+$	0.01	0.01	0.01						0.02
	$NiCO_{3\,(aq)}$	0.02	0.02	0.01	0.03	0.02	0.02	0.01	0.02	11.27
	$MgCO_{3\,(aq)}$	6.48	8.41	6.87	14.82	11.11	8.81	9.61	11.94	4.40
	$MgHCO_3^+$	6.11	6.51	6.01	5.33	5.61	4.77	4.75	4.34	0.96
	$CaHCO_3^+$	1.19	1.33	1.18	0.93	0.86	0.97	1.26	0.89	3.96
	$CaCO_{3\,(aq)}$	2.03	2.75	2.16	4.17	2.75	2.87	4.09	3.94	
	$NaCO_3^-$	0.17	0.16	0.15	0.26	0.24	0.21	0.27	0.27	0.27
	$NaHCO_{3\,(aq)}$	0.23	0.18	0.19	0.13	0.17	0.17	0.20	0.15	0.16
Fe^{+2}	Fe^{+2}	59.11	56.70	59.01	53.04	56.17	58.58	60.50	58.15	58.22
	$FeOH^+$	4.16	4.79	4.51	9.72	7.41	7.43	8.40	11.10	10.30
	$Fe(OH)_{2\,(aq)}$	0.01	0.01	0.01	0.06	0.03	0.03	0.04	0.06	
	$Fe(OH)_3^-$	0.01	0.02	0.02	0.23	0.09	0.07	0.10	0.24	0.19
	$FeCl^+$	0.17	0.11	0.12	0.10	0.14	0.12	0.14	0.13	0.13
	$FeSO_{4\,(aq)}$	36.54	38.36	36.33	36.86	36.17	33.77	30.83	30.32	31.11
K^{+1}	K^{+1}	95.23	94.71	95.38	94.69	95.11	95.91	96.33	96.34	96.23
	$KCl_{\,(aq)}$	0.21	0.15	0.15	0.14	0.18	0.15	0.17	0.16	0.16
	KSO_4^-	4.56	5.14	4.47	5.17	4.71	3.94	3.51	3.50	3.61
Mg^{+2}	Mg^{+2}	67.72	66.03	68.02	65.43	66.93	69.37	71.77	71.30	70.82
	$MgOH^+$	0.05	0.06	0.05	0.12	0.09	0.09	0.10	0.14	0.13
	$MgCl^+$	1.20	0.80	0.88	0.75	1.02	0.90	1.01	1.01	1.00
	$MgSO_{4\,(aq)}$	31.03	33.12	31.05	33.70	31.96	29.64	27.12	27.56	28.06
Na^{+1}	Na^{+1}	96.29	95.90	96.42	95.89	96.20	96.83	97.15	97.16	97.07
	$NaCl_{\,(aq)}$	0.22	0.15	0.16	0.14	0.19	0.15	0.17	0.17	0.17
	$NaSO_4^-$	3.50	3.95	3.42	3.97	3.61	3.02	2.68	2.67	2.76
Ni^{+2}	Ni^{+2}	64.88	62.81	64.98	60.07	62.78	65.23	67.28	65.42	65.36
	NiOH+	1.44	1.68	1.57	3.48	2.62	2.62	2.95	3.95	3.66
	$Ni(OH)_{2\,(aq)}$	0.32	0.46	0.38	2.03	1.09	1.02	1.26	2.28	1.97
	$Ni(OH)_3^-$				0.03			0.01	0.03	0.02
	$NiCl^+$	0.74	0.49	0.54	0.44	0.62	0.55	0.61	0.60	0.59
	$NiSO_{4\,(aq)}$	32.59	34.54	32.52	33.93	32.86	30.56	27.87	27.72	28.39
	$Ni(SO_4)_2^{-2}$	0.02	0.02	0.02	0.02	0.02	0.01	0.01	0.01	0.01

Table A9.10*(cont)* Predicted (*MINTEQ* modelling) species distribution in the pore-water extracted from borehole P1T.

	Sample number	*3*	*5*	*7*	*9*	*11*	*13*	*15*	*17*	*19*
	Average Depth (m)	*3.75*	*6.75*	*9.75*	*12.75*	*15.75*	*18.75*	*21.75*	*24.75*	*27.75*
	Species name	*% of total element concentration*								
Pb^{+2}	Pb^{+2}	13.57	11.71	12.89	5.90	8.15	8.61	8.01	5.85	6.31
	$PbOH^{+}$	60.28	62.39	62.13	68.22	67.75	68.89	70.19	70.45	70.39
	$Pb(OH)_{2\,(aq)}$	5.35	6.74	5.94	15.86	11.22	10.65	11.89	16.21	15.08
	$Pb(OH)_3^{-}$	0.03	0.04	0.03	0.20	0.10	0.08	0.10	0.19	0.16
	$PbCl^{+}$	2.14	1.26	1.48	0.60	1.11	1.00	1.01	0.74	0.79
	$PbCl_{2\,(aq)}$	0.07	0.03	0.03	0.01	0.03	0.02	0.03	0.02	0.02
	$PbSO_{4\,(aq)}$	16.74	15.80	15.83	8.18	10.47	9.90	8.15	6.09	6.73
	$Pb(SO_4)_2^{-2}$	1.83	2.03	1.66	1.04	1.17	0.85	0.63	0.45	0.52
SO_4^{-2}	SO_4^{-2}	61.39	59.48	61.30	61.14	62.05	64.21	62.33	64.16	64.02
	$ZnSO_{4\,(aq)}$	0.02	0.03	0.02	0.02	0.02	0.02	0.02	0.01	0.01
	$MgSO_{4\,(aq)}$	31.08	32.65	31.34	32.17	31.84	28.72	28.67	28.72	28.49
	$CaSO_{4\,(aq)}$	6.15	6.75	6.22	5.71	4.97	5.91	7.69	5.98	6.31
	$NaSO_4^{-}$	1.07	0.82	0.88	0.73	0.90	0.90	1.07	0.87	0.91
	KSO_4^{-}	0.29	0.26	0.23	0.22	0.22	0.22	0.22	0.25	0.25
Zn^{+2}	Zn^{+2}	51.34	47.91	51.05	35.22	42.35	45.17	44.77	37.42	38.99
	$ZnOH^{+}$	9.08	10.17	9.80	16.22	14.02	14.40	15.61	17.93	17.33
	$Zn(OH)_{2\,(aq)}$	4.04	5.50	4.70	18.89	11.65	11.15	13.25	20.68	18.60
	$Zn(OH)_3^{-}$	0.10	0.16	0.12	1.19	0.52	0.44	0.57	1.20	1.01
	$ZnCl^{+}$	0.57	0.36	0.42	0.25	0.41	0.37	0.40	0.33	0.35
	$ZnOHCl_{(aq)}$	2.11	1.63	1.64	2.44	2.80	2.37	2.79	3.17	3.07
	$ZnSO_{4\,(aq)}$	28.28	28.89	28.02	21.81	24.31	23.21	20.34	17.39	18.57
	$Zn(SO_4)_2^{-2}$	4.47	5.37	4.25	3.99	3.94	2.89	2.26	1.87	2.09

APPENDIX 10

Saturated paste analysis of the borehole tailings samples: raw data to supplement Chapter 4

Table A10.1 pH, electrical conductivity (EC), water content (WC) and element concentrations of saturated pastes extracts done on tailings samples taken from borehole P1T.

Sample	*Depth*	*pH*	*EC*	*WC*	*Al*	*Ba*	*Ca*	*Cd*	*Cu*	*Fe*
	m		*mS m^{-1}*	*wt.%*			*mg l^{-1}*			
P1T - 1	0 – 1.5	7.99	576.6	30.119	1.618	bd	434.800	bd	bd	0.054
P1T - 2	1.5 – 3.0	8.09	490.2	22.747	1.229	bd	285.300	bd	bd	0.044
P1T - 3	3.0 – 4.5	8.30	472.7	27.556	1.456	bd	399.200	bd	bd	0.047
P1T - 4	4.5 – 6.0	8.32	451.9	29.116	1.286	bd	277.400	bd	bd	0.038
P1T - 5	6.0 – 7.5	8.29	461.6	27.570	1.447	bd	307.300	bd	bd	0.046
P1T - 6	7.5 – 9.0	8.30	406.9	28.222	1.122	bd	170.200	bd	bd	0.035
P1T - 7	9.0 – 10.5	8.31	420.8	24.259	1.249	bd	133.400	bd	bd	0.035
P1T - 8	10.5 – 12.0	8.33	390.5	24.095	1.147	bd	149.700	bd	bd	0.043
P1T - 9	12.0 – 13.5	8.32	588.7	24.589	1.544	bd	622.200	bd	bd	0.047
P1T - 10	13.5 – 15.0	8.38	441.5	24.723	1.234	bd	258.300	bd	bd	0.035
P1T - 11	15.0 – 16.5	8.26	544.2	25.291	1.547	bd	513.800	bd	bd	0.054
P1T - 12	16.5 – 18.0	8.18	383.2	25.339	1.100	bd	249.600	bd	bd	0.029
P1T - 13	18.0 – 19.5	8.23	431.1	25.297	1.348	bd	286.500	bd	bd	0.037
P1T - 14	19.5 – 21.0	7.95	405.2	27.728	1.133	bd	240.800	bd	bd	0.035
P1T - 15	21.0 – 22.5	8.26	430.0	27.561	1.155	bd	307.100	bd	bd	0.046
P1T - 16	22.5 – 24.0	8.16	415.7	25.271	1.044	bd	211.500	bd	bd	0.043
P1T - 17	24.0 – 25.5	8.31	415.1	26.249	1.301	bd	271.100	bd	bd	0.087
P1T - 18	25.5 – 27.0	8.06	396.6	25.551	1.231	bd	215.000	bd	bd	0.096
P1T - 19	27.0 – 28.5	8.25	432.7	24.868	1.405	bd	339.300	bd	bd	0.091
P1T - 20	28.5 – 30.0	8.18	472.5	26.322	1.420	bd	308.200	bd	bd	0.103

Sample	*Hg*	*K*	*Mg*	*Mn*	*Na*	*Ni*	*Pb*	*S*	*Sr*	*Zn*
					mg l^{-1}					
P1T - 1	0.330	57.860	1005.000	0.527	87.320	0.025	0.009	1937.000	0.866	6.330
P1T - 2	0.201	72.090	1034.000	0.896	143.300	0.006	0.006	1829.000	0.510	1.370
P1T - 3	0.244	81.960	894.300	0.068	205.100	0.120	0.025	1656.000	0.489	1.574
P1T - 4	0.192	54.770	659.500	bd	122.300	0.069	bd	1198.000	0.325	1.231
P1T - 5	0.216	75.410	678.200	0.234	164.200	0.023	0.006	1316.000	0.388	2.036
P1T - 6	0.177	65.750	638.400	bd	152.900	bd	bd	1151.000	0.413	1.155
P1T - 7	0.206	73.180	1056.000	bd	198.600	0.006	bd	1737.000	0.452	1.870
P1T - 8	0.189	88.960	720.800	bd	197.000	0.017	bd	917.000	0.308	1.128
P1T - 9	0.264	55.660	1089.000	1.133	109.800	0.052	0.031	1954.000	0.401	14.308
P1T - 10	0.163	53.450	639.300	bd	123.700	0.018	bd	1275.000	0.242	1.966
P1T - 11	0.216	75.590	850.100	0.702	171.900	0.071	0.030	1520.000	0.507	8.910
P1T - 12	0.158	52.310	534.700	bd	118.800	0.002	bd	1108.000	0.330	1.434
P1T - 13	0.137	62.860	593.000	bd	152.100	0.018	0.004	1356.000	0.475	2.422
P1T - 14	0.097	57.370	564.500	bd	144.300	bd	bd	1176.000	0.450	1.517
P1T - 15	0.132	56.770	575.800	bd	131.300	0.007	bd	1270.000	0.344	1.335
P1T - 16	0.132	58.760	680.400	bd	111.000	0.004	0.001	1447.000	0.269	1.058
P1T - 17	0.124	62.540	1053.000	bd	121.400	0.007	0.011	1612.000	0.473	1.050
P1T - 18	0.319	60.700	592.700	bd	113.700	0.000	0.011	1300.000	0.542	1.006
P1T - 19	0.222	69.380	647.400	0.081	148.000	0.014	0.009	1477.000	0.437	1.456
P1T - 20	0.135	68.080	875.600	0.206	133.900	0.023	0.019	1101.000	0.823	2.908

bd: below detection

Table A10.2 pH, electrical conductivity (EC), water content (WC) and element concentrations of saturated pastes extracts done on tailings samples taken from borehole P3T.

Sample	*Depth*	*pH*	*EC*	*WC*	*Al*	*Ba*	*Ca*	*Cd*	*Cu*	*Fe*
	m		*mS m^{-1}*	*wt.%*			*mg l^{-1}*			
P3T - 1	0 – 1.5	7.74	618.3	28.967	2.046	bd	515.800	bd	0.106	0.149
P3T - 2	1.5 – 3.0	7.54	575.2	32.073	1.876	bd	422.400	bd	0.057	0.128
P3T - 3	3.0 – 4.5	7.89	493.6	28.344	1.538	bd	400.600	bd	bd	0.071
P3T - 5	6.0 – 7.5	7.56	555.4	30.209	1.662	bd	519.800	bd	bd	0.083
P3T - 6	7.5 – 9.0	7.90	503.2	31.604	1.365	bd	356.200	bd	bd	0.049
P3T - 7	9.0 – 10.5	7.77	419.3	26.291	1.294	bd	249.000	bd	0.018	0.044
P3T - 8	10.5 – 12.0	7.82	475.9	27.628	1.410	bd	353.600	bd	bd	0.046
P3T - 9	12.0 – 13.5	7.84	386.1	29.421	1.347	bd	229.800	bd	0.011	0.051
P3T - 10	13.5 – 15.0	7.92	426.0	27.473	1.459	bd	274.500	bd	bd	0.061
P3T - 11	15.0 – 16.5	7.11	394.4	26.320	1.363	bd	312.200	bd	0.011	0.041
P3T - 12	16.5 – 18.0	7.86	366.2	25.948	1.083	bd	265.600	bd	0.009	0.040
P3T - 13	18.0 – 19.5	7.46	414.4	27.058	1.203	bd	257.100	bd	bd	0.031
P3T - 14	19.5 – 21.0	7.91	390.3	33.788	1.222	bd	246.100	bd	bd	0.032
P3T - 15	21.0 – 22.5	7.42	421.1	27.432	1.158	bd	307.900	bd	bd	0.032
P3T - 16	22.5 – 24.0	7.80	409.4	32.729	1.231	bd	265.000	bd	bd	0.031
P3T - 17	24.0 – 25.5	7.76	425.7	30.256	1.240	bd	225.200	bd	bd	0.031
P3T - 18	25.5 – 27.0	7.82	434.1	29.921	1.267	bd	276.800	bd	bd	0.081
P3T - 19	27.0 – 28.5	7.76	463.4	27.821	1.696	bd	365.500	bd	0.015	0.052
P3T - 20	28.5 – 30.0	7.90	384.4	33.593	1.325	bd	246.600	bd	bd	0.035

Sample	*Hg*	*K*	*Mg*	*Mn*	*Na*	*Ni*	*Pb*	*S*	*Sr*	*Zn*
					mg l^{-1}					
P3T - 1	0.237	66.510	1121.000	0.624	93.930	0.120	0.152	1721.000	1.452	5.138
P3T - 2	0.240	94.570	824.100	0.924	219.400	0.000	bd	1377.000	1.072	2.196
P3T - 3	0.117	65.650	661.100	0.105	143.400	0.049	bd	1051.000	0.422	1.636
P3T - 5	0.157	58.310	800.300	0.220	111.800	0.004	bd	1308.000	0.597	2.906
P3T - 6	0.110	52.910	728.100	bd	110.700	bd	bd	1080.000	0.578	1.534
P3T - 7	0.122	67.660	555.700	bd	137.600	bd	bd	841.500	0.363	1.144
P3T - 8	0.128	57.700	643.500	bd	143.600	bd	bd	1021.000	0.463	2.032
P3T - 9	0.101	42.390	534.500	0.450	79.280	bd	bd	816.200	0.493	1.228
P3T - 10	0.092	54.520	624.500	bd	105.800	bd	bd	952.100	0.657	1.829
P3T - 11	0.086	56.630	563.200	bd	113.700	bd	bd	918.500	0.488	1.593
P3T - 12	0.082	59.490	476.100	bd	127.100	bd	bd	689.500	0.349	0.971
P3T - 13	0.086	69.210	508.000	bd	167.000	bd	bd	789.400	0.410	1.229
P3T - 14	0.088	45.650	452.400	bd	119.700	bd	bd	662.400	0.457	1.111
P3T - 15	0.086	56.880	519.800	bd	160.400	bd	bd	736.200	0.425	1.156
P3T - 16	0.105	45.190	487.800	bd	118.800	bd	bd	719.900	0.467	1.478
P3T - 17	0.098	62.800	519.800	bd	173.500	bd	bd	787.000	0.603	1.474
P3T - 18	0.103	49.790	528.300	bd	138.100	bd	bd	792.400	0.557	1.414
P3T - 19	0.705	52.390	634.700	0.210	128.500	bd	bd	1063.000	0.996	3.528
P3T - 20	0.173	50.260	448.300	bd	115.400	bd	bd	694.800	0.579	1.664

bd: below detection

Note: There was insufficient sample available to do a saturated paste on P3T-4

Table A10.3 pH, electrical conductivity (EC), water content (WC) and element concentrations of saturated pastes extracts done on tailings samples taken from borehole P2A.

Sample	*Depth*	*pH*	*EC*	*WC*	*Al*	*Ba*	*Ca*	*Cd*	*Cu*	*Fe*
	m		*mS m^{-1}*	*wt.%*			*mg l^{-1}*			
P2A - 5	6.0 – 7.5	7.76	476.6	26.359	1.756	bd	386.500	bd	0.052	0.093
P2A - 8	10.5 – 12.0	7.55	585.5	23.810	2.088	bd	521.300	bd	0.109	0.132
P2A - 15	21.0 – 22.5	7.76	542.3	24.814	1.736	bd	426.100	bd	0.116	0.092
P2A - 19	27.0 – 28.5	7.72	398.4	26.107	1.697	bd	346.000	bd	0.097	0.075

Sample	*Hg*	*K*	*Mg*	*Mn*	*Na*	*Ni*	*Pb*	*S*	*Sr*	*Zn*
					mg l^{-1}					
P2A - 5	0.092	47.440	593.200	0.325	116.900	0.034	0.050	1390.000	0.403	3.896
P2A - 8	0.194	55.750	831.700	2.064	112.700	0.073	0.039	1692.000	0.309	20.480
P2A - 15	0.305	67.090	1186.000	1.613	130.300	0.121	0.121	1359.000	0.195	16.176
P2A - 19	0.286	47.160	469.700	bd	83.900	0.014	0.042	951.500	0.390	3.162

bd: below detection

Table A10.4 pH, electrical conductivity (EC), water content (WC) and element concentrations of saturated pastes extracts done on tailings samples taken from borehole P4C.

Sample	*Depth*	*pH*	*EC*	*WC*	*Al*	*Ba*	*Ca*	*Cd*	*Cu*	*Fe*
	m		*mS m^{-1}*	*wt.%*			*mg l^{-1}*			
P4C - 8	10.5 – 12.0	7.85	532.0	29.714	1.623	bd	422.600	bd	0.036	0.057
P4C - 15	21.0 – 22.5	7.84	336.0	34.430	1.331	bd	262.100	bd	0.005	0.037
P4C - 19	27.0 – 28.5	7.81	303.6	36.092	1.145	bd	271.900	bd	0.046	0.036

Sample	*Hg*	*K*	*Mg*	*Mn*	*Na*	*Ni*	*Pb*	*S*	*Sr*	*Zn*
					mg l^{-1}					
P4C - 8	0.338	61.240	720.400	0.090	168.400	bd	0.007	1277.000	0.735	3.290
P4C - 15	0.067	42.660	717.800	bd	104.900	bd	bd	1268.000	0.469	0.990
P4C - 19	0.030	50.370	347.000	bd	130.300	bd	bd	554.400	0.414	1.125

bd: below detection

Table A10.5 pH, electrical conductivity (EC), water content (WC) and element concentrations of saturated pastes extracts done on tailings samples taken from borehole P6C.

Sample	*Depth*	*pH*	*EC*	*WC*	*Al*	*Ba*	*Ca*	*Cd*	*Cu*	*Fe*
	m		*mS m^{-1}*	*wt.%*			*mg l^{-1}*			
P6C - 2	1.5 – 3.0	7.64	641.0	21.554	1.688	bd	557.900	bd	0.072	0.080
P6C - 8	10.5 – 12.0	7.45	578.0	25.130	2.080	bd	546.700	bd	0.117	0.115
P6C - 15	21.0 – 22.5	7.68	537.0	23.943	1.911	bd	586.300	bd	0.162	0.105
P6C - 19	27.0 – 28.5		472.9	23.029	1.658	bd	297.800	bd	0.021	0.087

Sample	*Hg*	*K*	*Mg*	*Mn*	*Na*	*Ni*	*Pb*	*S*	*Sr*	*Zn*
					mg l^{-1}					
P6C - 2	0.169	91.340	1068.000	bd	153.600	0.205	0.013	1850.000	0.773	7.156
P6C - 8	0.189	73.040	727.900	0.821	142.000	0.095	0.120	1397.000	0.569	9.846
P6C - 15	0.266	61.910	570.300	0.339	96.070	0.063	0.167	1056.000	0.817	5.964
P6C - 19	0.162	57.180	678.800	bd	105.100	bd	bd	1131.000	0.612	2.674

bd: below detection

Table A10.6 pH, electrical conductivity (EC), water content (WC) and element concentrations of saturated pastes extracts done on tailings samples taken from borehole P7C.

Sample	*Depth*	*pH*	*EC*	*WC*	*Al*	*Ba*	*Ca*	*Cd*	*Cu*	*Fe*
	m		*mS m^{-1}*	*wt.%*			*mg l^{-1}*			
P7C - 2	1.5 – 3.0	8.30	581.9	19.967	1.832	bd	485.200	bd	0.153	0.121
P7C - 5	6.0 – 7.5	8.06	591.2	21.922	2.010	bd	475.700	bd	0.125	0.163
P7C - 8	10.5 – 12.0	8.38	583.3	24.169	1.798	bd	535.700	bd	0.089	0.124
P7C - 15	21.0 – 22.5	8.16	445.8	25.033	2.106	bd	546.200	bd	0.217	0.163
P7C - 19	27.0 – 28.5		511.0	24.928	2.432	bd	528.900	bd	0.299	0.162

Sample	*Hg*	*K*	*Mg*	*Mn*	*Na*	*Ni*	*Pb*	*S*	*Sr*	*Zn*
					mg l^{-1}					
P7C - 2	0.158	71.050	1202.000	2.446	91.130	0.035	0.073	2060.000	0.671	5.664
P7C - 5	0.202	73.920	1168.000	3.010	141.200	0.354	0.074	2079.000	0.560	6.950
P7C - 8	0.238	45.860	859.000	2.554	116.300	0.160	0.036	1603.000	0.312	27.420
P7C - 15	0.188	43.830	538.600	3.060	75.020	0.103	0.108	1138.000	0.357	15.344
P7C - 19	0.183	53.680	696.100	3.124	95.840	0.104	0.217	1342.000	0.507	10.374

bd: below detection

Table A10.7 pH, electrical conductivity (EC), water content (WC) and element concentrations of saturated pastes extracts done on tailings samples taken from borehole P8C.

Sample	*Depth*	*pH*	*EC*	*WC*	*Al*	*Ba*	*Ca*	*Cd*	*Cu*	*Fe*
	m		*mS m^{-1}*	*wt.%*			*mg l^{-1}*			
P8C - 2	1.5 – 3.0	8.28	582.0	21.960	1.984	bd	512.800	bd	0.179	0.170
P8C - 6	7.5 – 9.0	8.14	567.7	23.935	1.891	bd	537.100	bd	0.131	0.081
P8C - 8	10.5 – 12.0	8.24	554.5	23.920	1.533	bd	522.500	bd	0.031	0.048
P8C - 11	15.0 – 16.5	8.13	508.3	26.244	1.233	bd	539.700	bd	bd	bd
P8C - 13	18.0 – 19.5	8.22	512.6	24.681	1.845	bd	533.000	bd	0.206	0.102
P8C - 15	21.0 – 22.5	8.20	503.7	24.457	1.610	bd	536.500	bd	0.034	0.051
P8C - 19	27.0 – 28.5	8.30	501.5	25.053	1.567	bd	542.300	bd	0.032	0.046

Sample	*Hg*	*K*	*Mg*	*Mn*	*Na*	*Ni*	*Pb*	*S*	*Sr*	*Zn*
					mg l^{-1}					
P8C - 2	0.213	122.700	846.90	1.322	118.400	0.246	0.213	1603.00	1.152	4.092
P8C - 6	0.205	64.540	891.00	0.667	113.000	0.166	bd	1646.00	1.100	8.958
P8C - 8	0.235	58.740	818.90	2.524	102.500	0.066	bd	1576.00	0.356	21.28
P8C - 11	0.235	57.210	730.30	1.041	99.320	bd	bd	1502.00	0.616	14.62
P8C - 13	0.249	55.640	694.10	0.614	92.620	0.149	0.184	1384.00	0.552	9.692
P8C - 15	0.151	52.470	698.50	1.057	79.740	0.007	bd	1459.00	0.216	10.564
P8C - 19	0.182	62.300	642.50	1.081	93.360	bd	bd	1394.00	0.000	10.804

bd: below detection

Table A10.8 pH, electrical conductivity (EC), water content (WC) and element concentrations of saturated pastes extracts done on tailings samples taken from borehole P9C.

Sample	*Depth*	*pH*	*EC*	*WC*	*Al*	*Ba*	*Ca*	*Cd*	*Cu*	*Fe*
	m		*mS m^{-1}*	*wt.%*			*mg l^{-1}*			
P9C - 2	1.5 – 3.0	8.15	650.3	21.903	1.755	bd	509.900	bd	0.073	0.087
P9C - 5	6.0 – 7.5	8.36	566.7	25.885	1.841	bd	586.900	bd	0.073	0.065
P9C - 8	10.5 – 12.0	8.24	505.3	23.816	2.062	bd	586.200	bd	0.141	0.082
P9C - 15	21.0 – 22.5	8.26	374.6	27.032	1.426	bd	307.700	bd	0.002	0.056
P9C - 19	27.0 – 28.5	8.77	407.3	24.387	1.293	bd	259.600	bd	0.012	0.055

Sample	*Hg*	*K*	*Mg*	*Mn*	*Na*	*Ni*	*Pb*	*S*	*Sr*	*Zn*
					mg l^{-1}					
P9C - 2	0.261	100.700	1184.000	1.682	147.000	0.202	0.021	2177.000	0.827	10.342
P9C - 5	0.270	57.460	803.000	0.408	116.300	0.063	0.000	1634.000	0.683	4.212
P9C - 8	0.187	43.770	669.300	0.233	94.790	0.072	0.128	1407.000	0.482	4.084
P9C - 15	0.104	49.040	542.300	bd	98.890	bd	bd	1115.000	0.456	2.514
P9C - 19	0.136	52.620	626.400	bd	107.300	bd	bd	1145.000	0.333	2.012

bd: below detection

APPENDIX 11

Data from *HYDRUS-2D* modelling

Table A11.1 Predicted annual change in the volume of water stored in the flow domain for each of the six* model simulations (volume of flow domain = 30 m × 60 m × 1 m).

Time	*Run 1*	*Run 2*	*Run 3*	*Run 4*	*Run 5*	*Run 6*
days	*Total volume of water stored in flow domain (m^3)*					
0	660.540	660.540	660.540	660.540	660.540	660.540
365	630.230	631.540	635.010	640.820	632.400	629.470
731	623.330	624.630	627.500	636.420	623.530	622.540
1096	616.850	617.440	620.830	637.020	616.900	615.800
1493	623.630	637.320	647.750	670.830	636.990	616.280
1827	615.830	630.640	644.420	670.980	631.370	611.130
2192	612.620	626.250	641.070	656.620	625.060	608.280
2556	611.140	627.910	645.530	663.070	626.980	606.840
2892	608.640	623.760	636.510	651.560	621.070	604.840
3288	606.560	621.910	632.250	644.560	617.790	602.810
3653	604.870	618.080	625.760	635.100	614.420	600.900
4018	604.030	618.440	627.390	640.830	615.680	599.820
4384	603.440	615.800	622.770	640.500	612.510	599.310
4749	609.200	621.870	630.660	655.060	620.140	604.860
5114	602.340	614.130	623.750	654.970	612.390	598.670
5479	603.840	615.170	623.380	660.160	617.330	598.120

*Run 1: Bare surface; Run 2: rock cladding with 50% reduction in evaporation; Run 3 rock cladding with 65% reduction in evaporation; Run 4 rock cladding with 80 % reduction in evaporation; Run 5: plant growth in rocky covering; Run 6: plant growth in bare tailings.

Table A11.2 Cumulative boundary fluxes for the 15 year simulation period (positive values indicate a net movement of water out of the flow domain).

Run No.	*Percentage reduction in evaporation*	*Cumulative atmospheric flux*	*Cumulative seepage flux*
		m	
Run 1	0	0.295	0.902
Additional Run	20	0.184	0.906
Additional Run	35	0.054	0.915
Run 2	50	-0.184	0.977
Run 3	65	-0.567	1.207
Run 4	80	-1.752	1.767
Run 5	-	-5.983	0.948
Run 6	-	-1.011	0.899

	Cumulative volume over the whole impoundment[1]	*Cumulative volume over the whole impoundment*
	m^3	
Run 1	154181.4	470809.2
Run 2	-96161.1	510124.5
Run 3	-296183	629958.3
Run 4	-914457	922374
Run 5	-3123300	495030
Run 6	-527742	469095.3

	Cumulative percentage infiltration[2]	*Cumulative percentage seepage*[3]
	%	
Run 1	4.729	14.442
Run 2	-2.95	15.648
Run 3	-9.085	19.324
Run 4	-28.051	28.294
Run 5	-95.807	15.185
Run 6	-16.188	14.389

1: All fluxes reported in depth measurements, transferred to volumes by multiplying by the footprint area of the impoundment (522 000 m^2).
2: Percentage infiltration calculated by dividing the cumulative atmospheric flux by the total rainfall of the simulation period (6.245 m).
3: Percentage seepage was calculated by dividing the cumulative seepage flux by the total rainfall of the simulation period (6.245 m).